Schweizerische Eidgenossenschaft
Confédération suisse
Confederazione Svizzera
Confederaziun svizra

Federal Department of the Environment,
Transport, Energy and Communications DETEC

Swiss Federal Office of Energy
Energy Research and Cleantech

Final report from 22 May 2026

SmallFLEX GOMS

Small Hydro Flexibility and Complementarity with Photovoltaic and Wind Production in Goms Region

---

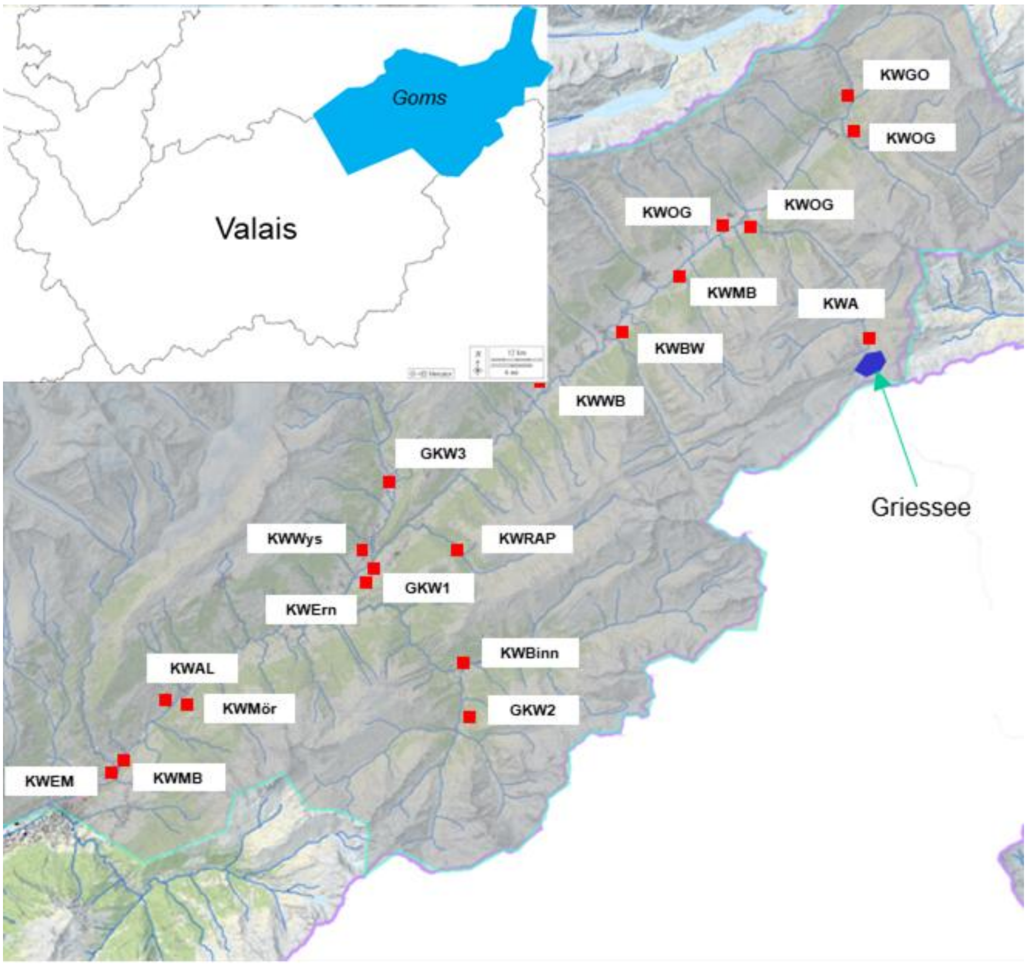

Source: @FMV 2022

Publisher:
Swiss Federal Office of Energy SFOE
Energy Research and Cleantech
CH-3003 Bern
www.bfe.admin.ch

Co-financing:
FMV SA
Rue de la Dixence 9, CP 506, CH-1951 Sion
www.fmv.ch
ALPIQ
Chem. de Mornex 10, 1003 Lausanne, Suisse
www.alpiq.ch

Subsidy recipients:
HES SO Valais
Rue de l'industrie 23, 1950 Sion
www.hevs.ch
HEIG-VD
Route de Cheseaux 1, 1400 Yverdon-les-Bains, CH
www.heig-vd.ch
HDE - Power Vision Engineering Sàrl
Rue des Jordils 40 1, CH-1025 St-Sulpice
www.powervision-eng.ch/
WSL - Swiss Federal Institute for Forest, Snow and Landscape Research
Zürcherstrasse 111, CH-8903 Birmensdorf
www.wsl.ch
ETHZ - Versuchsanstalt für Wasserbau (VAW)
Hönggerbergring 26, 8093 Zürich, Switzerland
www.vaw.ethz.ch

Authors:
Jean Decaix, Charly-Loup Lecointre, Vlad Hasmatuchi, Audrey Wesoly, Cécile Münch-Alligné, HES SO Valais, cecile.muench@hevs.ch
Mohammad Rayati, Luca Tomasini, Mokhtar Bozorg, HEIG-VD, mokhtar.bozorg@heig-vd.ch
Alirez Zobeiri, Florent Gauye, FMV, florent.gauye@fmv.ch
Jeremy Schmid, Claire Bussard, Matthieu Dreyer, Christophe Nicolet, Powervision Engineering, christophe.nicolet@powervision-eng.ch
Massimiliano Zappa, WSL, massimiliano.zappa@wsl.ch
Clara Streule, Adriano, Lais, Frederic Evers, Robert Boes, ETHZ VAW, boes@vaw.baug.ethz.ch
Bernard Valluy, ALPIQ, bernard.valluy@alpiq.com

SFOE project coordinators:
Karin Söderström, karin.soederstroem@bfe.admin.ch
Michael Moser, michael.moser@bfe.admin.ch

SFOE contract number: SI/502535-01

The authors bear the entire responsibility for the content of this report and for the conclusions drawn therefrom.

Summary

Background, Motivation and Objectives

The SmallFLEX Goms project builds on the initial SmallFLEX project, which identified new approaches to increase the flexibility of run-of-river hydropower plants. In the context of increasing integration of variable renewable energy sources, enhancing the operational flexibility of alpine hydropower is essential to support grid stability and optimise energy production. The main objective of the project is to confirm and implement these flexible operating modes under real operating conditions for the Gletsch–Oberwald power plant (KWGO). More broadly, the project aims to identify and exploit "hidden" flexibility in small and medium-sized hydropower plants with limited storage capacity, and to assess their potential role within Virtual Power Plants (VPPs).

Project Content and Methodology

The project started with a comprehensive inventory followed by a potential assessment of small and medium-sized hydropower plants in the Goms valley. Using a multi-criteria evaluation (including storage capacity, peak power, and risk factors), plants with limited storage capacity but high flexibility potential were ranked. The Merezenbach and Mörel power plants were selected for in-depth investigations with a view to on-site testing, while the Altstafel power plant was chosen for VPP studies.

For these plants, detailed transient hydraulic analyses were carried out using SIMSEN software to assess technical flexibility limits, quantify additional storage potential (in volume and energy), and evaluate options such as pumping integration. In parallel, a hydro-meteorological forecasting framework was developed to support short-term operation and long-term planning. This included forecasts of hydrological inflows, photovoltaic production, and wind generation, as well as simulations of hybrid energy systems combining these resources with storage.

A key focus of the project was the assessment of air entrainment risks when using hydraulic waterways as temporary storage. This issue was investigated through a literature review, physical modelling of the pressurisation process of the Mörel power plant, and numerical simulations, leading to the development of a structured engineering assessment methodology.

To validate these analyses, on-site experimental campaigns were conducted at Merezenbach and Mörel, supported by detailed monitoring and risk assessment procedures. In addition, the integration of flexible hydropower into a Virtual Power Plant framework combining hydropower, solar, wind, and storage was analysed using optimisation-based approaches. Finally, a business model was developed to evaluate the economic viability of these flexibility measures.

Main Results and Conclusions

The project demonstrates that significant flexibility can be mobilised in small and medium-sized run-of-river hydropower plants through adapted operating strategies, without major infrastructure modifications. Plants with limited storage capacity show the greatest potential, although technical limits arise from hydraulic transients and safety constraints.

Air entrainment was identified as a major limiting factor, making significant dewatering of headrace tunnels or hydraulic waterways generally inadvisable. Hydro-meteorological forecasts improve operational optimisation, particularly for hydropower and photovoltaic generation, while highlighting the importance of storage capacity. On-site tests at KW Mörel confirmed the feasibility of controlled dewatering and validated an additional flexibility of approximately ±3 MW.

Integration into a Virtual Power Plant improves profitability and reduces imbalance costs, with additional support provided by pumping and battery storage, although results remain sensitive to market conditions.

From an economic perspective, flexibility remains constrained by technical and environmental factors. Nevertheless, exploiting existing "hidden" flexibility can generate measurable benefits, with approximately **+1% additional winter revenue for KW Mörel**, as well as increases in **revenue and production of +3% and +2%, respectively, for KWGO**.

Zusammenfassung

Hintergrund, Motivation und Ziele

Das Projekt SmallFLEX Goms baut auf dem ursprünglichen SmallFLEX-Projekt auf, in dem neue Ansätze zur Erhöhung der Flexibilität von Laufwasserkraftwerken identifiziert wurden. Im Kontext der zunehmenden Integration fluktuierender erneuerbarer Energien ist die Verbesserung der betrieblichen Flexibilität alpiner Wasserkraftwerke von wesentlicher Bedeutung, um die Netzstabilität zu unterstützen und die Energieproduktion zu optimieren. Das Hauptziel des Projekts besteht darin, diese flexiblen Betriebsmodi unter realen Betriebsbedingungen für das Kraftwerk Gletsch–Oberwald (KWGO) zu bestätigen und umzusetzen. Darüber hinaus zielt das Projekt darauf ab, „verborgene" Flexibilitätspotenziale in kleinen und mittleren Wasserkraftwerken mit begrenzter Speicherkapazität zu identifizieren und zu nutzen sowie deren potenzielle Rolle in virtuellen Kraftwerken (Virtual Power Plants, VPP) zu bewerten.

Projektinhalt und Methodik

Das Projekt begann mit einer umfassenden Bestandsaufnahme und anschliessenden Potenzialanalyse der kleinen und mittleren Wasserkraftwerke im Goms. Mithilfe einer multikriteriellen Bewertung (einschliesslich Speicherkapazität, Spitzenleistung und Risikofaktoren) wurden Kraftwerke mit begrenzter Speicherkapazität, aber hohem Flexibilitätspotenzial priorisiert. Die Kraftwerke Merezenbach und Mörel wurden für vertiefte Untersuchungen mit Blick auf Vor-Ort-Tests ausgewählt, während das Kraftwerk Altstafel für VPP-Studien herangezogen wurde. Für diese Kraftwerke wurden detaillierte hydraulische Transientenanalysen mit der Software SIMSEN durchgeführt, um technische Flexibilitätsgrenzen zu bestimmen, zusätzliches Speicherpotenzial (in Volumen und Energie) zu quantifizieren und Optionen wie die Integration von Pumpbetrieb zu bewerten. Parallel dazu wurde ein hydro-meteorologisches Prognosemodell entwickelt, um den kurzfristigen Betrieb und die langfristige Planung zu unterstützen. Dieses umfasste Prognosen der hydrologischen Zuflüsse, der Photovoltaikproduktion und der Windenergieerzeugung sowie Simulationen hybrider Energiesysteme, die diese Ressourcen mit Speichern kombinieren. Ein zentraler Schwerpunkt des Projekts war die Bewertung der Risiken des Lufteintrags bei der Nutzung hydraulischer Wasserwege als temporäre Speicher. Diese Fragestellung wurde durch Literaturanalysen, physikalische Modellversuche zur Druckbeaufschlagung des Kraftwerks Mörel sowie numerische Simulationen untersucht und führte zur Entwicklung einer strukturierten ingenieurtechnischen Bewertungsmethodik. Zur Validierung dieser Analysen wurden Vor-Ort-Versuchskampagnen in Merezenbach und Mörel durchgeführt, unterstützt durch detaillierte Monitoring- und Risikobewertungsverfahren. Darüber hinaus wurde die Integration flexibler Wasserkraft in ein Konzept eines virtuellen Kraftwerks, das Wasserkraft, Solarenergie, Windenergie und Speicher kombiniert, mit optimierungsbasierten Ansätzen analysiert. Schliesslich wurde ein Geschäftsmodell entwickelt, um die wirtschaftliche Tragfähigkeit dieser Flexibilitätsmassnahmen zu bewerten.

Wichtigste Ergebnisse und Schlussfolgerungen

Das Projekt zeigt, dass in kleinen und mittleren Laufwasserkraftwerken durch angepasste Betriebsstrategien erhebliche Flexibilität mobilisiert werden kann, ohne dass grössere Infrastrukturanpassungen erforderlich sind. Kraftwerke mit begrenzter Speicherkapazität weisen dabei das grösste Potenzial auf, wobei technische Grenzen durch hydraulische Transienten und Sicherheitsanforderungen gesetzt werden. Lufteintrag wurde als ein zentraler limitierender Faktor identifiziert, weshalb ein starkes Entleeren von Druckstollen oder hydraulischen Wasserwegen im Allgemeinen nicht empfehlenswert ist. Hydrometeorologische Prognosen verbessern die Betriebsoptimierung, insbesondere für Wasserkraft und Photovoltaik, und unterstreichen gleichzeitig die Bedeutung von Speicherkapazitäten. Vor-Ort-Versuche am KW Mörel bestätigten die Machbarkeit einer kontrollierten Entleerung und validierten eine zusätzliche Flexibilität von etwa ±3 MW. Die Integration in ein virtuelles Kraftwerk verbessert die Wirtschaftlichkeit und reduziert Ausgleichskosten, zusätzlich unterstützt durch Pumpbetrieb und Batteriespeicher, wobei die Ergebnisse jedoch weiterhin stark von den Marktbedingungen abhängen.

Wirtschaftlich bleibt die Flexibilität durch technische und ökologische Rahmenbedingungen begrenzt. Dennoch kann die Nutzung bestehender „verborgener" Flexibilität messbare Vorteile generieren, mit rund **+1 % zusätzlichem Winterertrag für KW Mörel** sowie einer Steigerung von **Ertrag und Produktion um +3 % bzw. +2 % für KWGO**.

Résumé

Contexte, motivation et objectifs

Le projet SmallFLEX Goms s'inscrit dans la continuité du projet initial SmallFLEX, qui a permis d'identifier de nouvelles approches pour accroître la flexibilité des centrales hydroélectriques au fil de l'eau. Dans un contexte d'intégration croissante des énergies renouvelables variables, l'amélioration de la flexibilité opérationnelle des centrales hydroélectriques alpines est essentielle pour soutenir la stabilité du réseau et optimiser la production d'énergie. L'objectif principal du projet est de confirmer et de mettre en œuvre ces modes d'exploitation flexibles en conditions réelles pour la centrale de Gletsch–Oberwald (KWGO). Plus largement, le projet vise à identifier et exploiter les flexibilités « cachées » des petites et moyennes centrales hydroélectriques disposant de capacités de stockage limitées, ainsi qu'à évaluer leur rôle potentiel au sein de centrales virtuelles (Virtual Power Plants, VPP).

Contenu du projet et méthodologie

Le projet a débuté par un inventaire complet suivi d'une analyse de potentiel des petites et moyennes centrales hydroélectriques de la vallée de Conches (Goms). À l'aide d'une évaluation multicritère (incluant la capacité de stockage, la puissance de pointe et les facteurs de risque), les centrales présentant une capacité de stockage limitée mais un fort potentiel de flexibilité ont été classées. Les centrales de Merezenbach et de Mörel ont été retenues pour des investigations approfondies en vue d'essai sur site, tandis que la centrale d'Altstafel a été choisie pour l'étude des VPP. Pour ces centrales, des analyses détaillées de transitoires hydrauliques ont été menées à l'aide du logiciel SIMSEN afin d'évaluer les limites techniques de flexibilité, de quantifier le potentiel de stockage supplémentaire (en volume et en énergie) et d'étudier des options telles que l'intégration du pompage. En parallèle, un cadre de prévision hydrométéorologique a été développé pour soutenir l'exploitation à court terme et la planification à long terme. Celui-ci comprenait des prévisions des apports hydrologiques, de la production photovoltaïque et de la production éolienne, ainsi que des simulations de systèmes énergétiques hybrides combinant ces ressources avec du stockage. Un axe majeur du projet a porté sur l'évaluation des risques d'entraînement d'air lors de l'utilisation des voies d'eau hydrauliques comme stockage temporaire. Cette question a été étudiée au moyen d'une revue de la littérature, de modélisations physiques de la mise en charge de la centrale de Mörel et de simulations numériques, conduisant au développement d'une méthodologie structurée d'évaluation d'ingénierie. Afin de valider ces analyses, des campagnes expérimentales sur site ont été réalisées à Merezenbach et Mörel, avec un monitoring détaillé et des procédures d'évaluation des risques. En complément, l'intégration de l'hydroélectricité flexible dans un cadre de centrale virtuelle combinant hydroélectricité, solaire, éolien et stockage a été analysée à l'aide d'approches d'optimisation. Enfin, un business model a été développé afin d'évaluer la viabilité économique de ces mesures de flexibilité.

Principaux résultats et conclusions

Le projet démontre qu'une flexibilité significative peut être mobilisée dans les petites et moyennes centrales hydroélectriques au fil de l'eau grâce à des stratégies d'exploitation adaptées, sans modifications majeures des infrastructures. Les centrales disposant de faibles capacités de stockage présentent le plus grand potentiel, bien que des limites techniques apparaissent en raison des transitoires hydrauliques et des contraintes de sécurité. L'entraînement d'air a été identifié comme un facteur limitant majeur, rendant généralement déconseillé un dénoyage important des galeries ou conduites hydrauliques. Les prévisions hydrométéorologiques améliorent l'optimisation de l'exploitation, en particulier pour l'hydroélectricité et le photovoltaïque, tout en soulignant l'importance des capacités de stockage. Les essais sur site à KW Mörel ont confirmé la faisabilité d'un dénoyage contrôlé et validé une flexibilité supplémentaire d'environ ±3 MW. L'intégration dans une centrale virtuelle améliore la rentabilité et réduit les coûts liés aux écarts, avec un soutien supplémentaire apporté par le pompage et les batteries, même si les résultats restent sensibles aux conditions du marché. Sur le plan économique, la flexibilité reste contrainte par des facteurs techniques et environnementaux. Néanmoins, l'exploitation des flexibilités « cachées » existantes peut générer des bénéfices mesurables, avec environ **+1 % de revenu hivernal supplémentaire pour KW Mörel** ainsi qu'une augmentation du **revenu et de la production de +3 % et +2 % respectivement pour KWGO**.

Main findings («Take-Home Messages»)

WP1 – Implementation of SmallFLEX in KWGO

- Extended operating ranges can improve economic performance.
- Dewatering operations are feasible within physical limits.
- Feasibility confirmed based on site data and process-variable analysis.

WP2 – Selection of promising SHP

- Screening identified and ranked hydropower plants with additional flexibility potential.
- KW Merezenbach and KW Mörel selected as most promising; KW Altstafel for VPP integration.

WP3 – Hydraulic system flexibility limits

- Detailed modelling (SIMSEN) used to assess flexibility limits and dynamic behaviour.
- Additional storage and pumping potential evaluated.
- Hydraulic transients and shutdown scenarios analysed, including preliminary air entrainment risks.

WP4 – Hydro-meteorological predictions

- Forecasting framework developed for operational and long-term planning.
- Short-term forecasts improve management of hydropower and PV; wind remains uncertain.
- Storage availability is critical for flexibility.
- Hybrid system simulations highlight opportunities but require realistic demand scenarios.

WP5 – Risk of air entrainment

- Key air entrainment mechanisms identified and validated with physical modelling.
- Results show that fully emptying headrace systems is not recommended.
- A stepwise methodology was developed for assessing air entrainment risks.

WP6 – On-site experiments

- Robust preparation, monitoring, and risk assessment are essential for safe testing.
- Experiments at KW Mörel validated usable storage (~±3 MW flexibility) for primary control service.
- Data collected supports future operational improvements, despite limits at KW Merezenbach.

WP7 – Virtual Power Plant (VPP)

- Integration of hydropower, PV, wind, and storage improves profitability and flexibility.
- Pumping and batteries enhance value (arbitrage, imbalance reduction, ancillary services).
- Revenues are sensitive to market conditions.

WP8 – Business model

- Market revenues alone are insufficient; technical feasibility is the key.
- Aggregation (pooling plants) improves market access and unlocks ancillary service opportunities.
- Exploiting existing “hidden” flexibility offers the best cost-benefit, with revenue and production increases of up to +3% and +2% for KWGO.
- Flexibility provides additional but modest revenues (around +1% for KW Mörel), complementing rather than driving the business model.

Contents

List of figures

List of tables

1 Introduction

1.1 Context and motivation

The increasing penetration of photovoltaic generation in Switzerland, combined with periods of negative electricity prices and growing demand for ancillary services, creates new opportunities for distributed hydropower flexibility. While flexibility services are traditionally provided by large storage hydropower plants, pumped storage schemes or battery systems, these solutions are often not directly applicable to small and medium-sized run-of-river hydropower plants due to limited storage capacity, hydraulic constraints and economic scale effects. SmallFlex Goms addresses this gap by focusing on "hidden flexibility" within existing infrastructures, combining hydraulic engineering, forecasting, experimental validation and system-level integration through Virtual Power Plant concepts. This approach offers a pathway to unlock distributed flexibility with limited infrastructure investment, while making better use of existing hydropower assets.

The main motivation for launching the SmallFLEX Goms project is to build on the successful experience gained from the SmallFLEX project, which was conducted between 2018 and 2020[1]. The selected demonstration site was the small run-of-river power plant of Gletsch Oberwald (KWGO), owned by Forces Motrices Valaisanne (FMV). The results of the latter have clearly revealed the great potential of small run-of-river hydro power plants (SHP) in producing energy in peak hours as well as providing system services while maintaining the safety of the power plant and at the same time minimizing the environmental impacts related to hydropeaking.

Small Hydropower in Switzerland represents 10% of the hydroelectricity production with 3'400 GWh per year (around 5% of the annual electricity production of Switzerland) and an existing potential of 770 GWh/year (rapport de l'OFEN - Potentiel hydroéléctrique de la Suisse - Août 2019) has been estimated. More than 70% of this potential concerns the so-called "large" small hydropower plant with a mean installed power between 1 MW and 10 MW. The proposed project aims specifically at this type of hydro power plants and will try to increase their annual productions (mostly in winter) by employing a smart combination of the available additional resources. These could include using un-conventional spaces such as the desander and the upper part of the penstock as supplementary accumulation volumes (as in SmallFLEX project), coupling hydro generation with solar and wind energies, or even using pumping stations to save energy for peak production.

In addition to peak production, the mentioned actions could also help the plant owners to better plan their assets and use them for ancillary services as well. In fact, provision of grid services by hydroelectric power plants is a key factor associated with the energy transition. These services are vital for a stable operation of the grid, and thus, for the security of electricity supply in Switzerland. The massive integration of renewable energies such as solar and wind, which are intrinsically intermittent, results in a higher need for ancillary services. Hydropower energy is considered as a safe backup for such services. Traditionally, this task has been undertaken by large hydro power plants. However, with the emergence of the smart and local grids, the role of small hydro power plants becomes more crucial. Moreover, the need for flexibilities (ancillary services) is increasing year by year while the possibility for installing new large hydro power plants is limited. Many of the small hydro power plants might have a very small capacity that does not make them eligible for ancillary services, however, by integrating a number of small power plants (a pool of hydro power plants or a combination of hydro, wind and solar assets), the asset managers could call for these services, too. This definitely brings additional profits to the companies and also contributes to a better grid stability in the national level. These operations, however, require much higher levels of flexibility in the hydro section. The turbines must be ready to operate in off-design conditions and undergo fast transitions. To guarantee that these demands could be borne safely, further analysis and tests must be performed on each machine to define its limits in terms of operating modes.

[1] https://www.aramis.admin.ch/Texte/?ProjectID=40717

Concretely, the proposed project of ‘SmallFLEX Goms’ aims at addressing the following issues:

- How will the proposed actions in SmallFLEX project respond in real operations?
- How could the SmallFLEX project experience be transposed to other powerplants?
- How could we widen the production and flexibility possibilities beyond the SmallFLEX out-comes? In other words, how could we integrate additional sources like solar, wind, pumping, and so on into the previously approved approach to improve the performance of the plants?
- What would be the associated risks (technical, environmental, etc.) with the new functionalities and operation modes of the integrated systems and how could we address them?
- What will be the outcome of the proposed actions in terms of economic paybacks?

A particular attention will be paid to the following objectives:

- Demonstration of the flexibility of KWGO for a long-term operation.
- Definition of the main criterion and limits for a given run-off power plant to determine its flexibility.
- Evaluation of the complementarity of flexible medium and small power plant (run-off and storage) with new renewable production.

The obtained results through the proposed project will be of high value for the whole fleet of the Swiss hydropower production, as the potential for small hydro is quite high and demand for this sector is rising to answer to the long-term energy policies and decarbonization. The results and recommendations are believed to be directly applicable to many hydro power plants in Switzerland. This clearly shows the usefulness and the necessity of conducting the proposed project.

1.2 Project objectives

The SmallFLEX Goms project aims to discover new production and flexibility opportunities for small and medium hydropower, including these three main research paths:

- Applying the flexibility solutions to a region with several hydro power plants. This requires the evaluation of the potential of each plant at the first place, and then, leads to new challenges regarding connecting the plants together and having a virtual pool of small hydro power plants that can work together for peak production and system services.
- Integration of new solutions such as solar, wind, pumping stations, etc. to further increase the production capacity and flexibility. This brings in several new challenges in terms of coordination between the assets and choosing the optimal combination/solution in real time. This also requires preparing the system for being resilient against unforeseen events such as unpredicted cloudy skies and instantaneous peaks in energy demand.
- Implementation of the proposed actions in real practice and evaluation of the actual benefits and risks in place; and at a later stage, applying the solutions to other power plants and evaluating the economic profits in Goms region thanks to new operation modes.
- The above-mentioned goals are divided to the following tasks, which will be followed and evaluated during the project:
- Implementing the results of the ‘SmallFLEX’ project to the KWGO hydro power plant and evaluating the outcomes of such modifications in a realistic manner over a three-year horizon.
- Evaluating the existing potentials in the Goms region based on the methodology developed through the ‘SmallFLEX’ project.
- Improving (short-term) weather predictions and including the results for optimizing the exploitation program.

- In-depth analysis of air entrainment risks in penstock due to flexible operations of small hydro power plants.
- Design of Virtual Power Plants (VPP's) by aggregating all the available potentials in a region including hydro, solar, wind, pump-turbine cycles, etc in order to optimize the utilization of these potentials in energy and ancillary service markets.
    - Performing on-site experimental campaigns to evaluate the proposed scenarios and solutions in practice and ensure that these actions do not threaten the installation safety.
    - Evaluating the economic benefits of the selected scenarios for the whole region of Goms.

2 Methodology

The project focuses on the Goms region, situated in the northwest of Canton of Wallis. This region includes many small hydro power plants and holds considerable potential in terms of solar energy production. This makes this region a great candidate for the proposed project. Figure 1 (left) shows the hydrological map of the region with a non-exhaustive list of the existing hydro power plants.

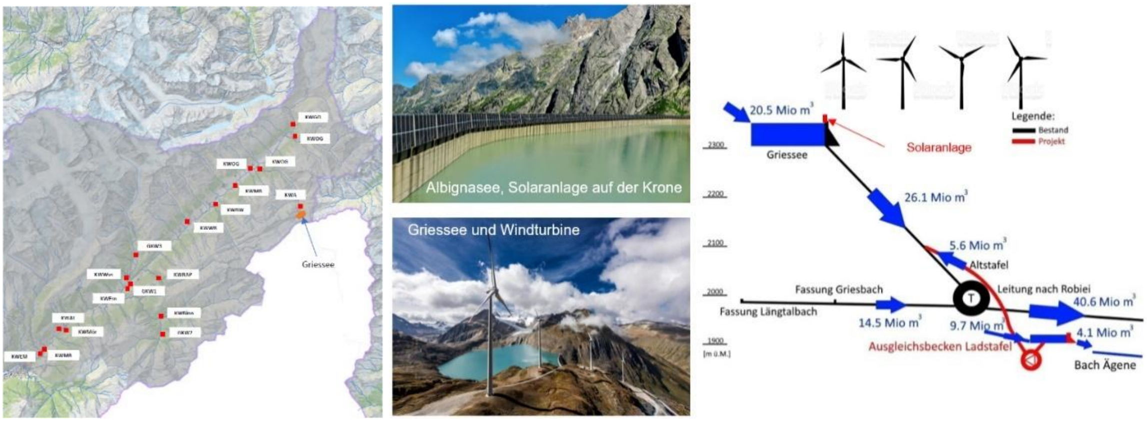

Figure 1: Hydrological map of Goms region with some existing hydro power plants and possible combination of hydro, solar, and wind generation close to Griessee lake.

An example of the ideas explained earlier related to creating an optimal combination of hydro, wind and solar generation is depicted on the right of Figure 1. This figure shows the Griessee lake as well as the installed wind turbines at its vicinity and highlight the potential of installing additional photovoltaic solar panels in the region to boost the production. The possibility to refurbish the Altstafel power plant, KW Aegina AG, as a pumped storage facility will be investigated in the project. Apart from this site gathering hydro, wind and solar, the following hydro power plants have been identified in the Goms region, at the beginning of the project, as potential candidates to be operated in a more flexible way.

Table 1 – List of the power plants in the Goms region.

- KW Gletsch-Oberwald
- KW Merezenbach
- KW Wannebode (Blinnenwerk AG)
- KW Walibach / Grafschaft
- KW Mörel (Aletsch AG)
- KW Bitsch (KW Massaboden)
- KW Bitsch (Electra Massa)
- KW Münstigertal
- KW Binn

Rhonewerke AG

- KW Ernen
- KW Mörel

KW Obergoms AG

- KW Gere
- KW Ulrichen
- KW Niderbach

Gommerkraftwerke AG

- KW Rappental (GKW1)
- KW Saflisch (GKW2)
- KW Heiligkreuz (GKW2)
- KW Fieschertal (GKW3)
- KW Wysswasser
- Neubrigg / Mubisa (GKW1)

A wide variety of power plants are available, with outputs ranging from less than 200 kW to over 300 MW. Some power plants have a storage basin, others are run-of-river. From an electromechanical point of view, some power plants are equipped with Pelton turbines, others with Francis turbines.

In order to provide concrete answers to the issues raised, 9 work packages in total have been structured for the SmallFLEX Goms project, which are explained in detail in Figure 2 below.

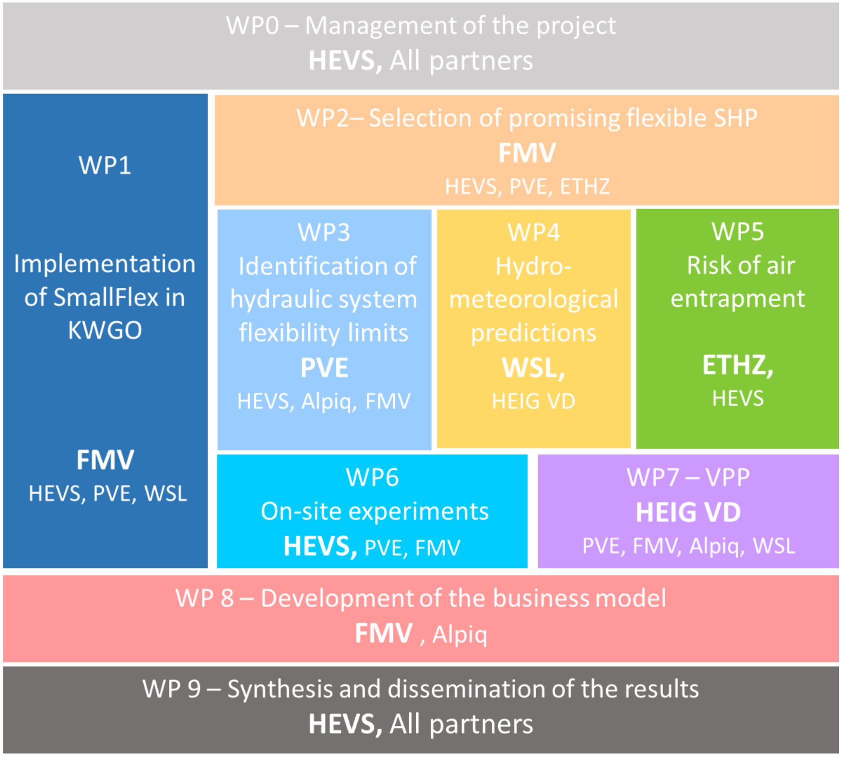

Figure 2: Project organisation

Hereafter are described in detail, the activities planned in the different WPs.

WP0 – Management of the project

Lead: HEVS, **partners:** all

This WP includes the fundamental actions required to guarantee the correct execution of the project throughout its lifecycle. This WP is led and handled by HEVS acting as the coordinator between partners and convene regular progress meetings to guarantee successful communication between the partners and the WP as well as the execution of the project. Three tasks have been defined:

- T0.1: Organisation, preparation, participation, and synthesis of the meetings
- T0.2: WPs coordination and information exchange support
- T0.3: SFOE annual reports and tracking of the deliverables.

WP1 – Implementation of SmallFLEX in KWGO

Lead: FMV, **partners**: HEVS, HDE, WSL

This work package deals with the implementation of the flexible operating mode based on the use of the upper part of the head race tunnel as an additional storage volume, demonstrated in the SmallFLEX project, at the Gletsch Oberwald (KWGO) hydropower plant. The following activities have been considered for this purpose; two tasks have been defined:

- T1.1: Implementing the new exploitation modes in KWGO power plant following the conclusions of the previous SmallFLEX project (HEX, HEVS VS)
- T1.2: Long-term monitoring of the new operation mode (FMV, HEVS, HDE)

WP2 – Selection of promising flexible SHP

Lead: FMV, **partners**: HEVS, HDE, ETHZ

This work package deals with the selection of power plants for which the implementation of the results and the developed methodology in the SmallFLEX project KWGO could be applied. The following activities have been considered for this purpose:

- T2.1: Exhaustive inventory of the hydropower plants and their potential in the Goms region: data availability, relevance, potential (FMV, HEVS)
- T2.2: Screening and ranking of the relevant power plants based on specific criteria and methodology to select the most promising plants. (FMV, HEVS, HDE, ETHZ)

WP3 – Identification of hydraulic system flexibility limits

Lead: HDE, **partners**: HEVS, ALPIQ, FMV

The aim of this work package is to perform an extensive hydraulic analysis of the flexibility potential of a selection of promising hydropower plants, via the following tasks:

- T3.1: Technical site visits of the selected plants (HEVS, HDE, FMV, Alpiq)
- T3.2: Determination of the extended operation modes of the power plants available and new storage capacity both in volume and energy, risk of air entrainment, turbine flexibility, variable speed) (HEVS, HDE, Alpiq, FMV)
- T3.3: Sizing of new storage and pumping capacity for the selected storage case study(ies) (Alpiq, HDE, FMV, HEVS)
- T3.4: Quantifying the peak production capacities, system services (SDL), etc. (HDE in coordination with WP4. HEVS, FMV, Alpiq)

WP4 – Hydro-meteorological predictions

Lead: WSL, **partner:** HEIG-VD

The aim of WP4 is to assess the suitability of the current FMV hydropower plants in the Goms valley for flexible operation from the point of view of the hydrological characteristics of the corresponding catchments. A second goal is to investigate how water discharge at selected HP intakes (e.g., Griesbach), and ultimately HP production, matches with the production of wind and solar electricity at corresponding HP infrastructures in order to optimize a joint operation. To this end, we will further develop and operate our hydrometeorological forecast system based on the hydrological model PREVAH and the corresponding operational information platform, https://hydro.slf.ch/sihl/gletsch, which was created during SmallFLEX Gletsch. The following subtasks are planned:

- T4.1 Demonstration of hydrometeorological forecasts for flexible operation of small HP plants (WSL, HEIG-VD)
- T4.2 Assessment of FMV small hydropower plants in the Goms valley with regard to their suitability for flexible operation from the point of view of hydrological preconditions (WSL, HDE)
- T4.3 Assessment of climate change impact on the potential for flexible operation of the small HP plants (from a hydrological point of view) (WSL)

WP5 – Risk of air entrainment

Lead: ETHZ, **partners:** HEVS

WP5 extends the work conducted within the preceding SmallFLEX project and aims at reducing the uncertainties related to the assessment of the limitations to the flexible operation of existing hydropower facilities in terms of air entrainment. In addition, the work package aims at minimizing the necessity to conduct tests of different operation modes at the selected facilities. The work package includes hydraulic laboratory tests at the Laboratory of Hydraulics, Hydrology and Glaciology (VAW) at ETH Zurich (ETHZ).

- T5.1: Compilation and review of the state-of-the-art related to air entrainment and transport in hydraulic systems similar to the investigated facilities; (ETHZ)
- T5.2: Identification and assessments of uncertainties related to scale effects and geometrical variations as well as gaps in the state-of-the-art; (ETHZ, HEVS, HDE)
- T5.3: Design and construction of a hydraulic laboratory test at adequate scale according to the literature review; (ETHZ)
- T5.4: General model investigations of different operation modes and their effect on air entrainment and transport within waterway system; (ETHZ)
- T5.5: Detailed model investigations of different operation modes and their effect on air entrainment and transport within the waterway system; (ETHZ)

WP6 - On-site experiments

Lead: HEVS, **partners:** HDE, FMV

The goal of this work package is to validate the predicted potential in the previous work packages in real action for two hydro power plants and verify that the new operation modes will respect the security guidelines of each plant. To answer these questions, the following tasks have been defined:

- T6.1: Definition of the experimental protocols (instrumentation, program, identification, and limitation of the risks) (HEVS, HDE)
- T6.2: Installation of the Hydro-Clone system on 1 hydro power plant (HDE)
- T6.3: Performing on-site experimental campaigns in 2 hydropower plants (HEVS)
- T6.4: Analysis of the experimental results and validation of the operational limits of the power plant with respect to the identified storage potentials (HEVS)

WP7 – VPP

Lead: HEIG-VD, **partners:** HDE, ALPIQ, FMV, WSL

This work package deals with the optimal design and operation of a Virtual Power Plant composed by a set of distributed resources connected to a distribution grid in the vicinity of small-scale hydro power plants in order to optimize energy and flexibility (ancillary service) exchanges. Finally, to ensure secure operation of the VPP and validate provision of ancillary services, we perform a dynamic analysis and simulation of the VPP including dynamic model of the resources as well as the electric grid model. The optimization process will be formulated in two stages. The first stage deals with design of the components of the VPP (i.e., selection of possible resources including PVs, battery energy storage systems, wind turbines, pump-turbines, etc as well as optimal size and location of each resource connected to the grid). The second stage deals with optimizing the operation of the VPP components within various time horizons (weekly, daily, intra-day) with respect to market conditions, and uncertainties related to renewable generations and natural water discharge. In particular, the following activities are envisaged:

- Task 7.1 Optimal design of the VPP (HEIG-VD)
- Task 7.2 Optimal operation of the VPP (HEIG-VD, Alpiq)
- Task 7.3 Dynamic simulation of capability of provision of ancillary services regarding power system constraints (e.g., primary frequency control) (HEIG-VD, HDE). Physical emulation of the reduced-scale local grid in the ReIne reconfigurable distribution grid laboratory of HEIG-VD.
- Task 7.4 Revisiting the optimal design and operation of the VPP (HEIG-VD, FMV, HDE) and optimal design of VPP regarding the results of optimal operation (Task 7.2)

WP8 – Development of the business model

Lead: FMV, **partners:** ALPIQ

This work package investigates the economic aspects of the project and examines how the proposed flexibility potential will reflect in the real economic situation. This is realized via:

- T8.1: Economic analysis of the supplementary production thanks to the additional storage of each power plant (including KWGO) (FMV, Alpiq)
- T8.2: Economic analysis of the supplementary ancillary services of each of the selected plants. (FMV, Alpiq)
- T8.3: Performing a global economic analysis of the optimization of the regional potential. (FMV, Alpiq)

WP9 – Synthesis and dissemination of the results

Lead: HEVS, **partners:** all

This work package is structured to gather all the project results under the same umbrella and disseminate them in an appropriate manner. To achieve this goal, the following activities have been foreseen.

- T9.1 Publication of scientific articles (journal and conference papers).
- T9.2 Public deliverable with guidelines to make small/medium HPP more flexible.
- T9.3 Final public report mandatory by OFEN.

The initial planning for all these activities is described below:

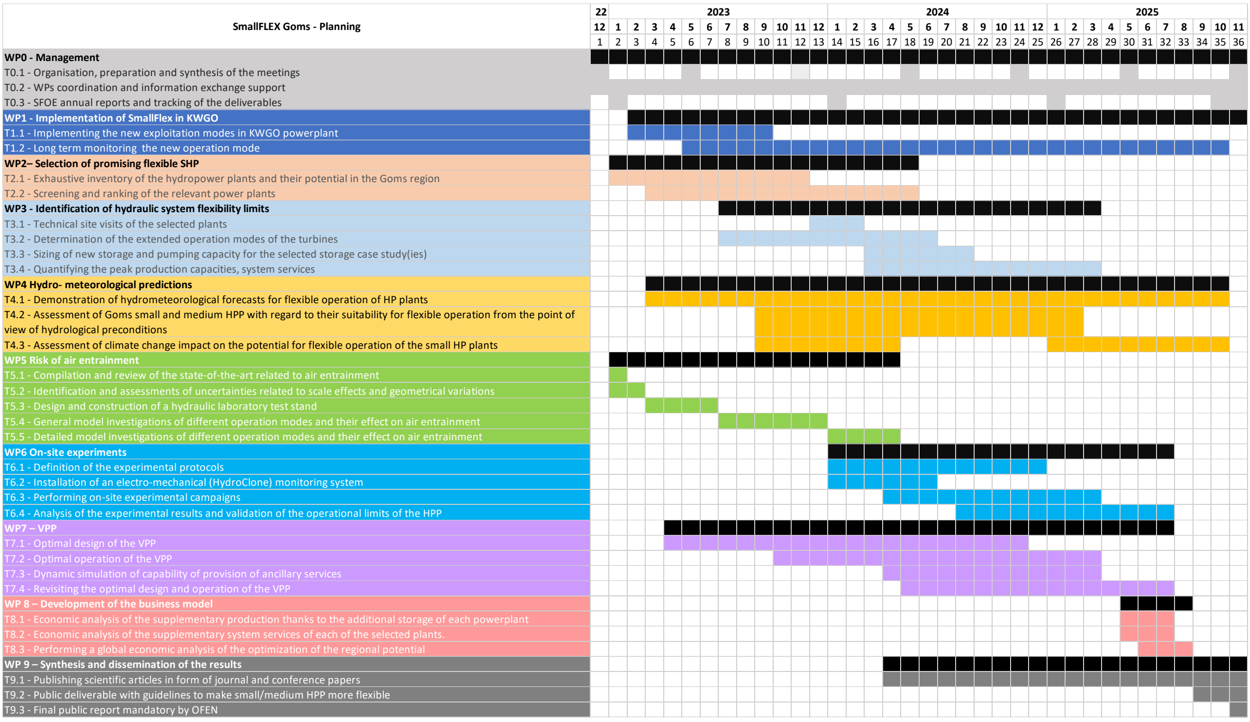

Figure 3: Initial project planning

3 Results and discussion

3.1 WP1 – Implementation of SmallFLEX in KWGO

Lead: FMV, partners: HEVS, HDE, WSL

The main goal of this work package is to implement for operation and to monitor the three modes of flexibility identified during the SmallFLEX project.

3.1.1. Monitoring of the FCR service system

An analysis of the data since 2019 have been performed to find the occurrences of some dewatering events of the desander, the overflow chamber and eventually the penstock. These occurrences are linked to the FCR (Primärregelleistung) service system that requires the use of a fraction of the water volume stored in the desander and the overflow chamber. Figure 4 shows the time history of the power and the frequency on Tuesday, October 17th, 2023, during two FCR events: one from 09:00 to 09:15 and a second from 10:00 and 10:15. For both cases, the power is increased by 0.3 MW consecutive to a drop in frequency of about 150 mHz. The increase in power goes hand in hand with a small decrease in the water level in the forebay tank. During these two events, the vibration level remains unchanged, as shown in Figure 5.

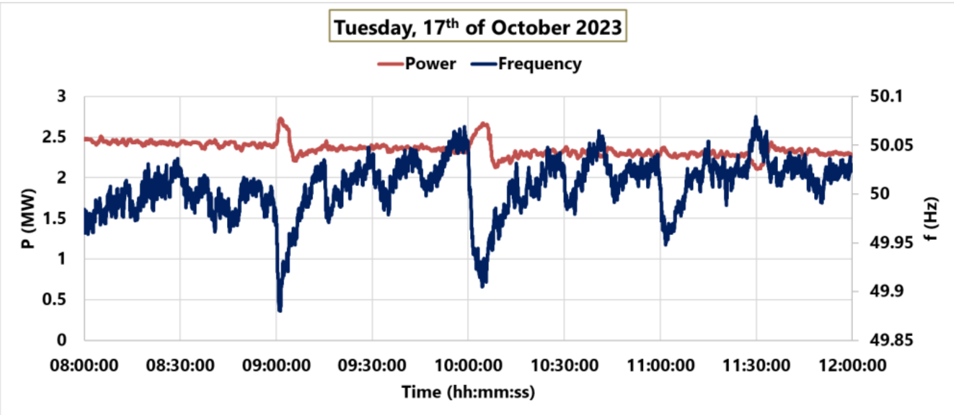

Figure 4: Time history of the power (left axis) and the frequency (right axis) on Tuesday, October 17th, 2023, with two FCR services activated between 09:00 and 09:15 and 10:00 and 10:15.

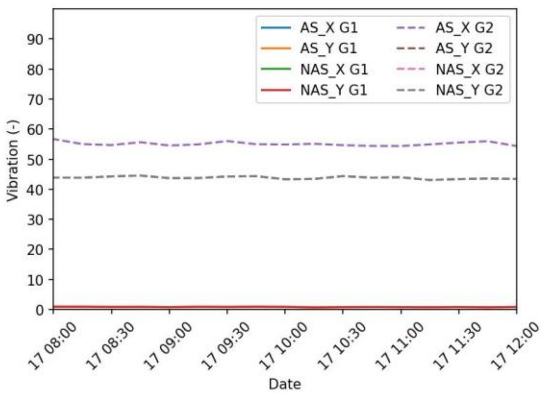

Figure 5: Time history of the maximum vibration level on Tuesday, October 17th, 2023, with two FCR services activated between 09:00 and 09:15 and 10:00 and 10:15.

From the available data, the dewatering of the desander, the overflow chamber and eventually the upper part of the penstock does not lead to an increase in the vibration level monitored along the turbine shaft.

This conclusion must be supported by additional data, acquired at higher powers and during longer times of operation.

3.1.2. Implementing the new exploitation modes in KWGO power plant – Dewatering operating protocol definition

In Figure 6 (and Appendix A), a proposal of a global logical scheme dedicated to the implementation of a permanent operation with dewatering of the KWGO powerplant is provided. Two possible modes are first considered, with a constant or with a variable upstream water level regulation respectively. The constant water level regulation is the current operating mode of the powerplant, using the water level in the desander as input. For this mode, two scenarios are basically used: the standard power production mode and the primary regulation production mode.

For the regulation with dewatering, two scenarios have been retained:

- The first one consists of one drawdown per day, using only one turbine unit. The dewatering cycle starts if the instantaneous inflow turbine discharge corresponds to a power between the allowed minimum (P_{turb_min}) and maximum (P_{den_max}) values. During the dewatering, the turbine is operated at a power equal to the minimum between the sum of the initial value P_{turb_ini} and a dewatering power shift (P_{den}), and the maximum allowed dewatering power P_{den_max}. The dewatering cycle is finished once the lower water level limit in the penstock is reached. The refilling phase is done at the minimum power P_{turb_min} until the maximum water level in the desander is reached. In the case of an insufficient inflow, the machine is stopped, and the refilling is continued. Once the refilling phase is finished (at maximum water level in the desander), the operating mode is switched back to the constant upstream water level regulation, until next day.
- The second one consists in operating the two units with the constant upstream water level regulation and primary grid control activated. Once the grid frequency is below the minimum allowed value, the operating power of the units is increased to reach the P_{reg} value and is maintained for 15 minutes, to cope with the grid regulation requirements. The refilling phase is done by operating the units with a power level P_{red} lower that the initial one. In the case of an insufficient inflow (water level still decreasing), the operating point of the units is reduced to the minimum turbine power level (2x P_{turb_min}) until the maximum water level in the desander is reached. Finally, an insufficient inflow condition even with a turbine power of 2 x P_{turb_min} conducts eventually to a decrease of the water level in the penstock until the lower limit is attained and the turbines are automatically stopped. Once the refilling phase finished (maximum water level in the desander reached), the operation is restarted either with the constant upstream water level regulation or back in the primary regulation with dewatering mode. Depending on specific water level variations during grid regulation, an additional pre-alarm may be implemented in this branch to cancel the regulation mode (*e.g.*, when the water level falls below a threshold at which the power peak can no longer be sustained for at least 900 s).

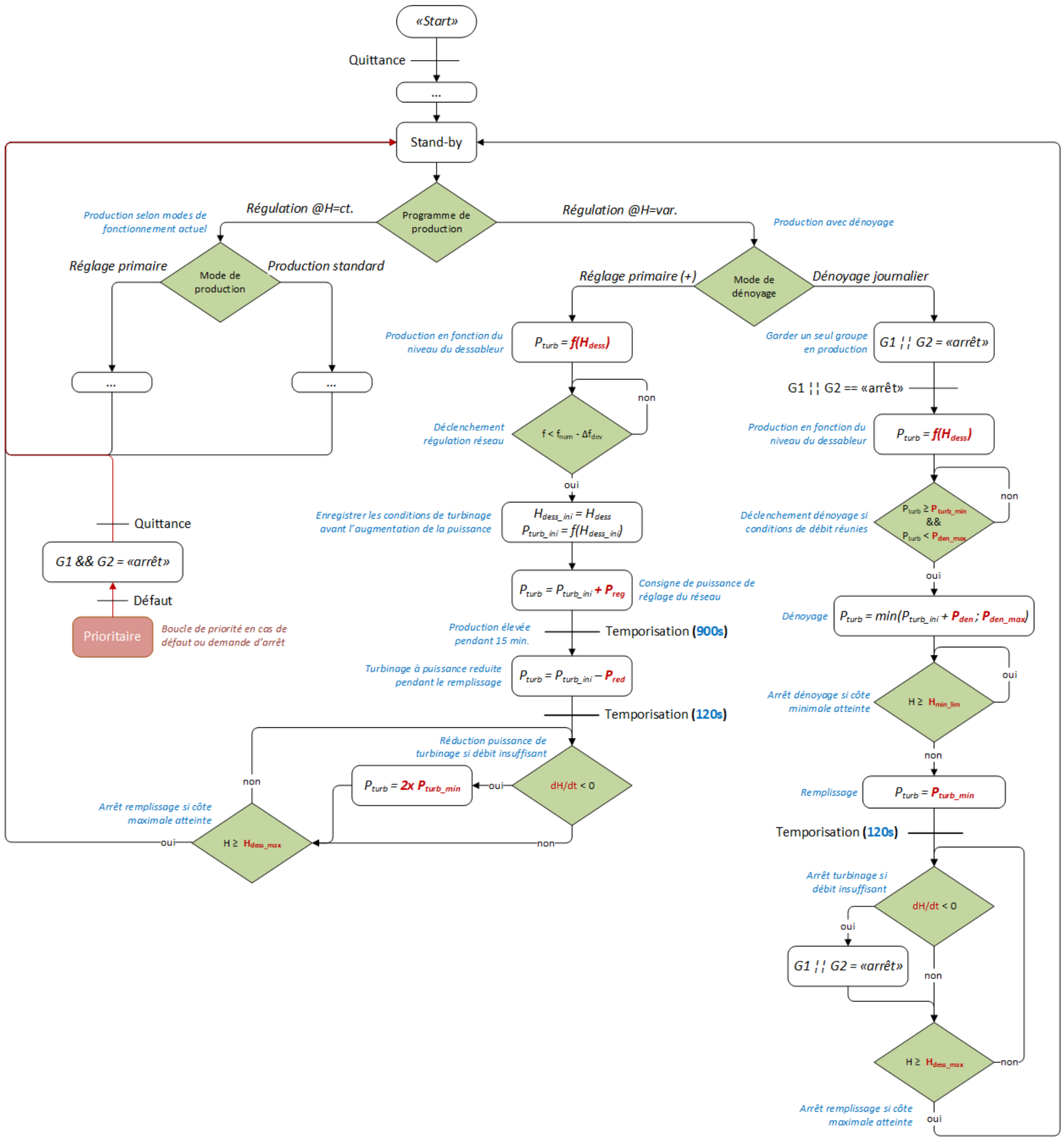

Figure 6: Proposal of a logical scheme for flexible operation with dewatering of KWGO.

The list of input variables necessary to operate the machines with one of these scenarios is provided in Appendix A. Part of these values is already specified based on the results of the previous SmallFLEX Project, 2021. The remaining values are defined considering the results of transient calculations performed by HDE: droop limits, economic considerations, as well as complementary safety limits identified during the implementation or commissioning stages. To ensure safe operation, in parallel with these controlled dewatering conditions, several additional alarms and faults have been defined for the control-command of the power units (see Appendix A). The analysis and implementation of the proposed operating scenarios are ongoing on the operator side, whereas commissioning will follow. A remote monitoring of all key parameters is planned during commissioning by HDE and HES-SO VS to ensure fully operational and safe behaviour of the control-command program for all implemented scenarios.

3.1.3. Water level prediction during dewatering/refiling procedures

The operation of the powerplant with flexible water level beyond the initial specifications (relatively small variation within the limits of the desander and the overflow chamber) requires a redundant survey of the water level over the full range. The direct water level measurement during the dewatering/refilling process, when the water level is below the floor of the overflow chamber by several tens of meters, has not been planned and is not technically an easy task. However, considering the basics of fluid mechanics, the estimation of the upstream water level with a given precision remains feasible. Thus, 15-minutes average data of several dewatering procedures performed during the period February-May 2025 has been recovered and analysed from the control-monitoring system of the powerplant.

In Figure 7, the schematic of the hydropower plant is introduced, along with the main reference levels and variables that governs the flow. At the top, the free surface level is characterized by the level z_0, a velocity C_0 (considered equal with 0) and the static pressure p_0 (equal with the atmospheric pressure). At the powerhouse, the reference plan z_{ref} gives the altimetric position of the two units (G_1 and G_2). Upstream the main valve of each unit, one may consider the $z_{1,2}$ altitude, $C_{1,2}$ discharge velocity and $p_{1,2}$ static pressure, measured with the help of the existing pressure taps, part of the base equipment of the two units. By applying the Bernoulli equation between the two reference points (0-1 and 0-2 respectively), in the case when only one unit operates, the water level can be obtained using the measured static pressure, the discharge velocity as well as the estimated head losses between the upstream (0) and downstream sections (1, 2).

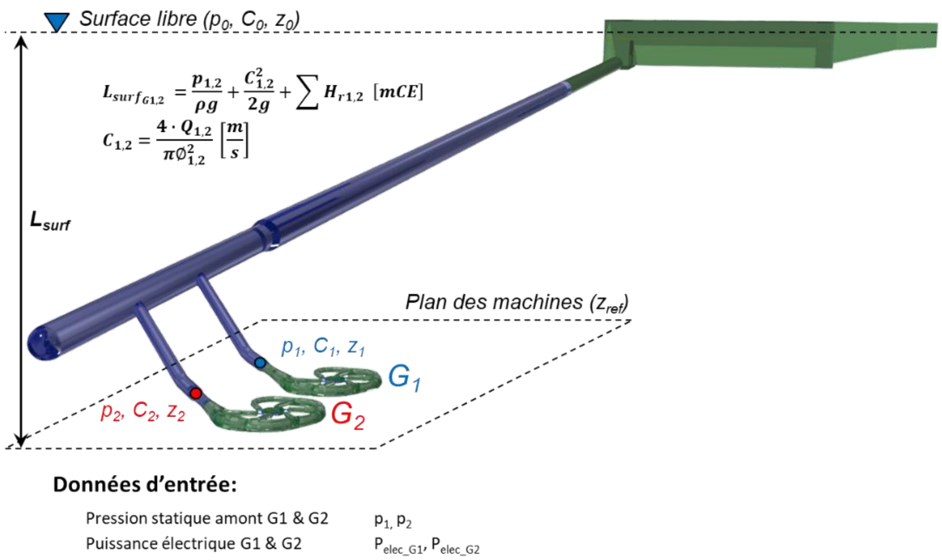

Figure 7: Schematic view of the KWGO hydropower plant and theoretical considerations used to estimate the water surface during dewatering with the help of upper static pressure and electrical power of the two groups.

The powerplant is not equipped with any permanent direct discharge measurement of each group. For regular operating conditions (water level variation only in the range of the desander and the overflow chamber), the discharge is predicted with the help of the injectors' position, pre-calibrated during the design and the commissioning phases. However, this law is not any more valid for large head variations encountered when dewatering the penstock. Anyway, using the results of the previous SmallFLEX project, the discharge can be estimated precisely using a surface fit model, depending on the direct measurements of the upstream static pressure and the electrical power. In Figure 8, two mathematical models for the discharge prediction using the electrical power of the groups at either constant nominal head (left) or with a variable head (right) are provided. Considered as more relevant for large water level variations, the second one is retained to estimate the upstream water level for further analyses.

The variation of the discharge (left) and the dynamic pressure (right) as a function of the electrical power is provided in Figure 9 for each unit. The estimated discharge obtained from both models are compared. The estimation of the dynamic pressure at the upstream of each unit is done with the linear 3D interpolation model since the input data contains values during dewatering phases with large level variations. The maximum dynamic pressure is about 1.3 mWC for the maximum power operating point. The points showing a large deviation from the rest of the values represent the deep dewatering phases present in the considered data set.

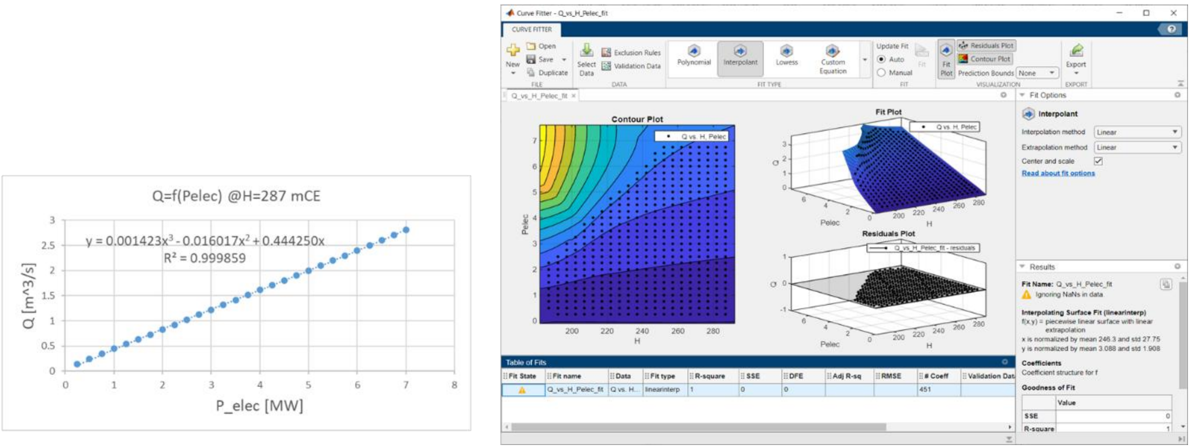

Figure 8: Mathematical model for discharge prediction using the electrical power of the groups: constant nominal head (left) or variable head (right) considerations, using the results of the SmallFLEX project, 2021.

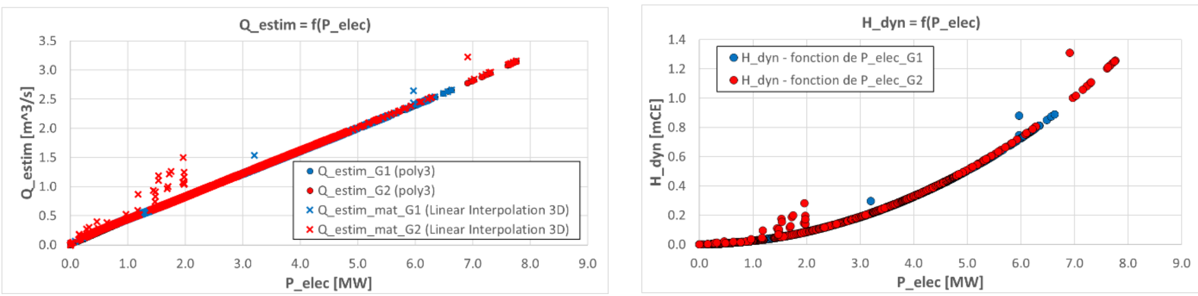

Figure 9: Resulting predicted discharge and dynamic pressure at the upstream of the two groups.

In Figure 10, the obtained static pressure variation upstream of each unit's valve with the estimated flow rate is provided. To assess the relation derived, the values were selected with the adjacent group stopped. The source of the difference between the two static pressure variations, estimated at 1.43 mWC (0.14 bar), is unknown. Anyway, a level difference between the two pressure sensors used for these upstream valve measurements is suspected to be the cause. The points showing large deviations mainly correspond to the deep dewatering phases.

The variation of the head losses with the estimated discharge, obtained from the estimated gross head, the variation of the static pressure, and the variation of the dynamic pressure is provided in Figure 11. Only values with the adjacent group stopped have been selected. The obtained variations allowed extracting one single head loss curve for both groups ($k = 0.06275$ mWC/(m^6/s^2)). The effect of the adjacent unit operation on the head losses has been neglected.

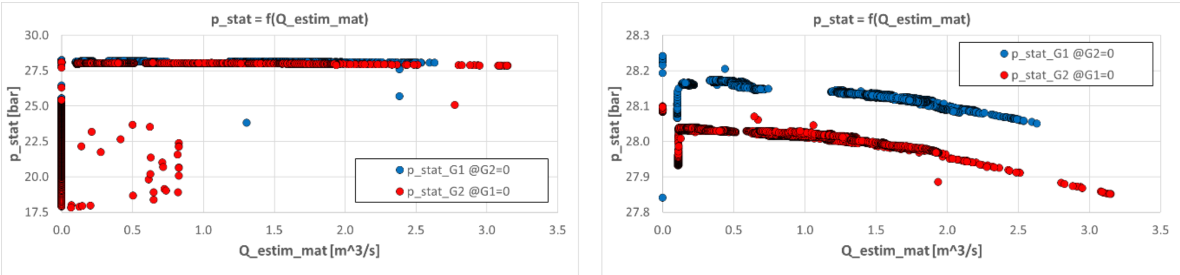

Figure 10: Resulting upper static pressure versus predicted discharge at the upstream of the two groups.

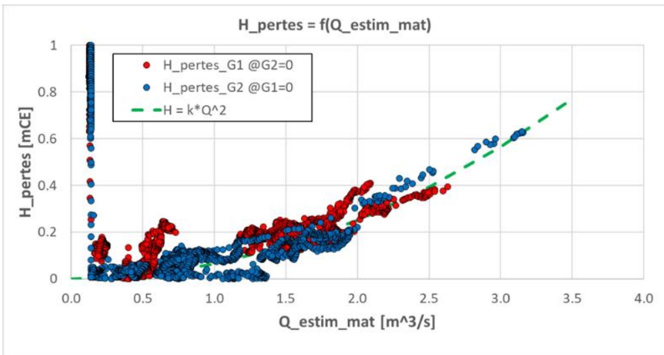

Figure 11: Resulting head losses estimation at the upstream of the two groups.

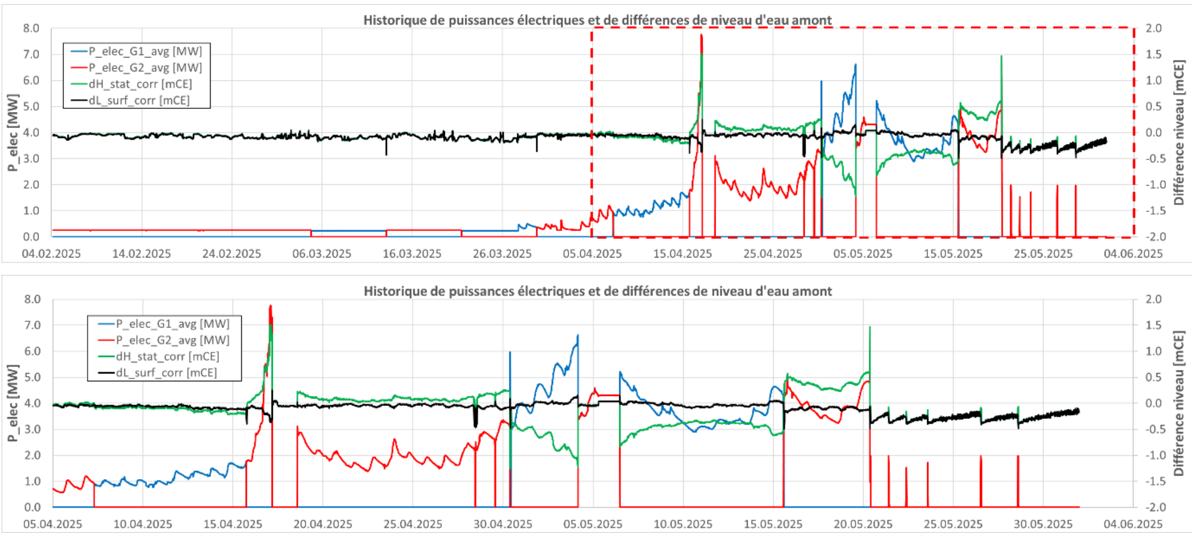

Figure 12: Time-history of electrical power and difference of predicted upper water level using measurements at each group - full available period (top) and zoom on the April 5th-June 4th, 2025, period.

The time-history variation of the electrical power and the upstream water level difference estimated based solely on the static pressure and, again, on the total pressure upstream of each unit is presented in Figure 12. The upper plot shows the results for the whole considered period, whereas the lower plot shows the results from the April 5th to June 4th, 2025, period. The period from February to March is characterised by a very low power operation (values close to the minimum power), whilst values up to around 7.5 MW may be noticed for the unit G_2. Regarding the water level estimation, a difference of ±1.5 mWC is obtained between the two static pressure direct measurements (ignoring the dynamic pressure and losses), whereas the obtained difference drops below ±0.5 mWC when the total pressure is considered, which shows a satisfying precision in terms of redundancy for both safety and regulation control purposes.

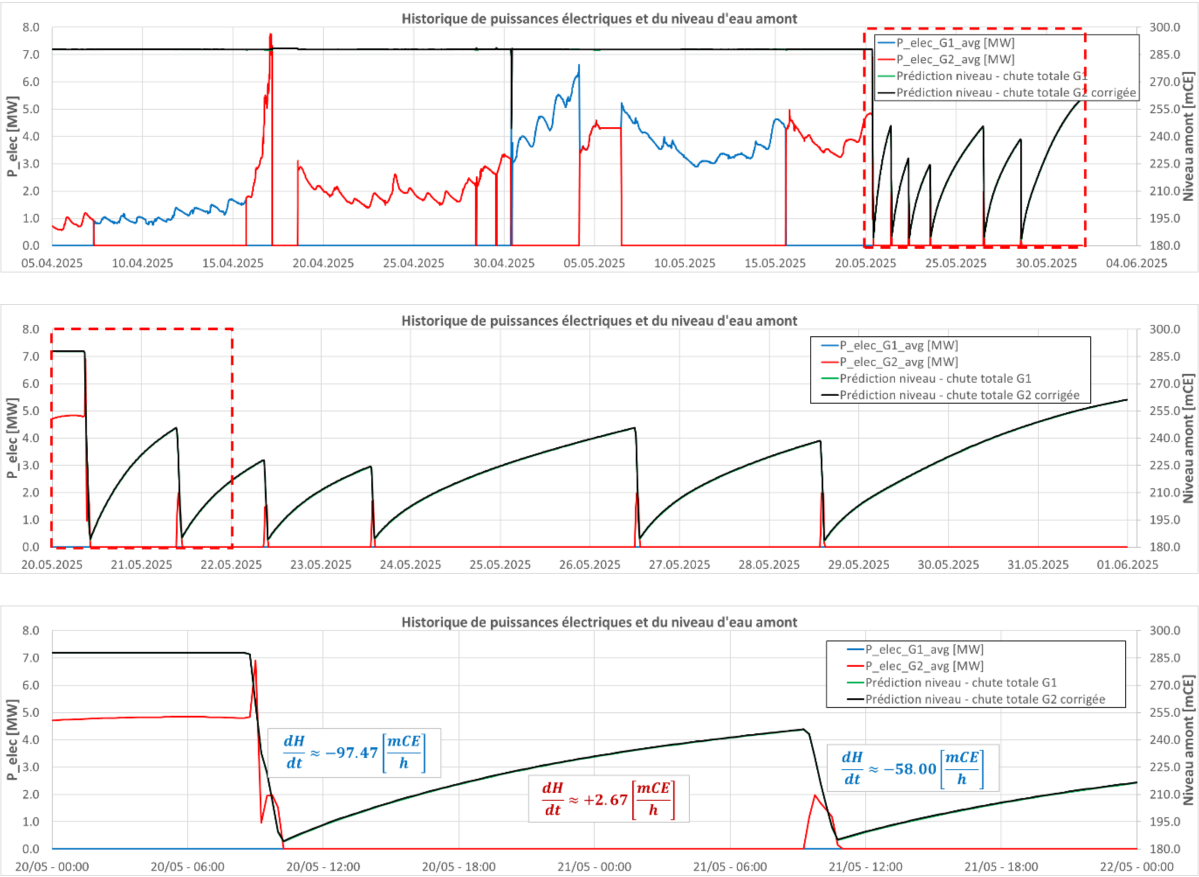

Figure 13: Time-history of electrical power and the predicted upper water level using measurements at each group: 05.04 - 04.06 2025 period (top), zoom on the 20.05 - 01.06 2025 period (middle) and on the 20-22.05 2025 (bottom).

In Figure 13, the time-history variation of the electrical power and the upstream water level estimated from the total pressure upstream of each unit is provided for the period from April 5th to June 4th, 2025 (top), with a zoom on the 05.04 - 01.06 2025 period (middle) and on the 20-22.05 2025 period (bottom). At least six sequences of dewatering followed by refilling of the penstock have been identified during the period from May 20th to June 1st, 2025. The dewatering tests were carried out with only the unit G_2 in operation. The first dewatering was performed on May 20th, 2025, with a maximum turbine output of 7 MW. The following five dewatering sequences were conducted with a turbine output of 2 MW, down to a water level of 190 mWC in the penstock (the limit tested during the previous SmallFLEX project, 2021). This value is beyond the 232 mWC retained as permanent dewatering limit for the future. Dewatering rates of −97.47 mWC/h and −58 mWC/h (a bit larger than the safe limit recommended by the expert for a permanent operation without long-term impact on the penstock) were estimated for the first two sequences, respectively. A refilling rate of 2.67 mWC/h has been estimated for the first refilling phase, which respects largely the value recommended by the expert. The remaining dewatering/refilling phases were not evaluated. The difference between the predicted upstream water level with the help of the estimated upstream total pressure at the unit G_1 and unit G_2 respectively is almost undetectable on the plots. This proves the robustness of the applied methodology to predict the water level and the feasibility of using these two available static pressure sensor measurements as an input for the permanent flexible water level operation of the KWGO.

Finally, a comparison of the upstream water level differences obtained based solely on the static pressure and again on the total pressure upstream of each group, as a function of the total electrical power, and that of each group, is provided in Figure 14.

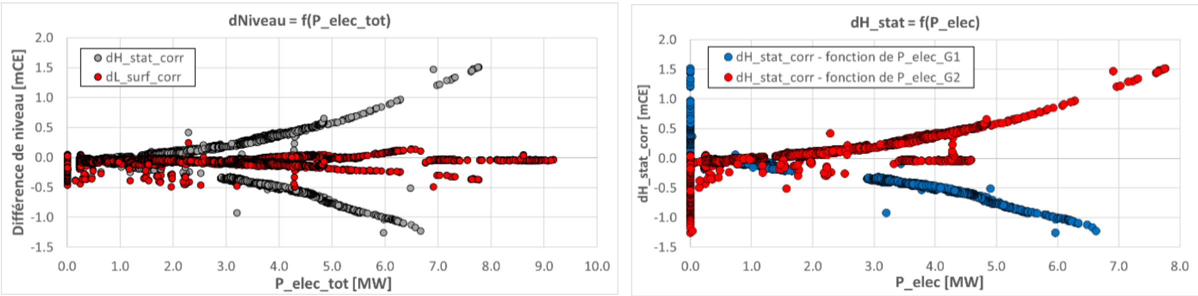

Figure 14: Evaluation of predicted water level using only the static pressure (right) or the total pressure, including the head losses (left) from measurements at each group.

The estimation of the upstream water level based solely on the static pressure shows a deviation of ±1.5 mWC (in addition to the base offset of 1.43 mWC, likely caused by the position of the pressure sensors installed in the powerhouse). When also considering dynamic pressure and head losses (with some approximation), a deviation of only ±0.5 mWC is obtained for the prediction of the upstream water level using the two existing pressure sensors.

This deviation could certainly be further reduced by using the fine-tuned parameters of the HydroClone system of the KWGO. The obtained results indicate a level of accuracy likely sufficient for the redundant use of these sensor signals in the control and monitoring of the plant operation during the dewatering and refilling phases of the upper part of the penstock. The results do not exclude the transient phases present in the analysed data. Anyway, a slight adjustment may still be necessary for the estimation of the upstream water level (considering the exact position of the pressure sensors relative to the machine floor), to cope with the direct water level measurements into the forebay tank and into the desander.

Conclusions and perspectives

The actual instrumentation of the powerplant reveals robust enough to ensure a permanent flexible operating with dewatering, based on pressure static and electrical power measurements as well as turbine discharge and head losses prediction, with a precision of ±0.5 mWC. The addition of an ultrasonic water level measurement at the settling basin would improve the inflow discharge prediction at the overflow chamber.

3.2 WP2 – Selection of promising flexible HPP

Lead: FMV, partners: HEVS, HDE, ETHZ

3.2.1. Description of the HPP fleet

A list of the power plants in the Goms region has been drawn (see Figure 15 for a spatial representation). For each power plant, the owners have been contacted. Some of them do not wish to respond to this request, so the information required to assess the hidden flexibility potential was found in another way and may therefore be incomplete. Table 2 gathers the main known information for each power plant.

Table 2: Main characteristics of the power plants in the Goms region.

Power Plant	H_n [m]	Q_{BEP} [m^3/s]	P [MW]	Winter production	Turbine	Penstock (diameter, length, and slope)
1 KW Altstafel (KW Aegina AG)	417	2.8	9.2	78%	1 x Francis	ø: 700 mm L: 800 m slope: 51%
2 KW Gletsch-Oberwald	287	5.7	14	10%	2 x Pelton	ø: 2800 mm L: 2117 m slope: 13%
3 KW Merezenbach	504	0.5	1.9	27%	1 x Pelton	ø: 450 mm L: 1114 m slope: 45%
4 KW Wannebode (Blinnenwerk AG)	147.5	1.625	2.1	20%	1 x Pelton	ø: 711 mm L: 475 m slope: 39.2%
5 KW Walibach / Grafschaft	772	0.53	2 x 1.8	20%	2 x Pelton	ø: 500 mm L: 3637 m slope: 22%
6a GKW1 / Rappental (Gommerkraftwerke AG)	62	2	0.5 + 0.8	20%	2 x Francis	
6b GKW1 / Neubrigg (Gommerkraftwerke AG)	720	4.5	25	24%	2 x Pelton	ø: 990 mm L: 1826 m slope: 41% (max 61%)
7 GKW2 / Saflisch (Gommerkraftwerke AG)	341	0.5	1.2	32%	1 x Pelton	ø: 500 mm (estimation) L: 1480 m slope: 27%
8 GKW2 / Heiligkreuz (Gommerkraftwerke AG)	680	6.6	3 x 13	16%	3 x Pelton	ø: 1400 mm L: 3100 m slope: 23%
9 GKW3 / Fieschertal (Gommerkraftwerke AG)	509	15	2 x 32	9%	2 x Pelton	ø: 1650 mm L: 1500 m slope: 35% (max 41%)
10 KW Wysswasser (Gommerkraftwerke AG)	37	10	2 x 1.55	20%	2 x Francis	

11 KW Ernen (Rhonewerke AG)	269	14	2 x 16	30%	2 x Francis double	ø: 1850 mm L: 571 m slope: 55% (max 59%)
12 KW Mörel (Rhonewerke AG)	248	24	3x17 + 0.3	29%	3 x Francis double + 1 x Pelton	$ø_1$: 3100 mm L_1: 28 m (estimation) $slope_1$: 85% $ø_2$: 2460 mm L_2: 397 m $slope_2$: 80%
13 KW Aletsch (Aletsch AG)	675	7.5	38	19%	3 x Pelton	
14 KW Massaboden (Bitsch)	44	21.5	2 x 4	31%	2 x Francis doubles	L: 70 m slope: 54%
15 KW Gere (KW Obergoms AG)	244	3	4.6 + 1.5	27%	2 x Pelton	L: 2720 m
16 KW Ulrichen (KW Obergoms AG)	273	1.1	2.3	15%	1 x Pelton	L: 2100 m
17 KW Niderbach (KW Obergoms AG)	653.5	0.15	0.8	15%	1 x Pelton	L: 2200 m
18 KW Münstigertal (KW Obergoms AG)	220	0.1	0.18		1 x Pelton	
19 KW Binn (Rhonewerke AG)	23	1.5	0.25		2 x Francis	
20 KW Bitsch (Electra Massa)	718	55	340	78%	3 x Pelton	slope: 70%

**Blank box indicates that the information is missing.*

Despite the strong diversity of the layout of the plants' hydraulic systems, some common features can be identified. The following main types of waterway design can be distinguished (Figure 15): (1) All water ways are pressurized, (a) without surge tank and (b) with surge tank connecting a gently inclined headrace tunnel to the strongly inclined penstock; (2) The power waterways consist of one or several free surface headrace tunnels and the pressurized penstock (a) without and (b) with surge tank. Figure 15 provides a map of the hydropower plants and indicates the location of the specific parts of their hydraulic system.

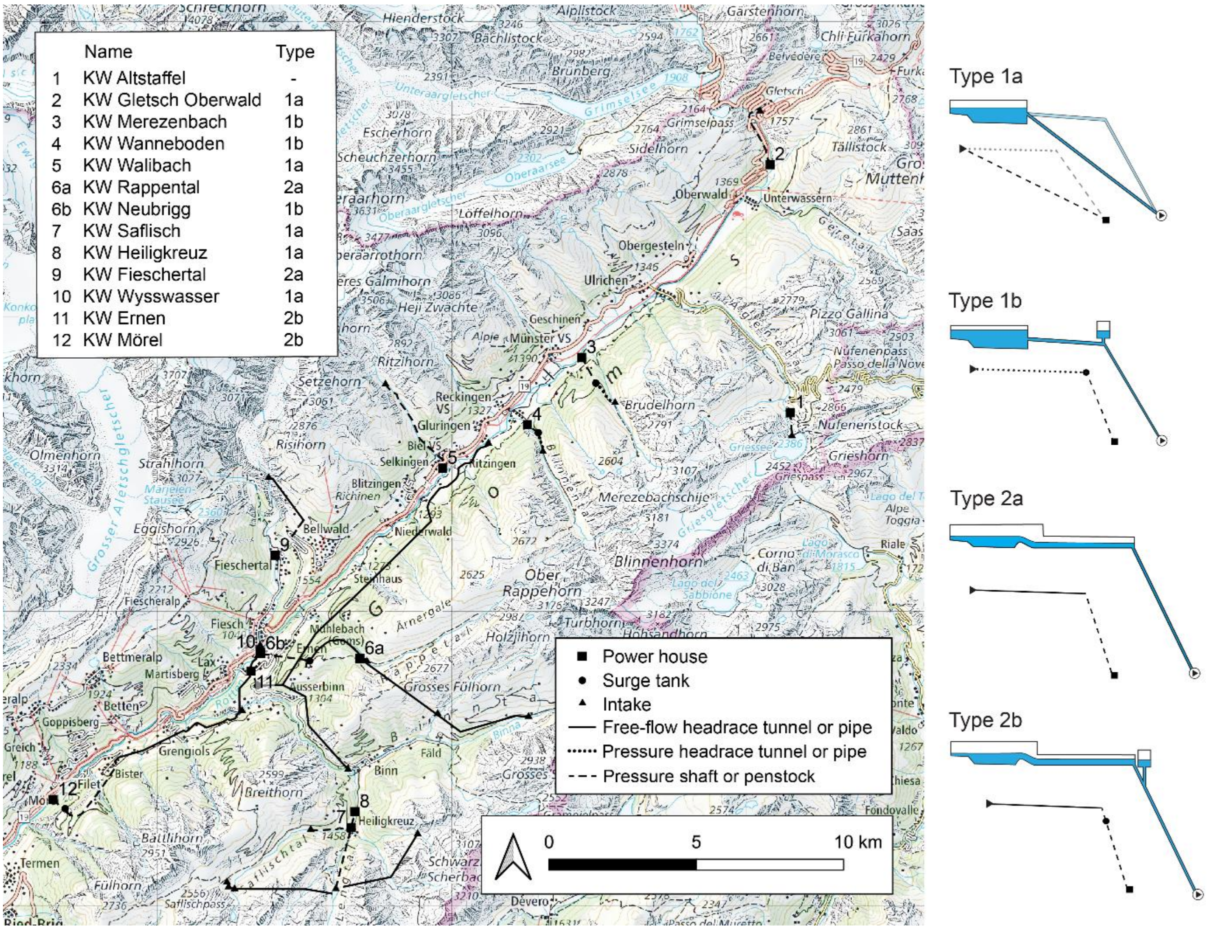

Figure 15: Localization of the HPPs considered in the project and classification of their waterway design. (Map: Federal Office of Topography swisstopo)

3.2.2. Selection of the HPPs

Although it was possible to find information on power plants whose owners do not wish to participate, their interest is of prime importance to be selected as demonstrator for WP6, since their agreement is required to carry out any on-site tests. Figure 16 is a map showing the different sites and the interest of the owners. Over twenty-one power plants, seven (*i.e.*, one third) agreed to share information and will be considered for the final selection of two power plants where on-site measurements will be carried out for WP6.

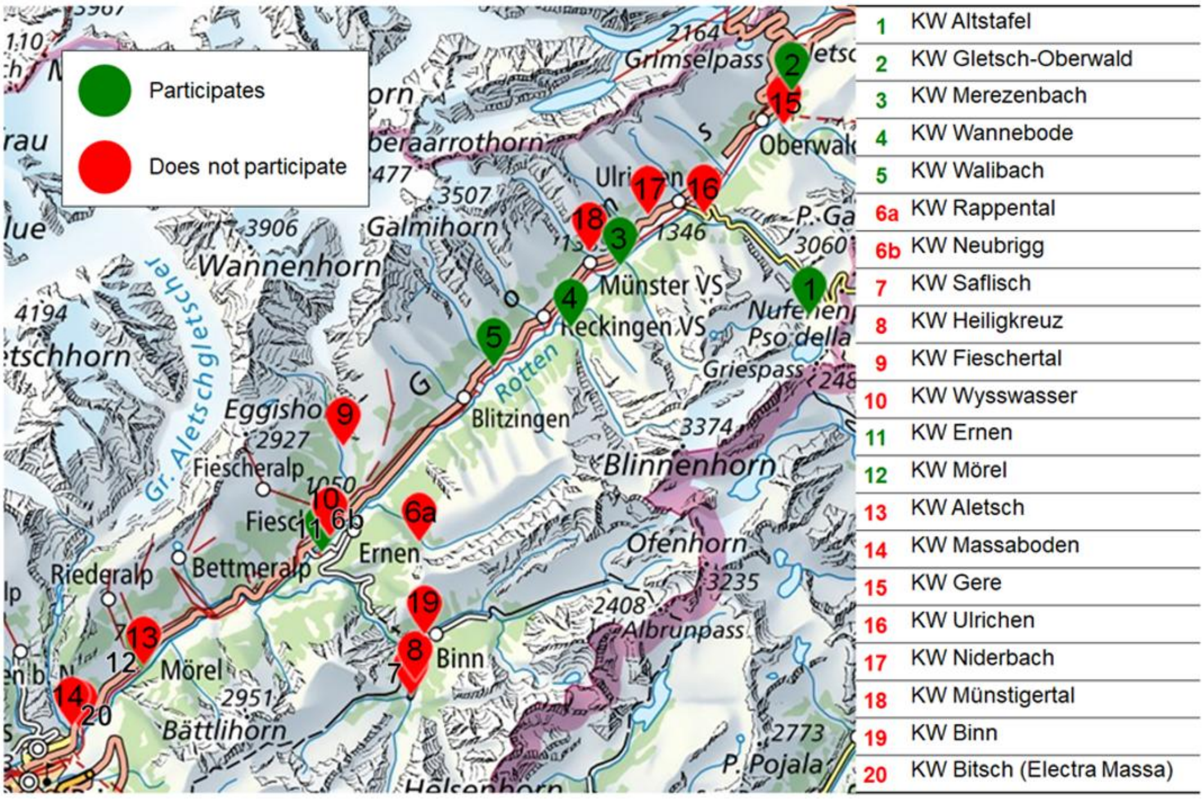

Figure 16: Map of the power plants and whether they intend to participate in the project or not. (Map: Federal Office of Topography swisstopo).

Among the seven power plants, two of them (KW Altstafel[2] and KW Ernen) have storage capacities, therefore they are omitted from the final selection. Consequently, the five remaining power plants are ranked considering five criteria:

- 1. The storage volume.
- 2. The power peak.
- 3. The duration of the power peak.
- 4. The energy produced.
- 5. The risk of air entrainment.

The values of the first four criteria are given in Table 3 for each power plant. Regarding the risk of air entrainment, Figure 17 presents the pipe Froude numbers as a function of the pressure shaft/penstock slope and compares them to the critical pipe Froude number $F_{w,c}$. The pilot plant KWGO, which is characterised by an unusually large pressure shaft diameter relative to its design discharge Q_d, exhibits a value of $F_w = 0.2$, well below all thresholds. In contrast, all other HPPs fall within the scatter band of experimental data or clearly exceed it, implying that even large air pockets would be transported downstream to the turbines. The critical pipe Froude number provides a useful exclusion criterion: if the pipe Froude number in a penstock exceeds $F_{w,c}$, air entrainment must be prevented. However, pipe Froude numbers below the threshold cannot be interpreted as evidence of safe operation, as small air bubbles may still be conveyed downstream. The criterion therefore allows early identification and exclusion of unsuitable cases, but positive confirmation of operational safety requires more detailed hydraulic

[2] KW Alstafel is however considered in the WP7 focusing on the VPP. See a description of the power plant in section 3.2.3.3.

analysis. Based on this evaluation, lowering the water level into the pressure shaft/penstock is not advisable for the investigated HPP fleet, except for the pilot plant KWGO.

Table 3: Assessment of the Energy Flexibility Potential of Hydroelectric Power Plants with Limited Storage Capacity.

	KW Gletsch-Oberwald	KW Merezenbach	KW Wannebode	KW Walibach	KW Mörel
Storage volume (m³)	6 909	1 195	2 811	234	1 076
Power peak (MW)	0.8	0.1	0.1	0.2	3.1
Duration of the power peak (min)	213	398	288	74	7
Energy (MWh)	38	11.5	8	3.5	5

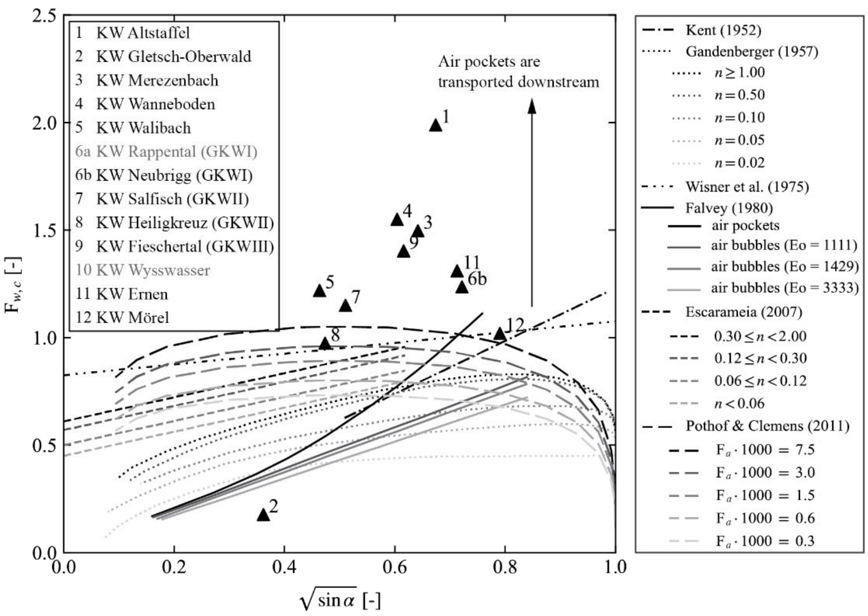

Figure 17: Comparison of different studies on the clearing flow number $F_{c,w}$ of air pockets in pipes, depending on pipe inclination α, dimensionless air velocity F_a or relative air pocket sizes n. For $F_{c,w}$ above the lines, air pockets are cleared from a pipe system, thus the entire air is transported downstream. For the considered plants in the Goms region, $F_{c,w}$ in the penstocks at design discharge Q_d are indicated. Figure from WP5 led by ETHZ.

For each criterion, the hydropower plants are ranked from the best rank, 1, to the worst rank, 5. Then, the sum of rank is calculated. Lower is the sum, better is the flexibility potential.

For the storage volume, the power peak, the duration of the peak and the energy produced, the best rank is for the highest value. For the risk of air entrainment, the best rank corresponds to the lowest clearing flow number (see Figure 17). Table 4 shows the ranking of the hydropower plants for each criterion and the sum. KWGO is the power plant with the highest flexibility potential with a sum of rank equal to 8, followed by KW Merenzenbach with a sum of 14, KW Mörel with a sum of 16, KW Wannebode with a sum of 17 and finally KW Walibach with a sum of 20.

The selection of the hydropower plants for the WP3 and WP6 is based on this ranking. Since KWGOis the topic of the WP1 and has been already studied in the previous SmallFLEX project, **the two selected hydropower plants are KW Merenzenbach and KW Mörel**.

Table 4: Ranking of the potential flexibility by criterion.

	KW Gletsch-Ober-wald	KW Merezenbach	KW Wannebode	KW Walibach	KW Mörel
Storage volume (m3)	1	3	2	5	4
Power peak (MW)	2	4	5	3	1
Duration of the power peak (min)	3	1	2	4	5
Energy (MWh)	1	2	3	5	4
Risk of air entrainment and transport according to ETHZ	1	4	5	3	2
Sum of rank	**8**	**14**	17	20	**16**

3.2.3. Description of the selected HPPs for further investigations

3.2.3.1. KW Mörel

KW Mörel forms the second stage of the *Ernen-Mörel* cascade, which, with an average annual production of more than 400 GWh, makes a significant contribution to the utilization of hydropower in the upper Rhone. The RoR-HPP has been operated by *Rhonewerke AG* since 1943.The plant exploits the *Rhone* River between the confluence of the *Fiescherbach* (elevation about 1000 m a.s.l.) and the water intake of the HPP *Massaboden* in *Mörel* (elevation about 737 m a.s.l.), with a gross head of about 248 m. In total, it uses a catchment area of about 530 km^2. The design discharge of the HPP is Q_d = 24 m³/s. The powerhouse is equipped with three Francis turbines rated at 17 MW each (Figure 18), plus one Pelton turbine rated at 0.3 MW (additional information in Table 5).

Figure 18: View of the three double-Francis units of the Mörel hydropower plant.

Table 5: KW Mörel main characteristics.

Turbine type	Horizontal axis double-Francis turbine
Number of units	3
Number of guide vanes	20
Number of runner blades	15
Gross head	248 m
Nominal discharge	3x 7.93 m^3/s
Nominal rotational speed	750 rpm
Total nominal electrical power	3x 17 MW

The waterways of HPP *Mörel* consist of a free-flow headrace tunnel of approximately 7 km length, followed by a pressurised headrace tunnel of about 3 km, and a 670 m long penstock equipped with a surge tank. Under normal operation, pressurisation occurs in the overflow chamber of *Eggen* (see Figure 19), which is widened in cross-section. Two side weirs in the chamber evacuate excess water (overflow crest on level 985.13 m a.s.l.), while the turbined discharge enters a circular pressurised tunnel (see Figure 19, Figure 62). Upstream of the chamber, the free-flow headrace tunnel has a modified horseshoe profile with a width of 2.8 m. In the region directly upstream of the overflow chamber (km 5.7–6.8), the tunnel slope *S* is first 2.2 ‰ over a length of 0.9 km (km 5.7–6.6), followed by a steeper 4.5 ‰ section over 0.2 km (km 6.6–6.8) leading into the overflow chamber.

The pressurised headrace tunnel was renewed in the 1980s. Downstream of the overflow chamber, the original tunnel extends for 67 m with a slope of 3.6 ‰. This is followed by a 27 m long connecting tunnel with a slope of 85%, which leads into the new pressurised headrace tunnel. The new tunnel extends over approximately 2.8 km with a positive slope of 2.2 ‰. At the junction between the original pressure tunnel and the connecting tunnel, there is a mitre bend with both a change in slope and a horizontal bend of 26° to the left. The crest of the bend lies at *H* = 984.17 m a.s.l. At the transition from the connecting tunnel to the new pressure tunnel, the alignment again combines a slope change with a horizontal bend of 23° to the left. After a total length of about 2.9 km, a connection to the existing surge tank is provided on the right-hand side. The crown of the connecting tunnel (*D* = 2.5 m) aligns flush with the crown of the new pressurised headrace tunnel. Immediately downstream, a valve chamber equipped with a throttle valve connects to the pressure shaft. The pressure shaft has an internal diameter of *D* = 2.5 m and a slope of 80% over a length of 385 m and a slope of 1% over a length of 285 m.

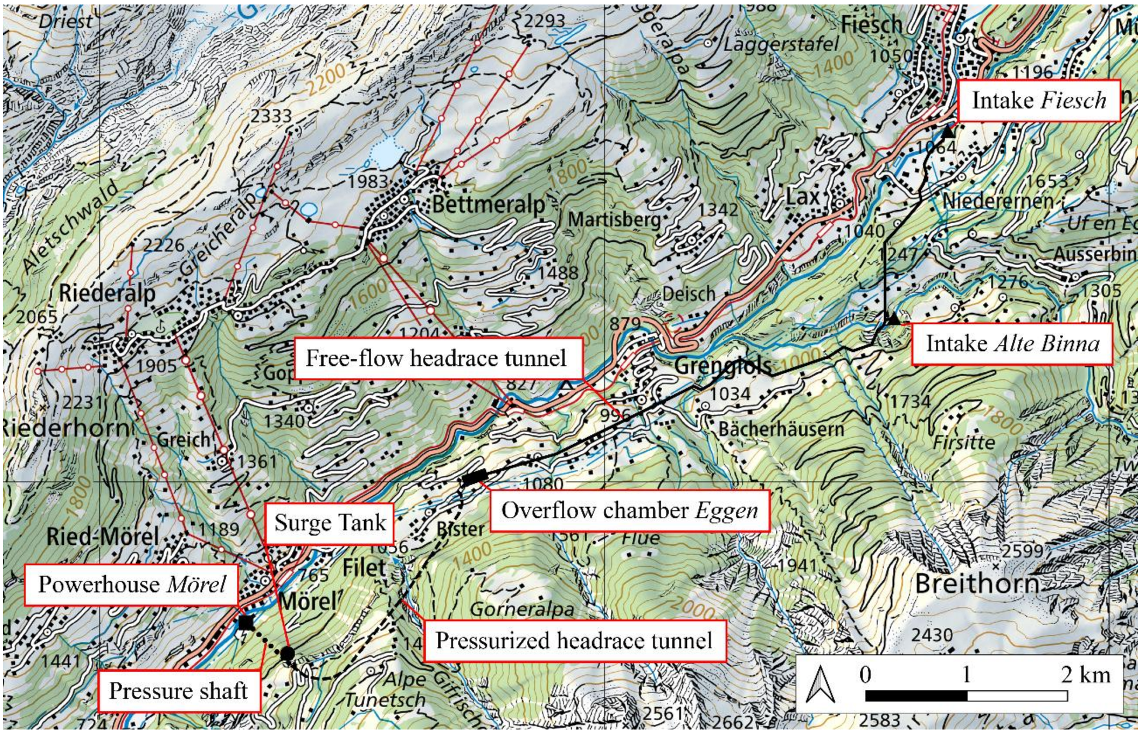

Figure 19: Overview of the HPP Mörel. (Map: Swiss Federal Office of Topography swisstopo)

The crests of the side weirs in the overflow chamber are located at 985.13 m a.s.l., which defines the maximum water level at this location. Under normal operation, the water level in the overflow chamber H_{oc} is regulated at this elevation by turbine control. The corresponding backwater curve extends into the 2.2 ‰ sloped section of the free-flow headrace tunnel.

Figure 20a) illustrates, as an example, the backwater profile for a discharge of Q_{in} = Q_{out} = 5 m^3/s at normal operation with H_{oc} = 985.13 m a.s.l. If, during flexible operation, the outflow discharge is increased (e.g. to Q_{out} = 10 m^3/s), the corresponding backwater curve must be considered. Upstream of

the intersection of the two backwater curves the inflow of Q_{in} = 5 m^3/s is conveyed, while downstream the outflow is Q_{out} = 10 m^3/s. The additional volume required to satisfy the increased outflow is provided by a drawdown of the water level, corresponding to an upstream movement of the intersection. Figure 20a) further illustrates an exemplary end of a flexible operation, with a drawdown of dH_{oc} = 0.5 m.
Figure 20 b) and c) illustrate the available storage volume V as a function of the drawdown height dH_{oc} for different discharge configurations. Note, that this calculation only considers the available storage volume in the free-flow headrace tunnel, so that the available storage volume in the overflow chamber *Eggen* itself and in the surge tank is not considered. In both cases, V approaches a plateau at large dH_{oc}. This behaviour reflects the diminishing backwater effect during drawdown. Once the water level lowering reaches the point where the free-flow headrace tunnel flows at its uniform depth for Q_{in}+dQ, no further drawdown is possible with Q_{out}, thus defining the maximum storage volume of the free-flow headrace tunnel. Figure 20 b) shows results for an inflow of Q_{in} = 5 m^3/s with different discharge increases dQ = Q_{out} − Q_{in}. The available storage volume decreases with larger dQ, because higher discharges correspond to greater uniform flow depths.
Figure 20 c) compares results for different inflows Q_{in} each with an increase of dQ = 1 m^3/s. The available storage volume of the free-flow headrace tunnel, and thus the flexibility potential, decreases with higher inflows for the same reason: larger inflows produce higher uniform flow depths in the tunnel.

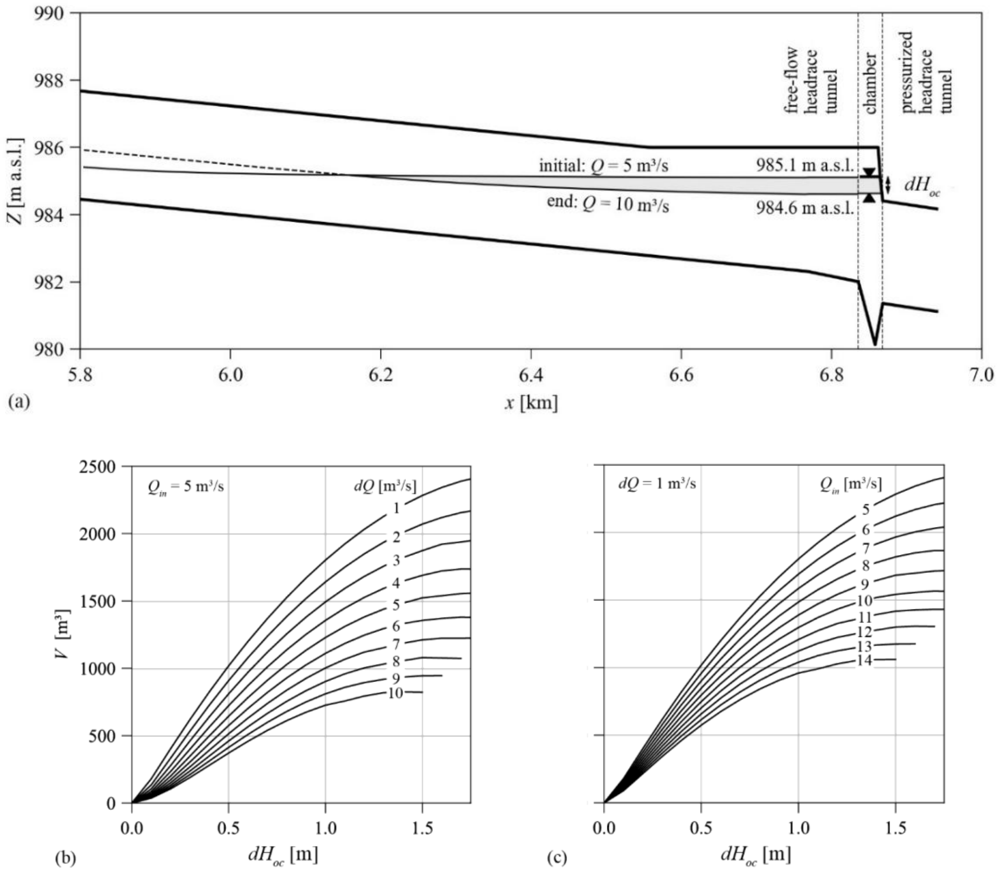

Figure 20: (a) Exemplary backwater curves in the free-flow headrace tunnel of HPP Mörel for different inflow and outflow discharges, illustrating the drawdown of the water level in the overflow chamber during flexible operation. (b), (c) Available storage volume V of the free-flow headrace tunnel as a function of drawdown height dH_{oc} for different discharge configurations.

3.2.3.2. KW Merezenbach

The hydroelectric scheme on the Merezenbach was commissioned in 1959 (Gardet, 1961) and is operated by Elektrizitätswerk Obergoms ewo. All structures are located within the municipality of Münster. The layout of the scheme is shown in Figure 21. The water intake, including a desander, is situated at an elevation of 1840 m a.s.l. From there, the water is conveyed along the left-hand side of the Merezenbach valley via a submerged intake (forebay tank) into a pressure pipeline made of prefabricated centrifugal cement elements with an internal diameter of 0.70 m. The hydraulic roughness of these elements is assumed as k_s = 1.25 mm. The headrace pipe is 1090 m long and connects to a surge tank at an elevation of H = 1 832.10 m a.s.l. The surge tank, with an internal diameter of 1.2 m and a height of 27 m, extends to the upstream end of the penstock. The penstock, with a length of 1 114 m and a diameter of 0.45 m, conveys the water to the power station (Figure 21) located near the left bank of the Rhône River, opposite Münster. A short tailrace channel returns the water to the Rhône. The power plant is equipped with a Pelton turbine (Figure 22), whose characteristics are provided in Table 6. The scheme is classified of type 1b (Figure 15).

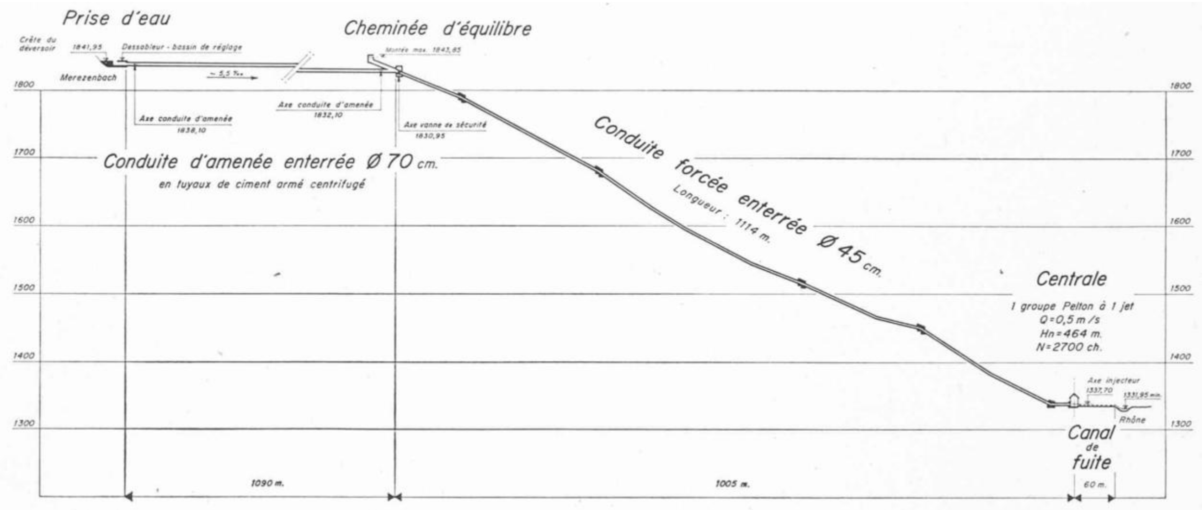

Figure 21: Longitudinal profile of the KW Merezenbach (Gardet, 1961).

Table 6: KW Merezenbach main characteristics.

Turbine type	Horizontal-axis Pelton turbine
Number of injectors	1
Gross head	504 m
Nominal discharge	500 l/s
Nominal rotational speed	1’000 rpm
Nominal electrical power	1’890 kW
Average yearly electrical production	7.5 GWh

Figure 22: Outside and inside views of the KW Merezenbach hydropower plant.

3.2.3.3. KW Altstafel

KW Altstafel, located near the Nufenen pass, is the first hydropower plant in the Maggia cascade, channelling water from the Gries reservoir to the Lake Maggiore in the canton of Ticino. Commissioned in 1959, the plant is owned by Aegina AG, whose shareholders are Officine Idroelettriche della Maggia SA (50%), FMV (35%), and EnAlpin AG (15%). The Gries reservoir lies at 2 386 m above sea level at the foot of the Gries Glacier and has a storage capacity of 18 million m^3. It is retained by a 60 m high gravity dam with a crest length of 400 m. The reservoir provides an energy storage capacity of 88 050 MWh, and the annual production of KW Altstafel is approximately 92 GWh. The power plant is equipped with a 9 MW non-regulated Francis turbine (Figure 23) operating at 1 500 revolutions per minute and benefits from an average head of 384 m. The water is then conveyed through a 13 km tunnel toward Robiei. Near the dam, Gries Wind AG has operated Enercon E-92 wind turbines since 2016 (Figure 24). With an installed capacity of 2.3 MW, the wind farm produces around 10 GWh per year—enough to supply approximately 2 850 households. In addition, the potential deployment of alpine photovoltaic installations near the Gries reservoir is currently being investigated. The coexistence of hydropower, wind energy, and prospective solar production within the same alpine environment makes KW Altstafel an ideal demonstration site for implementing a Virtual Power Plant (VPP), the central focus of WP 7.

Figure 23: non-regulated Francis turbine equipping the power plant of KW Altstafel (source: HES-SO).

Figure 24: Wind turbine near the dam of Gries (source: Wikipedia).

3.3 WP3 – Identification of hydraulic system flexibility limits

Lead: HDE, partners: HEVS, ALPIQ, FMV

The aim of this work package is to perform an extensive hydraulic analysis of the flexibility potential of a selection of promising hydropower plants identified in the WP2, which will serve as a basis for WP6, WP7, WP8 and WP9. The kick-off meeting was successfully held on August 25, 2023, bringing together key collaborators from FMV, Alpiq, HES SO Valais, ETH, HEIG-VD, and WSL. The initial discussions during the kick-off meeting helped shape the project's direction, especially regarding the selection of potential hydropower plants for evaluation. Based on the work carried out in WP2, the HPP of KW Merenzenbach, KW Mörel and KW Altstafel were selected to carry out a more detailed assessment of the flexibility potential of these plants.

3.3.1. Site visits

A task of this work package involves conducting technical site visits to the selected plants, see Figure 25, to provide valuable insights into the operational aspects and general layout, which is a fundamental step in the evaluation process. The site visit at the KW Merezenbach hydropower plant took place on the 24th of June 2024, and the visit of KW Altstafel took place on the next day, the 25th of June 2024. The visit at the KW Mörel hydropower plant took place on the 17th of July 2024. FMV managed and coordinated the scheduling of these visits, ensuring efficient organization. The site visits enabled strong collaboration among the project's various partners.

Figure 25: Photos of the SmallFLEX Goms team during the visits of KW Merezenbach and KW Mörel in June and July 2024.

3.3.2. 1D Modelling

After the selection and data collection of the different hydropower plants included in the study, a detailed modelling phase was carried out to determine the new storage capacities in terms of both volume and energy. To achieve this, each plant was accurately modelled using the SIMSEN software, allowing for a comprehensive analysis of their dynamic behavior and performance under various operating conditions. Full 1D-models of the KW Mörel, Altstafel and Merezenbach power plants were developed using the SIMSEN software, based on available detailed drawings and data. These models are illustrated in Figure 26, Figure 27 and Figure 28.

The modelling approach was based on a detailed representation of the hydraulic system components. The upstream reservoirs, headrace galleries, forebay tanks and penstocks were modelled using one-dimensional hydraulic elements to capture the unsteady flow dynamics. The turbines were represented by their four-quadrant characteristic to account for their complete operating range, including runaway modes. The tailrace tunnels and downstream reservoirs were also included to ensure realistic boundary conditions and an accurate simulation of the overall hydraulic transients.

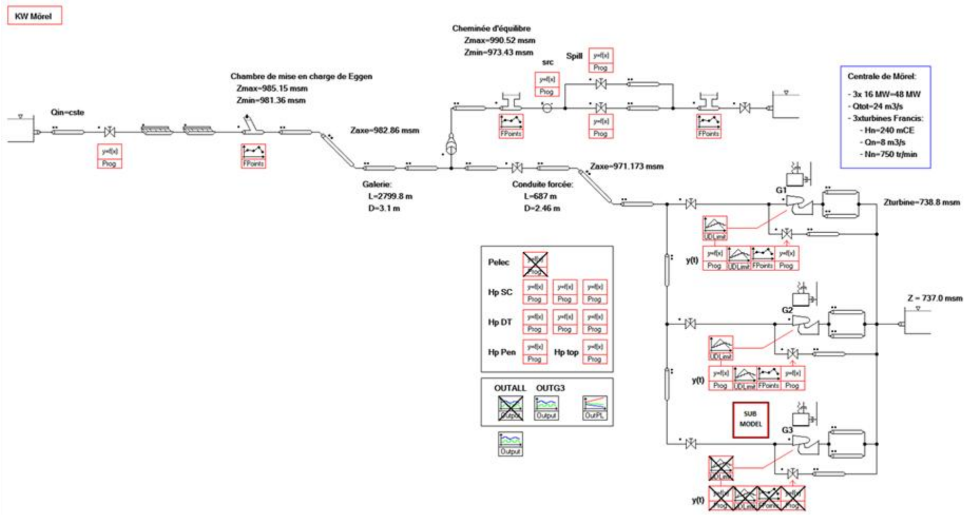

Figure 26: SIMSEN model of KW Mörel.

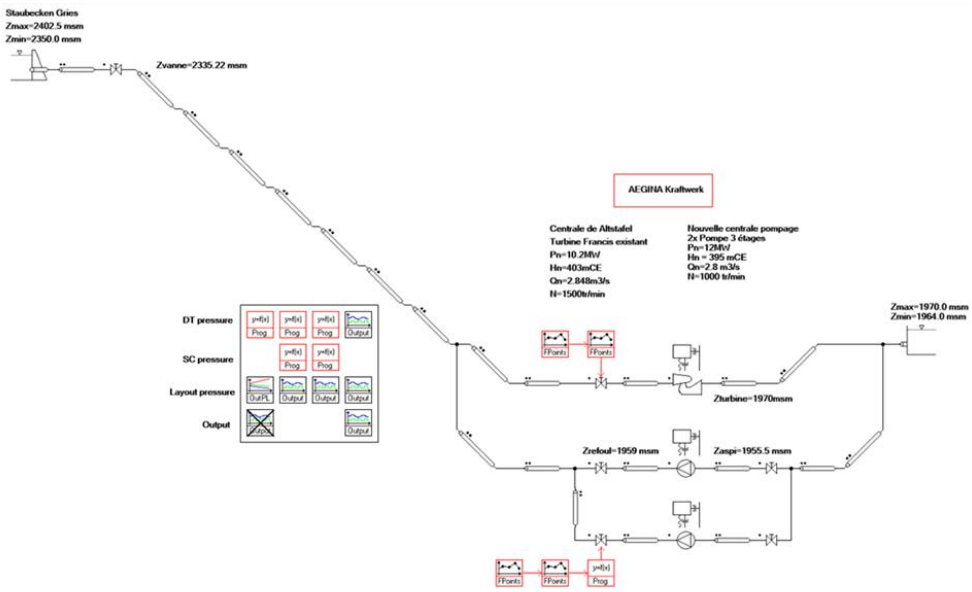

Figure 27: SIMSEN model of KW Altstafel.

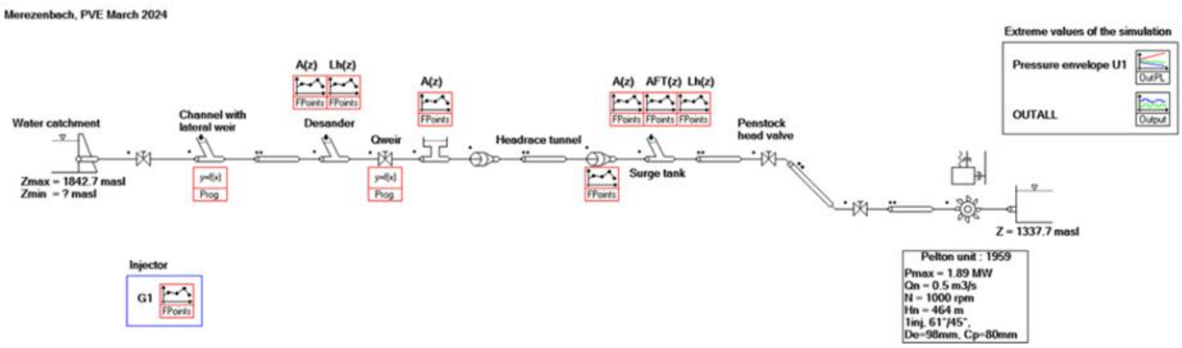

Figure 28: SIMSEN model of KW Merezenbach.

The validation of the SIMSEN models was carried out using time series measured during on-site tests, such as emergency shutdowns and quick shutdowns of the generating units for the different SIMSEN models. The comparison between measured data and simulation results makes it possible to validate the numerical model and to rely on it confidently for subsequent studies.

The Mörel SIMSEN model was calibrated and validated based on two main on-site tests: an emergency shutdown of a single unit at Pmax (17 MW), and a simultaneous emergency shutdown of three units at reduced power (5 MW). These transient sequences made it possible to validate the transient behavior of the turbine unit, including the pressure relief valve and the unit inertia, as well as the dynamic response in the differential surge tank equipped with check valves.

Figure 26 and Figure 27 illustrate the comparison of pressures at the base of the penstock between measurements and simulations for both tests. A good agreement can be observed between the two. The water hammer phenomenon shows excellent consistency between measured and simulated results. The first pressure peak is very well reproduced, as is the initial phase of the mass oscillation. The small pressure discrepancies in the three-unit test result from assuming identical PRVs across all units, although data were only available for Unit 3.

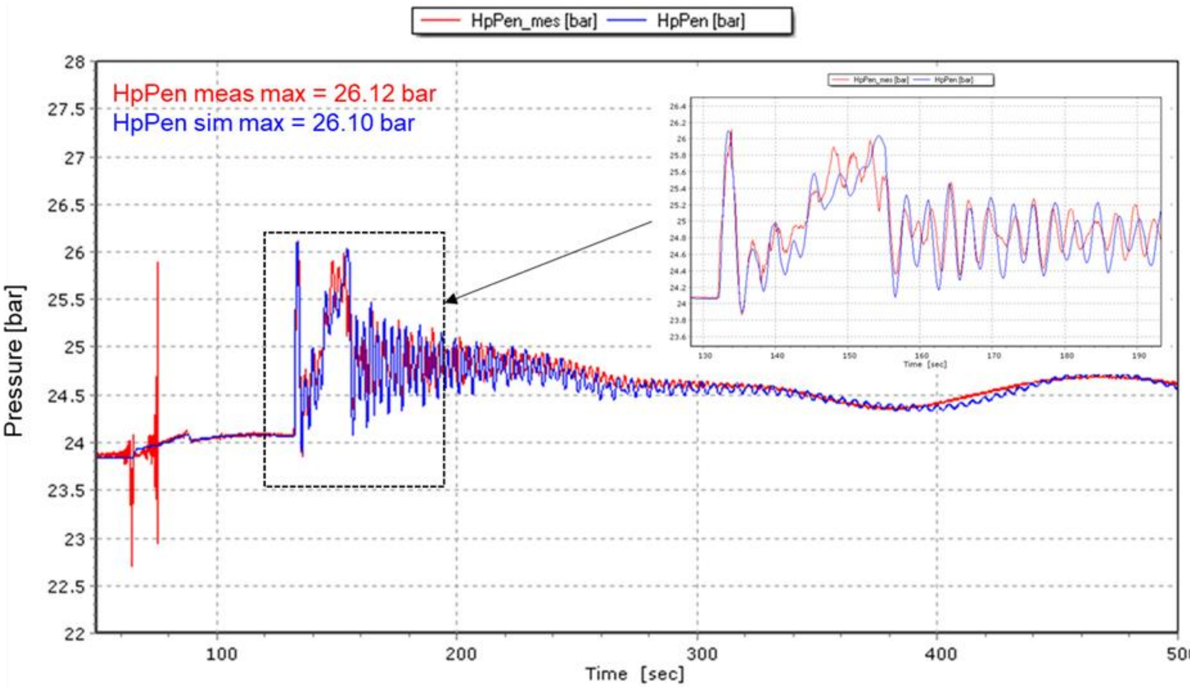

Figure 26: Comparison between measured (red) and simulated (blue) pressure in the penstock during the on-site test: emergency shutdown (ESD) of a single unit at 17 MW.

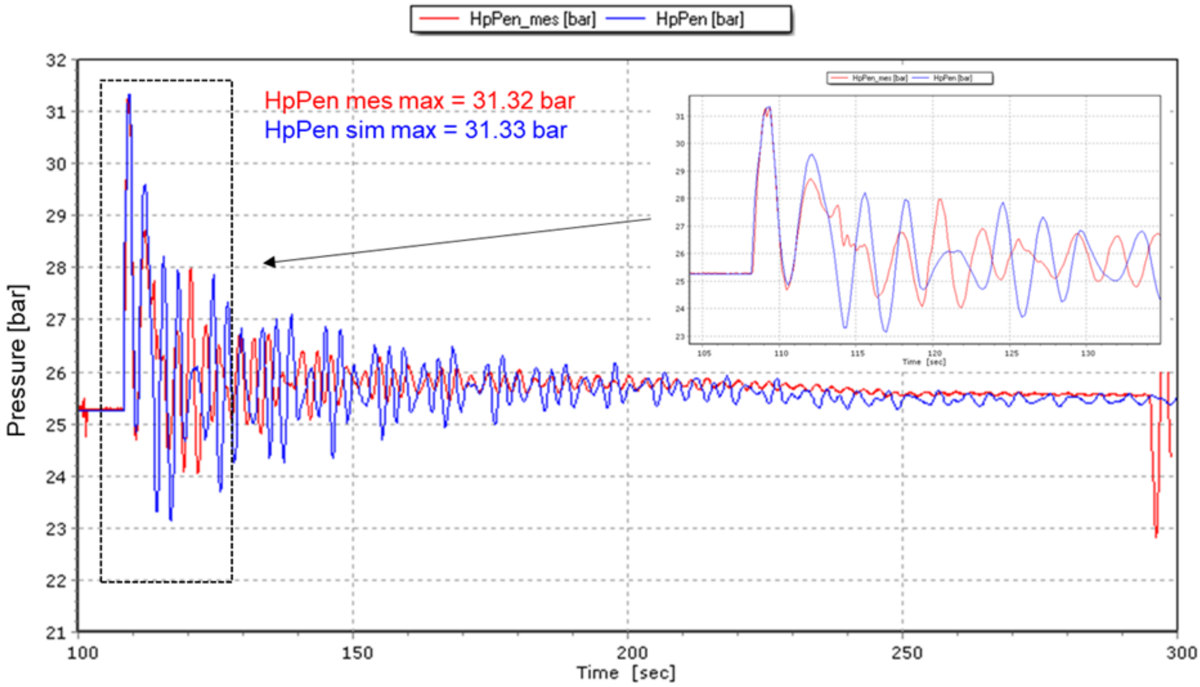

Figure 27: Comparison between measured (red) and simulated (blue) pressure in the penstock during the on-site test: emergency shutdown (ESD) of three units at 5 MW.

Once the models were established and validated, they allowed the investigation of transient phenomena, for instance during turbine or pump emergency shutdowns or primary control regulations. Concerning KW Mörel, the partner ETHZ calculated the water level in the Eggen loading chamber for different inflow (at the Eggen overflow chamber) and turbined discharges. The SIMSEN model was used to simulate emergency shutdowns for each calculated setpoint. The transient behavior during an emergency shutdown for the case where Q=24 m^3/s, both inflow and turbined flow, is show in Figure 29. Mass oscillations are observed in the headrace gallery, the Eggen overflow chamber, and the surge tank. No critical effects are detected under this specific load condition using 1D hydraulic transient model.

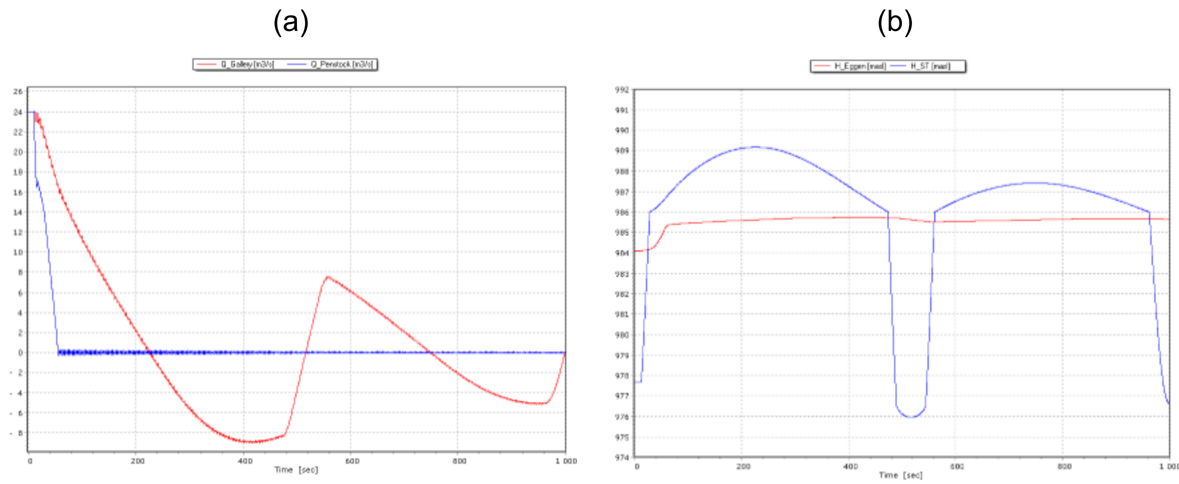

Figure 29: Simulated transient behaviour of discharges (a) in the headrace tunnel (red) and penstock (blue) and water levels (b) in the Eggen overflow chamber (red) and surge tank (blue) in the case of an ESD at Q=24 m^3/s at the Mörel hydropower station.

After collecting data for the selected plants, the new storage capacity of the selected HPP was assessed in terms of both volume and energy. Then a detailed calculation of the available storage volumes and corresponding energy potential was performed for the Merezenbach and Mörel HPP. These values were subsequently compared with the primary frequency regulation requirements of the units, according to the Swissgrid criteria, expressed as $\Delta P = P_n / B_s \cdot \Delta f / f_n$. The following Table 7 summarizes the available storage volumes and the corresponding regulation capacities derived from these calculations and from the geometric layout of the different components, such as the headrace tunnel, penstock, forebay tank and surge tank.

For the Merezenbach HPP, the required power regulation of 0.19 MW over 15 minutes (900s at 48.6 l/s equal 44 m^3 of additional turbined water) can be easily achieved using approximately 10% of the headrace tunnel available volume. In contrast, the surge tank alone cannot provide the full amount of energy required, supplying only about 67% of it. The combination of the desander and the pressurised chamber, however, offers sufficient storage capacity to perform the required primary regulation, corresponding to about 158% of the required energy.

For the Mörel power plant, the regulation can be performed for both single-units and two-units operation modes, corresponding to a total power regulation of 2 and 3 MW, and 4 and 6 MW respectively. These cases reflect different permanent droop (B_s) settings applied in the unit governor, which results in different power step responses. Specifically, droop values of 4% and 2.67% were considered for the respective power steps of 2MW et 3MW. For the single-unit operation, the Eggen overflow chamber provides sufficient energy for the required primary regulation, corresponding to 130% of the energy demand. The surge tank alone is also capable of covering the primary regulation requirement, with an approximately 392% of energy required.

However, under two-unit operation, the Eggen overflow chamber no longer appears sufficient to supply the total energy required for primary regulation, providing only 75% for the 2 MW per unit case and 43% for the 3 MW per unit case. In this configuration, the surge tank volume remains sufficient to supply the required energy for a 15-minutes regulation period. The dewatering of the Eggen overflow chamber appears to be a critical aspect, as discussed in WP5. Therefore, the use of the surge tank located downstream of the Eggen overflow chamber, beyond the siphon section, does not seem to be of practical interest.

Table 7: Assessment of new storage capacity of the selected HPPs in terms of volume and energy, according to the primary regulation requirements and geometric layout.

	Storage and Energy Capacity			Primary Control Requirements			
	Volume available [m3]	Energy available [MWh]	Contribution to energy demand (%)	Power regulation dP [MW]	Discharge regulation dQ [m3/s]	Energy requirement [MWh]	Volume requirement [m3]
Merezenbach - 1 unit operation							
Headrace tunnel (Qin=0m3/s)	417.8	0.45	956.4%				
Surge tank (Qin=0m3/s)	29.3	0.03	67.1%	0.19	0.0485	0.048	43.7
Desander + pressurised chamber (Qin=0m3/s)	69.1	0.08	158.2%				
KW Mörel - 1 unit operation							
Eggen forebay tank (Qin=0m3/s)	1076.0	0.65	130.0%				
Eggen forebay tank (VAW - Qin=5m3/s)	**1400.0**	**0.85**	169.1%	2.00	**0.920**	0.50	828.0
Surge tank	3250.0	1.96	392.5%				
Eggen forebay tank (Qin=0m3/s)	1076.0	0.63	84.2%				
Eggen forebay tank (WAV - Qin=5m3/s)	**1350.0**	**0.79**	105.6%	3.00	**1.420**	0.75	1278.0
Surge tank (Qin=0m3/s)	3250.0	1.91	254.3%				
KW Mörel - 2 unit operation							
Eggen forebay tank (Qin=0m3/s)	1076.0	0.65	65.0%				
Eggen forebay tank (WAV - Qin=5m3/s)	**1250.0**	**0.75**	75.5%	4.00	**1.840**	1.00	1656.0
Surge tank (Qin=0m3/s)	3250.0	1.96	196.3%				
Eggen forebay tank (Qin=0m3/s)	1076.0	0.63	42.1%				
Eggen forebay tank (WAV - Qin=5m3/s)	**1100.0**	**0.65**	43.0%	6.00	**2.840**	1.50	2556.0
Surge tank (Qin=0m3/s)	3250.0	1.91	127.2%				

Simulations of the ancillary services at the Mörel plant, performed using a 1D SIMSEN model, showed that the primary response to a 200 Hz frequency drop, with one or two units in service, fulfils with the 30 second response profile required by Swissgrid for power steps of 1 MW, 2 MW, and 3 MW per unit. The delay before the Eggen overflow chamber begins to empty is well above 900 s for power steps of 1 MW, 2 MW, and 3 MW, assuming inflows in the chamber of 5 m³/s and 8 m³/s. For larger power steps of 6 MW, the primary response leads to the Eggen chamber emptying below 984 m altitude, when considering the free-surface model of the upper tunnel. Additionally, under this scenario, the model predicts a supercritical flow condition (Fr > 1), implying a risk of a hydraulic jump. In summary, primary regulation for power steps of 1 MW to 3 MW per unit appears to comply with normal safe operating conditions. On-site tests to validate these simulations were conducted and are presented in WP6.

Table 8: Results of the 1D simulation of new storage capacity of the selected HPPs, in terms of volume and energy, according to the primary regulation requirements and geometric layout.

	Initial steady state values						After 900s (primary regulation requirements)								
	PG1	PG2	PG3	H Eggen	HST	Qtot in	dP	dQ	H Eggen min	dH Eggen	Hst max	Hst min	V inflow	V ouflow	dV Eggen
Scenario	[MW]	[MW]	[MW]	[masl]	[masl]	[m3/s]	[MW]	[m3/s]	[masl]	[m]	[masl]	[masl]	[m3]	[m3]	[m3]
REG01 - 1MW - Qin=5m3/s	0.0	0.0	10.8	984.9	984.6	5.0	1.0	0.43	984.7	0.16	985.1	983.8	5 098	5 124	26.0
REG02 - 2MW - Qin=5m3/s	0.0	0.0	10.8	984.9	984.6	5.0	2.0	0.99	984.4	0.41	985.7	982.9	5 556	5 621	65.4
REG03 - 3MW - Qin=5m3/s	0.0	0.0	10.8	984.9	984.6	5.0	3.0	1.66	984.1	0.75	986.6	981.6	6 073	6 212	138.6
REG04 - 1MW - Qin=8m3/s	0.0	6.0	10.8	984.9	984.2	8.0	1.0	0.43	984.7	0.19	984.6	983.4	7 952	7 982	30.1
REG05 - 2MW - Qin=8m3/s	0.0	6.0	10.8	984.9	984.2	8.0	2.0	0.86	984.4	0.42	984.9	982.6	8 297	8 365	67.6
REG06 - 3MW - Qin=8m3/s	0.0	6.0	10.8	984.9	984.2	8.0	3.0	1.31	984.2	0.69	985.4	981.8	8 633	8 757	124.2
REG07 - 4MW - Qin=10m3/s	0.0	10.8	10.7	984.9	984.0	10.0	4.0	1.83	984.1	0.79	985.5	980.8	10 939	11 097	158.0
REG08 - 6MW - Qin=10m3/s	*0.0*	*10.8*	*10.7*	*984.9*	*984.0*	*10.0*	*6.0*	*2.78*	*983.7*	*1.16*	*986.5*	*978.7*	*8 846*	*9 121*	*274.2*

Hydraulic transients were also simulated using the SIMSEN model of KW Merezenbach. The model was adapted to simulate hydraulic transients involving potential dewatering of the headrace tunnel and penstock. An open-channel flow model was implemented, capable of accurately representing free-surface conditions and transitions between pressurized and non-pressurized flow regimes. This approach allows to consider the storage capacity of the headrace tunnel of the power plant.

The Figure 30 (a-b) and Figure 31 (a-b) show the transient behavior during the response to a frequency drop followed by an emergency shutdown. The primary response corresponds to a frequency drop of Δf=200mHz, with a permanent droop of Bs=4%, resulting in a power variation of ΔP=0.19MW while the operating base power is 1.7 MW. The emergency shutdown occurs at different times corresponding to when the headrace tunnel is 25%, 50%, and 75% dewatered. The maximum pressure and maximum overspeed remain within the guaranteed limits and do not appear to be critical. Specifically, the maximum allowable overspeed is 1900 min^{-1} and the maximum pressure is 550 mWC. The simulation results show a maximum overspeed of 1708 min^{-1} and a maximum pressure of 512 mWC, both safely below the limits. As said earlier, the volume required to maintain the primary response for the minimum required duration of 900s corresponds to approximately 10% of the headrace tunnel volume.

(a)

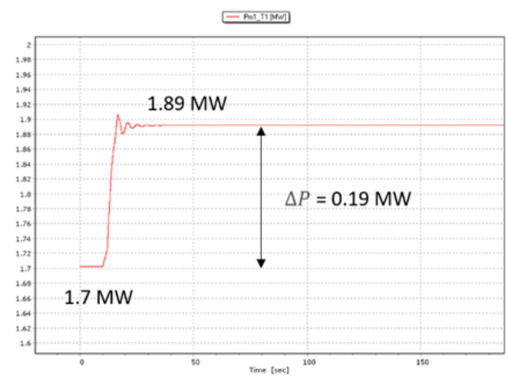

(b)

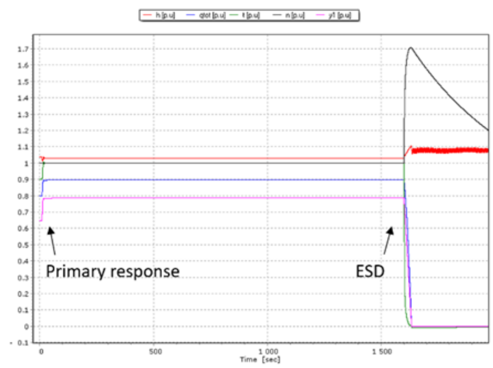

Figure 30: Simulated transient behaviour of (a) power and (b) unitary head, discharge, torque, speed and injector opening of the Pelton turbine in the case of a response to a frequency drop followed by an emergency shutdown at the Merezenbach hydropower station.

The Figure 31 (a) illustrates the time evolution of the water level in the headrace tunnel during Pelton turbine operation with an inflow equal to the turbine discharge of 0.4 m3/s, showing both the dewatering process and the use of the headrace tunnel storage capacity.

The Figure 31 (b) shows that the water level in the surge tank drops rapidly below the minimum admissible level after 10s for all scenarios. This minimum allowable limit is defined for normal conditions, however, in the case of dewatering, it is of limited relevance, as it cannot be met under all circumstances. But, in the case of 75% dewatering, the minimum level approaches the elevation of the surge tank diaphragm. This means that the surface of the water is so low that it is close to the connection between the headrace tunnel and the penstock. This indicates a risk of free surface vortex development in the surge tank, which could lead to air entrainment. Limiting the used volume of the headrace tunnel to 75% could help mitigate the risk of free-surface vortex formation in the surge tank. As reference, the surge tank weir is at 1844.7 m a.s.l., the diaphragm at 1832.1 m a.s.l., and the minimum and maximum allowable level are between 1834.5 m a.s.l. and 1843.85 m a.s.l. (representing 20% of the total volume).

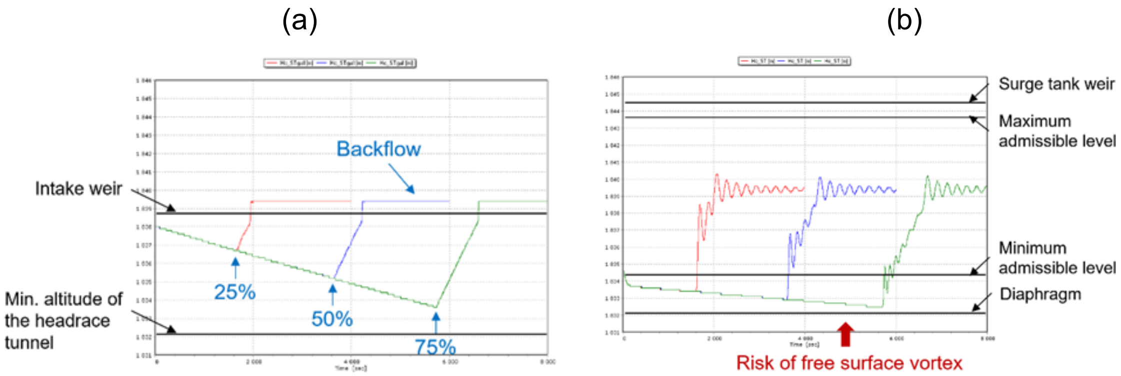

Figure 31: Simulated transient water levels (a) in the SIMSEN element modelling the loading chamber and headrace tunnel and (b) in the surge tank in the case of a response to a frequency drop followed by an emergency shutdown at the Merezenbach hydropower station, for dewatering levels of 25% (red), 50% (blue) and 75% (green) of the headrace tunnel.

3.3.3.CFD simulations

One of the objectives of WP3 is to carry out an initial evaluation of the risk of air entrainment in the selected powerplants. WP5 is fully dedicated to this topic and will conduct comprehensive evaluations of this risk. The following paragraphs describe the exploration of this issue through 3D CFD simulations, and final conclusions on the risk of air entrainment will be made in the WP5 (sect. 3.5.4).

Regarding the risk of air entrainment during the dewatering of the Merezenbach head race pipe, the simulation of the flow has been carried out by HEVS using Ansys® Fluent® on a domain including the forebay tank, the head race pipe (shortened in order to reduce the computational cost), the surge tank and the upper part of the penstock (see Figure 32). During the first 100 seconds, the discharge at the intake is set to 100 l/s and the water level to 1930.845 m a.s.l., and the discharge at the outlet of the penstock is set to 500 l/s. Consequently, the head race pipe dewaters as well as the upper part of the penstock. The free surface observed at the junction (see Figure 33) suggest a risk of air entrainment, which is critical for the safety operation of the Pelton turbine. Then, during the next 350 seconds, the outlet is closed, mimicking an emergency shutdown. Therefore, a wave goes back to the intake, and the pipes re-fill in water progressively. After 450 seconds, it is observed that a thin sheet of air is still present at the top of the head race pipe (see Figure 34). This feature suggests that some air is trapped in the pipe, which could be risky for the operation of the power plant.

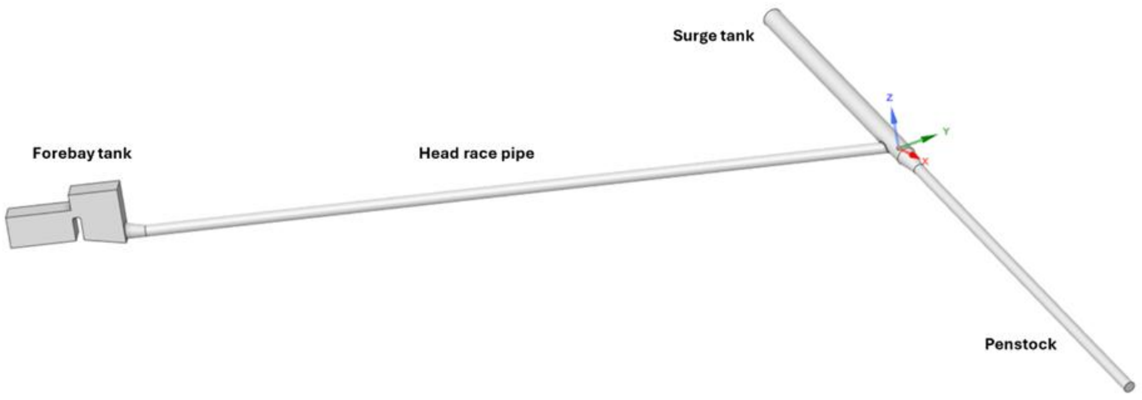

Figure 32: Computational domain considered for the simulation of the flow in the pipes during a dewatering event. The length of the head race pipe is shortened compared to the real length

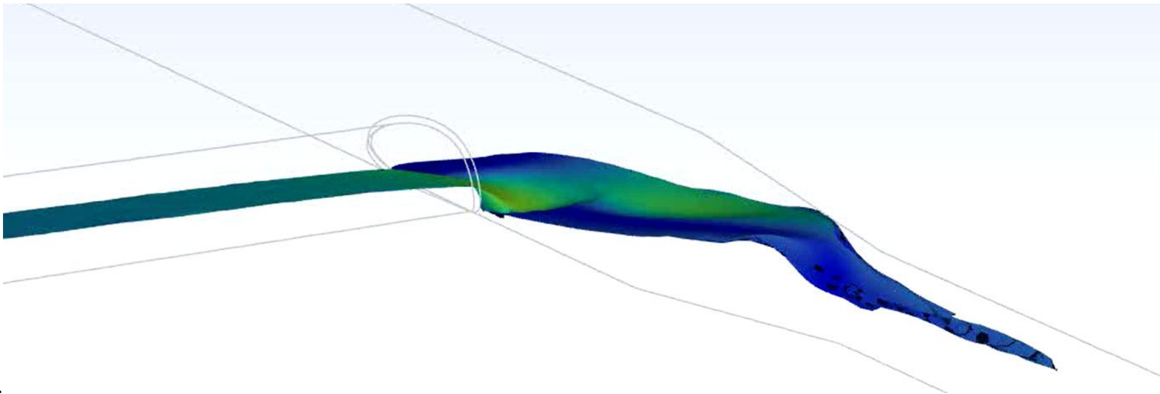

.

Figure 33: View of the free surface at the junction at the top of the penstock.

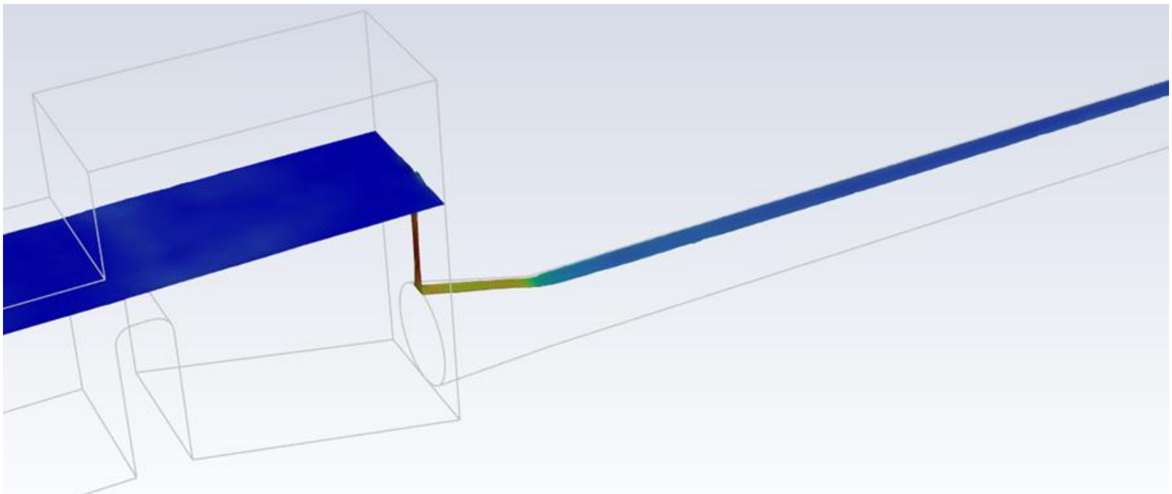

Figure 34: View of the free surface at the intake after 450 seconds during a dewatering/re-filling sequence of the head race pipe.

3D CFD simulations were also carried out by HDE for the Merezenbach surge tank to evaluate the risk of air entrainment. The 1D hydraulic simulations indicated that the water surface approaches the bottom of the surge tank during 75% dewatering of the headrace tunnel, so the water surface behavior at this low level is simulated. These simulations allow to evaluate the risk of free-surface vortices and air entrainment in the surge tank.

HDE carried out these simulations using both ANSYS® CFX® and OpenFOAM softwares. The aim was to compare the results from the well-established but expensive ANSYS® CFX® software and the newer and more affordable OpenFOAM software. Both sets of results converge to the same head loss values. The vortices predicted by OpenFOAM are stronger than those obtained with ANSYS® CFX®. The results obtained with OpenFOAM can therefore be considered conservative. These findings highlight the promising potential of OpenFOAM for such CFD analyses. For the CFD study of the free surface in the Merezenbach surge tank, the considered domain includes the surge tank and a section of both the penstock and the headrace tunnel, as can be seen in the Figure 35 below. A transient simulation is carried out, modelling a progressive emptying of the surge tank. The discharge entering the domain at the headrace tunnel is therefore smaller than the discharge exiting the domain through the penstock.

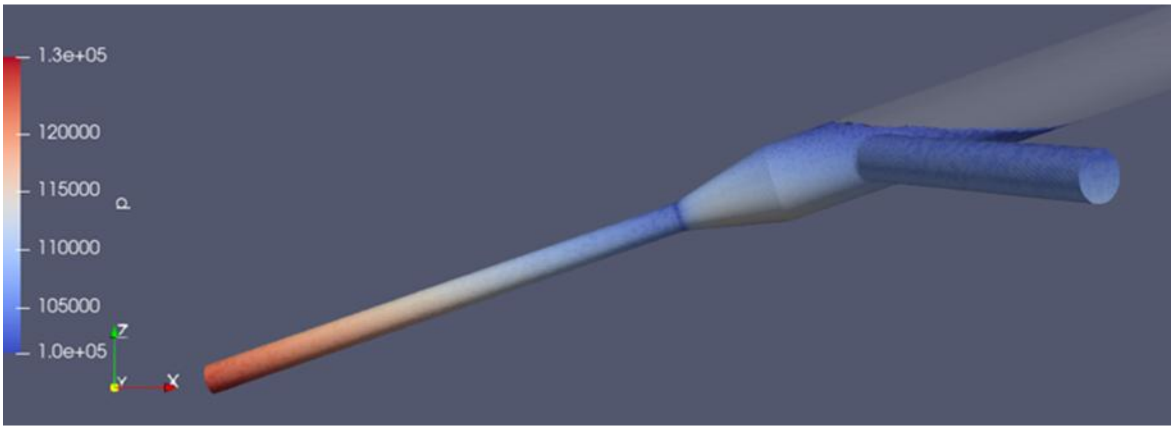

Figure 35: Free surface simulation 4 seconds after the emptying sequence start of the surge tank.

In Figure 36 a visualization of the simulated surface of the water in the surge tank is shown. A surface dimple is clearly visible, which indicates the development of a vortex of type 2 in the surge tank. The classification of the different types of surface vortices is shown in Figure 55. While the CFD simulation predicts a vortex of type 2 in the surge tank when the water level is low, it is recognized that CFD simulations usually underestimate the strength of free-surface vortices. In practice, vortices often develop at least one class beyond the level predicted by CFD models. In this case, the vortex would probably be of type 3 at least. Knowing that air bubbles start to be entrained at level 5, it cannot be ruled out that air entrainment may occur, though the likelihood and extent of such an event remain uncertain.

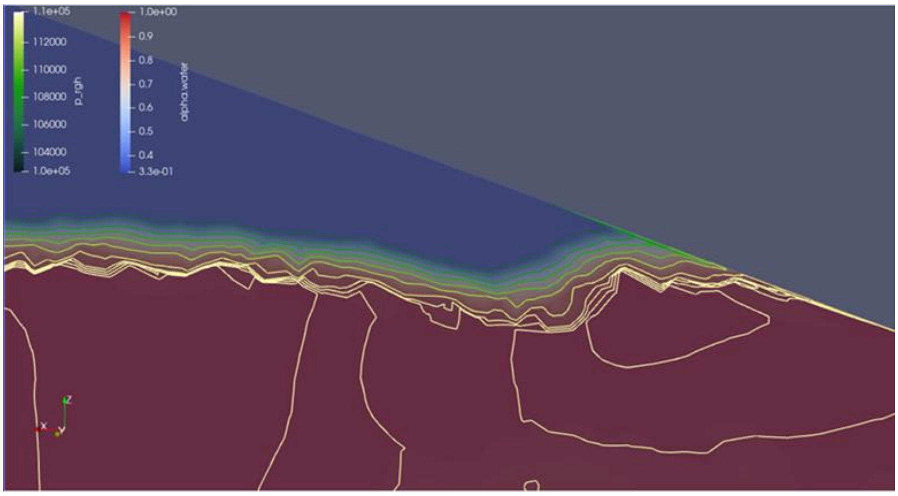

Figure 36: Visualisation of the free surface in the surge tank (OpenFOAM).

3.3.4. Sizing of the pumping capacity for KW Alstafel power plant.

The following paragraphs focus on the task of determining the appropriate storage and pumping capacity for the KW Altstafel power plant, based on the available preliminary civil engineering feasibility study.

In the feasibility study of the KW Altstafel pumping station variants, three types of pumps were evaluated. Standard industrial pumps, sourced from catalogue models, were considered unsuitable for the site's requirements. According to manufacturers, achieving the required flow rate (Q = 2 m³/s at a head of 400 m) would require many pumps, resulting in limited operational stability and low overall efficiency.

A customized version of the standard industrial pump, designed to meet the site-specific requirements, provides a viable solution, demonstrated by Sulzer's HPDM model with a configuration of three pumps (3 × Q = 0.8 m³/s at H = 400 m). This solution also helps reduce costs compared to developing a completely new pump design from scratch.

Finally, a prototype pump specifically designed for the site could reach very high efficiency, up to 90%. A detailed study on prototype pump variants was carried out to determine the optimal combination of pump quantity and stage configuration, ensuring a specific speed of *Nq ≥ 25* and a minimum submergence level of **-10 m**. Table 8 presents the results of the various pump variants. Meeting these criteria would allow the selection of either two three-stage pumps, each rated at 6 MW, or three three-stage pumps, each rated at 4.2 MW.

Table 8: Prototype design pump variants based on preliminary civil engineering feasibility study.

			1x Pump				2x Pump			3x Pump	
Characteristic of pump stage											
Mechanical power	Pm	[MW]	10	12.5	12.5	12.5	6.3	3.2	2	4.2	1.4
Nominal head	Hn	[m]	400	400	400	400	400	200	133	400	133
Nominal discharge	Qn	[m3/s]	2.28	2.81	2.87	2.87	1.4	1.4	1.4	0.92	0.96
Rotational speed	Nn	[rpm]	1500	1000	1500	750	1000	1000	1000	1000	1000
Specific speed	**Nq**	**[-]**	**25**	**18.7**	**28.4**	**13.9**	**13.2**	**22.7**	**30.1**	**10.7**	**25**
Mechanical time constant	Taum	[s]	3.9	3.9	4.1	3.8	3.3	2.8	2.5	3	2.3
Submergence	**Hs**	**[m]**	**-28**	**-19**	**-32**	**-12**	**-11**	**-7.6**	**-5.4**	**-7.2**	**-3**
Characteristic of pump											
Number stage	**e**	**[-]**	1	1	1	1	1	2	3	1	3
Mechanical power	Pm	[MW]	10	12.5	12.5	12.5	6.3	6.4	6	4.2	4.2
Nominal head	Hn	[m]	400	400	400	400	400	400	400	400	400
Characteristic of pumping station (total)											
Number pump	**Zp**	**[-]**	1	1	1	1	2	2	2	3	3
Total mechanical power	**Ptot**	**[MW]**	**10.0**	**12.5**	**12.5**	**12.5**	**12.6**	**12.8**	**12.0**	**12.6**	**12.6**
Total discharge	**Qtot**	**[m3/s]**	**2.3**	**2.8**	**2.9**	**2.9**	**2.8**	**2.8**	**2.8**	**2.8**	**2.9**
Efficiency	**eta**	**[%]**	**90%**	**88%**	**89%**	**86%**	**86%**	**89%**	**90%**	**86%**	**90%**

For the used civil engineering variant, a single-stage reversible Francis pump-turbine or centrifugal pump with a nominal power of 10 MW are not feasible in terms of hydraulic transients. In pump mode, low pressure could occur at the penstock inlet, potentially requiring operational limits on the minimum upstream reservoir level. In turbine mode, overpressure along the lined shaft reaches 142%, exceeding the maximum allowable service pressure of 132%, making operation unsafe. Consequently, this configuration cannot be recommended for the civil engineering variant without significant modifications.

The minimum submergence requirement of the pump could be reduced by using either multi-stage pumps or multiple multi-stage pumps operating in parallel. This approach also offers operational advantages, including improved availability and the possibility of operating a single unit even at lower upstream reservoir levels. Hydraulic transients indicate a risk of low pressure at the penstock inlet when the upstream reservoir is at its minimum level. Operational constraints or design modifications would therefore be necessary for this civil engineering variant. However, using multiple pumps or multi-stage pumps significantly improves the transient behaviour overall.

3.4 WP4 – Hydro-meteorological predictions

Lead: WSL, **partner:** HEIG-VD

The aim of WP4 is to assess the suitability of the existing hydropower plants in the Goms valley for flexible operation with a particular focus on the hydrological characteristics of their associated catchments. A second goal is to investigate the temporal alignment between water discharge at selected HP in-takes (e.g., Griesbach), and the resulting HP production with the generation of wind and solar electricity at corresponding HP infrastructures to optimize a joint operation.

Within this framework, WP4 develops and operates the hydro-meteorological prediction pillar of SmallFLEX Goms. The system delivers forecasts of river discharge, wind conditions and incoming solar-radiation, thereby supporting short-term operational decisions and enabling more flexible and integrated management of hydropower, photovoltaic and wind energy resources.

3.4.1.Hydrometeorological forecasts for flexible operation

The operational system is the most up to date version of the WSL forecasting tool that has been developed since 2007 (Zappa & Vogt, 2007). The gains by the scientific community in the forecasting of severe weather events and floods over the last decade has allowed the development of a new generation of flood warning systems which can provide reliable estimations of the discharge hydrograph with short-term (1–2 days) and mid-term (3–5 days) lead times. The main feature of the system is the propagation of numerical forecasts through the end-to-end chain and presenting it for decision support (Figure 37, Rossa et al., 2011, Zappa et al., 2010).

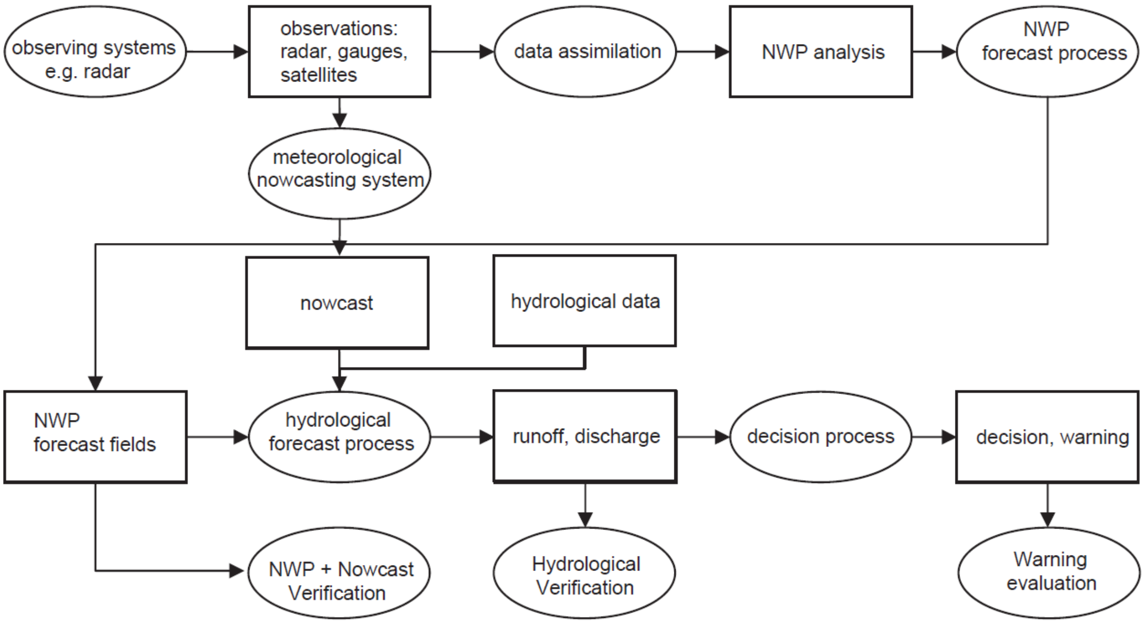

Figure 37: From Rossa et al., 2011: Schematic to depict the production chain of a flood forecasting, decision making and warning system. Boxes denote products while ellipses denote processes. Note that “NWP” may include any numerical forecast output, deterministic or probabilistic, e.g. ensemble prediction system (EPS) products.

A version of the operational system was implemented during the original “SmallFLEX Demonstrator for flexible small hydropower plant” project in 2021. The forecasts for the “Wasserkraftwerk Gletsch-Oberwald” have been operated by WSL ever since.

3.4.1.1. Ensemble hydrological forecasts

Extended-range hydrological ensembles arise from a hydrological model with numerical forecasts from an atmospheric prediction system. Such predictions can be accessed in Switzerland from Meteo Swiss. Downscaling methods are adopted to create inputs to operate a hydrological model at catchment scale (Addor et al., 2011). The atmospheric predictions are characterized by uncertainties. So-called ensemble prediction systems provide sets of equiprobable forecasts for the next hours to days, depending on the configuration of the prediction system operated by the national weather service (Zappa et al., 2011). The resulting probabilistic outputs of such a system are aligned with warning and operational use cases (Steeb et al, 2022; Rossa et al., 2011). Figure 38 presents the current version of tailored forecasts for the SmallFLEX “Gletsch” test case.

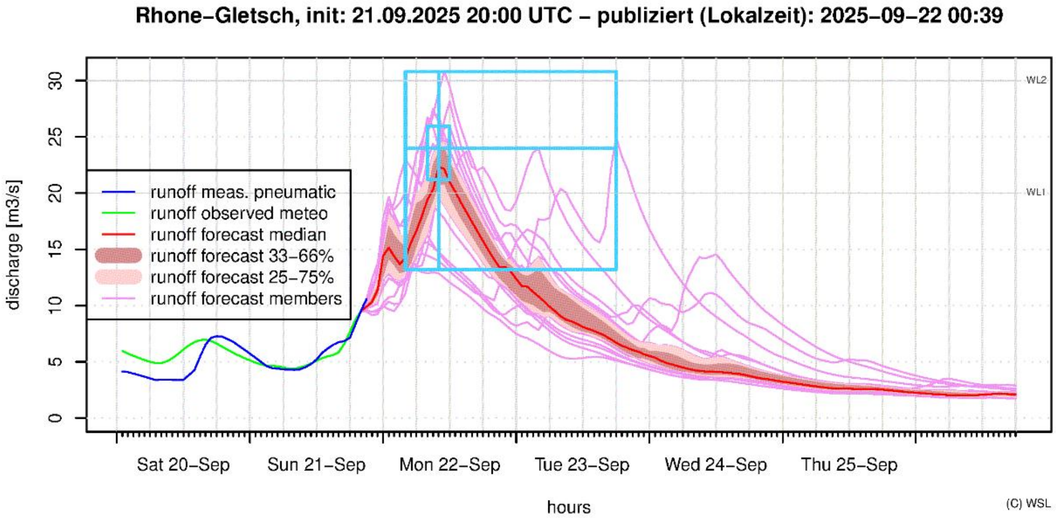

Figure 38: Sample of operational flood forecast issued for the Small-Flex Gletsch test bed on September 22nd 2025. The observed flood peak on was 15 m^3/s. 5 days ensemble prediction with 21 members.

3.4.1.2. The hydrological model PREVAH

The specific hydrological model adopted for the SmallFLEX test beds is PREVAH. Among a large variety of hydrological models used in Switzerland, PREVAH is the most used in operational hydrological context for both floods and droughts (Horton et al., 2021). PREVAH is a conceptual, semi distributed hydrological modelling system that represents catchments through hydrologic response units with shared physiographic properties (Viviroli et al., 2009). It simulates the water balance with explicit modules for snow accumulation and melt, interception, evapotranspiration, soil moisture dynamics, runoff generation and flow routing. For real time applications PREVAH is routinely forced with deterministic and ensemble numerical weather prediction and has been used as the hydrological engine in hydrometeorological ensemble prediction systems where probabilistic inputs (see next section). **For the SmallFLEX-Goms project, the data flow and data processing of PREVAH has been complemented with novel tool to extend the prediction to renewable energy sources.**

3.4.1.3. Numerical Weather Predictions

Numerical weather prediction (NWP) provides the meteorological forcing for our hydrological forecasts through a deterministic and probabilistic limited-area model and an ensemble system tailored to Alpine conditions (Rotach et al., 2012). The original SmallFLEX project (ended in 2021) implemented the COSMO-1 and COSMO-E NWPs. In 2024 MeteoSwiss deployed a novel NWP called ICON (https://www.meteoschweiz.admin.ch/wetter/warn-und-prognosesysteme/icon-prognosesysteme.html).

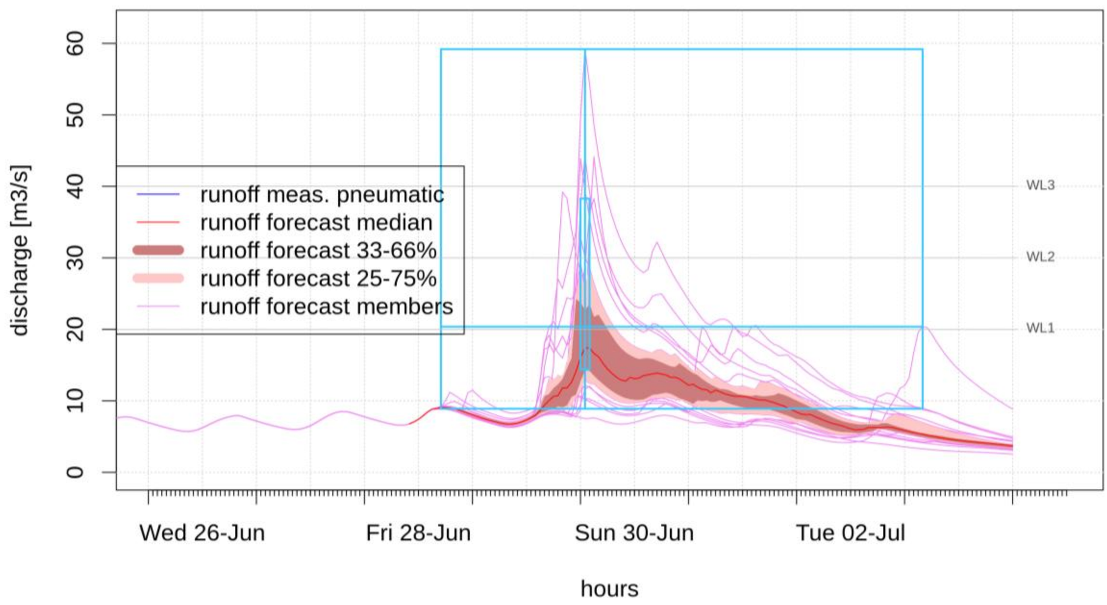

Figure 39: Operational flood forecast issued for the Small-Flex Gletsch test bed on June 28th 2024. The observed flood peak on was 20 m3/s.

Since June 2024, MeteoSwiss is operating the ICON (Icosahedral Non-hydrostatic) numerical weather prediction model to generate regional and local forecasts, particularly suited for the complex terrain of the Alps.

WSL configured the current operational forecasts for the SmallFLEX Goms project in early June 2024 (Figure 39).This was just in time to have a forecast for the large flood event of June 29th-June 30th in the Goms region (https://www.gemeinde-goms.ch/files/Online-Schalter/infoschreiben/35_Infoschreiben-Unwetter_Jul.2024.pdf).

3.4.1.4. New Toy model for forecasting renewable energies for flexible operations

Prior to this project the WSL operational furcating system was solely focussed on hydrological predictions. After the developments completed for WP4 we can deliver also energy forecasts. For this purpose, a tailored Toy model has been developed (see the Technical Report Wisskott, 2026 of D4.1 and D4.2). Energy – defined as the ability to do work – exists in several forms that can be transformed from one to another. Power is the rate of this transformation. It can thus also be of different forms; either electrical, mechanical, thermal, or hydraulic. Electricity can therefore refer to electrical energy or electrical power. The usual unit for electrical energy produced or consumed is kilowatt-hour (kWh), while electrical power is given in kilowatt (kW) (Jenkins, 2019).

The followings paragraphs will focus on the parsimonious algorithm that we used for all computations. The combinations of the algorithms build a flexible toy model that was the core of WP4 analyses.

For completing our task, we decided to setup a parsimonious toy model being able to generate robust estimates of renewable energy potential and production in operational mode. For this some standardized inputs are needed (Table 9).

Table 9 Definitions of the variable included in the standardized hydrometeorological input needed to feed the algorithms of the toy model as operationally generated by the real time system developed for SmallFLEX (see also Wisskott, 2026)

Variable	Meaning	Unit	Source	Application
year	Year	–	–	Timeline
month	Month	–	–	Timeline
day	Day	–	–	Timeline
pr	Precipitation	mm	CH2018	Water balance / Hydropower
ra	Global radiation	W/m^2	CH2018	PV power generation
re	Relative humidity	0–1	CH2018	PV efficiency correction
ss	Sunshine duration index	0–1	CH2018	Optional PV input
te	Daily mean temperature	°C	CH2018	Temperature correction for PV
tn	Daily minimum temperature	°C	CH2018	Optional
tx	Daily maximum temperature	°C	CH2018	Optional
wi	Wind speed	m/s	CH2018	Wind power generation
q	Discharge	mm/d	PREVAH	Run-of-river hydropower

The results obtained are to some extent synthetic. We used real data and realistic assumptions to estimate the amount of electricity that could theoretically be produced under the conditions given (power plant characteristics, available inputs). However, they do not consider real-time power plant operation or shutdowns. The calculated electricity is therefore considered a 'generation potential', even though, in this report, we will often refer to it by the term 'generation' for better readability. The Toymodel has three main components. Detailed information is provided in the two Deliverables of WP4 and in the additional technical documentation by Wisskott (2026). In summary, the three components consists of:

A) The Run-of-River (RoR) hydro power model simulates energy generation from natural water flow without significant storage capacity, making it dependent on instantaneous discharge rates. The hydrological runoff data is received from the hydrological model PREVAH. This data represents the entire water amount from the whole catchment area, supplied by glaciers and snow melting, and by rainfall. The potential electricity generation by a run-of-river RoR hydropower plant is a function of the time-varying effective streamflow Q [mm/d] ("q" in Table 9). Only a limited volume of streamflow can be used to generate electricity. Furthermore the turbine's design discharge and the environmental flow Q_{EF} [m3/s] that must be left in the river according to the law and the respective power plant's concession are accounted (Wechsler et al., 2023).

B) The PV model implements a physically based approach accounting for temperature-dependent efficiency losses and site-specific meteorological conditions. The power output of a photovoltaic plant under uniform solar radiation conditions can be evaluated as detailed in Micocci et al. (2025, see also supplements to WP4 deliverables). The temperature-dependent PV efficiency is accounted and clearly detectable in the hydrological future scenarios. Possible increase of available irradiance due to snow reflection in winter is neglected in the main outcomes of WP4 but has been presented in the analysis of Schenk (2023, see supplements to WP4).

C) The potential electricity generation by a wind turbine depends on the wind speed *U (t)* [m/s] ("wi" in Table 9), the air density and several turbine type specific parameters. The turbine type taken as model in this study is the Enercon E82 2MW (Bauer and Matysik, 2023; Enercon GmbH, 2016) which is considered suitable for alpine areas (Spielhofer et al., 2023). Wind turbines only operate within a certain range of wind speed specific to the turbine type (Spielhofer et al., 2023). This range is confined by an upper and a lower wind speed limit. At wind speeds beyond these limits, power generation is annotated as zero. To determine the electrical energy production of a wind turbine, the physical power of the airflow converted by the rotor must first be considered.

The operational implementations run for D4.1 consist of computations at hourly time step. The future scenarios calculations occurred at daily times step. In future simulations a disaggregation to hourly values has been implemented for the wind speed component. This is detaield in Wisskott (2026).

3.4.1.5. Selected hydropower plants in the Goms region

Finally, when combining the different energy sources, it is necessary to establish the number of units (hydropower plants, wind turbines and solar panels) to be considered for each source. The generation calculated with the “toymodels” equations and then multiplied by the respective number of units.

WP4 selected a subset of the 21 hydropower plants located in the Goms regions (WP). Three of the four plants (KW) presented in Figure 40 are configured as in the real world. The “Laengtalsbach” plant is operated as a virtual run-of-river plant (vKW), as simplification of the Altstafel plant. All these plants have been then virtually equipped with realistic solar and wind power farms. For sake of comparability all four plants used 3000 standard solar panels (LG375N1C-E6) and two Enercon E82 turbines (Schenk, 2023) as a complement to the hydropower plant.

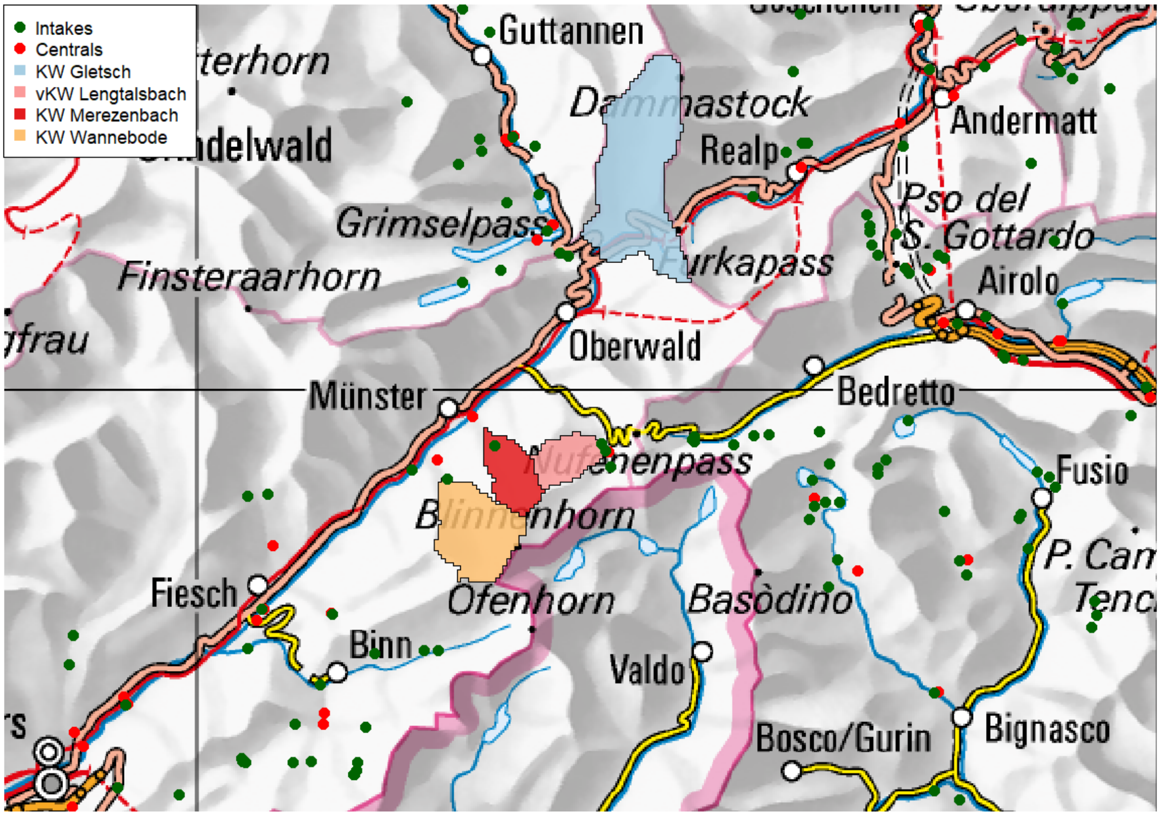

Figure 40: Testbeds retained for evaluating flexible real-time operations with hydrological forecasts.

The main characteristics of each hydropower plant concerning the RoR production are gathered in Table 10. The hydraulic head *H* for the semi-virtual Längtalbach plant is assigned by subtracting the elevation of the KW Ulrichen (1358 müM) from the elevation of the intake (1983 müM).

Table 10: Main characteristics of the considered hydropower plants for configuring the RoR module (section 4.2). The ares serves to transform the hydrological model outcomes from mm/h to m3/s. The head H is used to transform the used discharge into electrical energy. Each plant can force turbines with discharge volumes ranging between the prescribed environmental flows Q_e and the design discharge ot the plant Q_d.

Location	Type	Area [km^2]	H [m]	Q_d [m^3/s]	Q_e [m^3/s]
Gletsch	real	38.9	280	5.56	0.16
Längtalbach	semi-virtual	6.96	625	1	0
Merezenbach	real	7.8	504	0.5	0
Wannebode	real	17.4	171	1.625	0.1

3.4.1.6. Web Dashboard for Gletsch

The “gletsch.slf.ch” web dashboard is operated by WSL since the original SmallFLEX Project. It aggregates near–real-time observations (precipitation, snow, discharge) with MeteoSwiss numerical weather predictions (deterministic and ensemble NWP) and PREVAH hydrological forecasts and publishes them as simple station hydrographs and concise warning overviews for the target catchments.

The system presents both single-realization (deterministic) and ensemble summaries (median, percentile bands and optional member display) for risk-based decisions; where peak timing and magnitude are crucial the dashboard provides compact, uncertainty-focused summaries.

The dashboard is organized to navigate across target areas (horizontal bar) and forecasting products (left bar, Figure 41). In the following the products are shortly described.

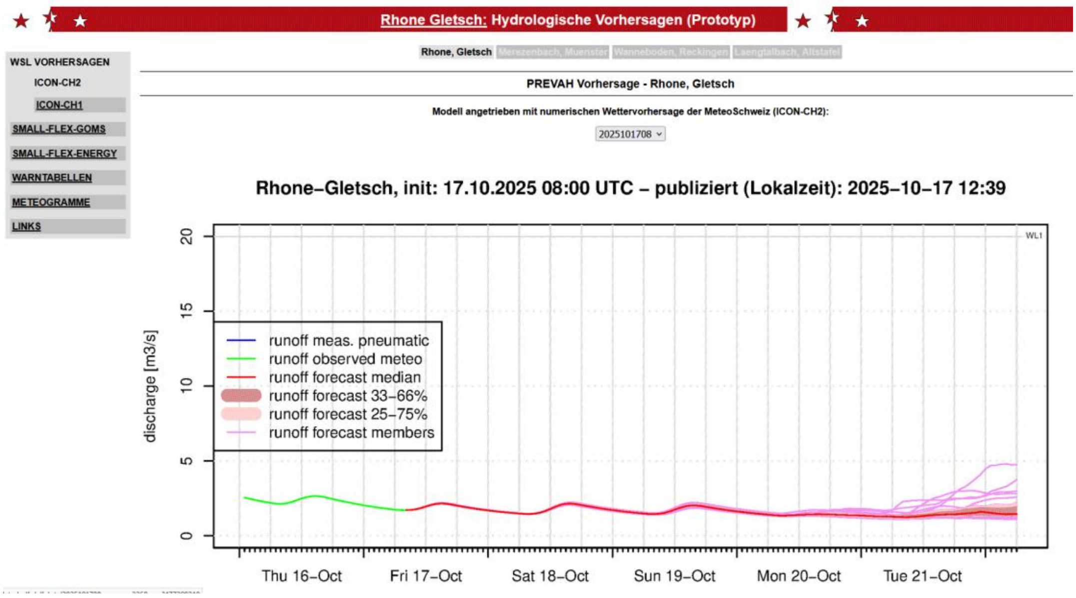

Figure 41: Welcome view of “gletsch.wsl.ch”

The forecasting product “WSL Vorhersagen” is the legacy of the original SMALL Flex project, where only the KW Gletsch was provided as real-time forecasts (Figure 41).

The forecasting product “Small-Flex Goms” extends the forecasting capabilities to all four considered plants.

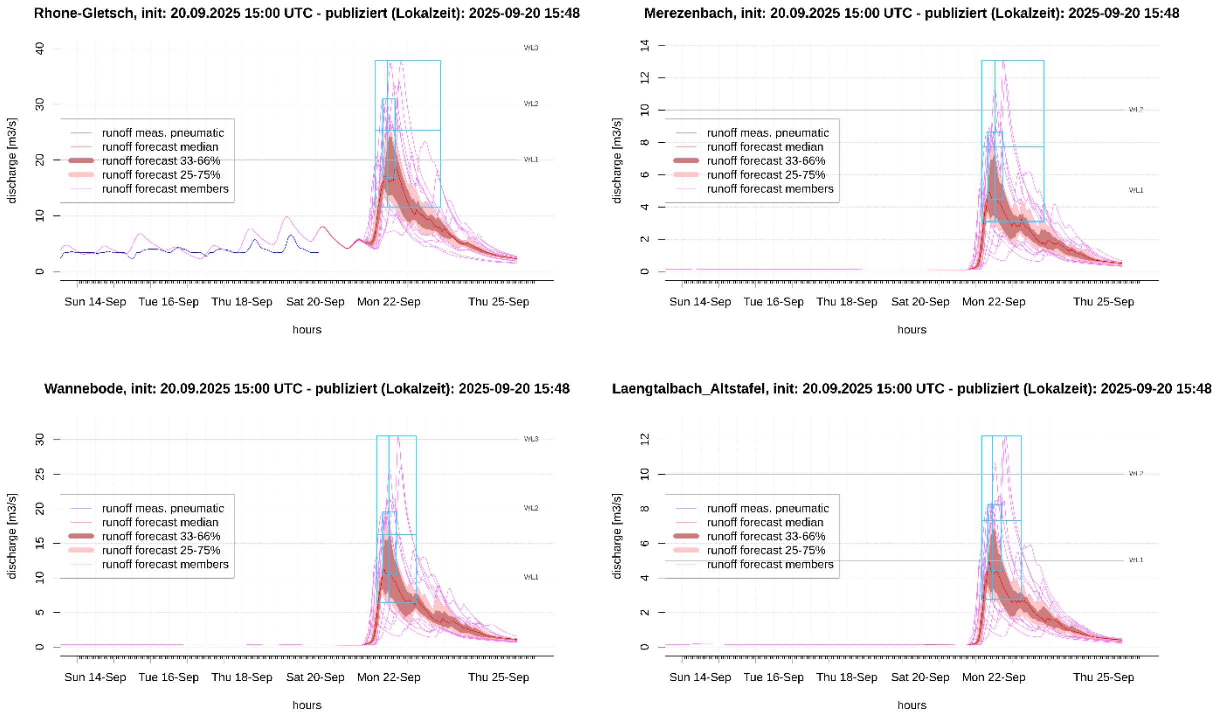

Figure 42: Archived operational discharge forecasts on September 20th 2025 for the four SMALL-FLEX-GOMS testbeds. Top-Left: KW Gletsch. Top-Right KW Merezenbach. Bottom-Left: KW Wannebode. Bottom-Right: KW Längtalbach.

This information is mostly useful to prevent damage to the intakes of the respective power plants by allowing good anticipation in closing the gates and avoiding that sediments and debris eventually reach the pipelines and the turbines. This information is updated several times per day allowing to react to changing predictions as the potentially harmful event is approaching, Figure 42 presents the streamflow forecasts for all four SMALL-FLEX-GOMS testbeds for the 20th of September 2025. The observed maximum discharge at the FOEN station in Gletsch occurred at 2 AM of September 22nd. The peak streamflow was 14 m3/s. The median of the forecasts two day ahead was about 17 m3/s.

The forecasting product “Small-Flex Energy” translates the hydrometeorological forecasts of the variables needed by the toy models into hourly energy forecasts. The forecasts of streamflow are needed to operate the RoR toymodel. The wind speed forecasts are needed for the “Wind Energy” toymodel. The PV toymodel is forced by the forecasts of both temperature and incoming global radiation. A sample of Energy forecasts is presented in Figure 43.

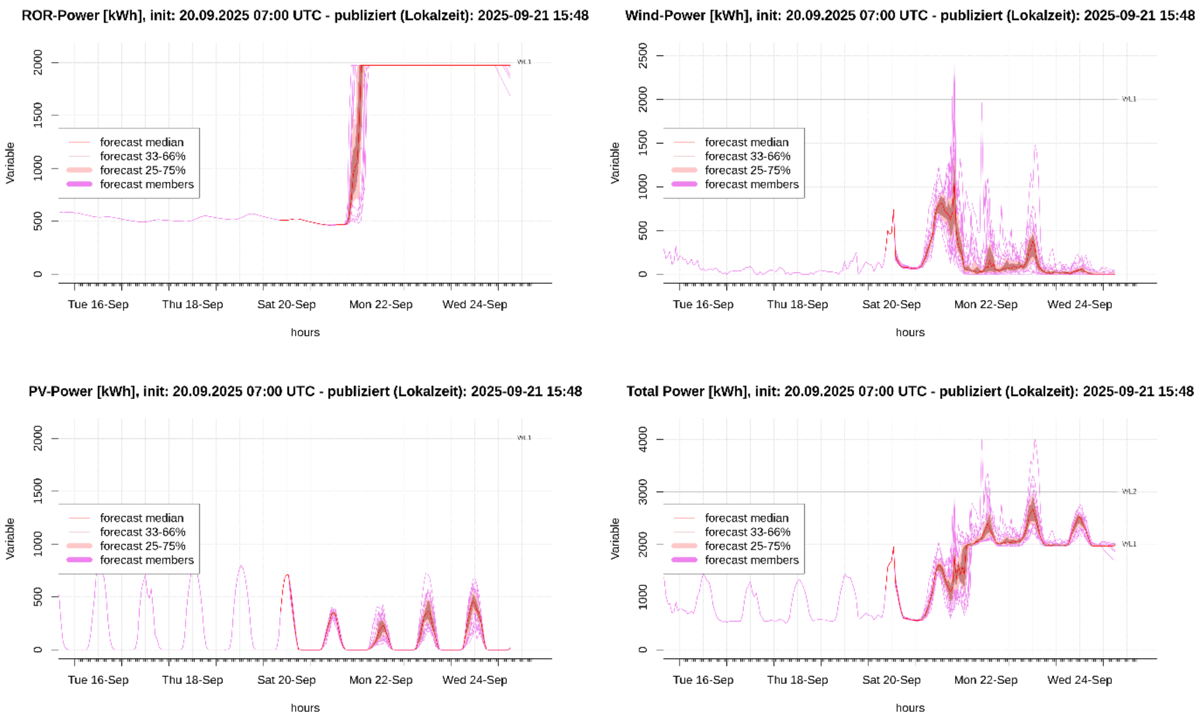

Figure 43: Archived 5 days operational forecasts of hourly Energy production (KWh) on September 20th 2025 for the KW Merezenbach. Top-Left: Run-of-River production. Top-Right: Wind Energy power. Bottom-Left: PV-power. Bottom-Right: total energy production.

The energy forecasts presented in Figure 43 are exemplary for the peculiarities of energy yield by the three sources of renewables to be considered for flexible operations of alpine run-of-river power plants:

- The ROR energy forecasts during low-flow periods do not show spread (Figure 43, top-left)
- During high-flow situation there is uncertainty about the timing when the maximum production capacity of the ROR plant is reached. Once this limit is reached additional streamflow overspills and is not used for hydropower production, unless storage capacity is also installed (Figure 43, top-left).
- Wind energy production is characterized by high uncertainty (Figure 43, top-right). Doubling the wind speed increases the power eightfold ($2^3 = 8$). It means that small increases in wind speed can lead to large increases in energy output, which may jeopardize any plans of production and flexible operation of small power plants with limited storage capacity for the next days.
- The photovoltaic energy predictions (lower-left panel in Figure 43) show a smaller variability and are strongly constrained by the yearly cycle of irradiance at a specific location. Under clear-sky conditions such forecasts might result in very reliable estimates of production for specific power plants in the alps. In our specific case we assumed a virtual PV-farm with 3000 standard panels.

3.4.1.7. Analysis of one year of real-time forecasts in the perspective of flexible operations

The real-time operations for D4.1 started in June 2024. For the evaluation, a set of 396 forecasts has been archived since then. Data are available for the four target areas listed in Table 10 and Figure 40. We had to record data gap in January-February 2025 (Figure 44).

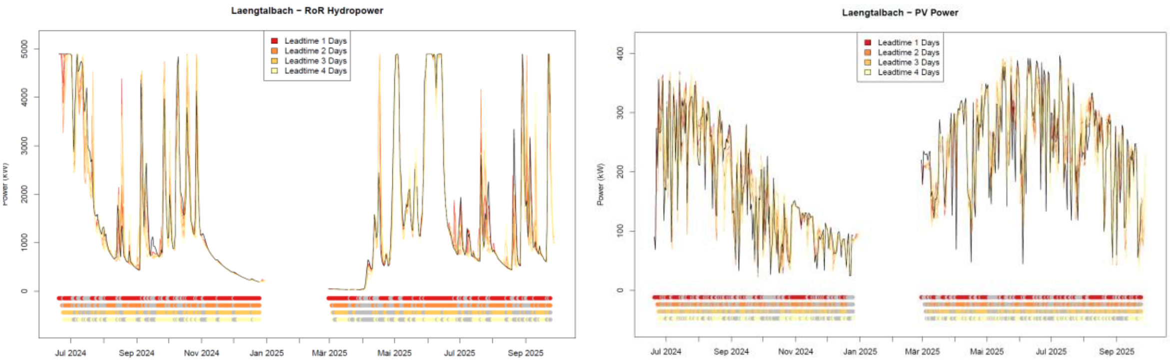

Figure 44: Daily energy yield estimations for the location Laengtalbach using observed meteorology (black line) and ICON2 predictions (colour according to lead time) as forcing for PREVAH and the toy models. Left: Run-of-River production. Right: PV-power. The four lines at the bottom of the forecasts indicate whether the black line falls within the interquartile range of the predictions for the four lead times (grey: no, color: yes). Analyses for all target areas and variables are summarized in Table 11 and included as supplement to deliverable 4.1 ("SmallFLEX_WP4_D4.1_SupplementAnalysis").

Bias of forecasted energy estimations

As a first term of comparison, the forecasted energy estimation has been compared to the reference obtained one day after meteorological observations have become available for a specific date. For the evaluation we take the output that is achieved by forcing the modelling chain (PREVAH & toy models) with the observed meteorological data as reference (LT=-1, "-1" means one day after a specific day is over and thus observed data are available). Subsequently, analyses for predictions with one to 4 days (LT=1, LT=2, LT=3, LT=4) ahead are evaluated. In the context of energy production, it is important to have reliable prediction one day ahead to plan operations and contribute to fulfil the local and regional demand.

Same day predictions (LT=0) are not useful for energy traders and operators. If the predictions one and two day ahead (LT=1 & LT=2) are skilful, then flexible production can be implemented and achieved. Paramount goal is therefore that predictions are not biased as compared to the effective energy potential production yielded by LT=-1.

Table 11 Average bias in forecasted energy estimations for the four operational small-flex power plants. Analyses are detailed per lead time (days), locations and renewable energy source. The last column cumulates all three energy sources. White background means no/small bias. Red fields indicate underestimation and blue fields overestimation of energy yield between reference and predictions

		Lead time	RoR	Wind	PV	All
Gletsch						
		1	0%	-74%	11%	-1%
		2	-1%	-74%	9%	-2%
		3	-1%	-72%	10%	-3%
		4	-2%	-71%	9%	-3%
Laengtalbach						
		1	0%	49%	0%	0%
		2	0%	53%	-1%	1%
		3	-1%	68%	-1%	1%
		4	-1%	76%	-2%	3%
Merezenbach						
		1	-1%	7%	1%	0%
		2	-2%	15%	1%	-1%
		3	-2%	30%	0%	-2%
		4	-2%	27%	0%	-1%
Wanneboden						
		1	0%	7%	1%	0%
		2	-1%	15%	1%	0%
		3	-1%	30%	0%	0%
		4	-1%	27%	0%	2%

Table 11 summarizes the average bias in percent between the estimated energy production with one to four days prediction and the reference. Following can be concluded:

RoR estimation have almost no bias. This is valid for all lead times and target areas. Consequently, predictions of RoR energy can be useful for flexible operations.

Wind energy predictions are largely biased, for all lead times and catchments. For the KW Gletsch location wind energy production is largely underestimated, while for the other three areas the wind energy prediction is higher than the obtained reference value. This makes wind energy predictions less suitable for flexible achievement of energy targets. Wind is a very local variable and there is a clear mismatch between the wind speed predictions in the numerical weather model and the local interpolation of wind speed based on observations in a standard meteorological network. For successful use of predictions to guide energy planning very targeted local analyses of real wind parks data must be planned and completed in the first years of operations, before using wind energy predictions for flexible operations of small hydropower systems.

The predictions of PV are in most areas unbiased (on average). As solar energy highly depends on the annual cycle of incoming global radiation, there is a kind of intrinsic persistence that is relatively easy to predict by the numerical weather models, also with several days of advance. From a theoretical point of view PV-energy is therefore valuable for planning of flexible operations. Nevertheless, also in case of PV, some bias arises, when the representativity of local observations mismatch as compared to the situation in the target area. In case of the KW-Gletsch plant, energy predictions are about 10% higher than the yield estimated by the reference at LT=-1. At such high elevations, there is probably no representative station of MeteoSwiss. The most representative station might be the one in Ulrichen, located at much lower altitude. In case of fog and low clouds such station might receive much less solar radiation than a potential PV-farm within the high elevation Gletsch basin. For maximising the usefulness of PV-energy predictions for flexible operations a year of effective production data should be analysed to explore ways to reduce biases arising by the local situation where the PV-farm is installed. For three of the four target areas in the small-flex Goms domain, PV-predictions are useful without need of further analyses.

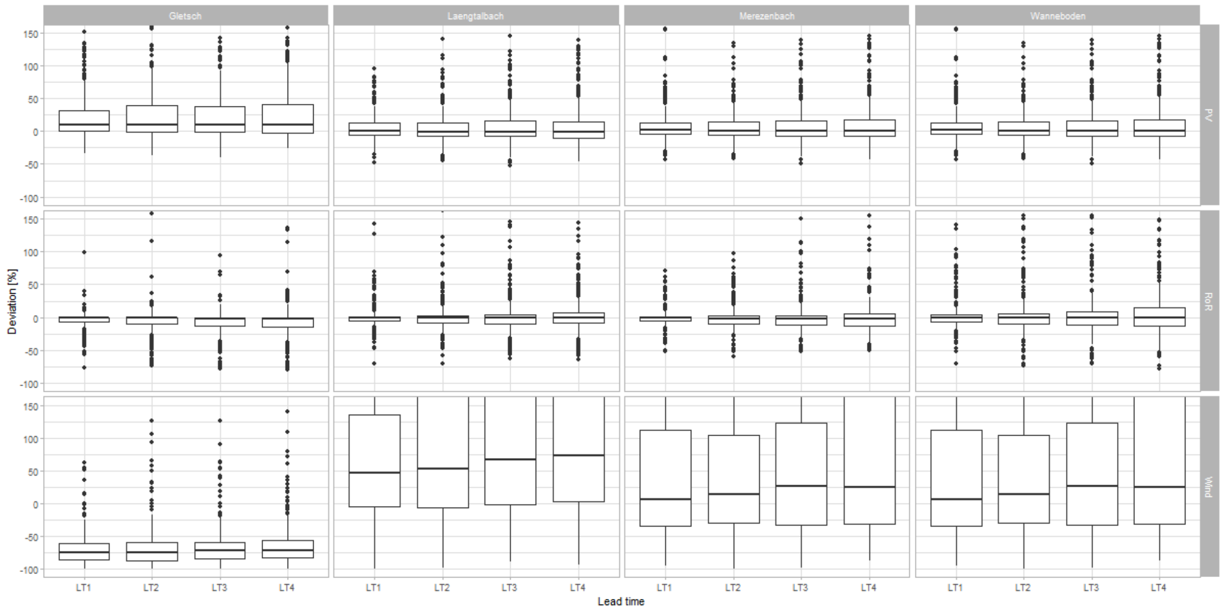

Figure 45 Bias in percent of daily energy yield estimations faceted by locations (columns), energy source (rows) and lead time (x-axis in the corresponding boxplot). The boxplots summarize the **deviation in percent** between the prediction and the reference. Values above zero are sign of positive and values below zero are sign of negative bias (see also table 4).

Figure 45 expands on the summary presented in Table 11. The boxplots summarizing all 396 forecast days indicate how reliable are the bias estimations in each area for the different energy sources and for different lead times. We can observe that:

The spread of the RoR boxplots is rather small and slightly increase from LT=1 to LT=4. KW Wanneboden has larger variability of deviation than the other target areas. The box of the whisker-plot (interquartile range) remains within a range of +/- 10% for both LT=1 and LT=2. These are the most interesting for flexible operation of the power plants. In other words: in more than 50% of the cases the RoR predictions are within +/- 10% of the reference for day-ahead and two-day-ahead energy planning.

The spread of the PV boxplots is larger than the one for RoR. Also, in this analysis the KW Gletsch displays worst prediction quality. In the other three KW more than 50% of the cases the PV predictions are within +/- 15% of the reference for day-ahead and two-day-ahead energy planning.

The deviation of the wind power predictions is very high and seldom within +/- 15% of the reference. Their usefulness for flexible energy operations of small power plants is therefore reduced.

Accuracy of ensemble-based decisions

Energy trades need to plan production some days and hours in advance. With uncertain predictions, a way to estimate how such decisions are useful need to be found. For the specific SmallFLEX framework it has been decided to investigate the frequency of occurrence of useful ensemble forecast following the principles of the Winkler's score as presented in Wilks (2011). Figure 44 illustrates the usefulness of the forecasts for each day in case of the RoR and PV predictions of the Laengtalbach. The horizonal lines in the lower part of the two-time series visualize which days are useful (color marker according to palette for each lead time) and which days resulted in poor forecasts (grey marker). Table 12 presents the correspondent analysis. Following the structure of the previous sections we list here the major findings:

- RoR predictions are useful in about 70% of the cases for LT=1. This quality decreases with increasing lead time. RoR predictions are particularly useful when all forecasts predict that the turbines can be run at maximum capacity and during long low-flow periods, when persistence is governing the drainage of the catchment.

- Also, this analysis confirms that wind energy predictions are poorest in all regions. Wind energy forecasts seem to be more useful for longer lead times. This is a bit misleading singe at longer lead times also the spread of the interquartile range is much higher.
- PV predictions are taxed as useful in half of the days. Also, in this case an increase interquartile range spread is yielding an improvement for later lead times as compared to LT=1.

Table 12 Percentage of useful forecasted energy estimations for the four operational SmallFLEX power. Analyses are detailed per lead time (days), locations and renewable energy source. The last column cumulates all three energy sources. Red fields indicate poor quality and green are sign of good performance. Graphical analyses for all target areas and variables are included as supplement ("SF_Analysis_SPREAD_IQR.pdf").

	Lead time	RoR	Wind	PV	All
Gletsch	1	70.6%	4.8%	44.1%	62.5%
	2	64.8%	3.6%	46.6%	59.8%
	3	64.1%	4.9%	50.0%	60.4%
	4	62.8%	8.4%	49.0%	60.5%
Laengtal-bach	1	71.6%	24.3%	54.2%	59.0%
	2	63.5%	30.6%	54.4%	57.0%
	3	64.3%	34.6%	58.9%	56.5%
	4	61.5%	43.5%	56.5%	59.4%
Merezen-bach	1	64.8%	26.1%	54.9%	57.7%
	2	58.5%	28.2%	57.8%	55.4%
	3	59.9%	35.9%	61.5%	57.3%
	4	57.9%	39.8%	59.9%	57.9%
Wanneboden	1	66.6%	26.1%	54.9%	56.7%
	2	55.4%	28.2%	57.8%	53.4%
	3	54.9%	35.9%	61.5%	53.9%
	4	52.9%	39.8%	59.9%	54.2%

3.4.2. Summary and recommendations from WP4 (part Forecasting)

WP4 (part Forecasting) assessed the potential for flexible operation of small hydropower (HP) plants in the Goms Valley using hydrometeorological forecasts.

Key Components are a state-of-the art hydrometeorological forecasting system and a newly developed "Toy Model for Energy Forecasting" (Wisskott, 2025). Three modules flexibly simulate energy production from several renewable sources:

- Run-of-River (RoR): Based on streamflow, head, and turbine efficiency.
- Photovoltaic (PV): Accounts for irradiance, temperature, and panel characteristics.
- Wind Energy: Based on wind speed, air density, and turbine specifications.

The tool has been implemented in R for operational use. Four HP plants in Goms have been retained. Three of them replicate the real settings of the power plants. One of them is semi-virtual. Each site was additionally virtually equipped with farms of 3000 PV panels and 2 wind turbines.

All analyses support the following conclusions:

- RoR forecasts: Very low bias across all sites and lead times → high reliability.
- PV forecasts: Generally unbiased, except at high-altitude sites like KW Gletsch.
- Wind energy forecasts: High bias and variability → low reliability.

For flexible operations following findings can be retained:

- RoR: ~70% of forecasts are useful for day-ahead planning.
- PV: ~50% useful; better at longer lead times.
- Wind: <30% useful; high uncertainty limits operational value.

Recommendations

- RoR and PV forecasts are suitable for flexible day ahead/two-day ahead operations.
- Wind forecasts require local calibration and further validation before operational use.
- Hybrid systems (RoR + PV) show promises for improving energy reliability in alpine regions.

Real Time tool:

The “gletsch.slf.ch” site has been upgraded. This real-time dashboard shows hydrological and meteorological forecasts. The SmallFLEX Goms option extends forecasts to all four plants, and the Small-Flex-Energy option converts in real time the hydrometeorological forecasts into energy predictions for RoR, PV, and wind. The forecasting system is operating as part of SmallFLEX Goms since end of June 2024.

3.4.3. Introduction WP4 – Hydrometeorological scenarios

The Swiss electricity generation is dominated by hydropower, *i.e.*, approximately 60% stem from this source (Karring and Raeck, 2019; SFOE, 2023). The energy strategy 2050 plans a further increase of hydropower generation (Bonalumi et al., 2021) but also an extension of wind and solar power plants (SFOE, 2021).

Variable renewable energy sources (VRES), such as wind power and solar photovoltaics, hold a pivotal role for the decarbonization of electricity supply systems all over the world (Kroposki et al., 2017).

Combining several renewable energy sources is seen as a strategy to mitigate climate change, as it can potentially attenuate the disadvantageous intermittency of some renewables and thus promote the use of renewable energy sources. The intermittent and hardly predictable nature of VRES (See also deliverable, previous sections of WP4 and Jurasz et al., 2020) is a challenge for the management of the electrical grid, which requires the supply to match the demand at any time (Lund et al., 2015). Integrating multiple renewables in a single hybrid power station is seen as a promising solution to facilitate the introduction of high shares of VRES in the energy mix (Delucchi and Jacobson, 2011), taking advantage of their complementarity to smooth out fluctuations and obtain more regular power generation profiles.

Some forms of hydropower, instead, are able to offer high quality energy, thanks to flexibility and storage capacity (Gernaat et al., 2017). This particularly applies to reservoir-based hydropower systems (Egré and Milewski, 2002); however, even in run-of-river plants with pondage the power output can be adjusted to a limited extent (Jurasz and Ciapała, 2018). The highest degree of flexibility is provided by pumped-storage hydropower plants: (Guittet et al., 2016; Hunt et al., 2020; Micocci et al., 2025).

We contribute to this field of research with conceptual case studies on complementing a Run-of-River hydropower plant with virtual wind and solar power plants in the Goms Region of canton of Valais in Switzerland. We aim to gain insight into how the performance of combined renewable energy sources in meeting electricity demand is impacted by the interplay between climate variability and the way the renewables are combined, under current hydrological and climate conditions as well as under future climate change.

3.4.3.1. Modelling framework in climate scenarios mode

The CH2018 scenarios

The transient daily streamflow scenarios used in this study were derived from the latest downscaled and de-biased Swiss CC Scenarios CH2018 (NCCS, 2018a), which are based on the EURO-CORDEX dataset (Jacob et al., 2014). The climate model ensemble CH2018 contains a total of 39 model members (Table 13) for three Representative Concentration Pathways (Moss et al., 2010):

- RCP 2.6 (Strong mitigation): Immediate global reduction of greenhouse gas emissions through CO2-free energy production stops emission increases within approximately 20 years. Global mean temperature rises by approximately 1.5°C above pre-industrial levels by the end of the 21st century.
- RCP 4.5 (Moderate mitigation): Greenhouse gas emissions are curbed but insufficiently. Atmospheric concentrations continue rising for another 50 years, preventing temperature stabilization by the end of the 21st century. The 2°C target of the Paris Agreement is not achieved, with global warming of approximately 2.5°C above pre-industrial levels.
- RCP 8.5 (No mitigation): Greenhouse gas emissions continue increasing without explicit climate protection measures. Global warming reaches 4–5°C above pre-industrial levels by the end of the 21st century.

CH2018 ensemble consists of different combinations of Regional Climate Models (RCMs) and General Circulation Models (GCMs) and the ensemble members. The model ensemble provides daily air temperature, precipitation, relative humidity, global radiation and near-surface wind speed (Brunner et al., 2019) as needed for forcing the hydrological model used.

Table 13 : The 39 model chains are based on the CH2018 climate scenarios (CH2018 – Climate Scenarios for Switzerland, 2018). The combination of TEAM (responsible institute), RCM (Regional Climate Model), GCM (Global Circulation Model), RES (spatial resolution), and RCP (Representative Concentration Pathways) defines the name of each model chain.

TEAM	RCM	GCM	Auflösung	RCPs
CLMCOM	CCLM4	HADGEM	EUR44	8.5
CLMCOM	CCLM5	ECEARTH	EUR44	8.5
CLMCOM	CCLM5	HADGEM	EUR44	8.5
CLMCOM	CCLM5	MIROC	EUR44	8.5
CLMCOM	CCLM5	MPIESM	EUR44	8.5
DMI	HIRHAM	ECEARTH	EUR11, EUR44	2.6, 4.5, 8.5
KNMI	RACMO	ECEARTH	EUR44	4.5, 8.5
KNMI	RACMO	HADGEM	EUR44	2.6, 4.5, 8.5
SMHI	RCA	CCCMA	EUR44	4.5, 8.5
SMHI	RCA	ECEARTH	EUR11, EUR44	2.6, 4.5, 8.5
SMHI	RCA	HADGEM	EUR11, EUR44	2.6, 4.5, 8.5
SMHI	RCA	MIROC	EUR44	2.6, 4.5, 8.5
SMHI	RCA	MPIESM	EUR11, EUR44	2.6, 4.5, 8.5
SMHI	RCA	NORESM	EUR44	2.6, 4.5, 8.5

3.4.3.2. The Hydrological Model for climate scenarios

The conceptual hydrological PREcipitation-Runoff-EVapotranspiration HRU Model (PREVAH; Viviroli et al., 2009) has been widely used to study the impact of climate change on discharge in Swiss catchments (Horton et al., 2022). For the CC impacts tasks, the gridded version (Bernhard & Zappa, 2012; Speich et al., 2015) with a spatial resolution of 200 x 200 m was used. In the version used, all model parameters had already been calibrated, and the model has been successfully applied in multiple studies (Brunner et al., 2019b, 2019a). The input data comprises temperature, precipitation, relative humidity, global radiation, wind speed, and sunshine duration in daily resolution. To ensure reliable melt estimates under evolving climate conditions, it is necessary to periodically update glacier extents. The implementation of the glacier module follows the methodology introduced by Zekollari et al. (2019) and its integration into PREVAH as described by Brunner et al. (2019a).

3.4.3.3. Simulation of scenarios

The CH2018 scenarios are finally used to force the hydrological model as part of a modelling chain leading finally to the estimation of impacts (Figure 46). Energy yield by power plants is accounted as an impact. Prior to the analyses, simulated time series are generally divided into four periods of the same length (30 years), namely:

- the reference period (1991-2020),
- the early period (2020-2049),
- the mid period (1945-2074) and,
- the late period (2070-2099).

The historical observations (available for 1981-2021) are shortened to 1991-2020 (historical period) to align with the reference climatology currently defined by the World Meteorological Organization (WMO).

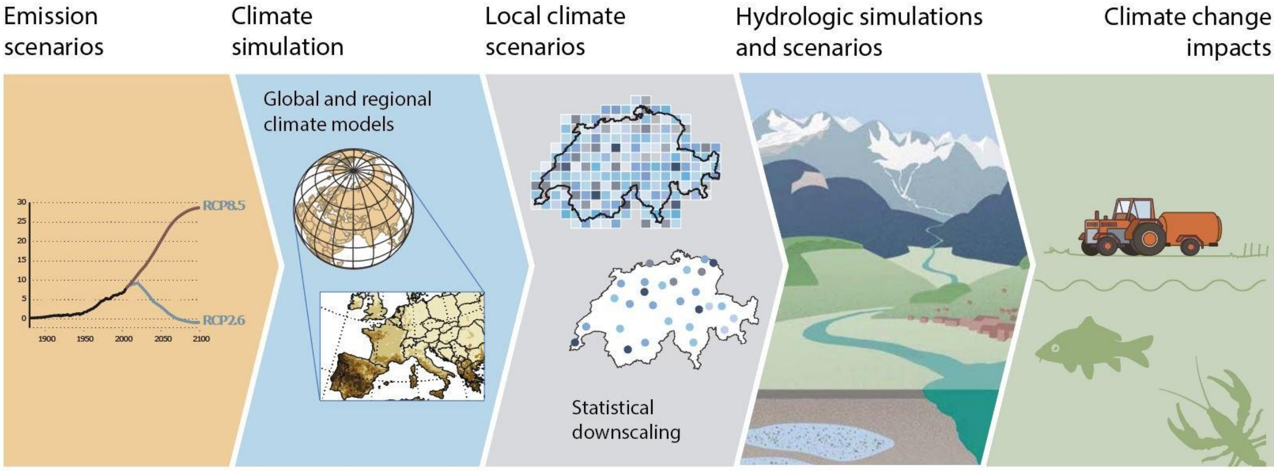

Figure 46: Basic description of the model chain framework of the Hydro-CH2018 CC impact assessments. The figure is slightly modified from the report by the FOEN (2021b). Energy yield by power plants is accounted as an impact.

3.4.3.4. Energy scenarios

After completion of the hydrological simulations data can be prepared to force the Toymodel presented in Wisskott (2026, see also deliverable WP4.1 and previous paragraphs in the sections of WP4). This flexible energy modelling framework for SmallFLEX Goms, includes a series of modules which provides a unified structure for simulating photovoltaic (PV), wind, and hydro power generation. The structure of the datasets comprises daily hydro-meteorological variables essential for energy system modelling, as detailed in Table 9. These variables span four distinct 30-year periods (see above) facilitating analysis of climate change impacts across different time horizons.

3.4.3.5. Case studies in the Goms region

WP 4 defined different case studies along the different stages of the project. A total of four studies in line with the objectives of SmallFLEX have been completed:

- Prior to the selection of the final target areas by WP2, Schenk (2023) developed as part of her Master Thesis at ETH a pilot study in the Goms region using near-real setting in the Binn valley. She completed a report on “Complementing a hydropower plant with solar and wind power plants: a conceptual study in the canton of Valais”. The hydropower plant that served as an example for her hypothetical hydropower plant is plant Nr. 500400 of the Swiss hydropower databases (WASTA), composed of four water intakes (SFOE, 2018). In her work, she used an early prototype of the Toymodel tools. She explored two simple “management strategies”. This master thesis is provided as supplement to this delivery. This work was supported by a collaboration with researcher from INRAE (Paris, France)
- Holovchak (2025) realized a study focused on three SmallFLEX target areas: Griessee, Merezenbach and Wannebode. His Bachelor Thesis on “Climate model-based simulation analysis of hydropower plant potentials: Numerical experiments on water storage strategies and complementary photovoltaic integration” focused on the flexible integration of hydropower, PV-energy and storage in a climate perspective. He transferred the Toymodel tools from R to Python and added features to flexibly cope with energy demand strategies and storage. This bachelor thesis is provided as supplement to this deliverable. This study was supported by researchers of the HAW Hamburg (Germany).
- Micocci et al. (2025 and 2026) realized a comprehensive study on hybridization of a storage hydropower plant with a floating PV farm for the Etzelwerk plant in the Swiss Pre-Alps. As this study is well in line with the goals of Small-Flex Goms. Dr. Micocci of the University of Bologna joined WSL for a 6-month collaboration on the SmallFLEX topics. The focus of the study was finally put on the

Lake Sihl, as the energy demand records and the absence of glaciers was better in line with the goals of our scientific colleagues in Bologna.

- To explore the sensitivity of climate impacts on energy estimation in the Goms region we created a set of ten target areas with different hydrological characteristics. This allowed a large sample analyses of possible impacts of CC on these systems. These analyses are the main part of this reporting.

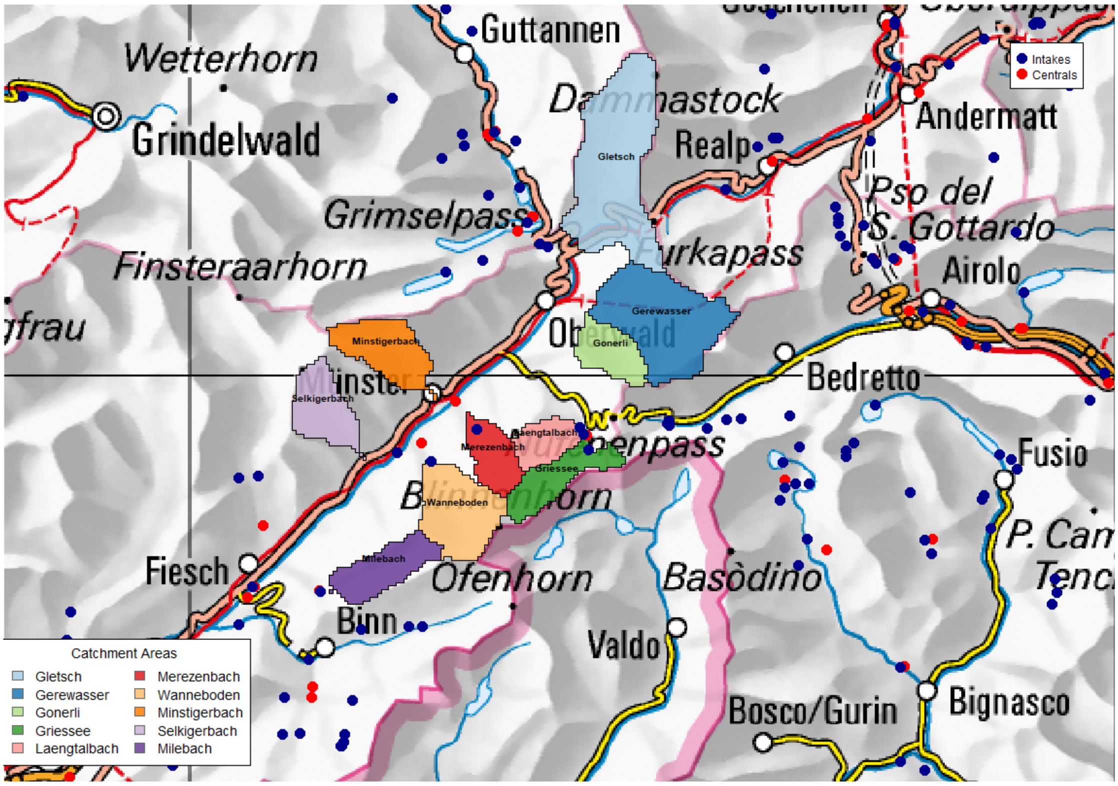

Figure 47: Testbeds for large-sample assessment of climate impacts on energy production in the Goms region.

Table 14: Main characteristics of the considered hydropower plants for the RoR model configuration. The catchment area converts hydrological outputs from mm/d to m^3/s, while the head H transforms discharge into electrical energy. Each plant operates between environmental flow Q_{EF} and design discharge Q_{HF}. Site types indicate real, virtual, or semi-virtual configurations.

Name	Head [m]	Q_{EF} [m³/s]	Q_{HF} [m³/s]	Catchment [km²]	Type
Gletsch	280	0.16	5.56	38.9	real
Gerewasser	265	0.14	3.00	24.0	virtual
Gonerli	385	0.075	1.00	5.78	virtual
Griessee	384	0.00	2.80	10.5	semi-virtual
Laengtalbach	625	0.00	1.00	6.96	semi-virtual
Merezenbach	504	0.00	0.50	7.8	real
Wanneboden	171	0.10	1.625	17.4	real
Minstigerbach	220	0.11	1.56	13.07	real
Selkigerbach	550	0.11	1.56	9.5	virtual
Milebach	729	0.14	1.56	12.4	semi-virtual

The study area comprises several catchment basins in the upper Rhône Valley, Switzerland, primarily located within the municipalities of Obergoms and Goms (Figure 47). Within these catchments, different types of power plants (Table 14) are considered, representing a mix of:

- Real power plants, corresponding to existing installations within the study area,
- Virtual power plants, conceptually designed based on regional hydrological and climatic characteristics, and
- Semi-virtual power plants, inspired by existing sites but modified.

All analyses are based on simulated climate and hydrological data, while the physical locations of the plants correspond to actual sites in the study region. The area exhibits typical alpine hydrological characteristics, with substantial influences from glacial melt, seasonal snow dynamics, and orographic precipitation patterns.

3.4.3.6. Climate change impacts

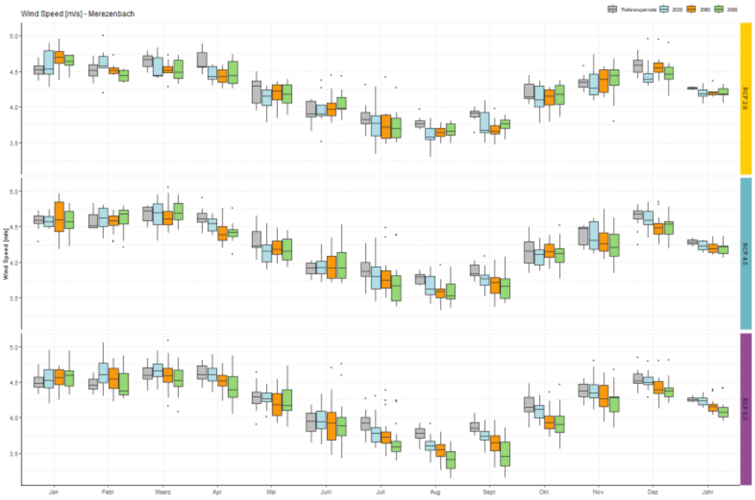

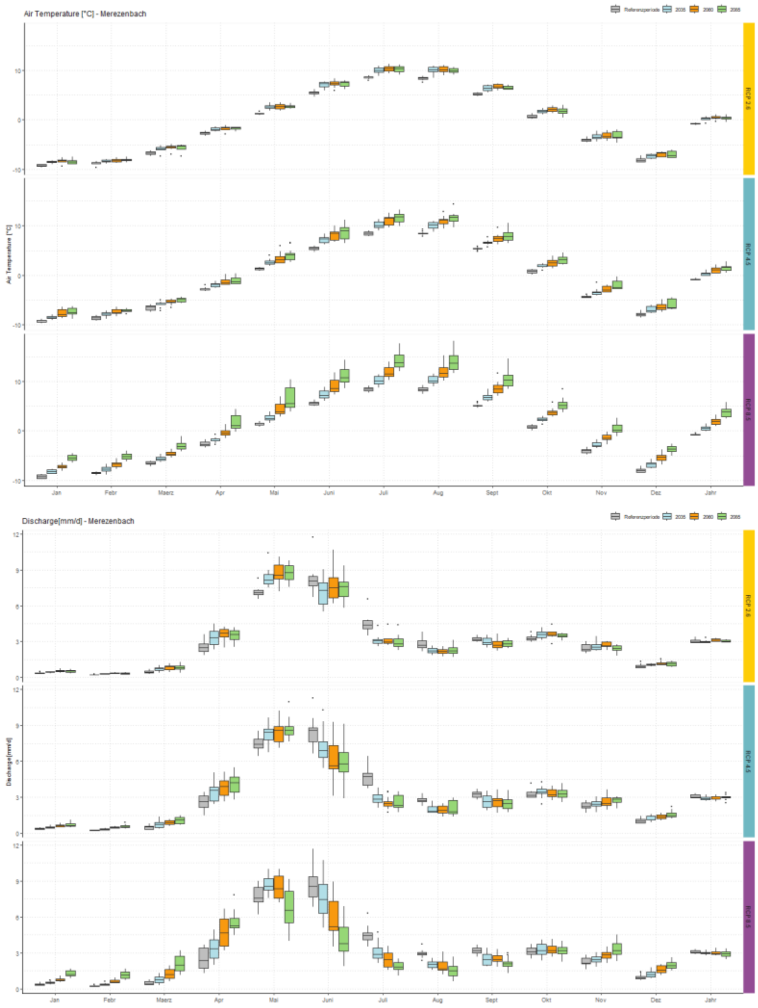

Figure 48 Simulated mean daily wind speed (top), air temperature (center) and streamflow (lower panel) faceted by month for the Merezenbach testbed. Each panel is separated by RCP scenario and divided into four 30-year periods: Reference (grey), early future (cyan), mid future (orange) and far future (green).

Figure 48 presents the baselines governing the changes of energy production with climate change as used in the frameworks defined to test prediction of future energy in the Goms regions. In case of the Merezenbach the average monthly values for wind speed, air temperature and streamflow are presented for different periods and emission scenarios. Changes are increasing from the reference period to the far future and difference are more uncertain for streamflow than for the other two variables. Such kind of analyses is available for 10 target areas and as absolute values (shown here), absolute difference between future periods and the 1991-2010 reference (grey in Figure 48) and as relative differences in percent (see next sections for annual and seasonal summaries).

3.4.3.7. Annual changes across variables and test beds

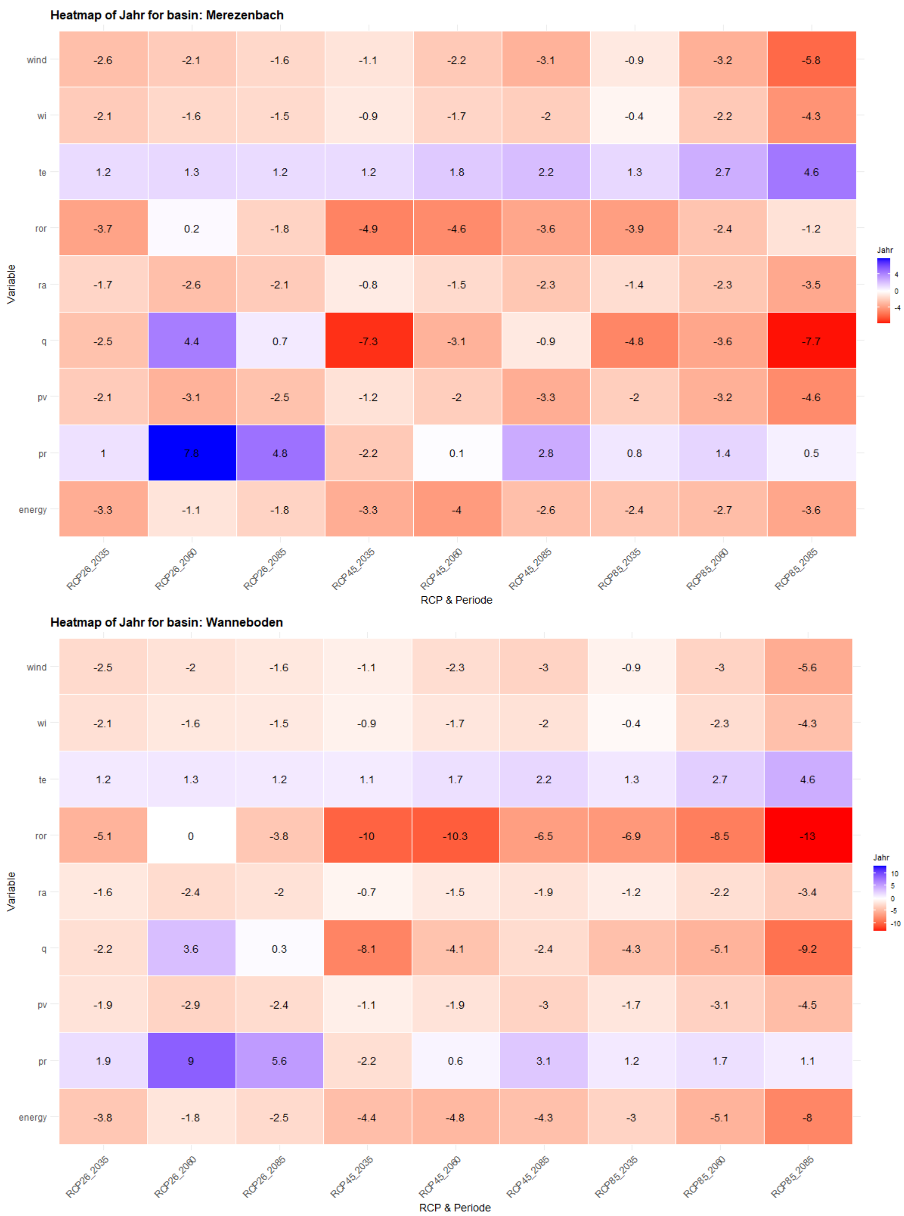

Figure 49 Simulated annual changes of main variables needed for flexible operations at Merezenbach and Wannebode (bottom). Each panel is separated by RCP scenario and period (x-component). At the y-axis the relevant variables for flexible energy assessment are found. “Wind” for wind power, “wi” for wind speed, ”te” for air temperature, “ror” for hydropower energy, “ra” for global radiation, “q” for streamflow, “pv” for photovoltaic energy, “pr” for precipitation and “energy” for the sum op “Win+ror+PV”. All changes beside air temperature are shown as deviation in percent between the scenario period and the reference period. The changes in air temperature are given in °K. Blue colour is sign of increase. Red colour of decrease.

Figure 49 presents the simulated annual changes of main variables needed for flexible operations at Merezenbach and Wannebode. The summary details the findings per RCP scenario and periods. For Merezenbach and Wannebode we can retain following findings:

- Wind speed and wind energy slightly decrease with largest negative impacts at the end of the century with the RCP8.5 scenario

- air temperature increases. At the end of the century up to 4.6 °K more could be achieved without climate mitigation. With climate mitigation warming could remain belo 2°K.
- The interplay between change in climate and changes in the cryosphere makes the changes of streamflow and hydropower energy very much variable across basins and scenarios. In some cases, despite reduction of streamflow by more than 5%, the change in RoR yield is only reduced by less than 2% as a better seasonal distribution of streamflow makes the plants more efficient across seasons. “ror” for hydropower energy, “ra” for global radiation, “q” for streamflow, “pv” for photovoltaic energy, “pr” for precipitation and “energy” for the sum op “Win+ror+PV”.

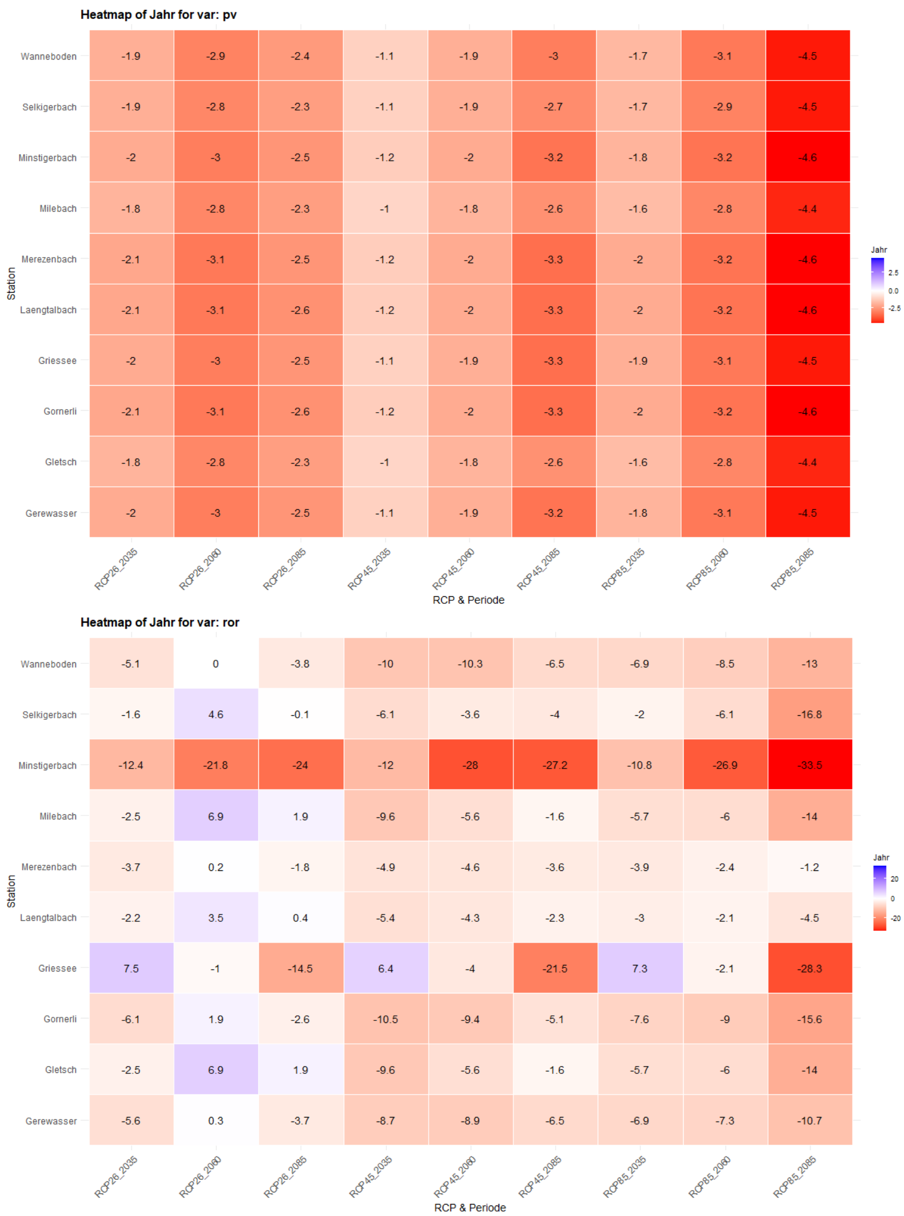

Figure 50 Simulated changes of two variables needed for flexible operations at all 10 testbeds (y-axis). Each panel is separated by RCP scenario and period (x-component). At top panel represents the PV energy changes. The bottom panel represents the RoR hydropower changes. All changes are shown

as deviation in percent between the scenario period and the reference period. Blue colour is sign of increase. Red colour of decrease.

Figure 50 presents details the simulated annual changes for the variables PV energy and RoR energy across all 10 target areas. The summary details the findings per RCP scenario and periods. We can retain following findings:

- The estimated changes in PV yield are not dependent from the location of interest. Such changes are only modulated by the average changes in air temperature and incoming global radiation. These are not varying at local scale
- The changes in RoR energy are modulated by the hydrological characteristics of the 10 investigated locations. Highest decrease in predicted RoR is obtained in catchments that are massively affected by reduction of their portion of glaciated areas (Griesse and Minstingerbach).
- In some areas RoR yield might increase as long as glacier melt is still advancing to the peak of melt amounts with progressing warming. Smallest decrease of RoR yield is achievable by implementing climate change mitigation strategies.

3.4.3.8. Seasonality of changes

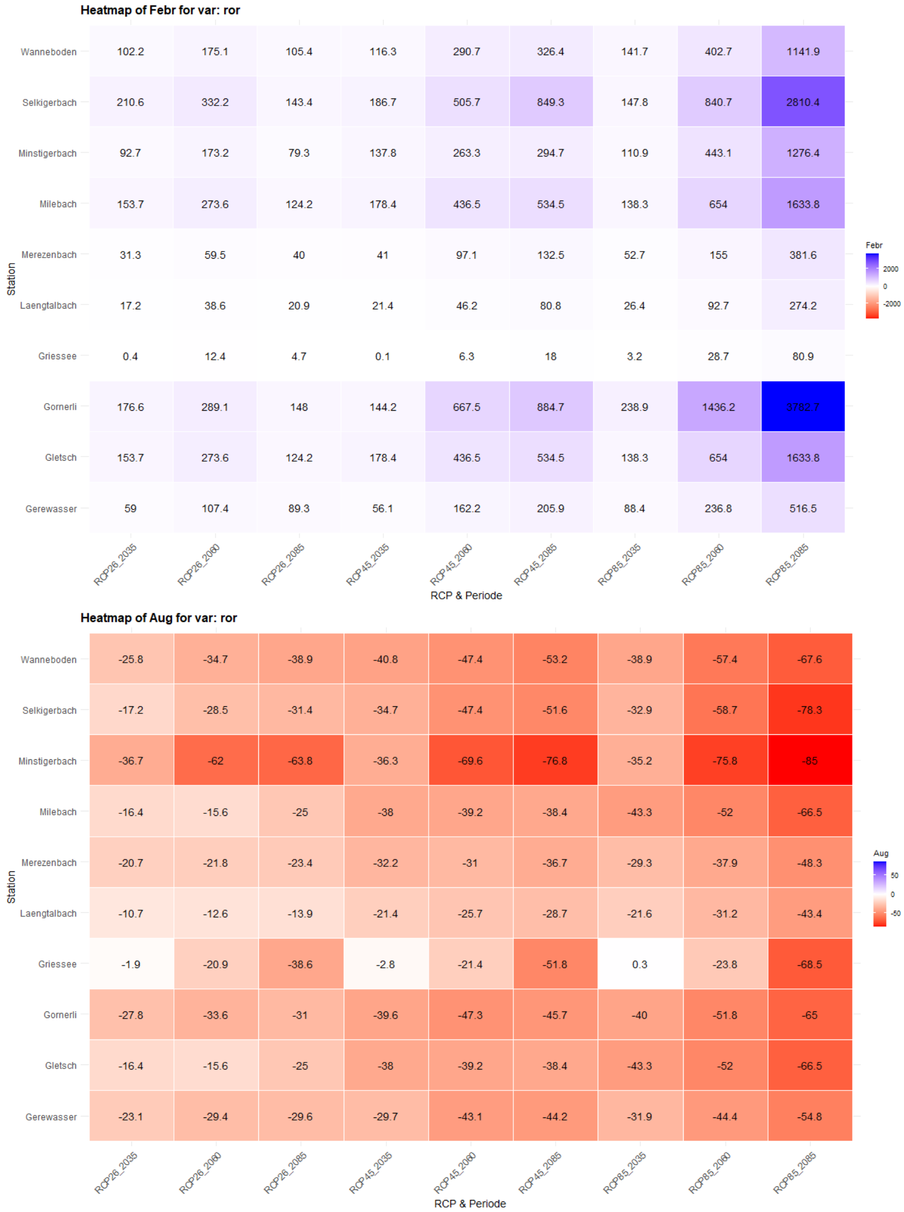

Figure 51 Simulated relative changes of RoR energy in February (top panel) and August (bottom panel). Each panel is detailed by RCP scenario and period (x-component). At the y-axis the 10 testbeds are found. Blue colour is sign of increase. Red colour of decrease. All changes are shown as deviation in percent between the scenario period and the reference period. Blue colour is sign of increase. Red colour of decrease.

Figure 50 is further detailed across seasons in Figure 51 for RoR. Figure 51 details the simulated changes for the variable RoR energy across all 10 target areas in February and August. The summary details the findings per RCP scenario and periods. We can retain following outcomes:

- The changes in RoR energy in February consist of strong to very strong percentual increase across all periods, emission scenarios and target areas.
- Also in this case are modulated by the hydrological characteristics of the 10 investigated locations. Furthermore, the change in seasonality of streamflow as coupled with the setup of the power plants results in increased efficiency in gathering water for power production in wintertime. Increase in

Winter production is surely a welcome outcome to overcome winter shortages in Energy when nuclear power plants wil be decommissioned.

- For similar reasons RoR yield will decrease in summer as snowmelt is anticipated to earlier months and glacier melt is shrinking year after year.

3.4.3.9. Summary of completed hybridization studies

Schenk (2003) combined different renewable energies in climate impact mode using so-called 'conceptual management strategies'. Such strategies determine the order in which the three energy sources are used, and the shares of each source needed to meet the electricity demand at a daily time step. These management strategies are defined according to the average historical climate (observations of the period 1991-2020) and then strictly analysed on how they perform in meeting electricity demand under climate conditions that deviate from the historical average. The respective performance of two management strategies was assessed: the first representing a more diverse combination (ranking the use of wind and solar before hydropower energy and thus using all sources throughout the whole year) and the second representing a less diverse combination (hydropower complemented by wind and solar energy in periods of low river discharge only).

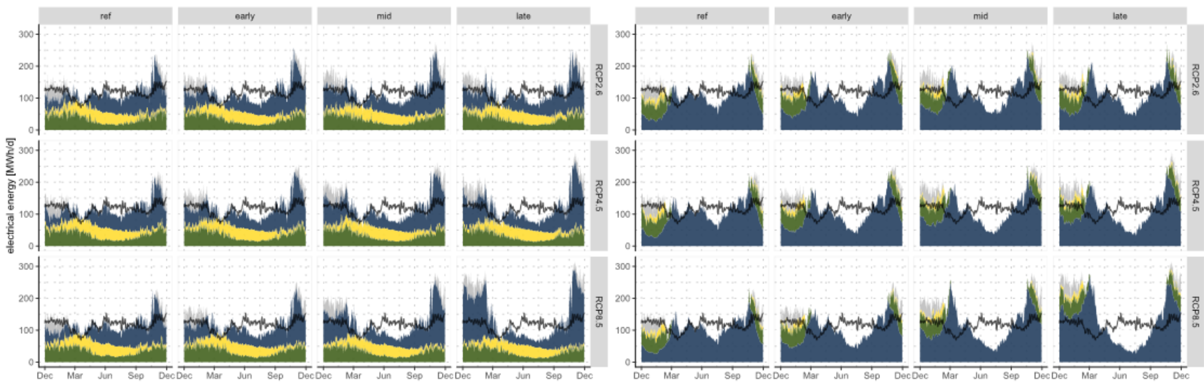

Figure 52 Left: Illustration of the outcome when applying the management strategy WSH to all climate change periods and RCPs. The color-code is equal to the one used to describe the management strategies in section 3.2 (green = wind power, yellow = solar power, blue = hydropower, grey = historical deficit). Coloured areas above the bold black line (electricity demand) mean overgeneration, while white areas below the black line mean undergeneration.

The results of Schenk (2023) indicate that the more diverse management strategy generally performs better in meeting demand under climate conditions that deviate from the average conditions used to define the strategies (compared to a less diverse strategy which relies mostly on one energy source only). This holds true for most future periods impacted by climate change analysed (Figure 52). For our setting, the more diverse management strategy could attenuate under-/overgeneration that arose from deviating climate conditions, regardless of whether this under-/overgeneration was showing a trend (future periods). This better performance is presumably due to the smaller share of one source when the same electricity demand is met by a combination of different energy sources, compared to a reliance on one source only. Schenk (2023) concluded that a diversification in renewable energy sources may potentially have a positive impact on the total electricity generation, as it seems to better support the system in meeting demand. The impacts of storage on similar setting was explored by Holovchak (2025) and Micocci et al (2026).

Holovchak (2025) investigate how to overcome the sensitivity of hydropower energy to climate change in the Alpine region. Previous studies have examined the impacts of climate change on the energy generation from hydropower plants and the benefits of complementarily combining different renewable energy sources. Holovchak (2025) contributed to this research field with a climate model-based simulation analysis of flexible operating strategies of small hydropower plants, using numerical experiments on virtual storage and the integration of complementary photovoltaic (PV) generation. It investigates the potential of stable energy production from small storage hydropower plants in the Goms region of the canton of Valais in Switzerland aiming at reduced seasonal fluctuations and increased annual yield consistency. He simulate daily hydropower and photovoltaic generation using climate projections from Swiss climate change scenarios CH2018 and the corresponding simulated discharge time series from the hydrological model PREVAH as detailed in previous sections. This study introduces and compares two reservoir operating strategies and assesses their effects on hydropower generation and overall energy balance under future climate scenarios. These methods define how potential hydraulic energy is utilized and how the available energy sources are prioritized.

Table 15 Merezenbach (increased reservoir capacity of 8 million m3): annual total hydropower generation with and without storage under each RCP scenario and projection period. The storage is operated with target production method.

RCP scenario	Projection	Without storage [MWh]	With storage [MWh]	Increase [%]
RCP2.6	ref	6999.045	9610.218	37.31
	2035	6773.273	9496.099	40.20
	2060	6981.909	9839.335	40.93
	2085	6841.237	9637.619	40.88
RCP4.5	ref	7036.195	9725.212	38.22
	2035	6619.038	9350.200	41.26
	2060	6646.634	9240.369	39.02
	2085	6822.986	9456.909	38.60
RCP8.5	ref	7008.930	9716.002	38.62
	2035	6697.602	9419.612	40.64
	2060	6920.518	9546.522	37.95
	2085	6942.991	9195.314	32.44

The results indicate pronounced issues in energy generation faced by the end of the century under scenarios with higher greenhouse gas concentrations in the atmosphere. For scenarios without climate protection, the annual hydropower production decreases by up to one quarter under high-emission scenarios for some analysed catchments due to large yearly discharge decrease. The simulations of virtual water storage address the seasonal and quantitative changes in discharge in the future and show a more balanced and reliable energy supply, reducing fluctuations. Compared to the run-of-river operating mode, this approach enhances mean annual generation by up to 40% in certain catchments (See Merezenbach in Table 15). The implementation of complementary photovoltaic plants enhances the flexibility of the system and overall energy generation results. We conclude that small storage hydropower plants may act as a main stabilizing element in future renewable energy systems when adequate storage can be installed.

Finally, a collaboration of WSL with the University of Bologna led to testing some of the SmallFLEX methods on a system located in the Swiss pre-alpine area. Micocci et al. (2025 & 2026) explored how renewable energy sources play a crucial role in improving hydropower system reliability (the Micocci et al. 2025 paper) and mitigating climate change (Micocci et al. 2026). In their study,they illustrated how climate change impacts can be integrated into the evaluation of a hybrid energy system that combines an existing pumped-storage hydropower plant with a conceptual floating photovoltaic installation. Climate change effects were estimated using 39 EURO-CORDEX model chains described in previous sections. Also, this study covered three future time periods and three emission scenarios. The simulations indicated a slight decrease in annual hydropower production, accompanied by a pronounced shift in seasonality, with an increase in winter production and a decrease in spring and summer. The annual solar energy yield also exhibits a modest declining trend over time, though no substantial changes in seasonality were projected. Despite these individual trends, hybridization enhances system resilience:

the complementary variability of the two energy sources at a seasonal scale helps to stabilize overall production. Moreover, the hybrid configuration enables strategic reservoir management by utilizing solar power for pumping in the spring to meet local water storage needs or maintaining higher environmental flows during summer months, thus compensating for the projected reduction in spring and summer run-off, affecting both reservoir inflows and downstream riverine habitats (Figure 53).

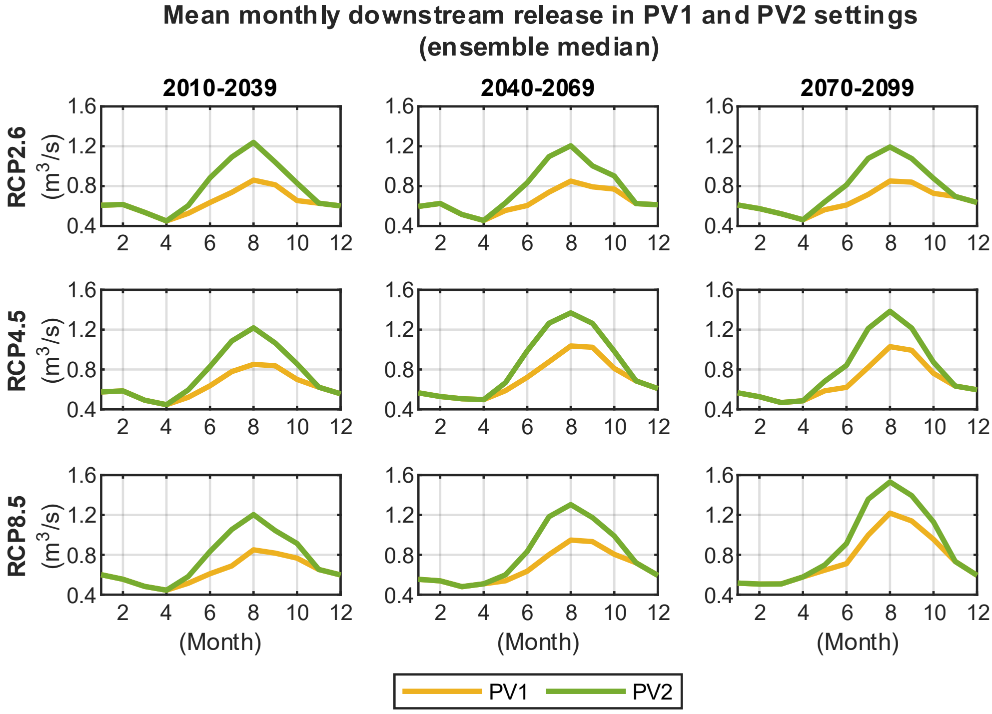

Figure 53 Multi-model ensemble median of 30-year average mean monthly downstream release in a setting without use of PV for mitigation of environmental stress (PV1) and with use of PV for reducing environmental stress in summer (PV2). The hybridization is detailed per each future period under different RCP scenarios.

3.4.4. Summary and recommendations from WP4 (part scenarios)

WP4 (part scenarios) assessed the potential for flexible operation of small hydropower (HP) plants in the Goms Valley using the CH2018 climate scenarios. The main conclusions are:

- Concerning future impacts local variability and changes of total energy potential are strongly governed by changes in the hydrological response (Discharge/RoR).
- Changes in Wind, Temperature, Radiation, Wind power and PV are found to be variable according to the adopted emission scenario, but no relevant location-dependent changes are found to be significant.
- PV show and increase in summer and a decrease in winter. RoR the other way round.
- Hybridization of hydropower plants with PV might be very attractive as long as storage of water is possible. We can confirm the literature recommendations that pumped-storage plants are the most promising for flexible operations.
- Best information for and from studies is achieved when a clear energy demand profile is available.

Recommendations

- RoR sensitivity to future climate should be the main criteria when assessing future potential for flexible operations of small plants in the Goms region and more in general in the European Alps.
- The exemplar analyses show that hybridization of hydropower with PV-Energy has large potential to accomodate both energy and environmental aspects.
- A careful planning of the storage of energy is key to optimize the flexibility of the system.

3.5 WP5 – Risk of air entrainment

Lead: ETHZ, partners: HEVS

The aim of this work package is to assess the risk of air entrainment into the pressurised system of hydropower plants (HPPs) operated flexibly. When parts of the headrace system are temporarily used as storage volume by lowering the water level, the transition between free-surface and pressurised flow is shifted or hydraulically altered. This can lead to undesired air entrainment.

To investigate this risk, a literature review was carried out to identify known mechanisms and consequences of air entrainment and air transport in power waterways. In parallel, a physical model of the Mörel HPP was built at VAW of ETH Zurich, where the influence of water level lowering on air entrainment could be experimentally studied.

In parallel to the physical experiment, numerical CFD simulations by HEVS was carried out (sect 3.5.3).

3.5.1. Literature review

Air entrapped in pressurised conduits is undesirable from both operational and safety perspectives. Stationary air pockets and entrained air bubbles cause additional head losses (backwater rise), reduce discharge capacity, and can promote corrosion. Moreover, entrained air can give rise to dynamic challenges in the form of unsteady flow behaviour, such as pulsations, pressure surges, and structural damage within the system. Of particular concern are air bubbles that rise to the soffit and accumulate into air pockets, which may blow back periodically once their volume reaches a critical size, or suddenly during shutdown. Due to these dynamic phenomena, the system components may be subject to unintended mechanical stresses (Möller, 2013). Air bubbles that reach the turbines can further reduce efficiency and, if imploding, potentially damage turbine components. In Pelton turbines, the sudden expansion of air bubbles at atmospheric pressure increases the spray angle of the jet (Figure 54), leading to reduced turbine efficiency (Staubli et al., 2009), and potentially cavitation erosion on the buckets (Mandal & Bajracharya, 2021).

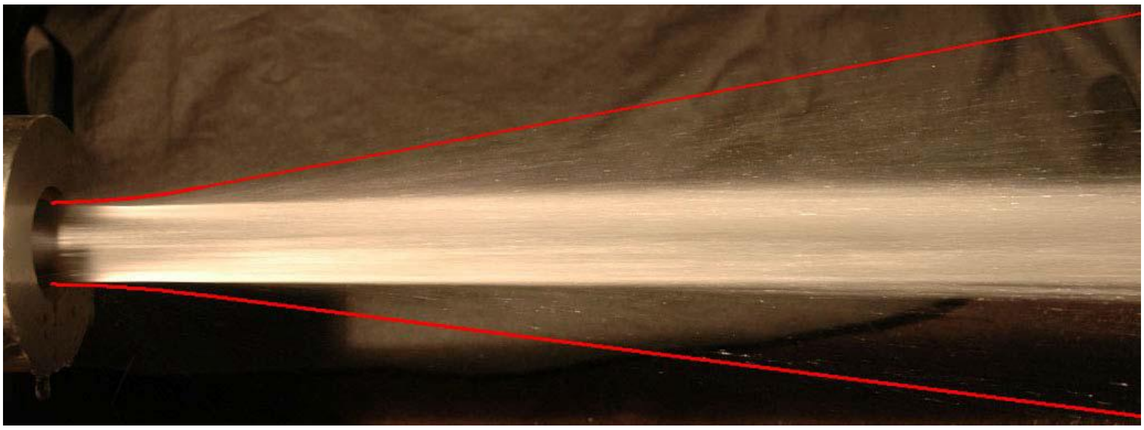

Figure 54: Jet dispersion due to air explosions, captured with a long exposure time (Staubli et al., 2009)

In addition to these hydraulic and mechanical effects, entrained air can dissolve under increasing pressure within the power waterway. When this pressurised water is released downstream, the rapid pressure drop can result in total dissolved gas (TDG) supersaturation. Prolonged exposure to elevated TDG levels can harm aquatic organisms, leading to gas bubble disease, where free gas bubbles form in blood vessels and tissues such as fins, eyes, and gills (Weitkamp and Katz, 1980). Recent assessments indicate that hydropower plants with secondary intakes and reaction turbines such as Francis or Kaplan turbines are particularly prone to TDG supersaturation, whereas Pelton turbines promote degassing and mitigate downstream effects (Pulg et al., 2024).

3.5.1.1. Air entrainment

The extent of air entrainment is commonly characterised by the relative entrainment rate, expressed as the ratio $\beta = Q_a/Q_w$ between the volumetric air (index *a*) discharge Q_a and the volumetric water (index *w*) discharge Q_w. The mechanisms governing this process depend on the flow conditions at the transition from free surface to pressurised flow. A lowering of the water level in power waterways causes a displacement of this transition and modifies the hydraulic conditions, which may give rise to air entrainment. Three processes are of relevance in this context. (1) Vortex-induced entrainment results from a rotational motion of the free-surface flow leading to a coherent surface vortex. (2) Air entrainment by a turbulent shear layer occurs when the impingement of an accelerated free-surface flow generates an unsteady shear interface with the pressurised flow, leading to air incorporation along the mixing layer. (3) Air entrainment by surface instabilities arises when growing disturbances at the water-air interface lead to the detachment and transport of air bubbles into pressurised flow.

(1) Vortex-induced air entrainment

Several investigations have addressed the occurrence of air-entraining vortices, with particular emphasis on pipe inlets in pump sumps and intake structures of hydraulic facilities. The development of such vortices is commonly described in terms of the circulation number N_Γ, which provides a measure of vortex strength. As the vortex strength increases, the core deepens until surface tension can no longer counteract centrifugal forces, at which point air bubbles are detached and entrained (Möller 2013). According to Alden Research Laboratory (ARL, Holden, USA), six vortex types (VT) can be distinguished (Figure 55): VT1 – coherent surface swirl, VT2 – surface dimple; coherent surface swirl, VT3 – dye core to intake; coherent swirl throughout the water column, VT4 – vortex pulling floating trash, but not air, VT5 – vortex pulling air bubbles, and VT6 – full air core to intake.

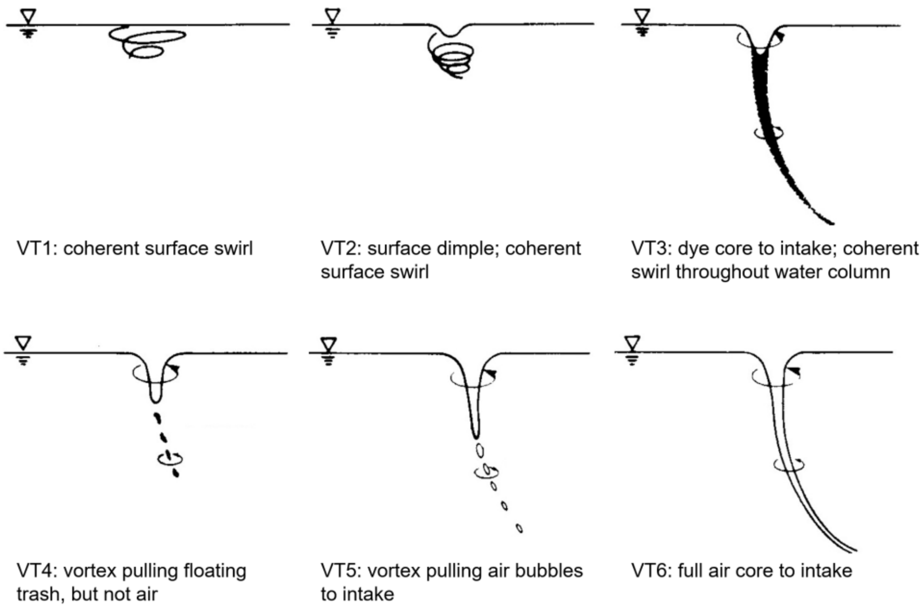

Figure 55: ARL vortex type classification (adapted from Möller, 2013)

The threshold for air entrainment by intake vortices is commonly described as the critical relative submergence depth $h_{s,cr} / D$ (*D*: diameter of the conduit) as a function of the intake Froude number, *i.e.* the pipe Froude number F_w (see Section 3.5.1.2). The most important approaches for predicting $h_{s,cr}$ at intakes of HPP are provided in Table 16. Gordon (1970) studied the flow at intakes of run-of-river HPPs with swirling flow problems, observing vortex formation during reservoir draw-down. Here, the characteristic length was defined as the height in the cross-section of the bulked-head gate, where also the velocity was measured. The two resulting design equations distinguish between symmetrical and asymmetrical approach flow conditions that are, however, not precisely defined. Gulliver et al. (1986) added more prototype investigations to Gordon's dataset and suggested more conservatively thresholds for the relative critical submergence $h_{s,cr}$ / D and F_w. Knauss (1987) recommended a linear relationship between the minimum relative critical submergence $h_{s,cr}$ and F_w as well as a minimum threshold of relative submergence for low Froude numbers. The equation is based on prototype observations with the intake Froude number is defined at the cross sections indicated with *d* or *b* in Figure 56.

It must be noted that the described studies reproduce strongly simplified geometries, not considering any site-specific, complex approach flow conditions. For evaluating the risk of vortex-induced air entrainment at specific hydraulic structures, hydraulic investigations remain necessary.

Table 16: Summary of the investigations on the critical relative submergence to avoid air entraining vortices.

Authors	**Criterion**	**Comment**
Gordon (1970)	$h_{s,cr} / D = 1.7F_w + 0.5D$	for symmetrical approach flow
	$h_{s,cr} / D = 2.3F_w + 0.5D$	for asymmetrical approach flow
Gulliver et al. (1986)	$h_{s,cr} / D > 1$ and $F_w < 0.5$	
Knauss (1987)	$h_{s,cr} / D = 2F_w + 0.5$ and $h_{cr}/D \geq 1…1.5$	

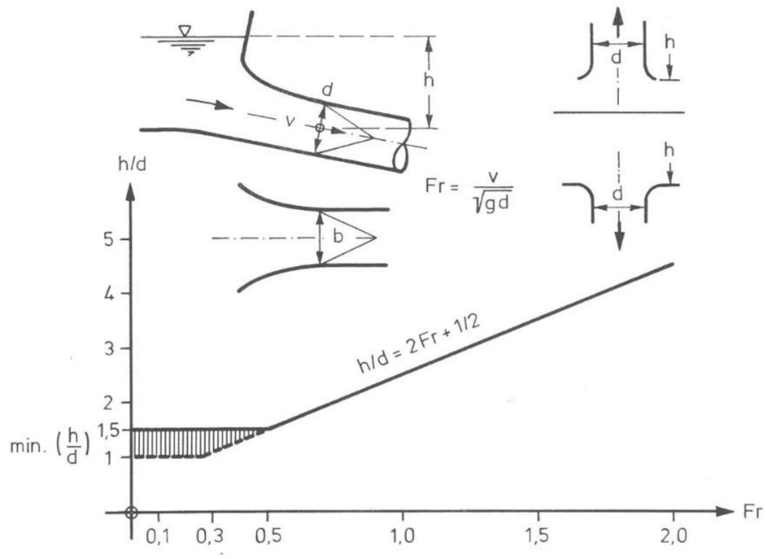

Figure 56: Relative critical submergence depth h_{cr}/D in function of intake Froude-Number F_w for intakes of HPPs (Knauss, 1987)

For the onset of air-entraining vortices at a horizontal intake, effects of viscosity and surface tension cannot be neglected. For an approximately correct modelling of these processes, the following threshold values must be observed according to Anwar et al. (1978):

- Radial Reynolds number $R_R = Q / (\nu h_s) > 3.0 \cdot 10^4$
- Weber number $W = v^2 \rho_w h_s / \sigma > 10^4$

with v : flow velocity, ν : kinematic viscosity of water, h_s : submergence height relative to intake axis, ρ_w : density of water and σ : surface tension.

(2) Air entrainment by impingement jet (turbulent shear layer)

Air entrainment by a turbulent shear layer occurs when a high-velocity free-surface jet impinges upon a slower pressurised flow, creating an unstable interface that induces air uptake. This process is governed by the velocity difference across the shear layer, turbulence intensity, and surface instabilities leading to bubble detachment and transport. Experimental studies have identified a critical onset velocity v_e for air entrainment, below which bubble formation does not occur. For instance, Bertola et al. (2018) observed that air bubbles begin to enter the flow when the impact jet velocity exceeds approximately 0.9...1.1 m/s, which is referred to as the onset velocity v_e.

$$\frac{\mu \cdot v_e}{\sigma} = 0.0109 \cdot \left(1 + 3.5 \cdot e^{-80 \cdot Tu}\right),$$

$$Tu = \frac{v'}{v},$$

with Tu : jet turbulence intensity, and v' : jet turbulence velocity at impingement.

Air entrainment in hydraulic jumps represents a specific case of shear-layer entrainment, occurring when supercritical free-surface flow transitions to pressurised or subcritical flow. Numerous studies have shown that the rate of air entrainment in hydraulic jumps can be described as a function of the Froude number at the jump toe F_0. Hydraulic jumps often develop downstream of submerged gates at low-level outlets. As a result, design equations frequently use the Froude number at the vena contracta F_c to estimate the expected air entrainment. The existing air entrainment equations and the experimental design of previous studies are summarised in Table 17.

Table 17: Design equations for air entrainment rate β through hydraulic jump in function of the Froude number F in the approach section (index 0) or in the vena contracta (index c) by various authors. Studies based on model tests are indicated with m, those based on prototype data with p. The dimensions (length L, slope S, width w and height h or diameter D) of the model facilities are indicated.

Authors	Equation	Data Source	Dimensions	F range
Kalinske & Robertson (1943)	$\beta = 0.0066(F_0 - 1)^{1.4}$ $\beta = 2.340F_0 - 5.248$	m	circular: D = 0.149 m, L = 10.7 m, S = [0, 30] %	2…30
Campbell & Guyton (1953)	$\beta = 0.04(F_c - 1)^{0.85}$	p		3…20
USACE (1964)	$\beta = 0.03(F_c - 1)^{1.06}$	p		3…40
Wisner (1967)	$\beta = 0.04(F_c - 1)^{0.85}$, $F_c < 6$ $\beta = 0.014(F_c - 1)^{1.4}$, $F_c > 6$	m & p	rectangular w = 1 m and 0.25 m, h = 0.1 m and 0.25 m, S = 0% *L not specified*	< 20
Sharma (1976)	$\beta = 0.0066(F_c - 1)^{1.4}$	m & p	rectangular: w = 0.1 m, h = 0.15 m, L = [2, 8] m S = 0%	6…40
Escarameia (2007)	$\beta = 0.0025(F_0 - 1)^{1.8}$	m	circular: D = 0.15 m, L = 3 m, S = [0, 41] %	1…3
Mortensen et al. (2011)	$\beta = 2.340F_0 - 5.248$	m	circular: D = [0.08, 0.59] m, L = [106, 53] D S = 4%	3…12

(3) Air entrainment by surface instabilities

When subcritical free-surface flow transitions to pressurised flow, air bubbles may detach from the water surface and become entrained into the pressurised flow (Figure 57). This entrainment is triggered by instabilities of the free surface, where surface waves grow until they promote bubble detachment. Such a mechanism can be interpreted as air entrainment by surface instabilities, in analogy to the destabilization processes at phase interfaces described by Wickenhäuser (2008).

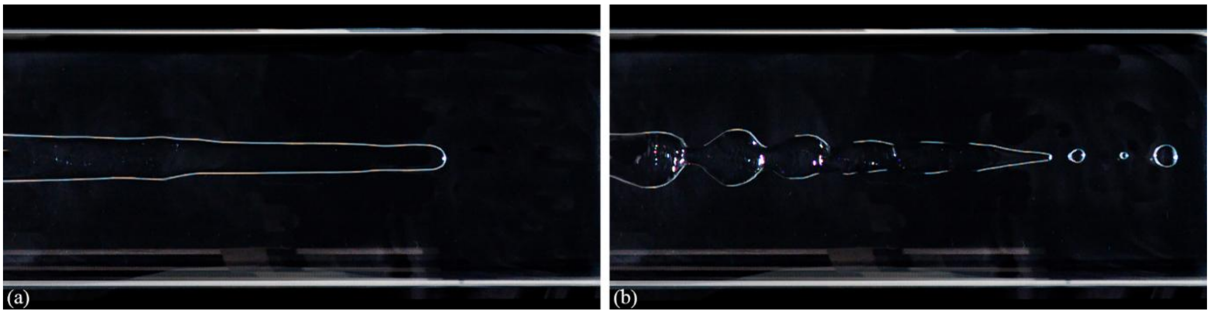

Figure 57: Observed transition from free surface to pressurised flow in an acrylic pipe with a slope *S* = 3.6‰ and diameter *D* = 0.19 m at (a) F_w = 0.20 and (b) F_w = 0.24 (top view). In (b) disturbance waves trigger air bubble detachment, resulting in their entrainment and transport.

3.5.1.2. Air transport

Once air has been entrained, a continuous air-water two-phase flow may develop downstream of the pressurisation. Such flows are described in terms of the superficial velocities U^s of the two phases, defined as the discharge of each phase divided by the total cross-sectional area *A*, *i.e.* for water and for air:

$$U_w^s = \frac{Q_w}{A}, \text{ and } U_a^s = \frac{Q_a}{A}$$

Based on these quantities, the pipe Froude number F_w (dimensionless superficial water velocity) and, in analogy, the air pipe Froude number F_a (dimensionless superficial air velocity) are introduced as

$$F_w = \frac{U_w^s}{\sqrt{gD}},$$

$$F_a = \frac{U_a^s}{\sqrt{\frac{\rho_w - \rho_a}{\rho_w} gD}},$$

with *g* = gravitational acceleration and ρ_a = densities of air.

Flow patterns

The commonly observed regimes of two-phase flow in closed horizontal conduits, i.e. air-water under pressure can be described as six distinct flow patterns, illustrated in Figure 58a (Rouhani & Sohal, 1983). Taitel & Dukler (1976) described the transition between these flow patterns theoretically and compared their results with data collected in a horizontal pipe with *D* = 0.025 m. A map of the flow patterns that develop as a function of the superficial water velocity U_w^s and the superficial air velocity U_a^s is provided in Figure 58b. At low air and water velocities, the flow is stratified with a smooth interface (SS: stratified flow, smooth. SS in contrast to free-flow conditions at atmospheric pressure). As the air velocity increases, the interface becomes wavy (SW: stratified flow, wavy). For increased water velocity, the air flow is intermitted by water, and elongated bubbles are transported at the pipe soffit (IP: intermittent flow, plug flow – also referred to as elongated bubble flow). At higher air velocities, water and air pockets alternate (IS: intermittent flow, slug flow). For very high water velocity and low air velocity, the air is transported as dispersed bubbles (DB: dispersed flow). At very high air velocity, the air accumulates at the centre and the water at the pipe wall (AA: annular flow).

Talley et al. (2015) characterise and visualise flow regime transition processes in horizontal gas–liquid two-phase flow.

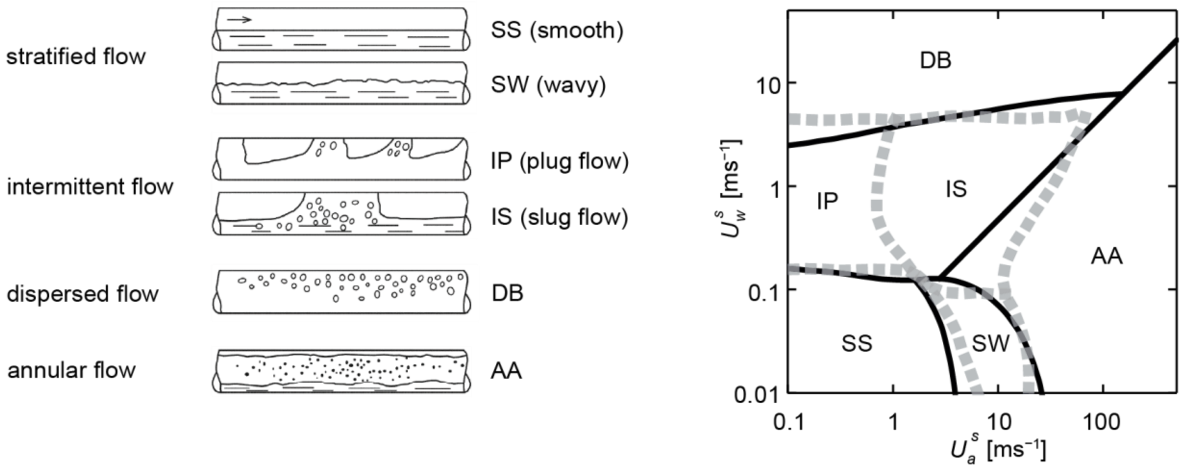

Figure 58: (a) Flow patterns according to Rouhani & Sohal (1983) (adapted from Hohermuth (2019)). (b) Comparison of theoretical (solid line) and observed (dashed line, data from Mandhane et al. (1974)) flow patterns in a horizontal pipe with D = 0.025 m (adapted by Hohermuth (2019) from Taitel & Dukler (1976)).

In hydraulic engineering applications the air velocity is generally limited by the drag of the water flow. As a result, for downward flow, the air velocity will not exceed the water velocity. The most commonly observed flow patterns of pressurised, downward air-water flow are therefore smooth stratified flow (SS) and elongated bubble flow (IP). As pipe diameters are generally larger in hydraulic engineering, the transition between the two patterns deviates from observations made in process engineering due to viscosity and surface tension effects. Wickenhäuser (2008) found that in horizontal to slightly inclined pipes ($S = 0\ldots1.7\%$) with $D = 0.484$ m the transition from stratified to elongated bubble flow occurs at higher superficial water velocities U_w^s than indicated in the flow pattern map by Rouhani & Sohal (1983) (Figure 59)

Bottin et al. (2014) illustrate the development of two-phase bubbly flow in a horizontal pipe with D = 0.1 m at the axial position x/D = 40 downstream of the inlet with the air bubbles being injected evenly across the inlet-section. This study also shows the flow patterns of stratified bubble (SB) and buoyant bubble (BB) flow during the development phase to a true dispersed bubble flow (Figure 59).

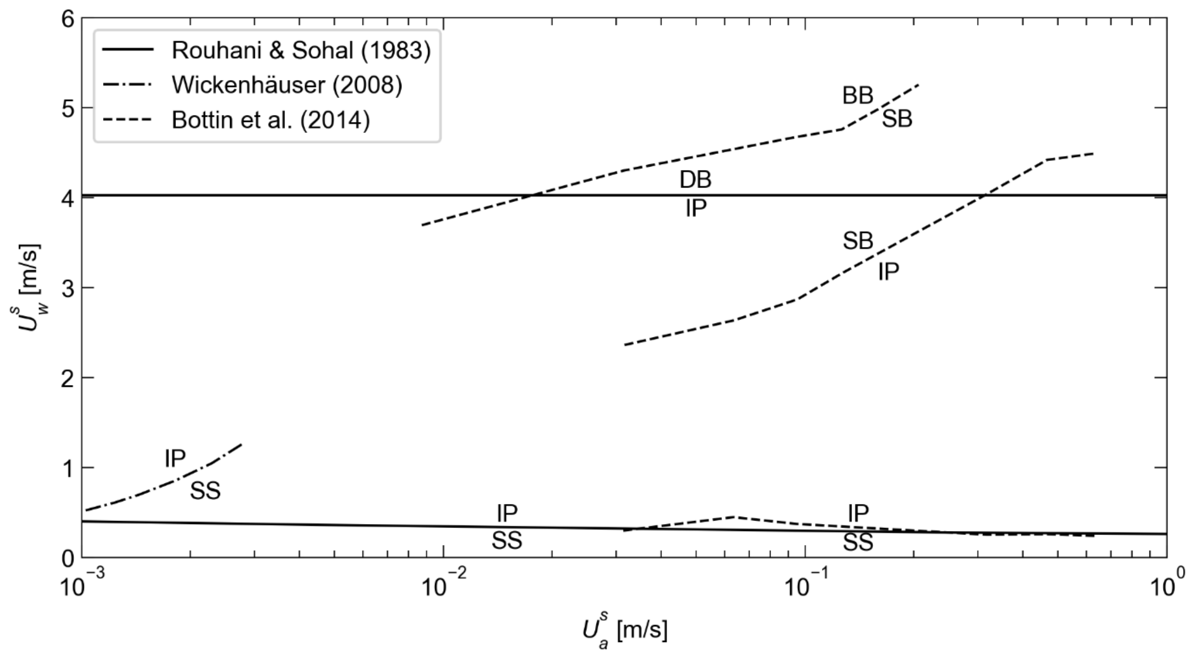

Figure 59: Regime transitions observed by Wickenhäuser (2008) in a horizontal pipe with D = 0.484 m from smooth stratified (SS) to elongated bubble (IP) flow (–·), and in the development phase 4 m downstream the inlet in a pipe with D = 0.1 by Bottin et al. (2015) from SS to IP, IP to stratified bubble (SB) and SB to buoyant bubble (BB) flow (--) in comparison with the flow pattern map by Rouhani & Sohal (1983) (—); adapted by VAW.

Kalinske & Robertson (1943) and Pothof & Clemens (2010) described similar flow patterns observed during model tests in downward sloping pipes. Kalinske & Robertson (1943) carried out their model tests in a pipe with D = 0.149 m at slopes between 0.2% and 30%, producing a hydraulic jump downstream of a sliding gate. Pothof & Clemens (2010) continuously injected air in the upstream horizontal section of a pipe with D = 0.22 m and let it accumulate to a large air pocket at the mitre bend into a downward slope with angles between 5° and 90°. Figure 60 visualises the observed flow patterns:

1. Stratified flow: The air pocket accumulating downstream of the hydraulic jump (Kalinske & Robertson, 1943) or at the mitre bend (Pothof & Clemens, 2010) fills the entire sloping reach, creating stratified flow conditions. All entrained air reaches the bottom of the slope where an air-entraining hydraulic jump establishes.
2. Blow-back flow: One (2a) or more (2b) air pockets form in the sloping reach, which include an air-entraining hydraulic jump at their downstream end. The air entrained by each hydraulic jump coalesces to form another air pocket. Periodically, the downstream air pockets blow out, i.e. rapidly move upstream, into the topmost air pocket. The air entrainment rate thus exceeds the average air transport capacity of the pipe flow.
3. Plug flow: The entrained air accumulates to air pockets, which are transported downstream. Hydraulic jumps within the air pockets are absent. Full air transport capacity is reached in this regime.
4. Bubbly flow: Air accumulation to larger pockets does not occur. All entrained air is transported as dispersed bubbles or small plugs.

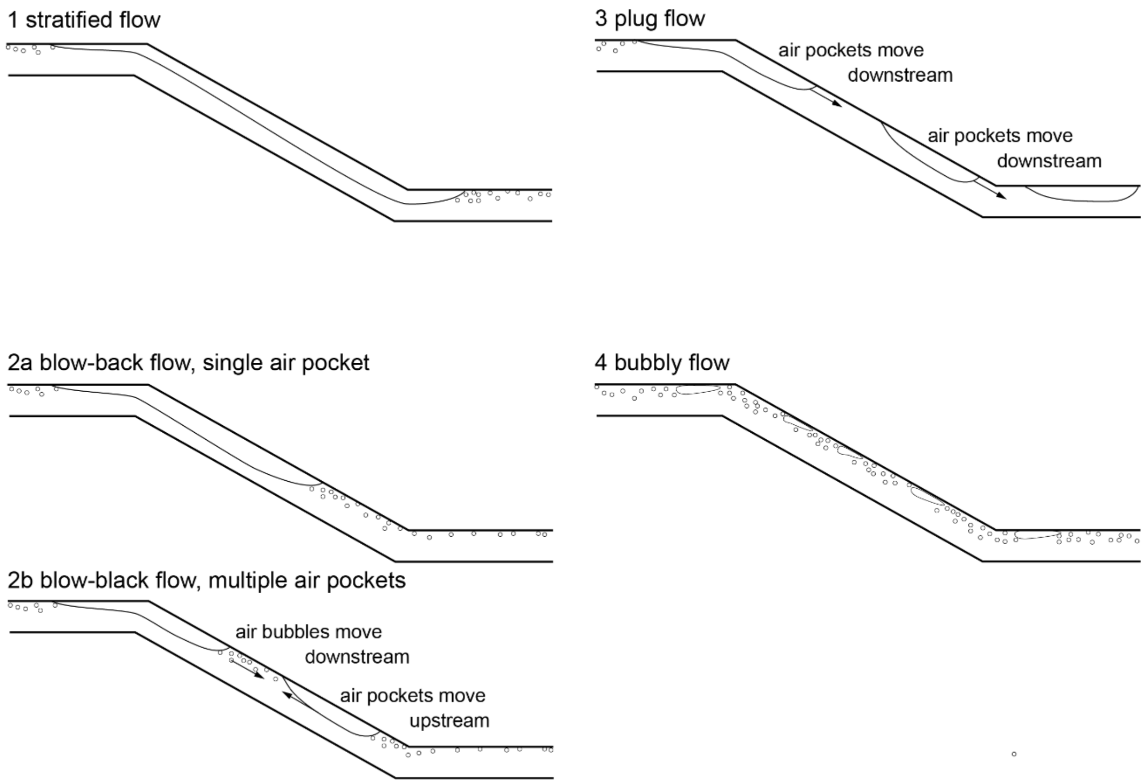

Figure 60: Visualization of the flow regimes described by Kalinske & Robertson (1943) and Pothof & Clemens (2010) for the experimental set-up of Pothof & Clemens (2010).

<u>Transport of single air bubbles or pockets</u>

The movement of individual bubbles or air pockets in pipes is governed primarily by inertial and gravitational forces. Depending on their shape, size, and the superficial water velocity U_w^s, air pockets may move upstream against gravity because of their buoyancy, or downstream if the drag on them exceeds their buoyancy. The threshold condition is expressed by the critical pipe Froude number $\mathsf{F}_{w,c}$, commonly referred to as the clearing flow number. Assuming constant bubble shape and a linear scaling of bubble diameter with pipe diameter, the equilibrium of forces for a stationary air pocket reduces to

$$\mathsf{F}_{w,c} = C_0 \sqrt{\sin\alpha} + C_1 ,$$

with coefficients C_0 and C_1 that can stem from laboratory data and α is the pipe inclination angle.

Table 18 summarises the empirical constants and the tested pipe diameters and angles of relevant studies from the literature. Kent (1952) suggested a relationship for air pockets with $L_b/D > 1.5$, where L_b = bubble length, although his own experimental data showed systematic deviations from the suggested formula, as later highlighted by Wisner et al. (1975). Wisner et al. (1975) compared their dataset with those of Kalinske and Robertson (1943) and Kent (1952), and defined a conservative envelope curve representing a lower bound for $\mathsf{F}_{w,c}$. Falvey (1980) pointed out that the motion of air bubbles and air pockets have to be considered distinctly, and that in the intermediate zone air bubbles and air pockets can move in opposite directions simultaneously, leading to a blow-back flow regime. Based on physical model experiments Escarameia (2007) proposed empirical constants as a function of the relative air pocket size $n = (4\ V_b)/(\pi\ D^3)$, where V_b is the air pocket volume.

Table 18: Empirical coefficients presented in the literature for the design equation of the critical pipe Froude number in the form $F_{w,c} = C_0\sqrt{\sin\alpha} + C_1$.

Authors	Coefficients	Experimental layout
Kent (1952)	C_0 = 1.23 C_1= 0	D = 0.1 m α = 15…75°
Wisner et al. (1975)	C_0 = 0.25 C_1= 0.825	D = 0.245 m α = 18.4°
Escarameia (2007)	C_0 = 0.56 $C_1 = \begin{cases} 0.45 & for \quad n < 0.06 \\ 0.50 & for \quad 0.06 \le n < 0.12 \\ 0.57 & for \quad 0.12 \le n < 0.30 \\ 0.61 & for \quad 0.30 \le n < 2.00 \end{cases}$	D = 0.15 m α = 0…22.5°

Wickenhäuser & Kriewitz (2009) carried out large scale model tests in horizontal to slightly inclined pipes (S= 0.4…8.7%) with a diameter of 0.484 m, revealing that the air flow number of the transported air $F_{a,t}$ increases with increasing pipe Froude number F_w. A critical F_w = 0.25 has to be exceeded for the air to be transported downstream. This means precisely that 1% of the air entrained is transported ($F_{a,t}$), while 99% rises back upstream. For F_w > 0.25 the entrained air is entirely or partially transported. This threshold is seen as the initiation of air transport and contrasts with $F_{w,c}$, at which all the air is transported downstream. The transported air discharge $F_{a,t}$ increases with increasing F_w and decreases with increasing pipe slopes S. For a given water pipe number F_w and slope there is a threshold value of transported air discharge $F_{a,t\max}$ representing a maximum air transport capacity. The results are presented in Figure 61, showing that the transport capacity features a high rate of decrease for smaller slopes and gets smaller for steeper slopes. However, the study investigated a rather limited range of slopes and pipe flow numbers.

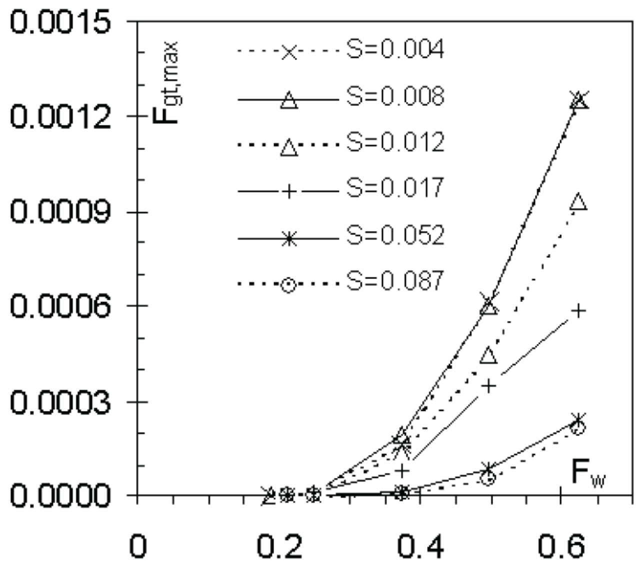

Figure 61: Air flow number of the maximum transported air $F_{a,t\max}$ as a function of the pipe slope S and the pipe Froude number F_w (Wickenhäuser, 2008).

Continuous air-water flow

The previous considerations refer to single air bubbles or pockets. However, air continuously entrained different bubble sizes can be expected to behave differently, as the clearing flow number $F_{w,c}$ for a single bubble varies depending on its volume and shape. Moreover, *e.g.* Kalinske & Robertson (1943) observed that small bubbles transported downstream coalesce to air pockets, which could become large enough to move upstream.

Pothof & Clemens (2010) investigated continuous air-water flows and described the transition from blow-back flow to plug flow as a critical condition corresponding to the attainment of the critical pipe Froude number $F_{w,c}$. At this transition, the air pockets remain stationary while hydraulic jumps at the downstream end of each pocket entrain the same volume of air as is introduced upstream. For this balance to hold, the tailwater depth beneath each air pocket must reach a constant value, since the air entrainment rate by a hydraulic jump depends on the Froude number at the jump toe. Based on the observation that the acceleration length under the air pocket is sufficient for the water flow to develop close to the uniform flow depth h_n, Pothof & Clemens (2010) derived the following analytical expression for the critical pipe Froude number:

$$F_{w,c1.5}(\alpha) = \frac{2\sin\alpha}{\lambda}\frac{D_h}{D}\left(\frac{A_n}{A}\right)^2 = \frac{A}{A_b}\frac{\cos\alpha}{\pi}\left[\frac{2}{3}\sqrt{\frac{4h_n}{D}-\left(\frac{2h_n}{D}\right)^2}\left(\frac{2h_n}{D}-3\right)\left(\frac{2h_n}{D}-\frac{1}{2}\right)+\arcsin\left(1-\frac{2h_n}{D}\right)+\frac{\pi}{2}\right], \quad \text{for}$$

$$F_a = 1.5\cdot 10^{-3}$$

where λ = friction factor, D_h = hydraulic diameter, A_n = cross-sectional area at uniform flow condition, and A_b = bubble cross-section.

It should be noted that the equation has been modified here, as the original publication contains a typographical error. The formulation was found to be in good agreement with experimental data at an air pipe Froude number of $F_a = 1.5\cdot 10^{-3}$. Pothof and Clemens (2011) extended their analysis and demonstrated that the air transport capacity increases exponentially with F_a. On this basis, they proposed the following relationship for the critical pipe Froude number as a function of the air pipe Froude number:

$$F_{w,c}(F_a,\alpha) = F_{w,c1.5}\cdot\ln\left[\left(\frac{F_a\times 10^7}{1.87}\right)^{\frac{1}{9}}\right]$$

Scale effects and model similitude

Froude scaling provides an appropriate framework for modelling air transport in closed conduits because the underlying force balance is primarily governed by inertia and gravity. However, Froude scaling ensures only geometric and kinematic similarity, while viscous and surface tension forces are not correctly scaled, i.e. full dynamic similarity is not achieved. The bubble geometry is governed by the Eötvös number

$$Eo = \frac{(\rho_w - \rho_a)gD^2}{\sigma},$$

which represents the ratio of gravitational to surface tension forces, with σ = surface tension at the water-air interface. The influence of surface tension decreases with increasing pipe diameter, and studies suggest that viscosity and surface tension effects become negligible for D > 0.175 m (Zukoski, 1966; Viana et al., 2003). In close agreement with the former, Pothof and Clemens (2011) showed that the effect of pipe diameter on the clearing flow number diminishes for D > 0.15 m and recommended a criterion of Eo > 5000, corresponding to D > 0.19 m for reliable investigation of $F_{w,c}$. The studies by Wisner et al. (1975), Escarameia (2007), and Pothof and Clemens (2011) satisfy this criterion.

3.5.2. Physical model experiments – case study KW Mörel

To determine the operational drawdown limit imposed by the risk of air entrainment, water-level lowering was investigated by means of physical model experiments. A scale model of HPP Mörel was constructed at the Laboratory of Hydraulics, Hydrology and Glaciology (VAW), ETH Zurich. The experiments aimed to analyse water-level lowering under different load cases, identify the associated air-entrainment mechanisms, and define threshold drawdown heights.

3.5.2.1. Experimental design

The physical model was designed according to Froude similitude with a geometric scale factor of $\lambda = 16.04$, giving a pipe diameter of $D = 0.19$ m, compliant with criterion for minimal scale effects. It covers a total reach of 165 m along the tunnel axis, compromising the last section of the free-flow headrace tunnel (30 m), the overflow chamber with the profile transition (31 m), the operational section of the original pressurised headrace tunnel (67 m), the connecting tunnel (27 m), and the first section of the new headrace tunnel (40 m) (Figure 62). The latter was simplified to be straight and horizontal, and was equipped with a de-aeration shaft, which is not present in the prototype. The free-flow headrace tunnel and the chamber were built from PVC and acrylic glass, while the adjacent pressurised headrace tunnel was realized in transparent acrylic pipe sections. Two automated valves allowed a controlled model inflow Q_{in} and outflow Q_{out} operation of the model. Instrumentation comprised two magnetic-inductive flow meters (MID) at the inlet and outlet, twelve relative pressure sensors, and one absolute pressure sensor installed in the deaeration shaft, enabling quantification of air transport. The physical model experiments covered five discharges Q = 5, 10, 15, 20, and 24 m^3/s.

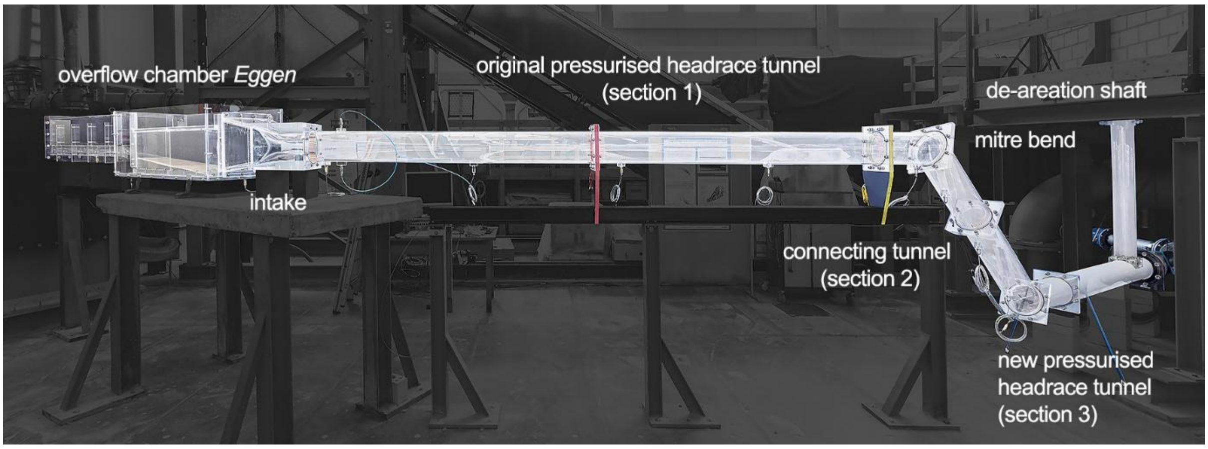

Figure 62: VAW physical model at scale 1:16.04

The examination of the air entrainment mechanisms was carried out under quasi-steady conditions ($Q_{in} \approx Q_{out}$) giving a total of 5 load cases LC (LC_05, LC_10, LC_15, LC_20, LC_24). A gradual drawdown of the water level was induced by setting Q_{out} slightly higher than Q_{in}, which produced a slow lowering of the water level, allowing for a systematic observation of the entrainment mechanisms at different water levels. Besides the entrainment of air, the entrainment of paper chads, manually added to the flow, was documented. The flow conditions were recorded by pressure measurements, and the entrainment mechanisms were documented by video recording.

The qualitative observations of the water level draw-down were made for steady inflow discharges Q_{in} = 5, 10, 15, and 20 m^3/s and transient outflow discharges increasing to Q_{out} = 10, 15, 20, and 24 m^3/s. This gives a total number of 10 load cases (LC_05-10, LC_05-15, LC_05-20, LC_05-24, LC_10-15, LC_10-20, LC_10-24, LC_15-20, LC_15-24, LC_20-24). The draw-down was documented by video recording at three camera positions.

3.5.2.2. Air entrainment mechanisms

Air entrainment into the pressurised system was observed at two locations (Figure 63).

a) At the intake of the original pressurised headrace tunnel (section 1), at water levels in the overflow chamber H_{oc} > 984.41 m a.s.l., i.e. pressurised flow in the circular headrace tunnel. Z = 984.41 m a.s.l. corresponds to the level of the soffit at the end of the intake structure.

b) At the mitre bend between section 1 and the connecting tunnel (section 2), at H_{oc} < 984.17 m a.s.l., i.e. free-surface flow along section 1. Z = 984.17 m a.s.l. corresponds to the level of the soffit at the mitre bend.

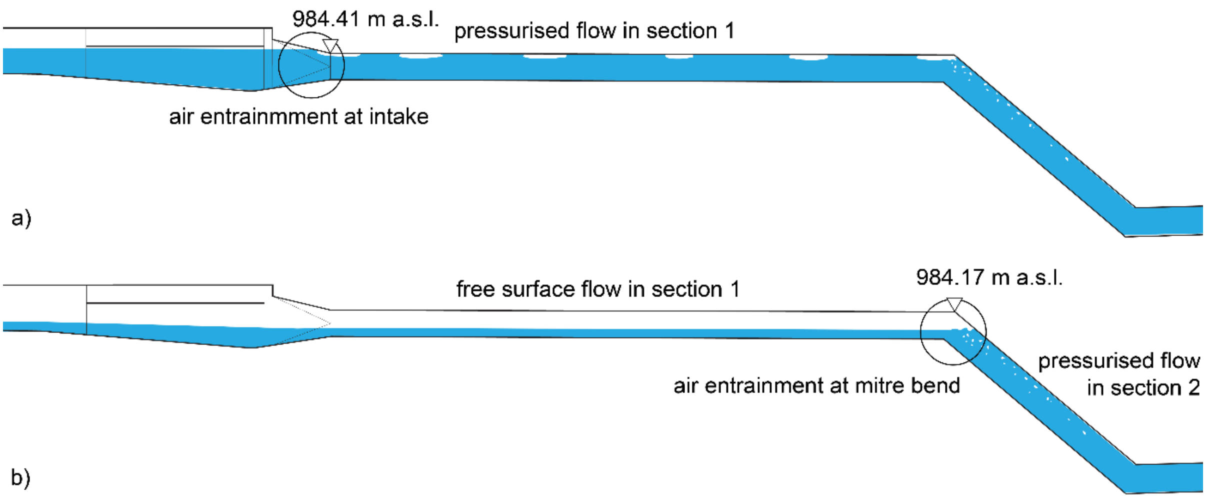

Figure 63: Air entrainment at a) the intake, and b) the mitre bend between section 1 and 2

a) Air entrainment at the intake

At the intake of the original pressurised headrace tunnel (section 1), instabilities of the free-surface in the overflow chamber and air entrainment into the pressurised section 1 were observed for the higher discharges (Q = 15, 20, and 24 m^3/s). Figure 64a shows the onset of air entrainment, considered as critical condition at which air bubbles detach from the free surface for those quasi-stationary load cases. At further lowering of the water level the air entrainment became continuous leading to elongated bubbly flow in section 2, as shown in Figure 64b. The flow conditions at which the onset and continuous air entrainment at the intake occurs is summarised in Table 19.

The visual observations show that the air entrainment mechanism is governed by surface instabilities, where disturbances at the free surface grow and eventually lead to the detachment of air bubbles. The occurrence of this air entrainment mechanism can be related to the pipe Froude number at the transition (sect. 3.5.1.1). The transition from the overflow chamber to the closed conduit induces a contraction of the flow area and a corresponding acceleration of the flow. The cross-sectional area, i.e. the flow velocity, at the transition from free-surface to pressurised flow depends on the water level in the overflow chamber H_{oc}. Under normal operation conditions (H_{oc} = 985.13 m a.s.l.), the pipe Froude number at the transition ranges between F_w = 0.05…0.25 for Q = 5 m^3/s…24 m^3/s. At lower water levels H_{oc}, F_w increases.

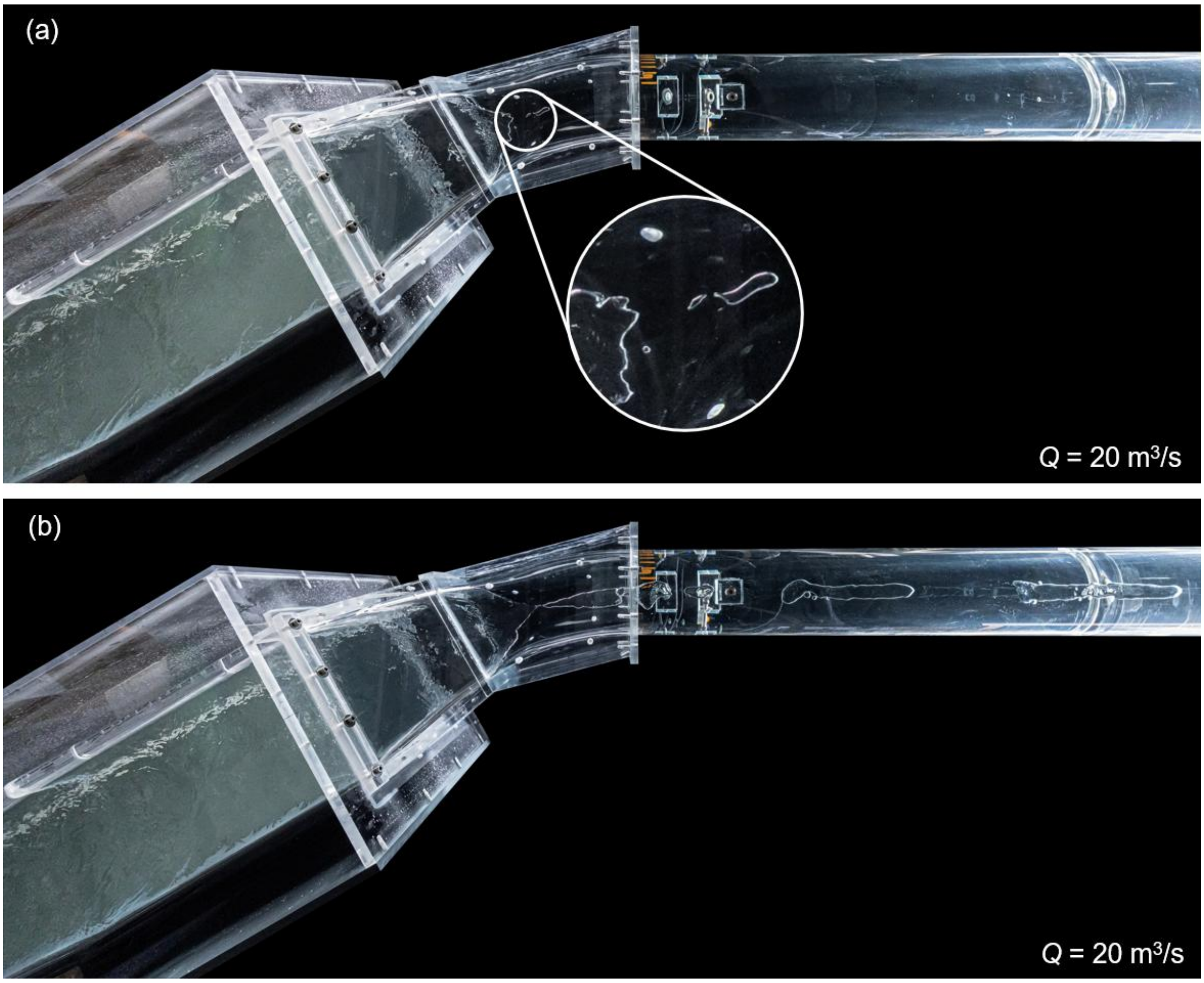

Figure 64: (a) Onset of air entrainment at the intake due to instabilities at the free surface leading to air bubble detachment and (b) continuous air entrainment at the intake due to instabilities at the free surface leading mainly to elongated bubbly flow in section 1.

Table 19: Critical water level at onset and continuous air entrainment in the overflow chamber $H_{oc,cr}$, water level drawdown ΔH_{oc} and pipe Froude number F_w at the transition from free surface to pressurised flow in the profile transition between the overflow chamber and the circular headrace tunnel.

Q [m³/s]	*entrainment type*	$H_{oc,cr}$ [m a.s.l.]	ΔH_{oc} [m]	F_w [-]
5	---------------------------- *not observed* ----------------------------			
10	---------------------------- *not observed* ----------------------------			
15	onset	984.69	0.44	0.24
15	continuous	984.54	0.59	0.30
20	onset	984.93	0.20	0.25
20	continuous	984.66	0.47	0.34
24	onset	985.19	-0.06	0.24
24	continuous	985.13	0.00	0.25

As summarised in Figure 65 and Table 19, the onset of air entrainment was consistently observed within a narrow range of pipe Froude numbers F_w = 0.24…0.25 across the investigated load cases, while continuous air entrainment occurred for F_w = 0.25…0.34. These findings are in good agreement with the results reported by Wickenhäuser & Kriewitz (2009), who identified a threshold of F_w = 0.25 for the onset of air transport (see Figure 61). Although the underlying mechanisms differ, the comparison indicates that the onset of bubble detachment observed in the present study occurs within a similar range of hydraulic conditions. The absence of air entrainment for Q = 5 and 10 m³/s, corresponding to maximum Froude numbers of F_w = 0.12 and F_w = 0.25, is consistent with this threshold interpretation.

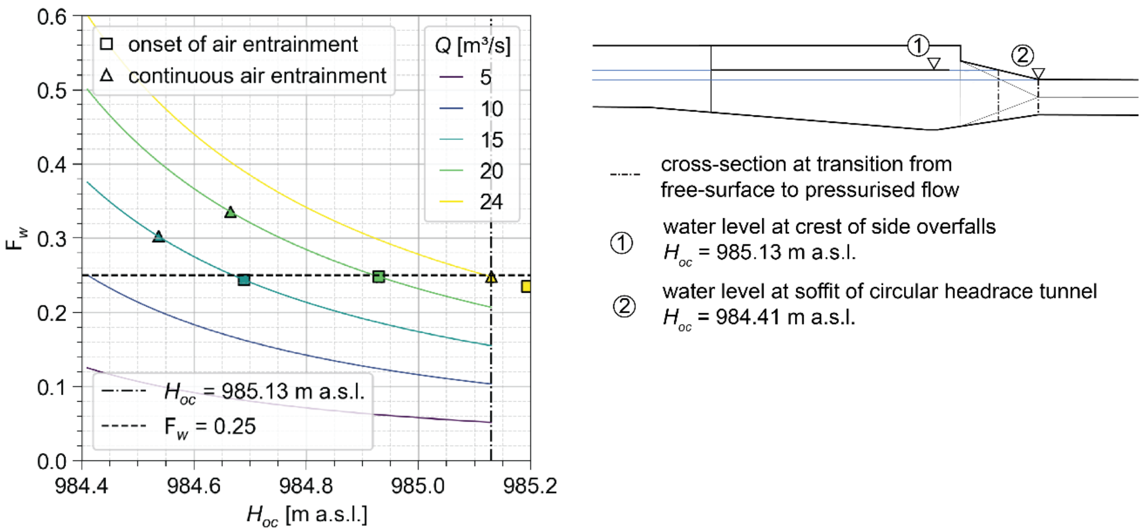

Figure 65: Pipe Froude number F_w observed at the onset and continuous air entrainment compared to with the threshold value for air transport F_w = 0.25 documented by Wickenhäuser (2008).

b) Air entrainment at the mitre bend

The air entrained at the outlet of the overflow chamber was transported in elongated bubbly flow along section 1 of the circular headrace pipe towards the mitre bend to section 2. Visual observations showed that at Q = 24 m³/s, all entrained air was further transported in section 2; for Q = 20 m³/s, only part of it was transported; and for Q = 15 m³/s, all entrained air accumulated at the mitre bend. This indicates that for Q = 20 and 24 m³/s, air entrainment at the mitre bend already occurred due to surface instabilities under pressurised flow conditions in the circular headrace pipe for velocities v > 0.7 m/s in the physical model (H_{oc} > 984.41 m a.s.l.). The control section for these load cases is therefore located at the outlet of the overflow chamber. In contrast, for Q = 5, 10, and 15 m³/s, air entrainment occurred only at lower degrees of partial filling in the circular headrace pipe. For these load cases, where the control section is at the mitre bend, four distinct air-entrainment mechanisms were identified (see Figure 66).

The first observation was the entrainment of paper chads at the water surface, by a vortex-like flow structure, which was classified as *pronounced VT4* (Figure 55). The *onset of VT5* was defined as the entrainment of the first air bubble into the pressurised system, which is defined as the onset of air entrainment in the model scale, following the definition by Bertola et al. (2018). This first bubble was later followed by more singular air bubbles, which, at first, were entrained at an unsteady rate, however with an interval of less than a minute. The moment when the entrainment rate was deemed continuous, was classified as *pronounced VT5*. Finally, air entrainment by an impingement jet was observed at the transition from the low-slope tunnel to the shaft with approach flow velocities higher than $v_e \approx$ 1 m/s. This phenomenon was attributed to the abrupt change in slope and tunnel curvature, which generated an acceleration of the flow and a turbulent shear layer at the impingement of the pressurised flow.

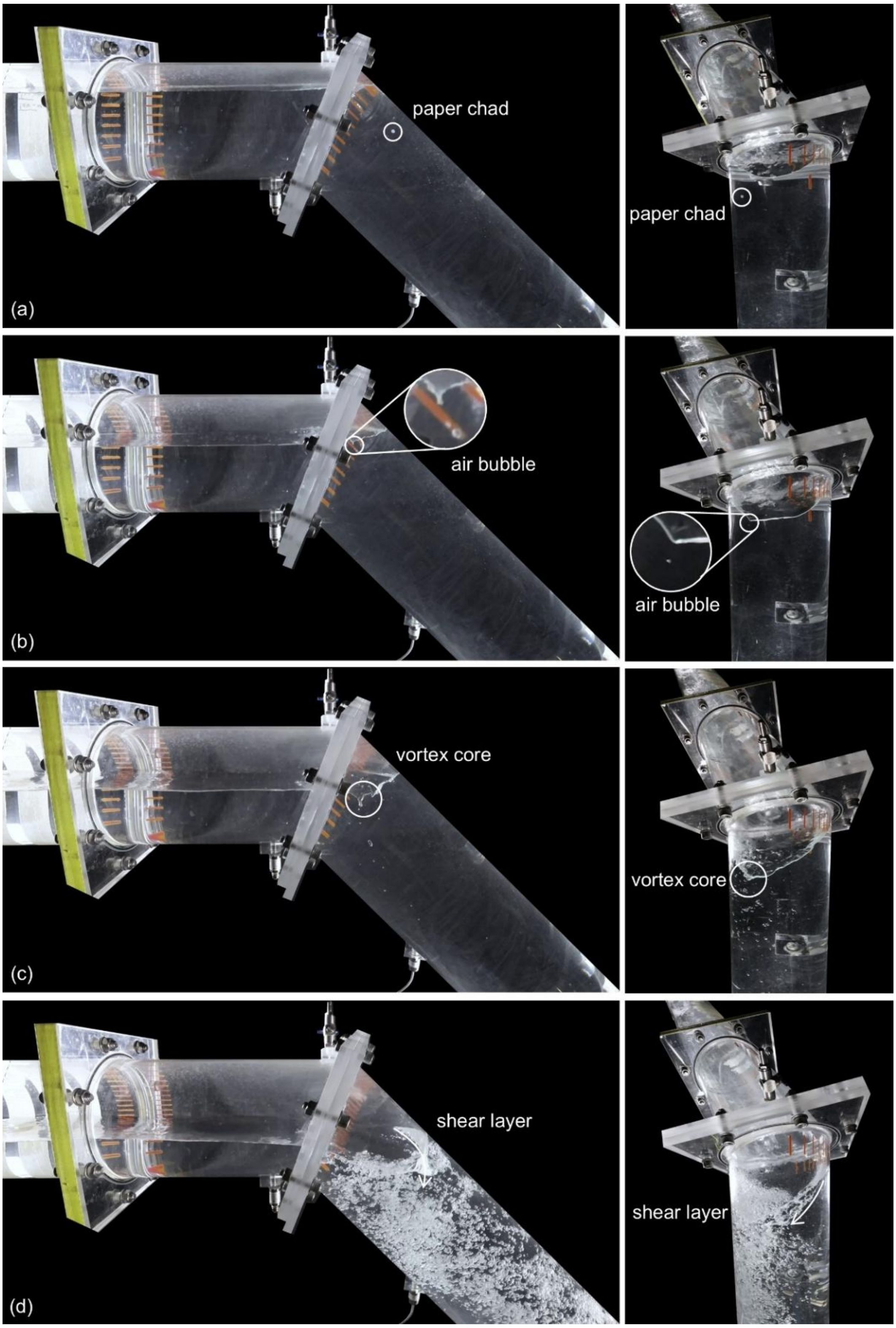

Figure 66: Side and top view of the four entrainment mechanisms at the mitre bend for Q = 10 m^3/s: (a) entrainment of paper chads (pronounced VT4), (b) entrainment of first air bubble (onset of VT5), (c) continuous air entrainment (pronounced VT5), and (d) air entrainment into the shear layer by an impingement jet

Table 20 summarises the occurrence of the different entrainment mechanisms across the load cases, including the corresponding water level in the overflow chamber H_{oc} and the associated drawdown height ΔH_{oc}. To quantitatively characterise the occurrence of air entrainment mechanisms and to evaluate the effects of viscosity and surface tension on the onset of air-entraining vortices, the flow conditions immediately upstream of the mitre bend (subscript 0) were evaluated. The measured flow depth h_0, the partial filling ratio Y_0, the approach flow velocity $v_{o,M}$, the Froude number F_0, the radial Reynolds $R_{R,M}$ and the Weber W_M numbers in the model (subscript M) at the onset of each entrainment mechanisms are given in Table 20. The approach flow depth h_0 is considered as the reference length and thus as the characteristic measuring unit for the submergence depth h_s in order to calculate $R_{R,M}$ and W_M (see eq. given in sect. 3.5.1.1).

Table 20: Occurrence of entrainment mechanisms with corresponding water levels in the overflow chamber and flow conditions upstream of the bend. The approach flow velocity $v_{0,M}$, the radial Reynolds number $R_{R,M}$ and the Weber number W_M are specified for model conditions.

Load case		Overflow chamber		Mitre bend approach flow					
Q [m³/s]	entrainment type	H_{oc} [m a.s.l.]	ΔH_{oc} [m]	h_0 [m]	Y_0 [-]	$v_{0,M}$ [m/s]	F_0 [-]	$R_{R,M}$ [-]	W_M [-]
15	*pronounced VT4*	-	-	-	-	-	-	-	-
15	*onset of VT5*	983.82	1.31	2.25	0.74	0.65	0.56	$1.0 \cdot 10^5$	500
15	*pronounced VT5*	983.72	1.41	1.96	0.64	0.75	0.74	$1.2 \cdot 10^5$	435
15	*shear layer*	983.73	1.40	1.47	0.48	1.07	1.28	$1.6 \cdot 10^5$	326
10	*pronounced VT4*	983.85	1.28	2.54	0.83	0.38	0.29	$6.1 \cdot 10^4$	251
10	*onset of VT5*	983.31	1.82	1.84	0.60	0.54	0.55	$8.3 \cdot 10^4$	182
10	*pronounced VT5*	983.29	1.84	1.48	0.49	0.71	0.84	$1.0 \cdot 10^5$	146
10	*shear layer*	983.27	1.86	1.17	0.38	0.97	1.33	$1.3 \cdot 10^5$	115
5	*pronounced VT4*	982.83	2.30	1.60	0.53	0.32	0.36	$4.8 \cdot 10^4$	39
5	*onset of VT5*	982.65	2.48	1.33	0.44	0.41	0.52	$5.8 \cdot 10^4$	33
5	*pronounced VT5*	982.62	2.51	1.02	0.34	0.58	0.86	$7.5 \cdot 10^4$	25
5	*shear layer*	982.64	2.49	0.75	0.25	0.89	1.55	$1.0 \cdot 10^5$	19

The data reveals a decoupling between the water level in the overflow chamber and the water level in the circular headrace tunnel. Specifically, while H_{oc} decreases between the occurrence of *pronounced VT4* and the *onset of VT5*, it remains essentially constant as the water level in the tunnel continues to lower. This behaviour was observed consistently for all investigated load cases (Q = 15, 10, and 5 m³/s). Once equilibrium flow conditions are established in the overflow chamber, its water level cannot fall further; any additional volume required to sustain the slightly increased outflow is supplied from the downstream headrace tunnel. This has direct implications for the practical implementation of flexible operation. Since the chamber is accessible and equipped with a level gauge, operational control would rely on its water level. However, once the water level in the chamber reaches equilibrium conditions, water levels in the tunnel and chamber decouple, resulting in a potential loss of control over the downstream hydraulic conditions and compromising operational safety.

The flow conditions at the mitre bend at the occurrence of the entrainment mechanisms are visually summarised in Figure 67. With the emptying of the tunnel, *i.e.* the decrease in partial filling ratio Y_0, the approach Froude number F_0 increases. The data reveals, that the entrainment mechanisms occur at similar approach Froude numbers across the load cases: The entrainment of paper chads (*onset of VT4*) occurs at F_0 = 0.29...0.39, entrainment of the first air bubble (*onset of VT5*) at F_0 = 0.52…0.56, continuous air entrainment (*pronounced VT5*) at F_0 = 0.74...0.86, and air entrainment and air entrainment due to the jet impingement at F_0 = 1.28…1.55, where $v_{0,M}$ corresponds well with the critical onset velocity v_e for air entrainment (see Table 20, sect. 3.5.1.1). The latter is below uniform flow conditions, *i.e.* there is a water level drawdown at the mitre bed towards the steeply inclined section, leading to an acceleration of the flow.

In the literature, air-entraining intake vortices are typically reported for approach flows characterized by an approach Froude number F_0 smaller than the intake Froude number F_w, i.e. under conditions of flow acceleration towards the intake (Table 16). In contrast, the present case exhibits an inverse behaviour: the approach flow is faster, and the flow decelerates during pressurisation. Figure 68 compares the intake geometry described by Knauss (1987) with the current configuration, showing that the critical relative submergence $h_{s,cr}/D$ can be interpreted analogously to the partial filling ratio $Y_0 = h_0/D$ (Table 20). Accordingly, Figure 67b contrasts the air-entrainment threshold proposed by Knauss (1987), derived from prototype observations, with the thresholds observed in the physical model. For the investigated load cases, the intake Froude numbers, i.e. the pipe Froude number F_w are below 0.5, which according to Knauss (1987) would require a minimum submergence of $h_{s,cr}/D$ = 1.0…1.5 to prevent air entrainment at an intake. In contrast, extending the curve $Y_{0,cr} = 2\ F_w + 0.5$ to values of $Y_0 = 0.5$ seems to correspond well with the observed situation at the mitre bend regarding the critical flow depth $h_{0,cr}$ required to prevent air entraining vortices. However, the onset of entrained paper chads (VT4) observed in the physical model lies below the extended empirical relationship, and not above the curve, where it would be expected as a non-air-entraining vortex type if the relationship were valid.

Froude scaling preserves only geometric and kinematic similarity, while viscous and surface tension effects are not correctly scaled (sect. 3.5.1.1). The relatively low observed Weber numbers $W_M < 10^4$ indicate that surface tension influences the onset of air-entrainment in the physical model (Table 20), thus the observed entrainment mechanisms are subject to scale effects. It means, that a vortex capable of entraining paper chads in the model is expected to entrain air in the prototype. For intake vortices, it is common practice to increase the vortex type by up to two when translating model results to prototype conditions (e.g., VT4 in the model corresponds to VT6 in the prototype). In the present case, however, the analogy with intake vortices is limited, making it difficult to predict prototype-scale entrainment mechanisms with certainty. Consequently, based on current knowledge and the experiences gained with the model, the extended linear relationship between the minimum partial filling of the pipe when approaching a mitre bend $Y_{0,cr}$ and the pipe Froude number F_w appears to represent a suitable threshold value for preventing air entraining vortices. For example: the critical partial filling $Y_{0,cr}$ amounts to 1 for Q = 10 m³/s with F_w = 0.25, which leads to the conclusions, that it is not advisable to empty the pressurised headrace tunnel for Q_{out} ≥ 10 m³/s.

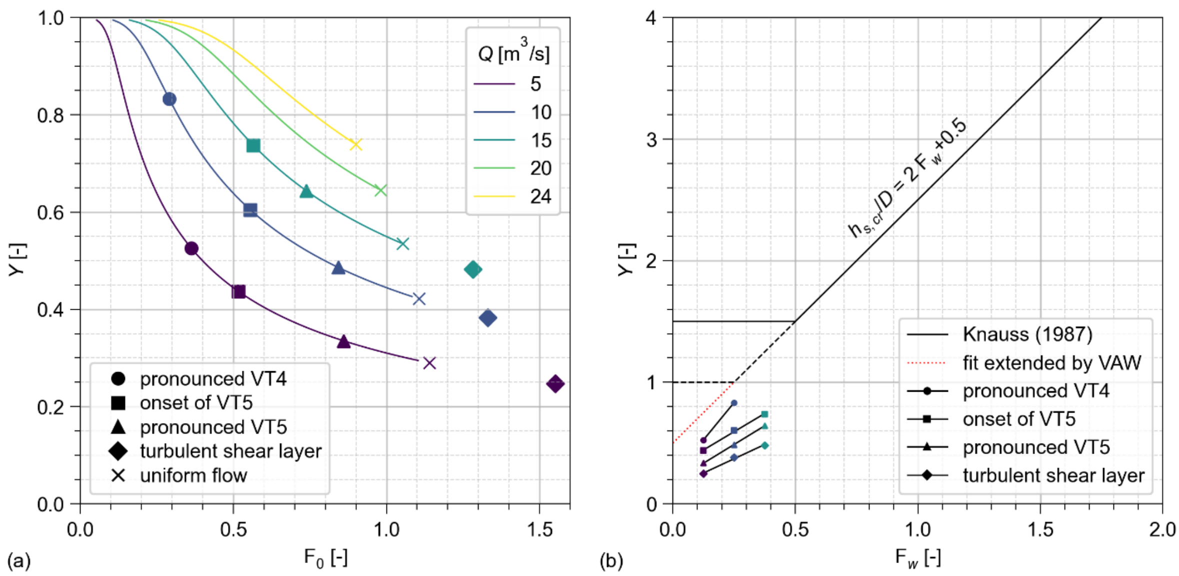

Figure 67: a) Partial filling ratio Y_0 and approach Froude number F_0 for the different load cases and thresholds for the entrainment mechanisms. (b) Comparison of the observed threshold partial filling ratio Y_0 for the different pipe Froude numbers F_w with the threshold proposed by Knaus (1987)

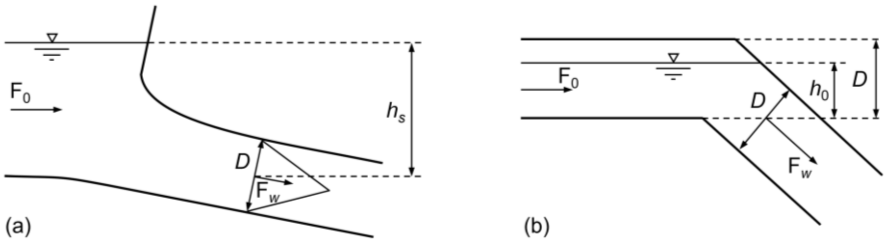

Figure 68 (a) Definition of the relative submergence depth h_s/D and intake i.e. pipe Froude number F_w by Knauss 1987. (b) Definition of the approach flow depth h_0 and Froude number F_0 in the present investigation.

3.5.2.3. Critical water level drawdown

The physical model investigations identified two governing mechanisms for the onset of air entrainment limiting the water level drawdown ΔH_{oc} in the power waterway of the HPP *Mörel* at flexible operation:

(a) Onset of air entrainment due to surface instabilities at the transition from free-surface to pressurised flow at the intake, occurring for discharges $Q_{out} \geq 10$ m³/s when the pipe Froude number at the transition from free surface to pressurised flow reaches the critical threshold $F_{w,cr} = 0.25$.

(b) Onset of air entrainment induced by vortex formation, occurring for discharges $Q_{out} < 10$ m³/s when the partial filling ratio of the free-surface flow approaching the mitre bend reaches the critical threshold $Y_{cr} = 2\ F_w + 0.5$.

Accordingly, a partial emptying of the pressurised headrace tunnel (section 1) is not advisable for $Q_{out} \geq 10$ m³/s. The critical water levels $H_{oc,cr}$ and the critical drawdown heights $\Delta H_{oc,cr}$ for the investigated load cases are given in Figure 69. They define the critical condition for the onset of air entrainment to which an additional safety margin should be applied to ensure safe operation.

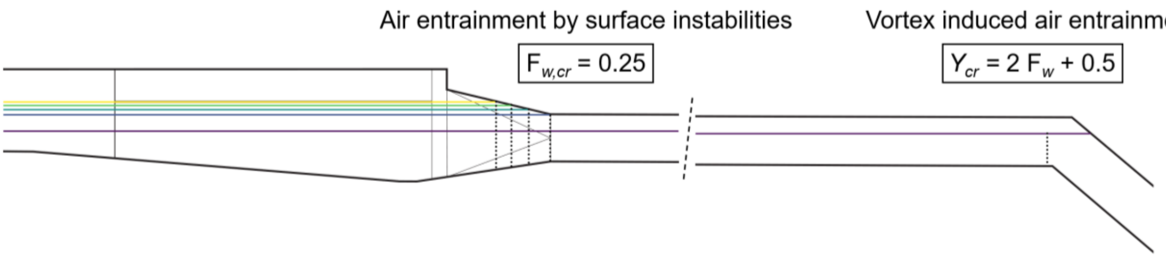

Q_{out} [m³/s]	$H_{oc,cr}$ [m a.s.l.]	$\Delta H_{oc,cr}$ [m]	surface instabilities at intake	vortex formation at mitre bend
24	985.13	0.00	x	
20	984.93	0.20	x	
15	984.69	0.44	x	
10	984.41	0.72	x	
5	983.35	1.78		x

Figure 69: Critical water levels in the overflow chamber Eggen $H_{oc,cr}$ and critical drawdown height $\Delta H_{oc,cr}$ for Q_{out}, if $Q_{out} > Q_{in}$.

3.5.3. CFD results – case study KW Mörel

In parallel to the experiment, numerical simulations of each quasi-steady operating condition were carried out using the Ansys Fluent software. A polyhedral mesh with 1.3 million of cells and an average y+

value around 10 was considered as enough refined for the simulations. The simulations solve the Unsteady Reynolds-Average Navier-Stokes (URANS) equations for a homogeneous two-phase flow with a specific numerical treatment for the free surface. The turbulence model considered is the realizable k-ε with a scalable wall function. According to the experimental set up, the mass flow rate is imposed both at the inlet and the outlet whereas an atmospheric pressure condition is set above the free surface. The outlet mass flow rate is controlled by using a function that forces the simulation to match the static pressure at the pressure probe 7 for the operating points 1 to 8 and the pressure probe 8 for the operating points 9 to 11. The momentum convective terms are discretized with a second order spatial scheme whereas for the turbulence convective terms a first order spatial scheme is used. The time step is set to 0.1s and time integration is performed with a first order implicit scheme.

Simulations are performed for 11 operating conditions split in three set according to the experimental data (see Table 20): OP1 (pronounced VT4) to OP4 (shear layer) corresponds to a flow rate of 5 m^3/s, OP5 (pronounced VT4) to OP8 (shear layer) corresponds to a flow rate of 10 m^3/s and OP9 (onset of VT5) to OP11 (shear layer) corresponds to a flow rate of 15 m^3/s.

The free surface corresponding to a water volume fraction of 0.1 and the locations of the pressure probes for the operating point OP1 are shown in Figure 70. The free surface is almost stable in agreement with the quasi-steady operating condition.

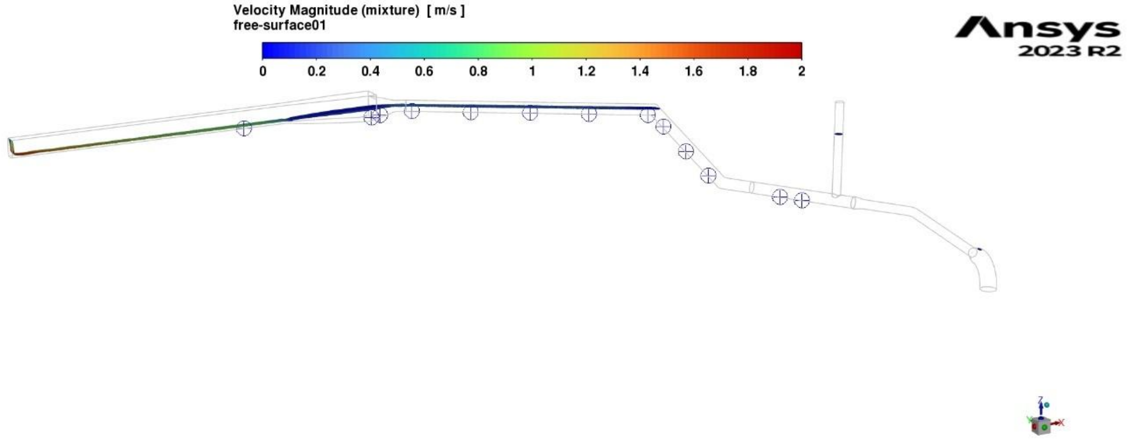

Figure 70: Free surface (iso-surface of the water volume fraction equal to 0.1) coloured by the velocity and location of the probes for the operating point OP1. CFD results.

The static pressure difference between the measurements and the simulations for each pressure probe and operating points is displayed in Figure 71. A discrepancy above 4 mbar is noticed for the probe 9 for the set of operating point OP1 to OP8. The physical model experiments demonstrated that pressure probe 9 exhibits unreliable measurement behaviour and is therefore not suitable for calibration purposes. Consequently, the observed discrepancy associated with this probe is not considered in the evaluation of the simulation accuracy. 94% of the data lies in a range between ± 2mbar, which corresponds to a variation of the free surface level of 2cm, i.e., equal to twice the mesh size in the core of the computational domain, which can be considered as the precision of the simulation.

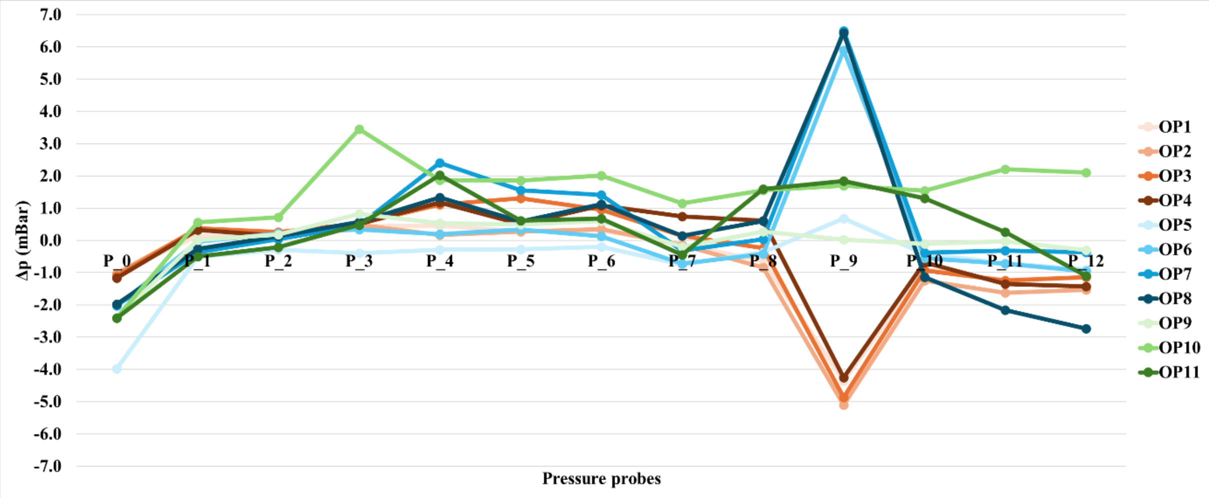

Figure 71: Static pressure difference between the measurements and the simulations for each pressure probe and operating point.

In Figure 72, the free surface and the streamlines coloured by the velocity magnitude are shown for the operating points OP5 to OP8 (load case with a flow rate of 10 m^3/s). For OP8, characterized by air entrainment in the experimental data, the velocity of the free surface upstream of the bend is around 1 m/s, in accordance with the experimental investigations.

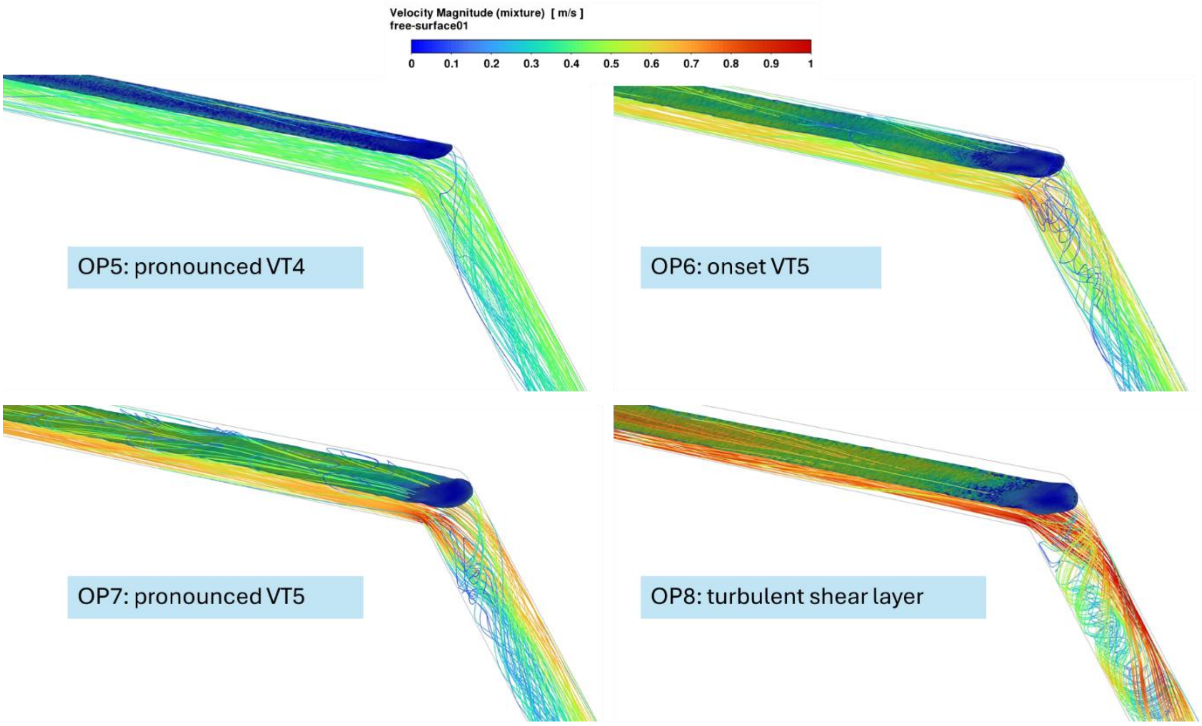

Figure 72: Free surface and streamlines coloured by the velocity magnitude for the operating point OP5 to OP8. CFD results. Observed VT in the physical model is specified.

3.5.4. Case study KW Merezenbach

In the following, the findings of the literature review and the physical model experiments are applied to evaluate the risk of air entrainment and transport when lowering the water level in KW Merezenbach headrace pipe (cf. sect. 3.3.3).

1. Vortex induced air entrainment at the surge tank

- The asymmetrical inflow from the pressurised headrace into the surge tank, combined with the acceleration towards the smaller penstock, promotes vortex formation.
- The critical cross-section with D = 0.45 m lies at the intersection between the penstock and the conical contraction at an elevation of H = 1831.31 m a.s.l. (see Figure 73, Section A-A). At Q_d = 0.5 m³/s the pipe Froude number is F_w = 1.50 at this location (v = 3.14 m/s).
- The critical submergence depth is $h_{s,cr} = (2F_w + 0.5)\cdot D$ = 1.57 m according to Knauss (1987) (see Table 16). This results in a critical water level of $H_{s,cr}$ = 1832.88 m a.s.l. in the surge tank, which lies 0.43 m above the soffit of the headrace junction.

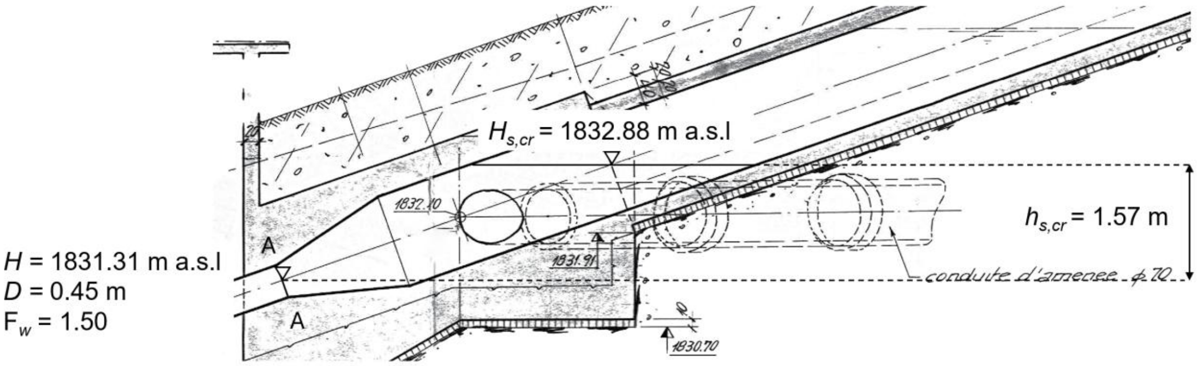

Figure 73: Critical submergence for vortex induced air entrainment into the penstock.

2. Pressure line in the headrace pipe

- The Darcy Weisbach friction factor in the headrace pipe is $\lambda = 0.023$ with $\frac{1}{\sqrt{\lambda}} = 2\log\left(3.71\frac{D}{k_s}\right)$ in the rough flow regime. The slope of the pressure line is thus $S_p = S_e = \frac{\lambda}{D}\frac{v^2}{2g} = 2.8‰$.
- With h_p = 0.43 m the pressure head at the junction and neglecting local losses the pressure line thus reaches the pipe soffit at $L = \frac{h_p}{S - S_p} = 158$ m, with S = 5.5 ‰ (section of transition from free-surface to pressurised flow). A backwater in the upstream section of the headrace establishes.
- In the approach to the backwater zone and at the beginning of the backwater, respectively, the normal flow depth is h_n = 0.44 m, corresponding to a filling ratio Y_n = 0.63 and a Froude number F_n = 1.03. At this Froude number, the flow is in a transitional regime (undular flow).

3. Air entrainment and transport in the headrace tunnel

- At the transition from free-surface to pressurised flow the surface instabilities trigger air bubble detachment, resulting in their entrainment as F_w > 0.25 (see Figure 57).
- The pressurised flow with F_w = 0.5 is capable of transporting air up to an air pipe Froude number of $F_{at,max} = 6\cdot10^{-4}$ according to Wickenhäuser (2008) (see Figure 59). This corresponds to β = 1.2‰ with a superficial water velocity $U_w^s = 1.3$ m/s and a superficial air velocity $U_a^s = 1.6\cdot10^{-3}$ m/s.
- According to Figure 59 elongated bubble flow is expected.

4. Air transport at the junction with the surge tank

- The elongated air pockets reach the junction with the surge tank, allowing most of the transported air to rise and be released at the free surface (see Figure 74).
- The release of air pockets generates water-hammer-like pressure peaks (Naudascher, 1991). Such pressure fluctuations may lead to mechanical stresses and unstable regulation behaviour.
- With v = 1.3 m/s the velocity of the jet entering the surge tank lies above the onset velocity v_e = 0.9...1.1 m/s according to Bertola et al. (2018). Therefore, air bubbles are also expected to be entrained in the turbulent shear layer caused by the inflowing jet (Wickenhäuser, 2008). The air bubbles disperse through turbulent diffusion but are also transport downstream by the mean velocity field and thus continue into the penstock (see Figure 74).

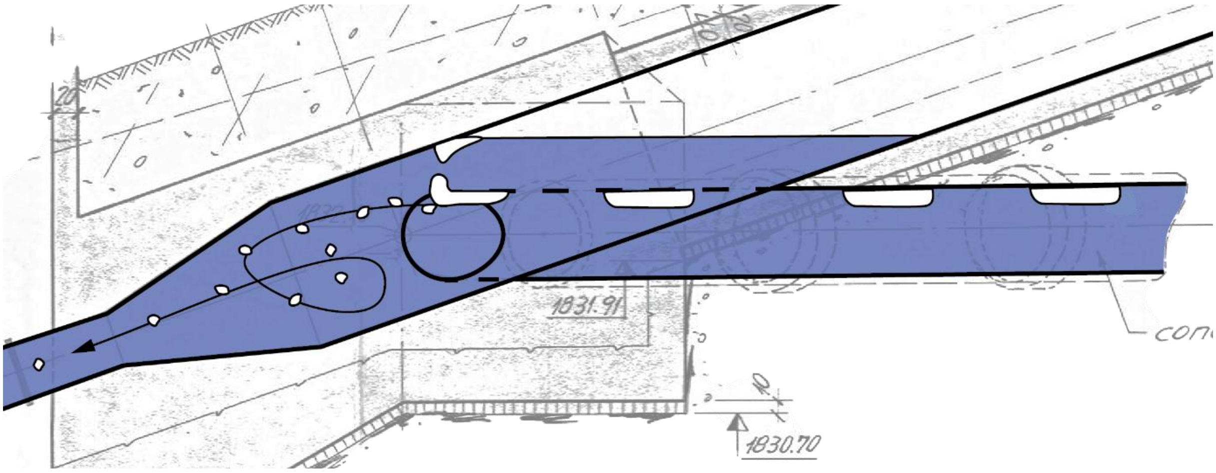

Figure 74: Air transported in plug flow regime to the junction with the surge tank where most of it rises to the water surface and part of its entrained by the turbulent shear layer of the entering jet and transported towards the penstock.

5. Air transport in the penstock

- With F_w = 1.5 the pipe Froude number in the penstock lies substantially above the clearing flow number $F_{w,c}$ (see Figure 17). Therefore, all air bubbles reaching the top of the penstock are expected to be transported towards the turbines.

The analysis indicates a risk of air entrainment and transport to the turbines for any dewatering of the headrace pipe which is unacceptable from operational safety perspective. Therefore, the flexibility potential is limited to a decrease of the water level in the desander and the forebay tank within the current operational limits.

3.5.5. Conclusions

Water level lowering during flexible hydropower operation is constrained by the risk of air entrainment and transport in pressurised power waterways, since these processes may lead to severe operational and structural issues. As even partial air transport may result in the formation and release of air pockets and associated blow-out, the critical condition for the assessment of flexible operation is the onset of air entrainment and transport, whereas the absolute amount of air entrained and transported is of secondary importance.

The clearing pipe Froude number $F_{w,c}$ represents the condition at which all entrained air, including large air pockets, is transported downstream. Values reported in the literature range between $F_{w,c}$ = 0.5…1.1, depending on pipe inclination and air discharge. The clearing pipe Froude number represents a reliable no-go criterion: its exceedance indicates complete downstream transport of entrained air, whereas its non-exceedance does not preclude partial air transport and possible local air accumulation.

For horizontal to slightly inclined pipes S = 0.4…8.7%, Wickenhäuser & Kriewitz (2009) reported the onset of air transport at pipe Froude numbers of approximately F_w = 0.25. Since steeper pipes require higher pipe Froude numbers for air transport, this threshold may be regarded as conservative also for steeper inclinations. The present findings further indicate that air entrainment by surface instabilities in partially filled conduits approaching pressurised conditions also initiates at approximately $F_{w,cr}$ = 0.25. A comparison indicates that, although the underlying mechanisms differ, the onset of bubble detachment occurs in a similar range of flow conditions as the reported threshold for the initiation of air transport. However, this value may be subject to scale effects and should therefore be interpreted with caution.

For vortex-induced air entrainment at submerged intakes, several empirical criteria for critical submergence exist in the literature. However, these criteria are generally based on simplified geometries and do not account for site-specific approach flow conditions. Reliable assessment therefore requires physical model experiments. Vortex-induced air entrainment may also occur at the transition from free-surface flow in a partially emptied, mildly inclined tunnel to a steeper pressurised tunnel section (mitre bend). The present results suggest that the critical partial filling ratio of the upstream free-surface flow may be estimated by $Y_{cr} = 2\ F_w + 0.5$. Since partial filling requires $Y < 1$, this criterion implies $F_w < 0.25$. According to Wickenhäuser & Kriewitz (2009) air entrained under these conditions is not expected to result in downstream air transport. Consequently, the critical partial filling ratio is of limited operational relevance, whereas the critical pipe Froude number $F_{w,cr}$ = 0.25 is the governing operational criterion, since its exceedance indicates conditions under which partial emptying is not advised.

The derived threshold relationships provide a practical basis for assessing air entrainment risk during flexible hydropower operation. In particular, the threshold F_w = 0.25 may be used as a conservative criterion for the onset of air entrainment by surface instabilities at the transition from subcritical free-surface to pressurised flow as well as for the onset of air transport.

3.6 WP6 – On-site experiments

Lead: HEVS, partners: HDE, FMV, EnAlpin, VAW

The objective of the experimental campaigns conducted in this project is to investigate and assess the flexibility potential of two hydropower plants, as predicted by 1D and 3D numerical simulations and reduced-scale model tests. In addition, the campaigns aim to verify that the proposed operating modes comply with the safety requirements of each plant. The two hydropower plants under study are Kraftwerk Merezenbach (KW Merezenbach) and Kraftwerk Mörel (KW Mörel).

3.6.1. KW Merezenbach and KW Mörel Test Cases

3.6.1.1. KW Merezenbach test case

Measurement objectives

A dedicated instrumentation system was deployed on site in December 2024 to evaluate the effects of dewatering the forebay tank and the headrace tunnel (see WP3 results). Energy production at the plant is highly seasonal, with approximately 6.8 GWh generated during summer compared to only 2.5 GWh in winter. The additional flexibility enabled by dewatering is therefore of particular interest during the winter season.

The primary objective of the measurement campaign is to provide a comprehensive characterization of the unit's behaviour across its full operating range. This includes steady-state operation, positive and negative power ramps, start-up and shutdown sequences, as well as emergency shutdown conditions. A second objective is to identify potential changes in system behaviour - hydromechanical, electrical, and overall stability - during the dewatering and refilling phases.

The investigated dewatering scenarios include both standard draining of the hydraulic system, following established procedures used during inspection periods, and temporary partial dewatering of the upper section of the headrace tunnel to provide ancillary services, particularly during low inflow conditions. Finally, the results of the measurement campaign are intended to validate the operational limits of the power plant in terms of flexibility and safety.

Identification and evaluation of risks and limits

Dewatering the hydraulic circuit of a power plant during operation entails several well-known effects and potential risks. Beyond possible air entrainment, the most immediate consequence is a reduction in the gross head - and consequently the net head - available to the turbine. This leads to a decrease in efficiency and may ultimately induce increased vibratory behaviour due to significant deviation from nominal design conditions. For a Pelton turbine, operation with a net head reduced to approximately one third of the nominal value may remain acceptable.

However, controlled dewatering at low turbine load, as typically performed during inspection procedures, is generally considered safe. Under such conditions, the unit is continuously monitored by an on-site vibration monitoring system, which triggers an emergency shutdown if critical thresholds are exceeded. In addition, the duration of operation under these potentially harsh conditions remains limited.

A second potential risk arises from uncontrolled transient events, particularly in the case of an emergency shutdown during dewatering, which may induce excessive pressure fluctuations within the hydraulic circuit. To assess these risks, 1D numerical simulations of critical scenarios were carried out by HDE using the SIMSEN software. The detailed results are presented in WP3 and summarized below.

The most critical risk during both dewatering and refilling phases is air entrainment. Air transported toward the injector may cause rapid expansion at the needle outlet, potentially leading to mechanical damage. In addition, trapped air pockets in the upper sections of the hydraulic circuit may pose a significant hazard in the event of an emergency shutdown.

The 1D SIMSEN simulations highlight the need for caution regarding power peaks during dewatering. At a base power of 1.7 MW, a transient peak of 0.19 MW (corresponding to an increase of 48.6 l/s in turbine discharge) with a constant inflow of 500 l/s causes the surge tank water level to briefly reach its minimum admissible value. On the headrace tunnel side, however, only about 10% of its volume is emptied over the 900 seconds required for primary ancillary services. Even after nearly 100 minutes of sustained peak operation, the water level remains above the elevation of the junction with the surge tank (1832.45 m a.s.l.), corresponding to approximately 75% dewatering of the headrace tunnel (HDE, WP3).

At this level of dewatering, the water surface approaches the bottom of the surge tank. Free-surface behaviour was simulated using ANSYS CFX and OpenFOAM, predicting the formation of a type-2 vortex. Since CFD simulations are known to underestimate vortex strength and given that air entrainment typically begins at vortex level 5, there remains a risk that air could be conveyed toward the turbine (HDE, WP3).

Further CFD analyses investigated a deep dewatering scenario below the junction between the headrace tunnel and the penstock, where air entrainment at the free surface was observed. This condition is reached after approximately 100 seconds for a turbine discharge of 500 l/s and an inflow of 100 l/s. A subsequent emergency shutdown simulation showed that a thin air pocket persisted at the top of the headrace pipe even after 450 seconds, indicating a potential risk of air entrapment (HEVS, WP3).

Consistent with the findings of WP3, WP5 also recommends adhering to the current operational water level limits. Accordingly, the definition of the testing scenarios incorporates the recommendations and constraints identified in both WP3 and WP5.

Experimental protocol

The experimental protocol primarily focuses on the characterization of the turbine under normal operating conditions.

A second test day involving dewatering was initially planned; however, no dewatering scenarios could be tested due to the contraindications identified in WP3 and WP5. In addition, dewatering following the standard drawdown procedure of the power plant was not feasible due to operational constraints.

One data acquisition system was installed by HES on December 3rd, 2024, and removed on October 7th, 2025. A dedicated test campaign was carried out on December 17th, 2024.

For this purpose, signals from several sensors permanently installed on the unit were recorded, and additional sensors were deployed (see the complete list in Table 21). Figure 75 show the schematic distribution of the sensors on the machine along with detailed photographs from the site.

Relative static pressure signals at several locations, as well as atmospheric pressure, turbine discharge, and injector position, were recorded at 1 kHz. In parallel, turbine casing vibrations, airborne noise, shaft displacement, and runner speed were acquired at 12.8 kHz using a National Instruments cDAQ-9189 data acquisition system equipped with dedicated input modules.

A dedicated LabVIEW interface running on a local PC was developed to enable continuous data recording. Two high-capacity SSDs were systematically used, allowing uninterrupted acquisition over several weeks. The system was connected to a GSM router to ensure remote access, enabling continuous monitoring of its status and remote control of data acquisition (start/stop) as required.

In addition, several SCADA variables were recorded, including the water levels in the forebay tank and desander, turbine discharge, injector opening, active and reactive power, static pressure upstream of the turbine, and runner rotational speed. These data were logged at a sampling interval of 1 second during the dedicated test day and 1 minute during the remainder of the monitoring period.

Table 21: List of existing and installed sensors in the KW Merezenbach.

#	*Variable*	*Sensor name*	*Fs*	*Range*
1	Ambient noise	Micro_Tu_512226	12.8 kHz	138 dB / 20 kHz
2	Key phasor pulses – Shaft rotation speed (VM600)	Keyphasor	12.8 kHz	0 – 5 V
3	Turbine casing Vibration X – Generator side	Tri100g Tu_X_2139607	12.8 kHz	± 100g
4	Turbine casing Vibration Y - Generator side	Tri100g Tu_Y_2139607	12.8 kHz	± 100g
5	Turbine casing Vibration Z - Generator side	Tri100g Tu_Z_2139607	12.8 kHz	± 100g
6	Turbine bearing Vibration X	Uni100gBe_X_5993577	12.8 kHz	± 100g
7	Turbine bearing Vibration Y	Uni100gBe_Y_5993578	12.8 kHz	± 100g
8	Injector Vibration X	Uni100gInj_X_5993581	12.8 kHz	± 100g
9	Rel. Shaft displacement X – Generator side (VM600)	WE_AS_X	12.8 kHz	0.3 – 4.3 mm
10	Rel.* Shaft displacement Y – Generator side (VM600)	WE_AS_Y	12.8 kHz	0.3 – 4.3 mm
11	Rel. Shaft displacement X – Non-Generator side (VM600)	WE_NS_X	12.8 kHz	0.3 – 4.3 mm
12	Rel. Shaft displacement Y – Non-Generator side (VM600)	WE_NS_Y	12.8 kHz	0.3 – 4.3 mm
13	Main inlet valve upstream relative static pressure	p_stat_up_P35510X08780595	1 kHz	0 – 100 barg
14	Main inlet valve downstream relative static pressure	p_stat_down_P35510X08780596	1 kHz	0 – 100 barg
15	Injector relative static pressure	p_stat_inj_P35510X08780598	1 kHz	0 – 100 barg
16	Atmospheric pressure	p_atm_M200C601052	1 kHz	0 – 1 bara
17	Discharge – Ultrasonic flow meter	q_ufm_W706BB02000	1 kHz	0 – 0.75 m^3/s
18	Injector position	x_inj_S43110X11476672	1 kHz	16 – 120 mm

** Relative displacement between the shaft and the bearing.*

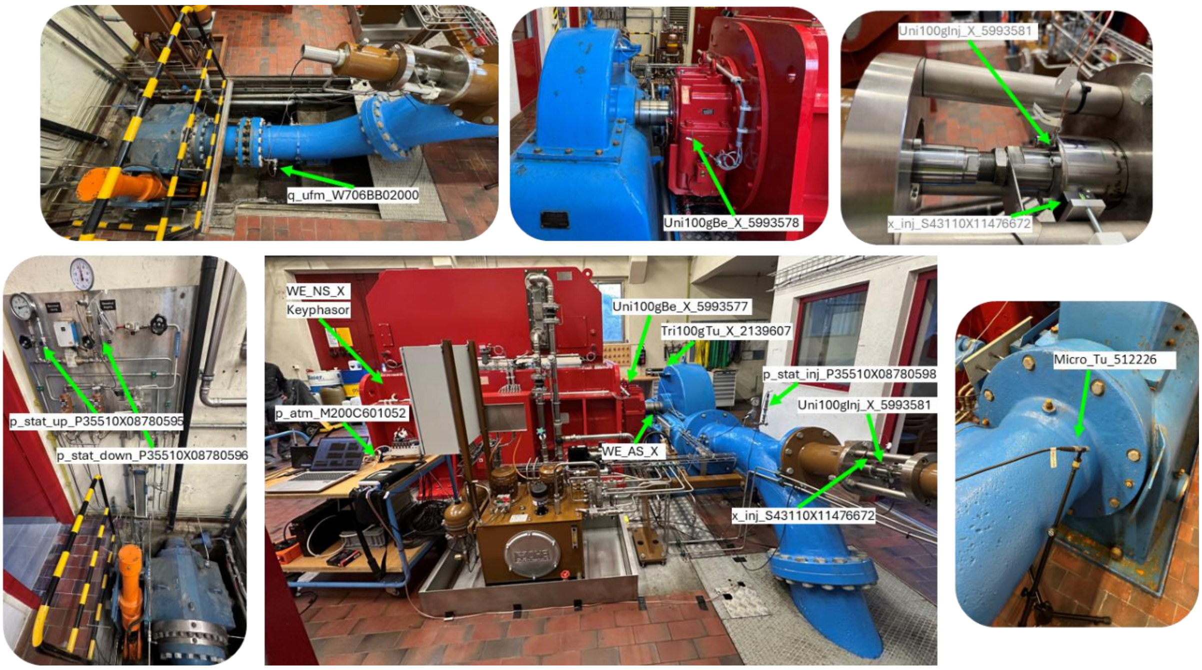

Figure 75: Photographs of existing and temporarily installed sensors in the KW Merezenbach.

In addition to a long-term free-run recording of the turbine under normal operating conditions, a dedicated testing program including turbine start-up, steady-state operation at several different power levels as well as dynamic transitions from P_{min} to P_{max} and vice versa, is depicted in the left column of Figure 76. The right column of Figure 76 presents the predicted evolution of the water level in the desander for five hypothetical intake flow rates. These predictions were used to support the test planning and to prevent unintended activation of the low-water-level alarm implemented in the plant control system. The red dashed line indicates the shutdown elevation, while the maximum level corresponds to the spillway elevation.

In practice, the water level may slightly exceed the side spillways (with a recorded maximum of 1840.6 m a.s.l.), and the operational minimum level was set more conservatively than the automated threshold (1840 m a.s.l.).

The proposed testing program was approved by the plant owner and successfully conducted remotely on December 17th, 2024.

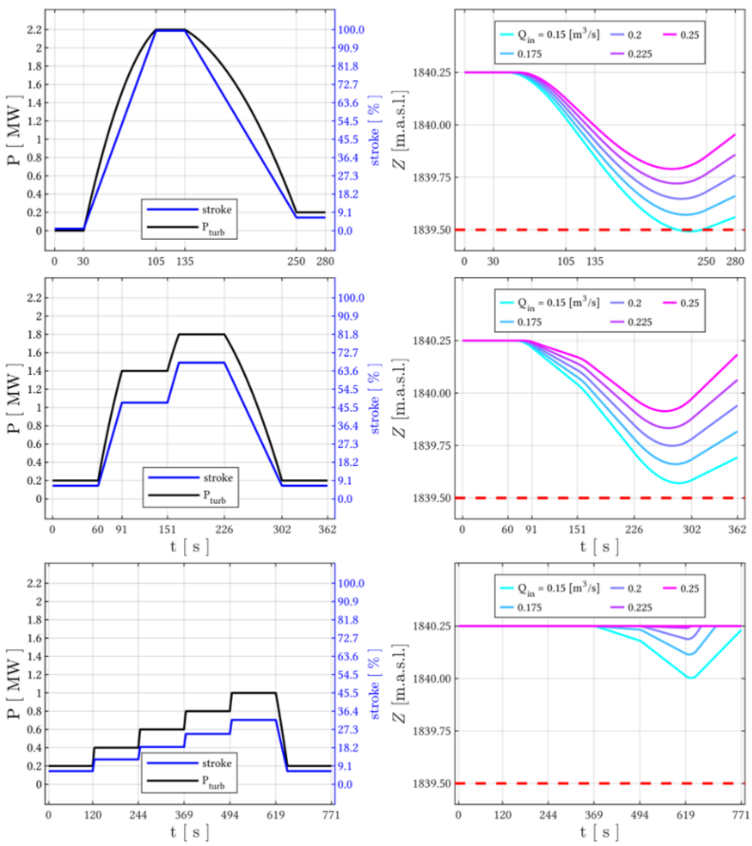

Figure 76: KW Merezenbach testing program including one power ramp and several power steps (left). Simulation of the resulting upstream water level according to five hypothetical intake flow rates (right).

3.6.1.2. Mörel test case

Measurement objectives

A dedicated set of instruments was deployed on site in 2025 to evaluate the effects of partial dewatering of the overflow tank and the headrace tunnel (see WP3 results) on the overall operation of the power plant, with a particular focus on Unit 3.

By contrast with the KWGO case study, where dewatering directly affects the head available to the turbine, this is not necessarily the case in the present study. Here, partial dewatering of the head-race tunnel - and potentially of the downstream gallery connecting the Eggen overflow chamber to the surge tank - may have a more indirect impact on turbine operating conditions. Furthermore, in addition to the water level monitoring sensors permanently installed at Eggen overflow chamber, two night-vision cameras were installed to monitor possible overflow or significant deep dewatering events during the planned flexible operating scenarios. Finally, the Hydro-Clone real-time simulation and monitoring system, acting as a physics-based digital twin, has been installed by HDE to continuously survey the plant's transient behaviour using boundary conditions measured and transmitted through the SCADA system.

These on-site measurements aim first at drawing an extensive radiography of one unit operation over its whole operating range. The turbine characterisation plan covers the transient and steady-state operating conditions, startup and shutdown as well as the emergency shutdown sequences. Then, the focus is put on the identification of any eventual behaviour change (hydromechanical, electrical, global stability, and so on) during the temporary partial dewatering/refilling of the headrace tunnel and of the overflow chamber induced by emulated ancillary service tests.

Experimental protocol

Figure 77 : Photographs of existing and temporarily installed sensors at KW Mörel.

The impact of partial dewatering of the Eggen's overflow chamber on the turbines must be tested in several stages. To begin with, information on turbine behaviour during normal operation must be gathered, allowing us to draw the reference behaviour during all regular operating conditions. On a second step, the eventual effects of dewatering on the turbines' behaviour are identified in comparison with the normal operation to exclude any eventual harsh condition. In addition to the operation of the turbines, the study of the Eggen's overflow free surface behaviour is mandatory to exclude any air entrainment into the downstream circuit (hardware gallery, penstock, and so on) which could, in the worst case, lead to the damage of the hydraulic circuit components.

To this end, a full set of mainly non-intrusive instrumentation was deployed on March 25th, 2025 on the Mörel KW units to determine the operation of the machines under the various operating conditions. The instrumentation is detailed in Table 22, whilst photographs with the different deployed instruments and the acquisition system are provided in Figure 77. One may state here that most instruments have been deployed mainly on the Unit 3.

Table 22 List of existing and installed sensors in the KW Mörel.

#	*Variable*	*Sensor name*	*Fs*	*Range*
1	Draft tube airborne noise - Turbine side	MIC_DT_TSU3_SN157775	12.8 kHz	0…20kHz
2	Draft tube airborne noise - Generator side	MIC_DT_GSU3_SN512227	12.8 kHz	0…20kHz
3	Turbine Vibration pos. -Y - Generator side flange m. 270°	Uni50gGSU3y_270deg_6003929	12.8 kHz	± 50g
4	Turbine Vibration pos. +X - Generator side flange m. 0°	Uni50gGSU3x_0deg_6003931	12.8 kHz	± 50g
5	Turbine Vibration pos. -Y - Turbine flange m. 0°	Tri50gTSU3y_0deg_6299439	12.8 kHz	± 50g
6	Turbine Vibration pos. -Y - Turbine flange m. 270°	Tri50gTSU3y_270deg_SN62999439	12.8 kHz	± 50g
7	Turbine Vibration pos. -Y - Turbine flange m. z0°	Tri50gTSU3y_z0deg_SN629939	12.8 kHz	± 50g
8	Turbine Vibration pos. +X - Turbine flange m. 0°	Uni50gTSU3x_0deg_SN6090061	12.8 kHz	± 50g
9	Draft tube static pressure - Turbine side	PRS_DT_TSU3_SN5431	1 kHz	6 bar (a)
10	Draft tube static pressure - Generator side	PRS_DT_GSU3_SN5432	1 kHz	6 bar (a)
11	Atmospheric pressure	PRS_ATM_SNK610AF01052	1 kHz	1 bar (a)
12	Spiral casing static pressure	PRS_SC_U3_SN6576	1 kHz	40 bar (a)
13	Penstock static pressure upstream unit valve	PRS_UpV_U3_SN6577	1 kHz	40 bar (a)
14	Guide vanes opening angle	ANG_GVO_TSU3_DIT2024001	1 kHz	± 45°
15	Guide vanes piston displacement	POS_GVO_TSU3_SN7000108188	1 kHz	100…600 mm
16	Flowrate of unit 3	Q_U3_SNH40F1702000	1 kHz	0…10 m^3/s
18	Vibration Z - Turbine bearing	VIB_VM600_WE_TL_Z_U3	12.8 kHz	100 mm/s
19	Position Z - Turbine bearing	POS_VM600_WE_TL_Z_U3	12.8 kHz	0,3…4,3 mm
20	Position Y - Turbine bearing	POS_VM600_WE_TL_Y_U3	12.8 kHz	0,3…4,3 mm
22	Position Y - Turbine to generator bearing	POS_VM600_WE_KL_Y_U3	12.8 kHz	0,3…4,3 mm
23	Position X - Turbine to generator bearing	POS_VM600_WE_KL_X_U3	12.8 kHz	0,3…4,3 mm
24	Vibration X - Turbine bearing	VIB_VM600_LA_TL_X_U3	12.8 kHz	100 mm/s
25	Vibration X - Turbine to generator bearing	VIB_VM600_LA_KL_X_U3	12.8 kHz	100 mm/s
26	Shaft rotation speed - Unit 1	Tacho_VM600_U1	12.8 kHz	-
27	Shaft rotation speed - Unit 2	Tacho_VM600_U2	12.8 kHz	-
28	Shaft rotation speed - Unit 3	Tacho_VM600_U3	12.8 kHz	-
29	Pressure regulator displacement – Unit 3	Nikon D800	30 fps	-

The absolute static pressure upstream the main valve, on the spiral casing as well as on the two draft tubes of the Unit 3, along with the atmospheric pressure, have been recorded at a rate of 1 kHz. The discharge of the same unit has been also acquired along with the guide vanes opening angle and piston displacement, at the same rate. Then, the vibration of the turbine casing, the airborne noise and the shaft displacement of the Unit 3, as well as the runner speed of the three units were recorded at 12.8 kHz, with the help of a National Instruments cDAQ 9189 digitizer equipped with several specific acquisition modules. A specific LabView software, running on a local PC, has been set up to record all this data continuously. Two fast SSDs with a large storage capacity have been systematically employed, allowing continuous data recording during several weeks. As for the KW Merezenbach test case, the system has been connected to a GSM rooter to guarantee a remote access to the PC, allowing us to permanently control the state of the system and to start/stop the recording. Several SCADA variables (mainly the water level at the Eggen overflow tank, the total turbine discharge, the distributor upstream static pressure, as well as the units' active and reactive power, guide vanes opening and rotational speed) have been recorded with a rate of 1 Hz for the full monitoring period.

Figure 78 : Setup of the visual stroke measurement system installed on the pressure regulator piston of Unit 3 at KW Mörel .

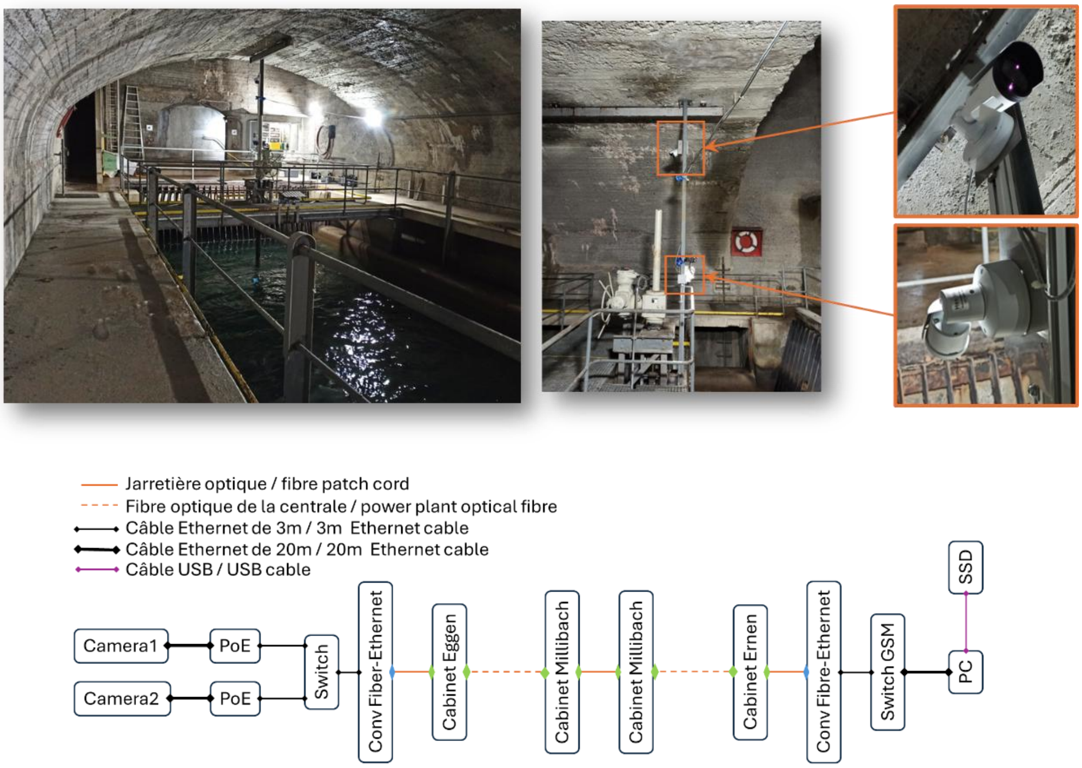

Figure 79 : Pictures of the two cameras installed at Eggen overflow tank on December 9th, 2025 (top) and the setup of the communication chain to remotely monitor the free surface (bottom)..

During the two specific test days, a Nikon D800 camera was installed to measure the pressure regulator piston stroke of Unit 3 during emergency shutdown events (see Figure 78). These data are required for calibration of the Hydro-Clone model. The piston displacement was determined through post-processing of video images recorded at 30 frames/s with a resolution of 1920 × 1080 pixels (spatial resolution of ~4 px/mm), using automatic detection of the piston position as it moves behind a millimetre-scale ruler. Synchronisation of the video with the other recorded signals was achieved through audiovisual sound impact detection.

As shown in the upper part of Figure 79, two cameras (Axis P1447 and M2025 models) with integrated infrared lighting were installed on December 9th, 2025, at the Eggen overflow tank to capture free-surface variations during the dewatering tests, on the upstream and downstream sides, respectively. The images from both cameras (with resolutions of 3072 × 1728 and 1920 × 1080) were recorded at 20 frames/minute, by intermittency over several weeks using a pre-programmed trigger. The timestamps of the recorded images and of the acquisition system deployed at KW Mörel were synchronised using GMT. The communication chain enabling remote control of the cameras is shown in the lower part of Figure 79. Each camera is powered by a PoE (Power over Ethernet) injector and connected to an Ethernet switch. Two Ethernet-to-optical-fibre converters (one at each end) are then used to communicate with the recording PC installed at the Ernen powerplant via an available optical fibre line of the Ernen-Mörel hydropower complex. Finally, a GSM switch installed upstream of the PC ensures remote access to all components, enabling configuration, real-time monitoring, recording control (start/stop), and data retrieval.

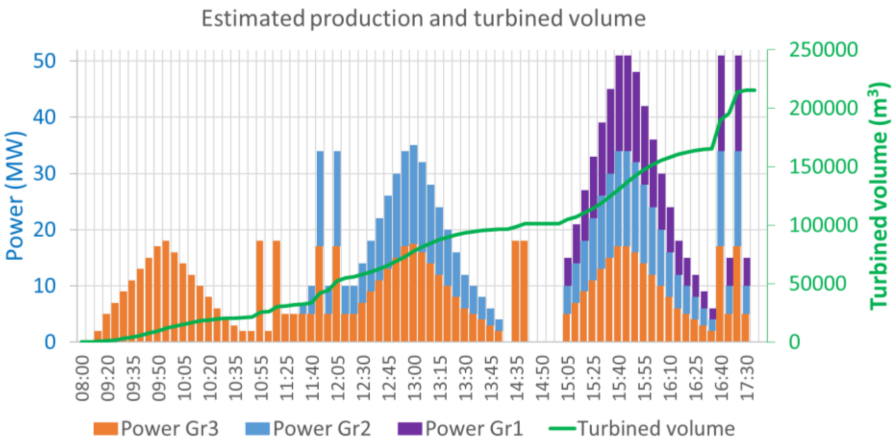

Figure 80 : Defined specific testing program to characterize the Mörel KW turbines' normal operation.

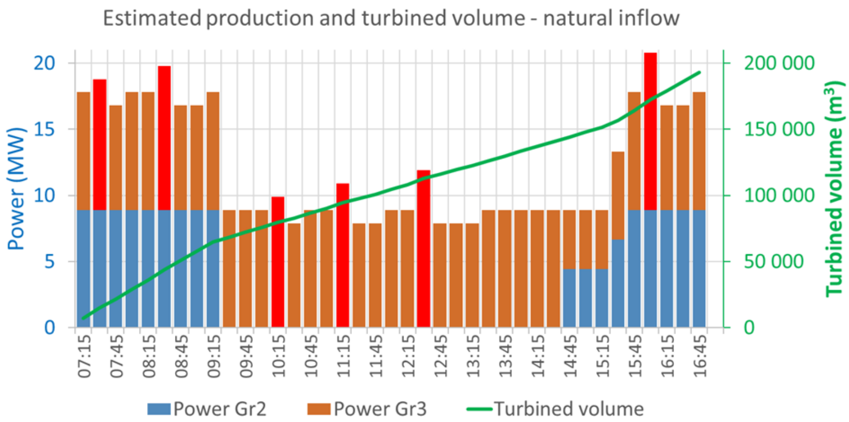

Figure 81 : Defined specific testing program to determine the dewatering effect of primary ancillary service at KW Mörel.

In addition to long-term free-run recording of turbines' operation, an extensive characterization testing program was prepared. This program included turbine start-up and shutdown, steady-state operation at various power levels, dynamic transitions between P_{min} to P_{max} and vice versa, emergency shutdowns, and various combinations involving one, two, and three operating units (see Figure 80). The power setpoints for each unit, as well as the estimated total cumulative turbine discharge, were provided to FMV several days in advance to prepare the production schedule and conduct the tests. The proposed testing program, approved by both the owner and the operator, was successfully carried out on site on June 17th, 2025.

A second testing program was designed to evaluate turbine hydromechanical behaviour and free-surface evolution at the Eggen overflow tank under various emulated primary ancillary service conditions. As illustrated in Figure 81, two sets of power peaks of 1, 2, and 3 MW (red bars) were planned for two different inflow rates of approximately 5 m³/s and 8 m³/s at Eggen. The power peaks were scheduled in accordance with the daily discharge profile of the selected test date. The available discharge strongly depends on natural meteorological inflows and fluctuations in energy market demand. This is illustrated in Figure 82, which shows the time history of total turbine discharge recorded at KW Mörel a few days prior to the testing campaign, which was successfully conducted on March 10th, 2026

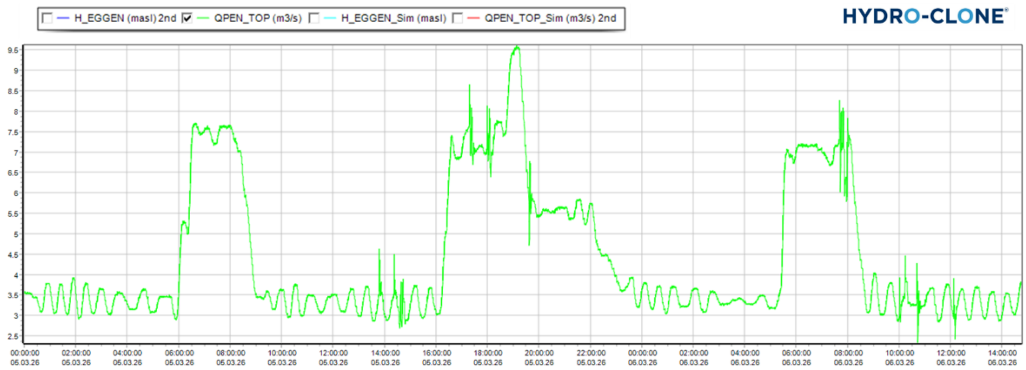

Figure 82 : Time history of total turbine discharge at KW Mörel on March 5th - 6th, 2026.

Identification and evaluation of risks and limits

Considering the outputs of WP3 and WP5, as well as all known limitations (physical and control-related) of the hydraulic circuit and the power plant, six main dewatering scenarios were identified and analysed in terms of objectives, expected effects, testing procedures, prerequisites, risks, and protective countermeasures. The first three scenarios consist of power peaks of 1, 2, and 3 MW, respectively, maintained for 900 s under an inflow condition of approximately 5 m³/s. The second set of three scenarios targets the same power peak amplitudes (1, 2, and 3 MW) over 900 s, but with an inflow condition of approximately 8 m³/s.

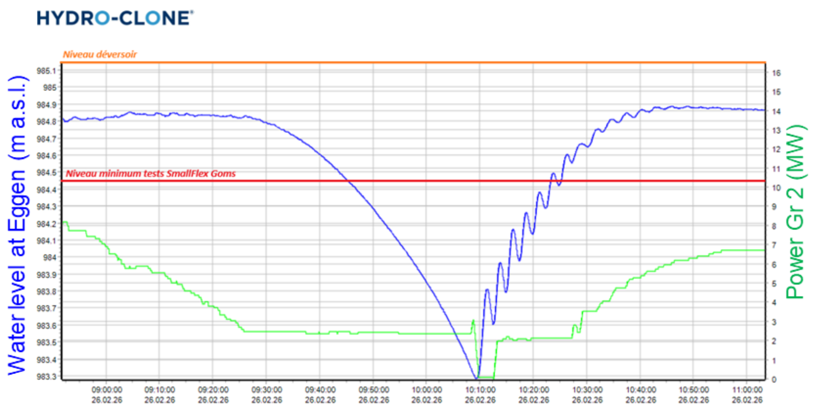

Figure 83 : Time history of a large water level variation event under regular operation, recorded at Eggen using the Hydro-Clone system on February 26th, 2026.

The testing procedure consists of increasing the power by 1, 2, or 3 MW (using the implemented control ramp), followed by a 900 s holding phase and then a reduction to a value below the initial one, allowing water level restoration at Eggen. Each testing cycle concludes with water level stabilisation in accordance with the inflow conditions before the next cycle is initiated.

The prerequisite is stable turbine operation with regulated water levels at Eggen (ideally close to overflow, while avoiding it), with one or two units operating at the same power depending on the inflow conditions (Unit 3 only for an inflow of ~5 m³/s, and Units 2 and 3 for an inflow of ~8 m³/s).

Among the expected effects, partial dewatering during positive power peaks and overflow at the end of the power peak cycles were identified in the Eggen overflow chamber. Additional water level fluctuations at Eggen and in the surge shaft, induced by turbine power variations, are also expected.

The identified risks, considered limited, include deep dewatering, air entrainment, sudden overflow, and air blasts in the Eggen chamber, as well as the potential triggering of an emergency shutdown.

The active protection measures implemented to ensure safe testing are based on the power plant's overall protection and monitoring system. These include conducting the tests under relatively low inflow conditions (depending on the testing period) and enabling full units' shutdown if necessary. In addition, the tests are monitored in real time by power plant operators and project engineers using the deployed HES-SO VS system, the SCADA system, the HydroClone system, and two cameras installed at Eggen.

The organisation of the tests required a thorough risk analysis to reassure FMV decision-makers regarding the proposed experiments. Moreover, conservative water level variation limits were adopt-ed compared to the operational limits of the power plant (see Figure 83: dewatering limit set at 984.45 m a.s.l. and weir crest at 985.15 m a.s.l.). An adapted test protocol and program were developed and updated several times to account for the daily discharge profile of the selected test date.

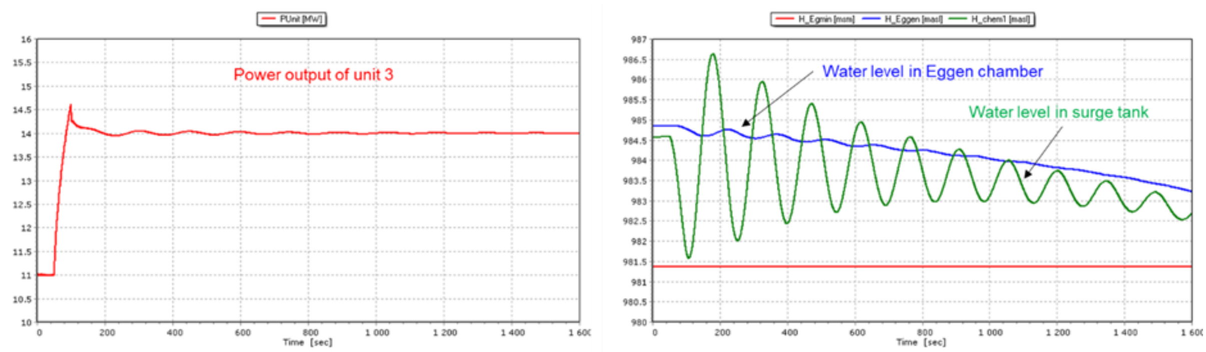

Figure 84 : Simulated transient behaviour of the surge tank and Eggen chamber water level (right) for a 3 MW power step (left) with an inflow of Q_{in} = 5 m³/s and an initial water level of 984.85 m a.s.l at Eggen.

Table 23 Predicted simulation results for the on-site tests of Eggen chamber dewatering.

	Initiale value						After 900s				
	PG1	PG2	PG3	Hegen	HST	Qtot	dP	Heggen min	dH Eggen	Hst max	Hst min
	[MW]	[MW]	[MW]	[masl]	[masl]	[m3/s]	[MW]	[masl]	[m]	[masl]	[masl]
REG01	0.00	0.00	11.00	984.85	984.58	5.00	1.00	984.68	0.17	985.08	983.82
REG02	0.00	0.00	11.00	984.85	984.57	5.00	2.00	984.44	0.41	985.66	982.89
REG03	0.00	0.00	11.00	984.85	984.57	5.00	3.00	984.10	0.75	986.63	981.58
REG04	0.00	6.00	11.00	984.85	984.15	8.00	1.00	984.66	0.19	984.55	983.4
REG05	0.00	6.00	11.00	984.85	984.15	8.00	2.00	984.43	0.42	984.94	982.64
REG06	0.00	6.00	11.00	984.85	984.15	8.00	3.00	984.16	0.69	985.35	981.81

In addition, predictive simulations of power step changes were performed for all six defined scenarios to support the preparation of the on-site tests. The load cases were defined based on the expected test conditions, with power regulation steps of 1, 2, and 3 MW using a single unit, for inflows of 5 m³/s and 8 m³/s, under steady-state water level conditions of 984.85 m at the overflow chamber. A loading and unloading rate of approximately 7.5 MW/min, measured on site, was applied, representing typical operating conditions.

Table 23 summarises the results of the different simulated scenarios and provides an overview of the expected dewatering levels in the Eggen chamber, with a maximum amplitude of 0.75 m for a power peak of 3 MW and an inflow of 5 m³/s. As illustrated in Figure 84 for this scenario, the load increase of Unit 3 induces significant oscillations in the surge tank (green), while the Eggen chamber exhibits a relatively smooth and quasi-linear drawdown, with slight mass oscillations induced by surge dynamics (blue). After approximately 900 s, corresponding to primary ancillary service requirements, a total level drop of about 0.75 m is noticed.

3.6.2. Installation of the Hydro-Clone system in one hydro power plant (HDE)

Hydro-Clone system (see Figure 85) is a real-time simulation and monitoring system based on a validated SIMSEN model of the hydropower plant. Acting as a physics-based digital twin, it continuously simulates the plant's transient behaviour using boundary conditions measured and transmitted through the SCADA system.

The main objective of Hydro-Clone is to ensure safe and efficient operation by detecting and preventing malfunctions or anomalies that could affect hydraulic transients. Through this predictive monitoring, the system helps reduce the risk of major incidents. In addition, it provides access to quantities that are difficult to measure directly, such as internal pressure fluctuations, thus enabling early detection of potential issues by means of virtual sensors. Over time, the continuous monitoring of transient regimes will contribute to optimizing operating parameters, reducing mechanical stresses, and extending the equipment's service life, while minimizing operational risks.

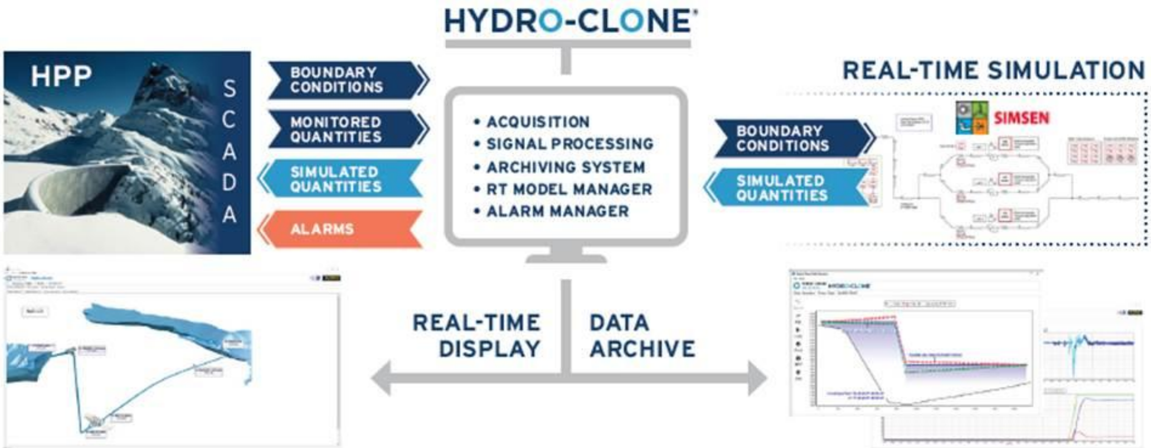

Figure 85 General concept of Hydro-Clone physics-based digital twin for HPP transient monitoring

The Hydro-Clone system has been successfully deployed at the Mörel hydropower plant in collaboration with Hydro Exploitation (HEX). The installation and commissioning were completed without major issues, enabling the system to operate as intended. The system proved to be particularly effective in supporting on-site testing activities, allowing continuous monitoring and data acquisition throughout the test phases. It provided valuable assistance during the dewatering tests of the Eggen chamber, where real-time data visualization was especially beneficial for tracking system behaviour and supporting operational decision-making under dynamic conditions. Overall, the Hydro-Clone system has demonstrated its relevance as a powerful tool for monitoring and analysing transient processes during field tests.

Some minor adjustments are still to be carried out, including the fine-tuning of the free-surface model using the available test data. However, the long-term monitoring system is fully operational and performing as expected. Additional modifications and new signals will be implemented following the maintenance of Units 1 and 2.

The Hydro-Clone interface provides real-time visualization of measured and simulated signals, enabling direct comparison between field data and digital twin outputs. This functionality facilitates im-mediate assessment of system behaviour during testing phases and supports the validation of the simulation model under actual operating conditions. Figure 86 shows the real-time trends displayed in the Hydro-Clone interface.

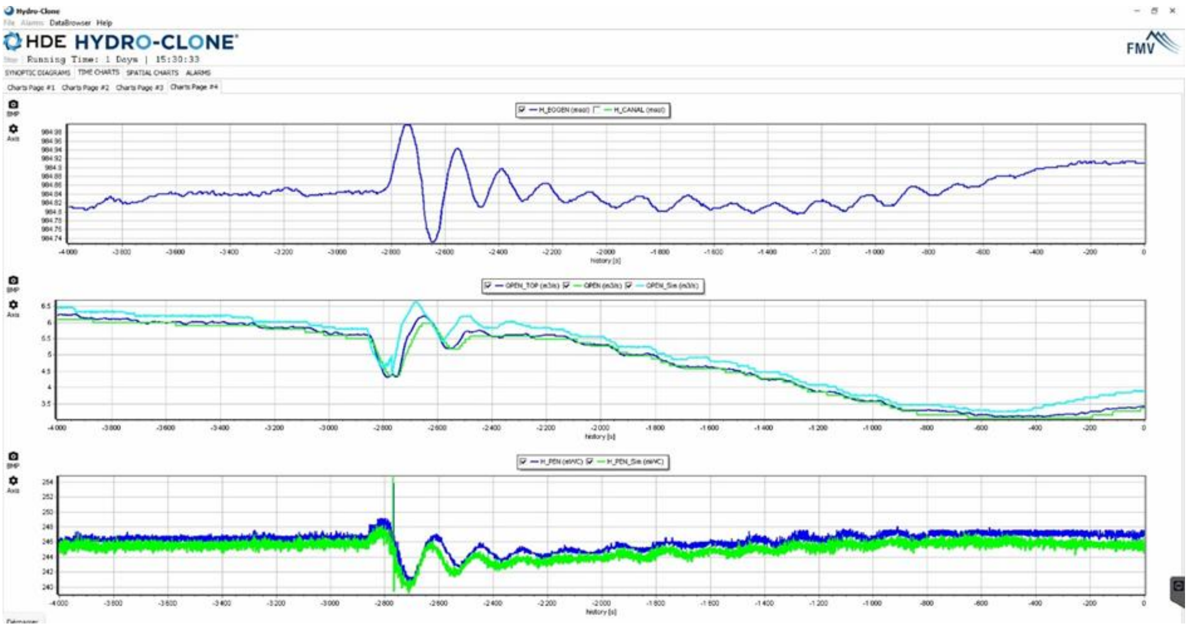

Figure 86 General concept of Hydro-Clone physics-based digital twin for HPP transient monitoring

3.6.3. Performing on-site experimental campaigns in two hydropower plants (HEVS)

3.6.3.1. KW Merezenbach test case

The instrumentation of the unit was carried out on December 3, 2024. Continuous data were recorded under free-run conditions (normal plant operation), with some interruptions, from December 2024 to October 2025. In total, 3’781.5 hours of data were acquired, corresponding to 51.2% of the overall monitoring period of 7’385.8 hours.

Figure 87 presents an overview of the maximum turbine power, turbine discharge, unit rotational speed, and the NI system recording periods over the entire measurement campaign, based on per-minute averaged data. The maximum turbine power values are computed over intervals defined by two consecutive start-stop sequences. The discharge exhibits a clear seasonal variation, along with shorter-term fluctuations associated with transient operating conditions.

Figure 88 provides an overall view of the variations in the main process variables throughout the entire measurement campaign, based on per-minute averaged data from both the HES-SO VS acquisition system and the SCADA system. A clear seasonal variation in discharge - and consequently in turbine power - can be observed. In contrast, only minor variations are noted in the upstream water level and in the static pressure downstream of the main inlet valve (MIV), reflecting the constant water-level control mode of the unit.

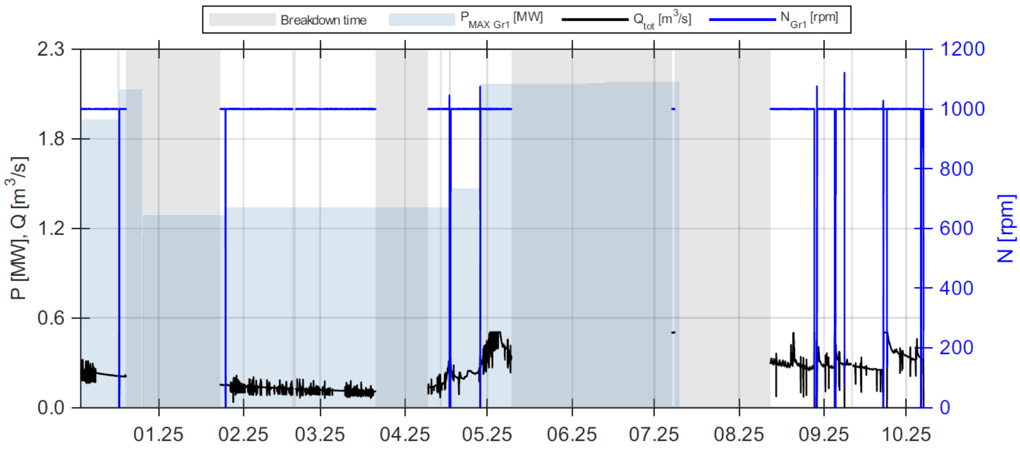

Figure 87: Overview of maximum turbine power, turbine discharge, rotational speed of the unit and breakdown recording periods of the NI system during the full KW Merezenbach measurements campaign.

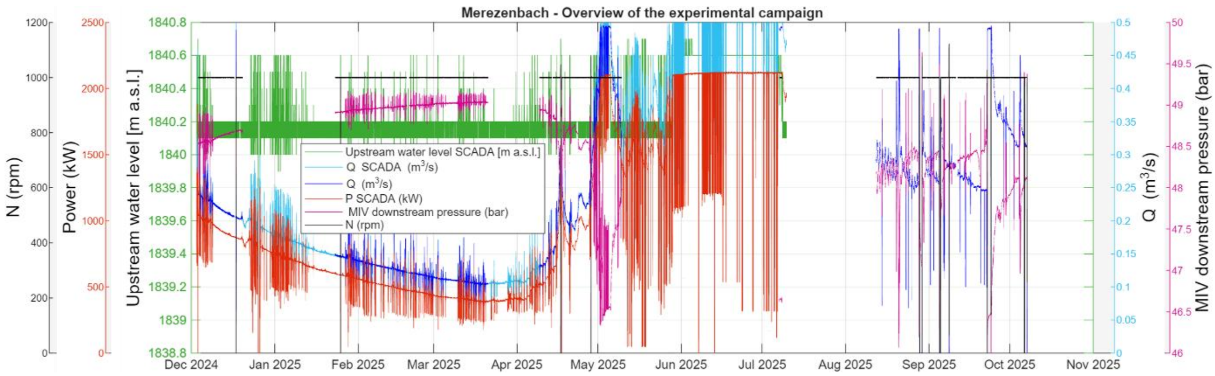

Figure 88: Overview of main process variables of KW Merezenbach turbine operation during the full measurement campaign.

A dedicated test campaign was conducted on December 17th, 2024, to get the standard operation of the turbine. An overview of the main process variables is provided in Figure 89, using per-second average data. The turbine start-up, dynamic transitions from P_{min} to P_{max} and vice versa as well as steady-state operation at different power levels may be clearly identified. Those specific tests allow to validate the measured signals, and to get the different relationships between the upstream water level, the static pressure near the injector, the discharge, and so on.

A second test day with dewatering was initially planned. However, for unavailability reasons (since a satisfactory time to stop the production couldn't be found), but also for safety reasons, given the conclusions of WP3 and WP5, this test has been unfortunately abandoned and the system removed on October 7th 2025.

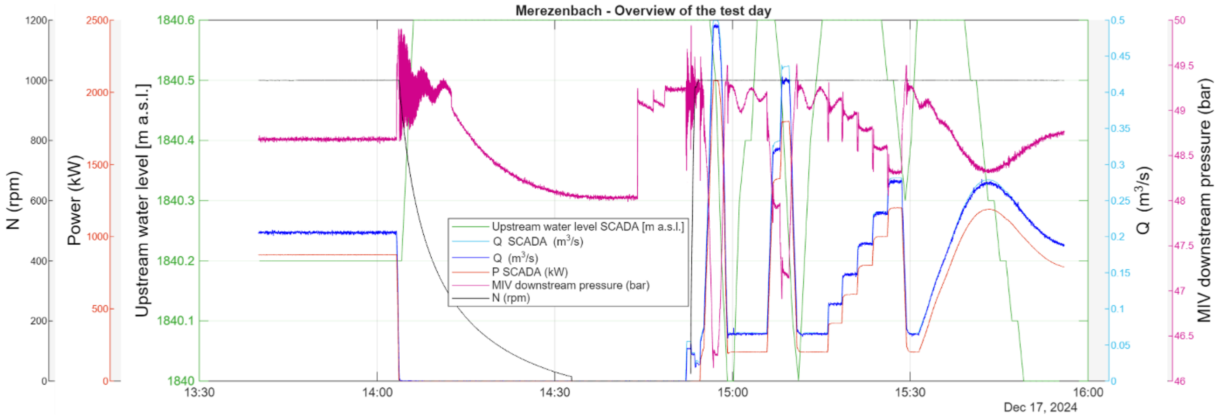

Figure 89: Overview of main process variables of KW Merezenbach turbine operation during the dedicated test day of December 17th, 2024.

3.6.3.2. KW Mörel test case

The instrumentation of Unit 3 at the Mörel powerplant was completed on March 25th, 2025. Pending the planning of a specific test day, continuous intermittent free-run measurements were performed since the instruments installation and ran until March 2026. On June 17th, a specific testing campaign, following the proposed operating plan (see Figure 80) has been successfully accomplished.

In Figure 90, the time-history of total discharge along with the electrical power of the three units is provided, from recorded SCADA data at 1 Hz. As shown in this figure, three planned sets of stationary power steps were performed:

- Unit 3 alone.
- Units 2 and 3 operating together at the same power.
- Units 1, 2 and 3 operating together at the same power.

Moreover, using the same configurations, several transient tests were carried out, from minimum to maximum power, and vice versa.

Finally, two emergency shutdowns were conducted with:

- Unit 3 operating at 17 MW (Pmax).
- Units 1, 2 and 3 operating at 5 MW each.

An additional unplanned emergency shutdown occurred due to a rapid rise in the tailrace water level during transient tests with all three units operating simultaneously at approximately 2 MW.

The instrumentation of Unit 3 was temporarily removed for maintenance on February 5th, and reinstalled on March 4th and 9th, 2026. On March 10th, a specific test campaign was conducted to measure the behavior of Unit 3 delivering power peaks of 1, 2, and 3 MW, with inflow conditions of ap-proximately 5 and 8 m³/s in the Eggen overflow tank.

In addition to the data recorded by the NI system deployed by HES-SO VS, data logged by the Hydro-Clone system and SCADA data from the power plant were collected during the test day.

Figure 91Figure 90 presents the time history of total discharge, along with the electrical power of Units 2 and 3 used during the tests, based on recorded SCADA and Hydro-Clone data. The six power peaks sustained over 900 s are indicated by light-blue hatched areas. In addition to these scenarios, an emergency shutdown of Unit 3 followed by a rapid restart was also tested. It is also worth noting that unit regulation throughout the day had to cope with variable inflow conditions at Eggen, which were relatively difficult to predict and compensate for.

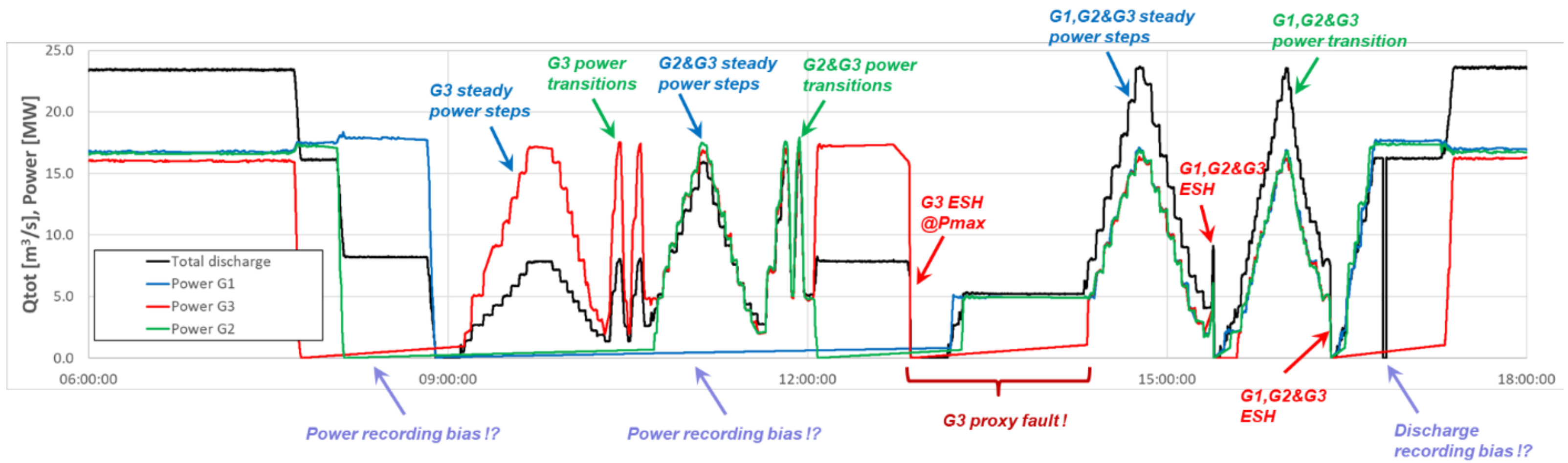

Figure 90 : History of total discharge and electrical power of the three units of KW Mörel during the specific test day of June 17th, 2025

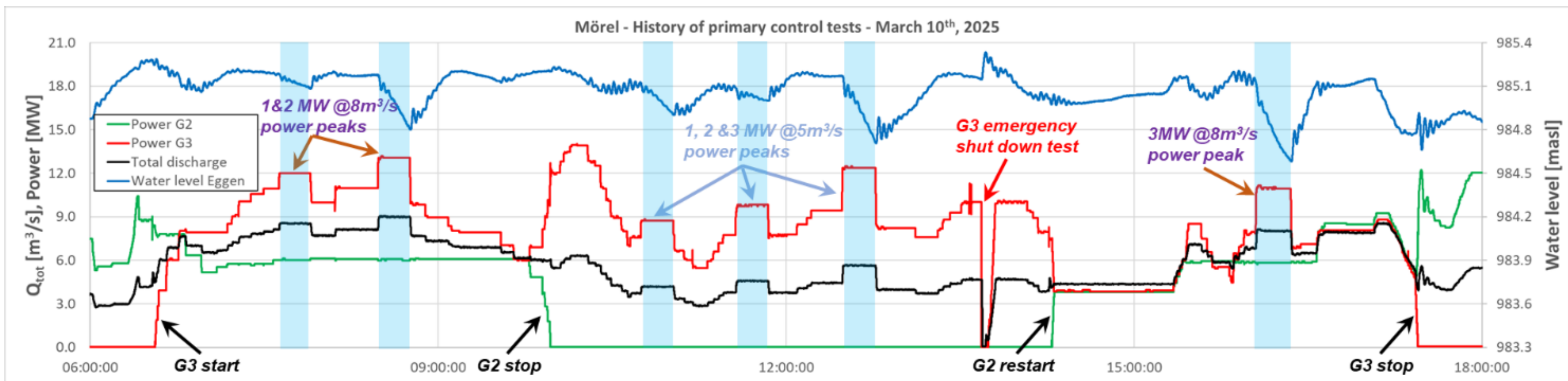

Figure 91 : History of total discharge and electrical power of the two used units of KW Mörel during the specific test day of March 10th, 2026

3.6.4. Analysis of the experimental results and validation of the operational limits of the power plant with respect to the identified storage potentials (HEVS)

3.6.4.1. KW Merezenbach test case

The longitudinal hydraulic profile of the plant, together with the principal equations used to determine the upstream water level, is presented in Figure 92. The static head is calculated using the static pressure measured upstream of the main inlet valve, rather than downstream of it. This approach avoids measurement loss (“blindness”) when the valve is closed, such as during normal or emergency shutdown of the unit.

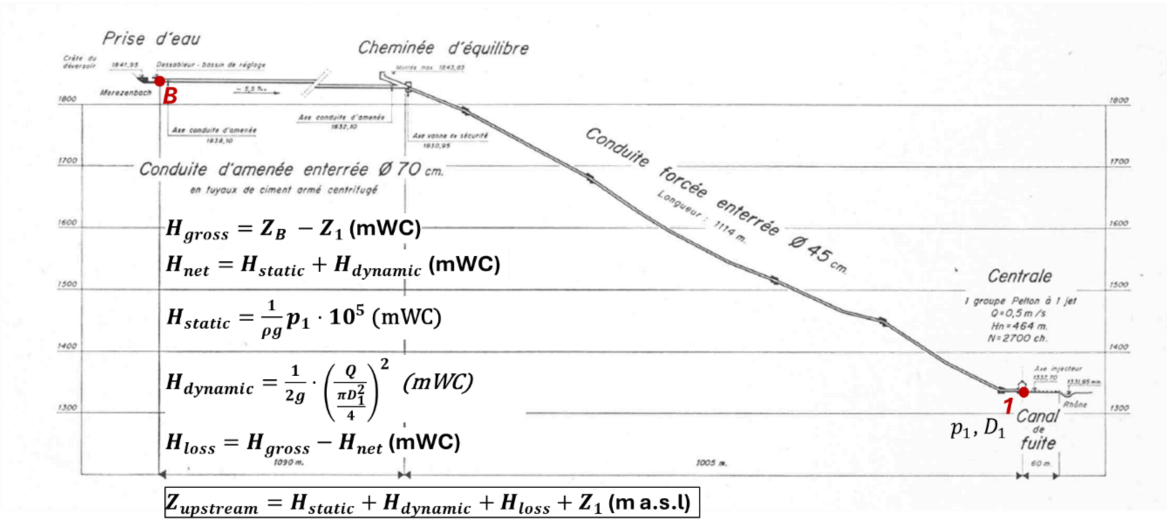

Constants:			
Water density	ρ	999.7	(kg/m³)
Gravitational acceleration	g	9.80665	(m/s²)
Turbine elevation	Z_1	1337.9	(m a.s.l)
Sensors-turbine elevation differences	dz_pstat_up	1.295	(m)
	dz_pstat_down	1.16	(m)
	$dz\_pstat\_up\_SCADA$	1.16	(m)
	dz_pstat_inj	0.395	(m)
Penstock inner diameter	D_1	0.2999	(m)
Measured quantities:			
Upstream water level	Z_B	SCADA	(m a.s.l)
MIV upstream static pressure	p_1	LabView + SCADA	(bar)
Discharge	Q	LabView + SCADA	(m³/s)

Figure 92: KW Merezenbach longitudinal profile along with mathematical formulation used to compute the upstream water level.

The estimation of the upstream water level requires the determination of both the static and dynamic net head, as defined by the mathematical formulation presented in Figure 92(where Z_1 is the elevation of the turbine). The corresponding static and dynamic net head values over the entire monitoring period are shown in Figure 93. These were computed using the measured static pressure upstream of the MIV and the turbine discharge, respectively. It should be noted that, for the HES dataset, the upstream MIV pressure signal was only available from January 23, 2025, due to a sensor malfunction. The red and orange curves, representing the dynamic head derived from LabVIEW and SCADA data respectively, exhibit a continuous variation over time. In contrast, the static head decreases as the discharge increases. The small average difference (approximately 2 mWC) between the static head values calculated from SCADA and LabVIEW data can be attributed to uncertainties in the altimetric positioning of the sensors, as well as to their respective measurement accuracies. While the uncertainty of the existing

SCADA sensor is unknown, the installed sensor has an accuracy of ±1.5 mWC. In addition, the SCADA pressure signal has a resolution of 0.1 bar (i.e., approximately 1 mWC), which explains both the thicker appearance and the higher variability of the light blue curve compared to the darker one. Despite these discrepancies, the resulting error remains relatively small, on the order of 0.4% of the total head.

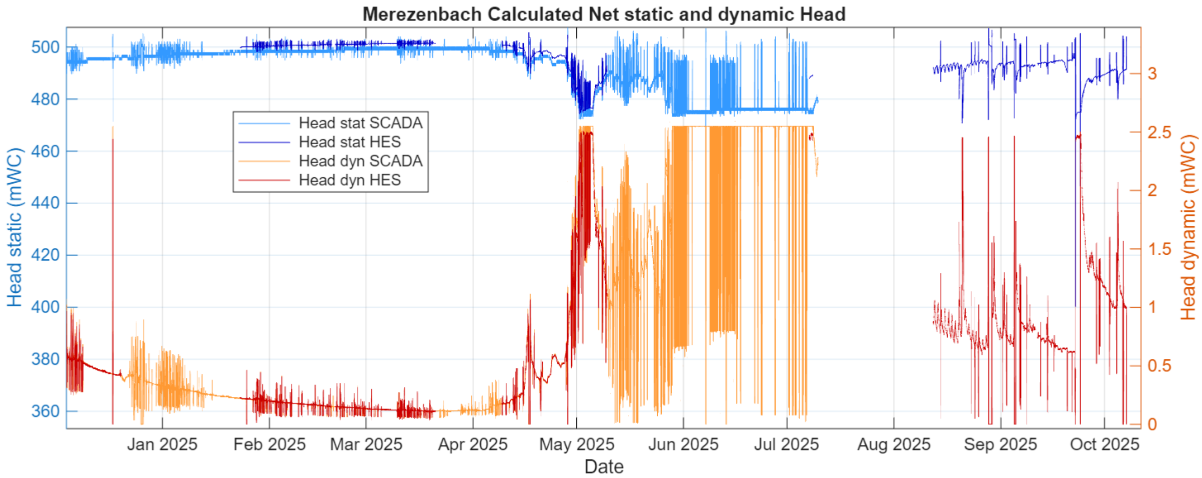

Figure 93 : History of the KW Merezenbach static and dynamic net heads calculated from the turbine upstream static pressure and discharge. Per minute averaged data used.

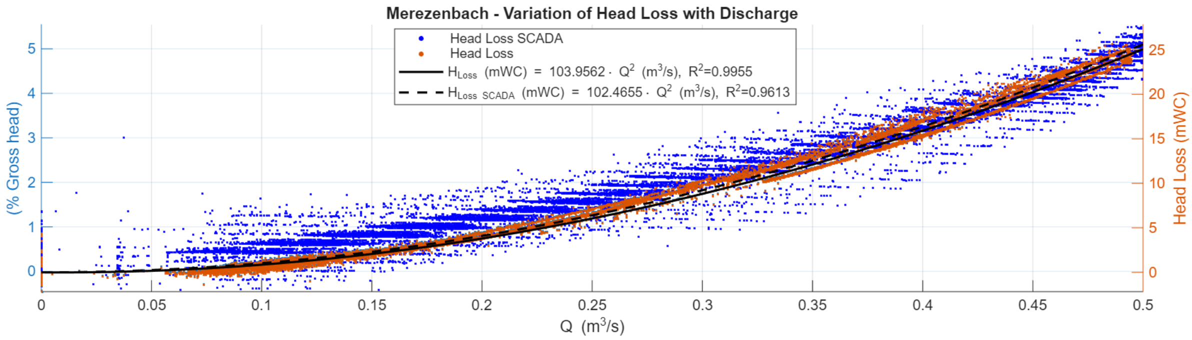

Figure 94 : Resulting KW Merezenbach estimated head loss and discharge relationship, obtained from LabView and from SCADA data. Per minute averaged data used.

Figure 94 presents the estimated head loss as a function of the discharge. The few negative values observed correspond to data recorded during transient conditions at low discharge. In these cases, the measured static head slightly exceeds the gross head obtained from SCADA data, with a maximum discrepancy of 0.83 mWC - considered acceptable in light of the previously discussed measurement uncertainties. Furthermore, the relative difference between the polynomial fitting coefficients remains below 2%.

Using the calculated dynamic and static net head, as well as the associated head losses, the estimated upstream water level is presented in Figure 95. The blue curve corresponds to values derived from SCADA pressure and discharge data, while the yellow curve is based on LabVIEW measurements. The measured water level provided by the plant is shown in green, indicating a generally good agreement with the estimated values. The mean deviation between the calculated and measured water levels is approximately 0.2 mWC for the LabVIEW-based estimation and 1.4 mWC for the SCADA-based estimation, corresponding to less than 1% of the total head.

However, the upstream water level cannot be reliably estimated during transient conditions. Due to the surge tank's reflection ("mirror") effect on pressure waves, as well as the communicating vessels effect between the headrace tunnel and the surge tank, the pressure measured at the turbine is no longer directly correlated with the upstream water level. An additional challenge arises from the extended free surface within the headrace tunnel, resulting from its gentle slope and complex hydraulic behaviour.

Under steady-state conditions, and during slow variations of the intake level, this free-surface elevation can be monitored with an accuracy limited by the sensor uncertainty (±1.5 mWC). Transient events can also be captured, as illustrated in the zoomed section highlighted in brown. However, during such events, the upstream free-surface elevation cannot be accurately inferred from pressure measurements alone.

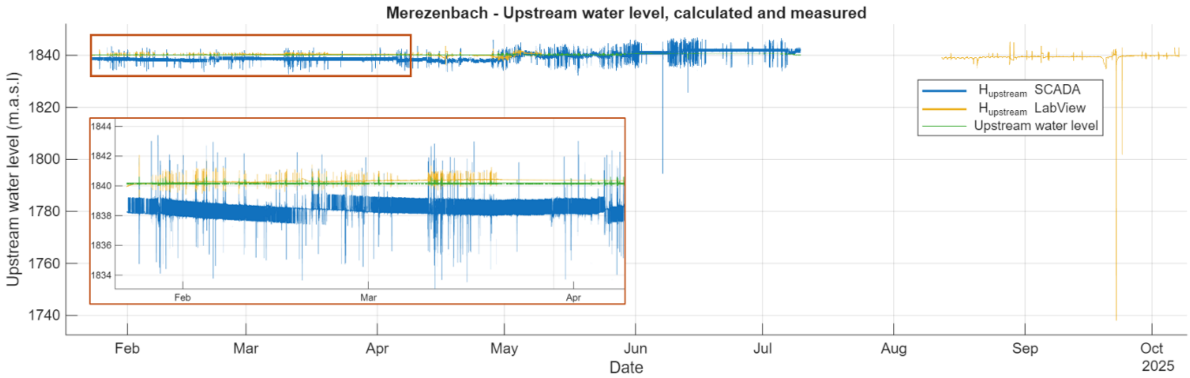

Figure 95 : Comparison between the measured and the calculated upstream water level using the Lab-view and the SCADA data. Per minute average used.

Figure 96 presents the turbine discharge as a function of the injector stroke (with 100% opening corre-sponding to 78 mm). The data, collected over three different years, show no noticeable drift over time.

For the vibration analysis, the standard deviation is used instead of the root mean square, as the mean values of the accelerometer signals are close to zero ([-0.02; 0.005] g). As shown in Figure 97, the standard deviation of the recorded acceleration increases monotonically with the generated power across the entire operating range, for all measurement points. This behaviour indicates that the turbine operates without significant resonance or hydrodynamic disturbances.

.

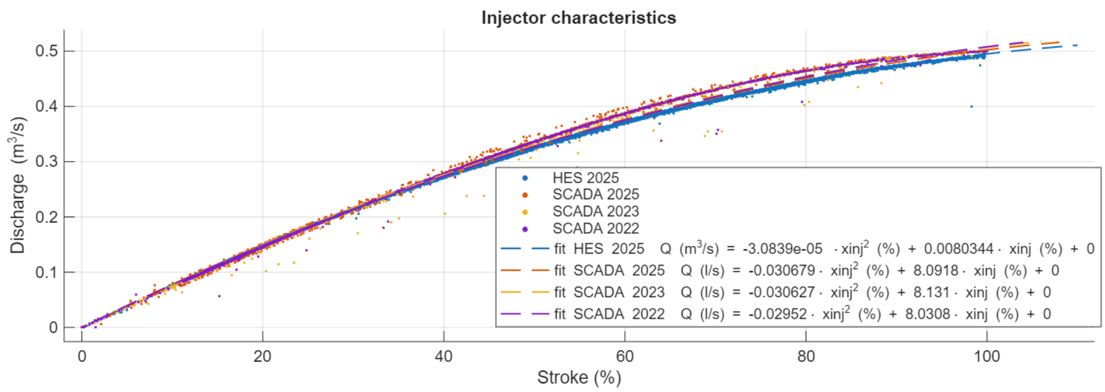

Figure 96 : KW Merezenbach turbine injector characteristics using data from 2022, 2023 and 2025. Per-minute averaged data used.

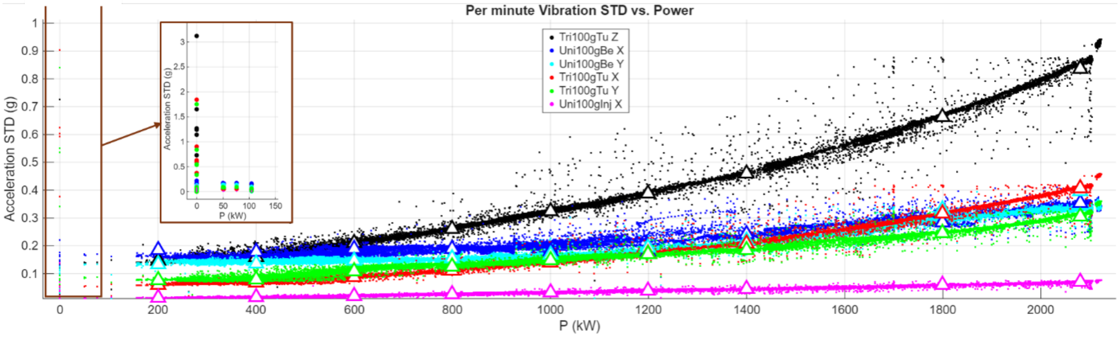

Figure 97 : KW Merezenbach vibration data per-minute STD from the whole test campaign. Triangles indicate the vibration STD during power steps depicted in Figure 98 using per-second data statistics.

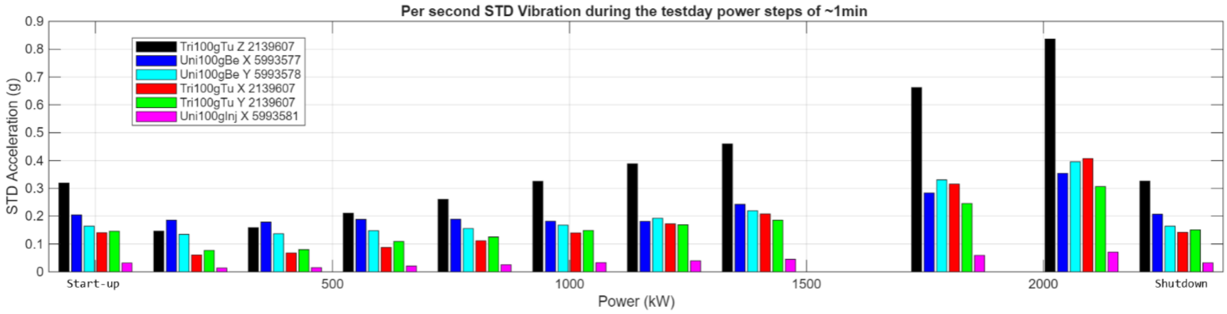

Figure 98 : KW Merezenbach vibration STD during power steps, start-up and shutdown. Per-second data statistics from the test day (December 17th, 2024).

The high-power outliers observed in Figure 97 correspond to measurements recorded on July 7, 2025, when the Merezenbach River reached full capacity. The highest standard deviation (STD) values are measured by the sensor installed on the turbine casing in the Z direction (aligned with the shaft axis), likely due to the cantilever configuration of the turbine shaft.

In contrast, the lowest vibration levels are observed in the injector mechanism area, particularly in the X direction (aligned with the flow), which is also the location farthest from the rotating assembly. It is also noteworthy that bearing vibrations exceed those measured on the turbine casing in the X and Y directions up to a power output of approximately 1’800 kW.

The highest vibration levels occur during start-up, when the jet impacts stationary buckets. As this phase lasts less than one minute, its contribution is not fully captured in Figure 97, which is based on per-minute statistics. Higher values are observed when considering per-second standard deviations (e.g., Tri100gTuZ ≈ 4 g, Tri100gTuX,Y ≈ 2.4 g, others < 0.2 g).

Figure 98 further illustrates the vibration levels during a complete start-up (from standstill to grid synchronization) and shutdown (from desynchronization down to 20% of nominal speed), alongside several steady-state operating points recorded during the test day. Both start-up and shutdown phases exhibit vibration levels comparable to those observed at approximately 1 MW of power generation.

The power-step values, represented as triangles in Figure 97, confirm that the tested steady-state operating points are representative of the turbine’s overall behaviour. Indeed, during normal operation, the turbine power continuously fluctuates due to the regulation strategy aimed at maintaining a constant upstream water level, resulting in continuous adjustments of the nozzle position.

Regarding the relative displacement between the shaft and the bearing casing (see Figure 99), the peak-to-peak values are plotted together with the standard limits applicable to this type and size of machine. The measurements remain nearly constant across the entire operating range and are well below both safety thresholds.

Furthermore, the relative displacement does not show a clear correlation with electrical power and appears to be primarily influenced by the rotational speed of the shaft.

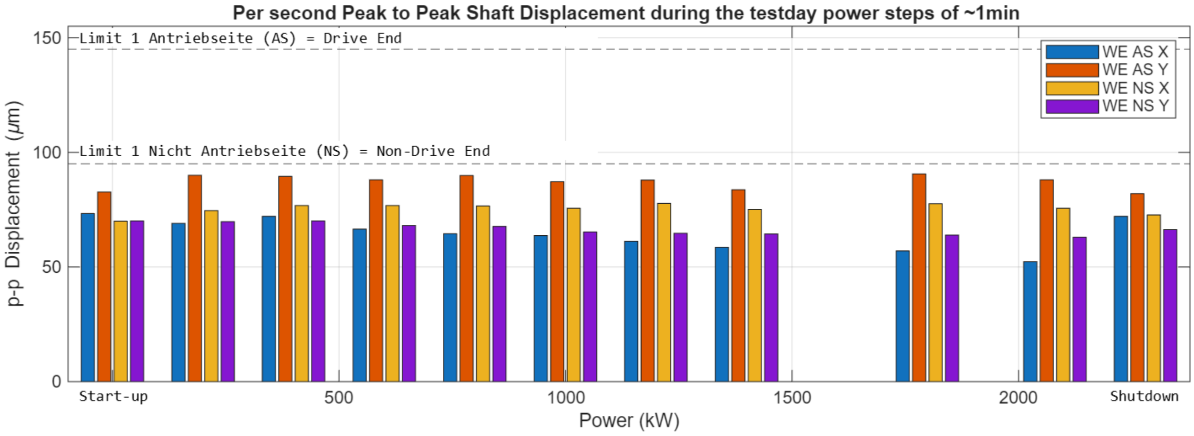

Figure 99 : KW Merezenbach vibration peak-to-peak during power steps, start-up and shutdown. Per-second data from the test day (December 17th, 2024) used.

3.6.4.2. KW Mörel test case

Recorded data validation

The data recorded using LabVIEW and the measurements obtained from the Hydro-Clone system were cross-validated based on the rotational speed of Unit 3, the pressure at the Main Inlet Valve (MIV) of Unit 3, as well as the discharge of Unit 3 and the total discharge signals. The synchronisation of the two datasets was achieved using rotational speed variations observed during start-up and shutdown sequences. It should be noted that the total discharge, measured upstream of the surge tank and logged by the Hydro-Clone system, is subject to a moving average of approximately 25 s.

The time histories of rotational speed, static pressure at the MIV, and discharge, recorded during the March 10th, 2026 test day, show in Figure 100 to Figure 102 good agreement between the measurements obtained from the two systems. The start-up of Unit 3, as well as the emergency shutdown followed by a rapid restart, can be observed in the rotational speed variations shown in Figure 100. The static pressure fluctuations induced by the Unit 3 pressure regulator drain test and the emergency shutdown are depicted in Figure 101. In Figure 102, the time periods during which the total discharge differs from the discharge of Unit 3 correspond to operation of the power plant with both Units 2 and 3 running simultaneously.

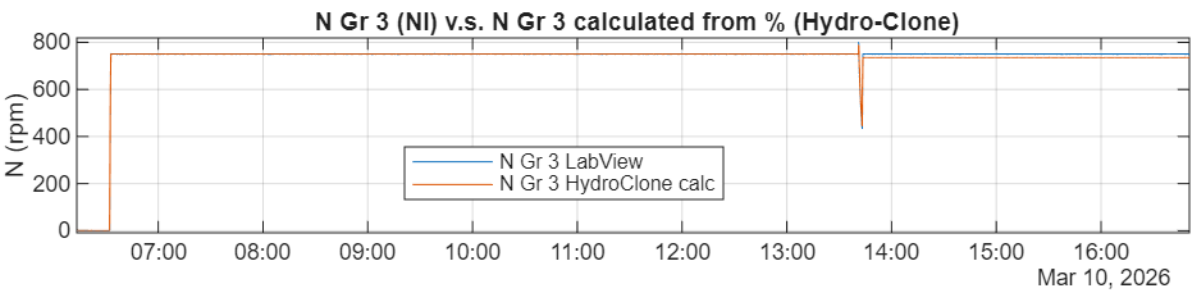

Figure 100 : Time-history of rotational speed of Unit 3 recorded using the NI and the Hydro-Clone systems during the test day of March 10th, 2026.

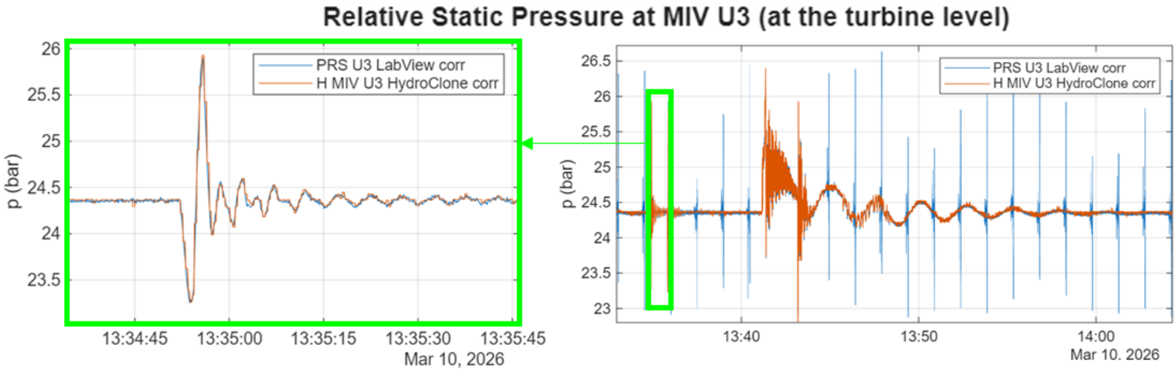

Figure 101 : Time-history of relative static pressure (at the turbine level) at the MIV of Unit 3, recorded using the NI and the Hydro-Clone systems during the test day of March 10th, 2026.

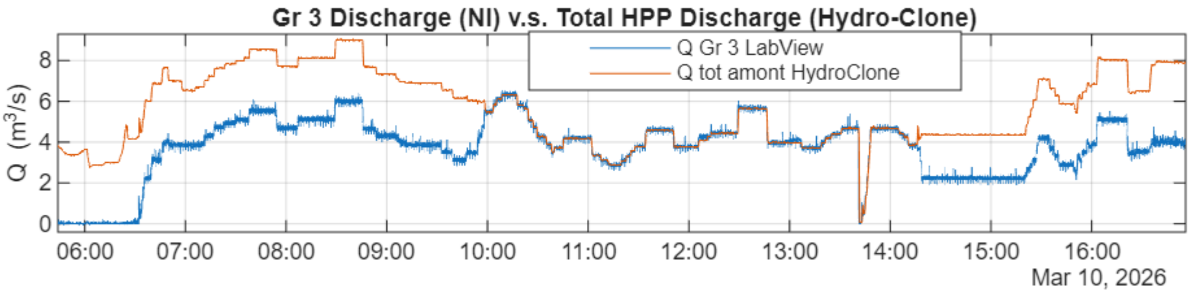

Figure 102 : Time-history of Unit 3 discharge and of total discharge, recorded using the NI and the Hydro-Clone systems, respectively, during the test day of March 10th, 2026.

Resulting dewatering induced by primary ancillary service tests

Figure 103 presents the six power peaks (where 1H designates a 1 MW power peak under high inflow conditions, and 3L corresponds to 3 MW under low inflow conditions) achieved with Unit 3 during the March 10th, 2026 test day, alongside the water level in the Eggen overflow chamber. The power set-points of Units 2 and 3 (depending on the configuration required by the available discharge) were controlled manually by the operator. Consistent initial conditions, with slight overflow at Eggen, were systematically established before and after each power peak. It should be noted that the operator had to manage variable inflow conditions, which were difficult to predict and compensate for throughout the day.

Regarding the water level, the minimum recorded value was 984.58 m a.s.l., which is 13 cm above the minimum authorised level (984.45 m a.s.l.) defined for these tests. In the 1D simulations, the initial water level was set to 984.85 m a.s.l. to avoid overflow. However, this condition proved difficult to maintain precisely on site due to inflow variations and transients between the surge tank and the Eggen chamber induced by turbine power (and thus discharge) changes. In practice, a slight overflow at the Eggen weir crest (located at 985.15 m a.s.l.), which contributed to stabilising the level, was ultimately used as the initial condition for the power peaks.

Table 24 presents the key results of the six ancillary service tests conducted on March 10th, 2026, at KW Mörel. From left to right, the table includes: the time required to reach the power peaks, the corresponding ramp-up rate, the water level at Eggen at the start of each peak, the measured dewatering after 900 s, the simulated dewatering after 900 s, the dewatering rate, and finally the ramp-down rate of Unit 3 power. Power peaks achieved with a load time of less than 30 s, highlighted in green, meet the Swissgrid qualification criterion for ancillary service provision. The slower ramp-up observed for peak 2L is attributed to manual unit regulation combined with head variations induced by hydraulic transients. The measured dewatering depths remain within the predicted range obtained from 1D simulations.

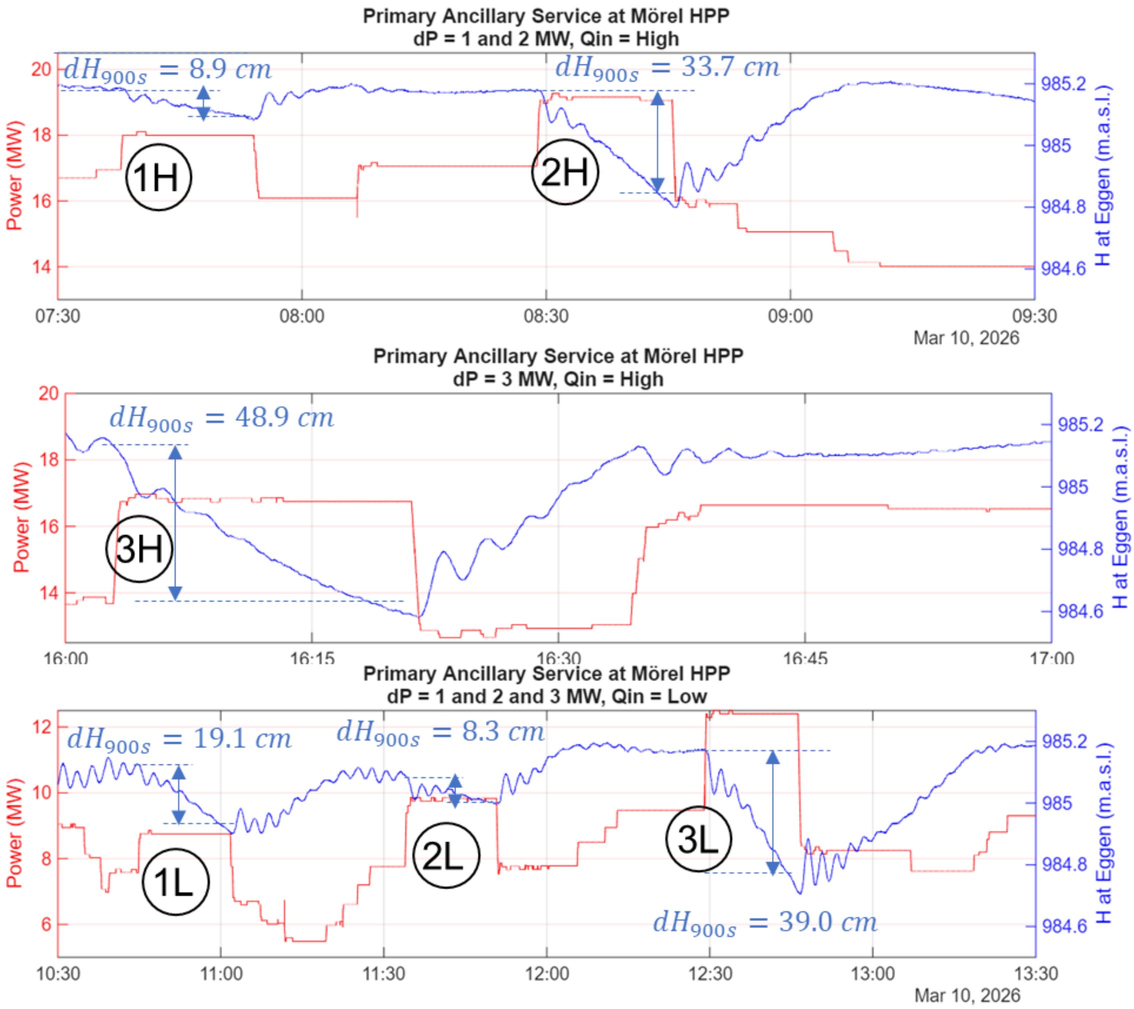

Figure 103 : Time history of Unit 3 power and Eggen water level variations during ancillary service tests conducted on March 10th, 2026, at KW Mörel.

Table 24 Key results of the six ancillary service tests conducted on March 10th, 2026, at KW Mörel.

	Dewatering						Refilling
Test	Load time dP [s]	Load rate dP/t [MW/min]	Initial level H_{start} [m a.s.l.]	Level decrease dH_{900s} [cm]	Simulated level decrease dH_{900s_1D} [cm]	Dewatering rate dH/t [cm/min]	Unload rate dP/t [MW/min]
1H	11.4	5.5	985.184	8.9	19.0	0.59	2.85
2H	22.4	5.35	985.180	33.7	42.0	2.25	7.15*
3H	26	7.08*	985.134	48.9	69.0	3.26	6.02*
1L	9.2	6.87*	985.124	19.1	17.0	1.27	3.82
2L	58.1	2.16	985.088	8.3	41.0	0.55	6.63*
3L	21.2	8.33*	985.17	39.0	75.0	2.60	6.67*

**Power ramp-up and ramp-down rates that allow 3 MW change in less than 30 s.*

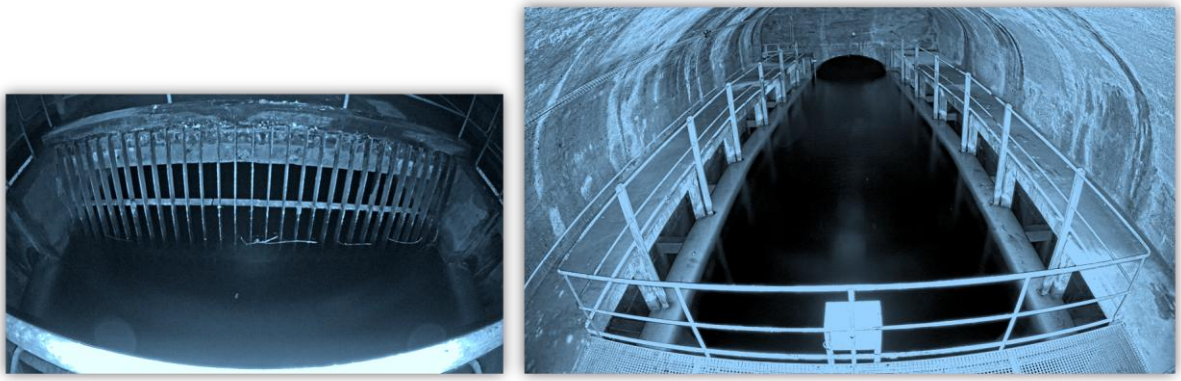

Figure 104 : Recorded downstream (left) and upstream (right) views at Eggen overflow tank during the 3 MW power peak with an inflow of ~8 m^3/s (test 3H) tested on March 10th, 2026.

Finally, Figure 104 provides visualisations of the upstream side of the overflow chamber and the downstream screen, based on recordings from two night-vision cameras installed at Eggen. During the three months between installation and the test day, images were periodically recorded to verify proper camera operation and to document standard operating conditions.

Water surface variations were recorded throughout the entire day of March 10th, 2026, both at the screen and on the upstream side, and video sequences were compiled for all tested scenarios. No major events (such as splashing, large waves, or air entrainment) were observed during the six tested power peaks. In contrast, more pronounced water surface variations were observed during the Unit 3 emergency shutdown test conducted on the same day, including overflow and backflow at the free surface.

Turbine behaviour under standard and primary ancillary service operation

To evaluate the potential impact of overflow chamber dewatering on the turbines, the behaviour of Unit 3 was first analysed under different net head operating conditions, influenced by the total discharge of the power plant and, implicitly, by the number of operating units and their setpoints. Starting Units 1 and 2 increases head losses in the penstock, thereby reducing the energy available to Unit 3, as shown in Figure 105 through the three variations coloured in blue, obtained from steady-state operating condition measurements during the first test day conducted on June 17, 2025.

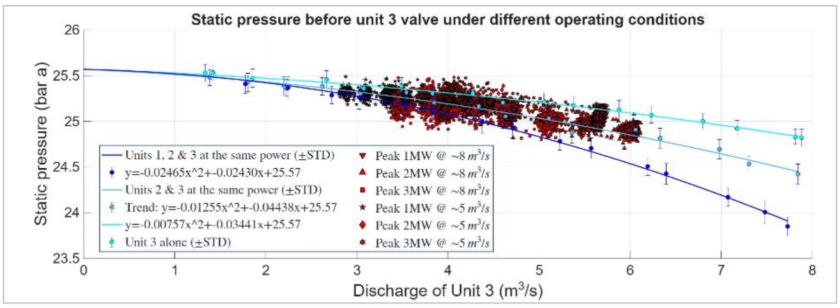

Figure 105 : KW Mörel - Unit 3 static head variation with the discharge depending on operating groups number on standard operation (blue) and during tested ancillary services (red).

The scattered points superimposed on this plot represent per-second average values obtained during the six ancillary services tested on March 10th, 2026. Considering that these points include both steady-state conditions and the numerous power changes carried out during the day, it can be concluded that the slight dewatering of the Eggen tank and the induced transients in the hydraulic circuit have no influence on the net head–discharge characteristic of the turbine.

Figure 106 shows the relationship between discharge and electrical power of Unit 3, depending on whether Units 1 and 2 were operated in parallel. It should be noted that the electrical power measured at the power plant and acquired through the SCADA system is subject to interpolation and temporal resolution effects. To account for this, a fitting was performed based on the corrected discharge, specifically for the test case in which Unit 3 was operated alone. When representing the three cases together, it becomes clear how much additional water is required to achieve the same electrical power output from Unit 3, which is consistent with the observed reduction in static pressure. Based on this information, the turbine characteristics can be presented under different operating conditions. As in the previous plot, the scattered points superimposed on these curves represent per-second average values obtained during the six ancillary services tested and show a remarkable agreement with the values obtained under steady-state operating conditions.

The left side of Figure 107 shows the peak-to-peak X, Y, and Z shaft displacement variations of Unit 3 as a function of electrical power, based on data recorded under steady-state operating conditions. The superimposed scattered points represent the corresponding per-second peak-to-peak displacement values obtained during the dewatering tests. In addition, the right-hand plot illustrates the evolution of the average static pressure and its standard deviation (STD) in both draft tubes (generator and turbine sides) as a function of electrical power, using data from the same steady-state operating conditions and from the ancillary services tests. These two plots reinforce the conclusion that the tested dewatering scenarios have no significant effect on turbine operation.

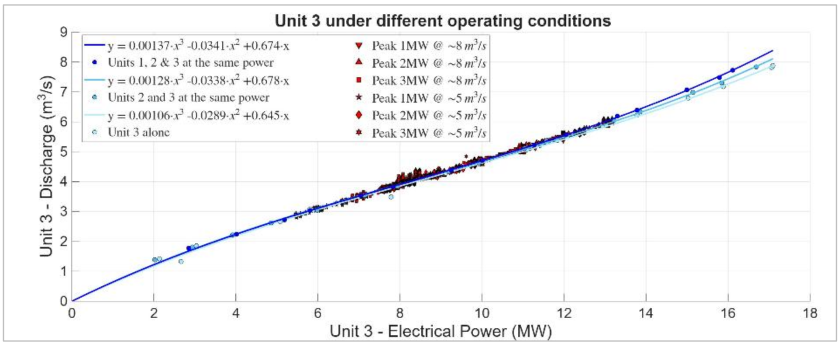

Figure 106 : KW Mörel - Unit 3 average discharge variation with the electrical power depending on operating groups number in standard operation (blue) and during tested ancillary services (red).

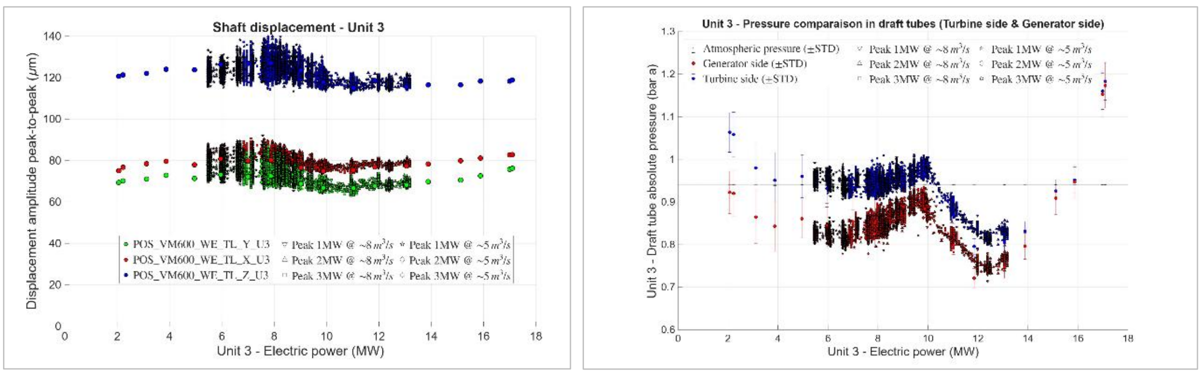

Figure 107 : Unit 3 turbine shaft peak-to-peak displacement (left) and draft tubes average and STD static pressure variations (right) with the electrical power in standard operation and during tested ancillary services.

Another approach to identifying potential perturbations affecting the turbine during dewatering operations is to perform a spectral analysis of the recorded signals, as illustrated in Figure 108 to Figure 110. This type of analysis provides insight into the global energy distribution across different frequency components throughout the operation.

The FFT (Fast Fourier Transform) cascades presented in Figure 108 highlight the main frequency response components detected by the two microphones positioned near the turbine draft tubes for several steady-state operating conditions of Unit 3 operating alone, ranging from 2 MW (blue) to 17 MW (red). The frequencies shown, f/n, are normalised by the runner rotational frequency (12.5 Hz). It can be observed that most components within the frequency spectrum up to 50 f/n are associated with speed-driven phenomena, including hydraulic and electromagnetic rotor-stator interactions dominating the turbine and generator operation, respectively - as well as residual shaft eccentricities, imbalance, and related effects.

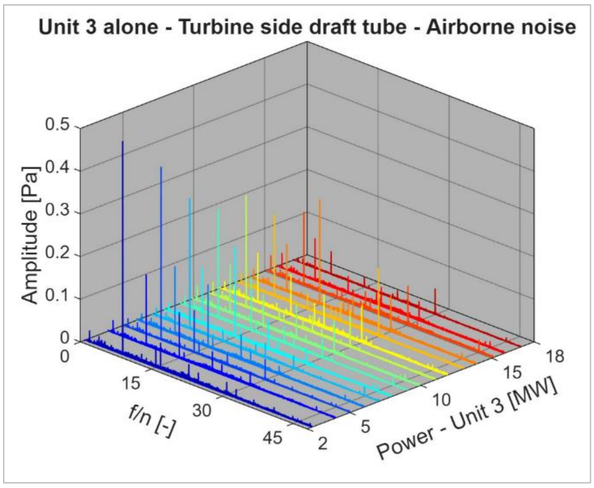

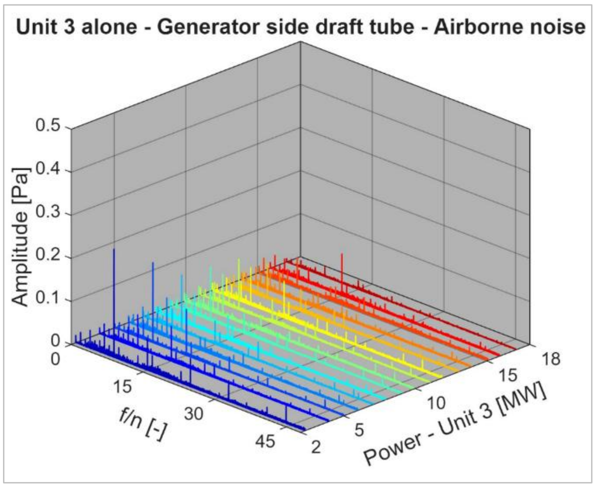

Figure 108 : FFT distribution as a function of the Unit 3 power for the airborne noise measured on the generator side draft tube (left) and the turbine side draft tube (right).

The following figures present examples recorded with Unit 3 operating alone during start-up, minimum-to-maximum and vice versa power transitions, an emergency shutdown, and a power peak of 3 MW under an inflow condition of approximately 5 m³/s. The signals from the two microphones oriented toward the draft tubes of Unit 3, as well as from the pressure sensors installed on the draft tubes, have been considered.

Several identified spectral response components follow the runner rotational speed. For instance, during start-up, these components evolve with speed until reaching a steady value once the generator is synchronized with the grid (e.g., 12.5 Hz corresponds to the runner rotational frequency, while 187.5 Hz corresponds to the blade-passing fundamental frequency induced by the 15 runner blades). Other spectral components can be linked to magnetic phenomena originating in the generator, typically at multiples of 50 Hz.

During the start-up sequence, no distinct frequency excitation is observed; instead, the overall energy level increases progressively as the runner approaches its nominal speed. Similarly, during power transient operations, the spectrograms do not reveal any specific frequency excitations. However, the spectrogram of static pressure in the draft tube (Figure 110) shows higher energy levels at part-load and full-load conditions compared to intermediate regimes.

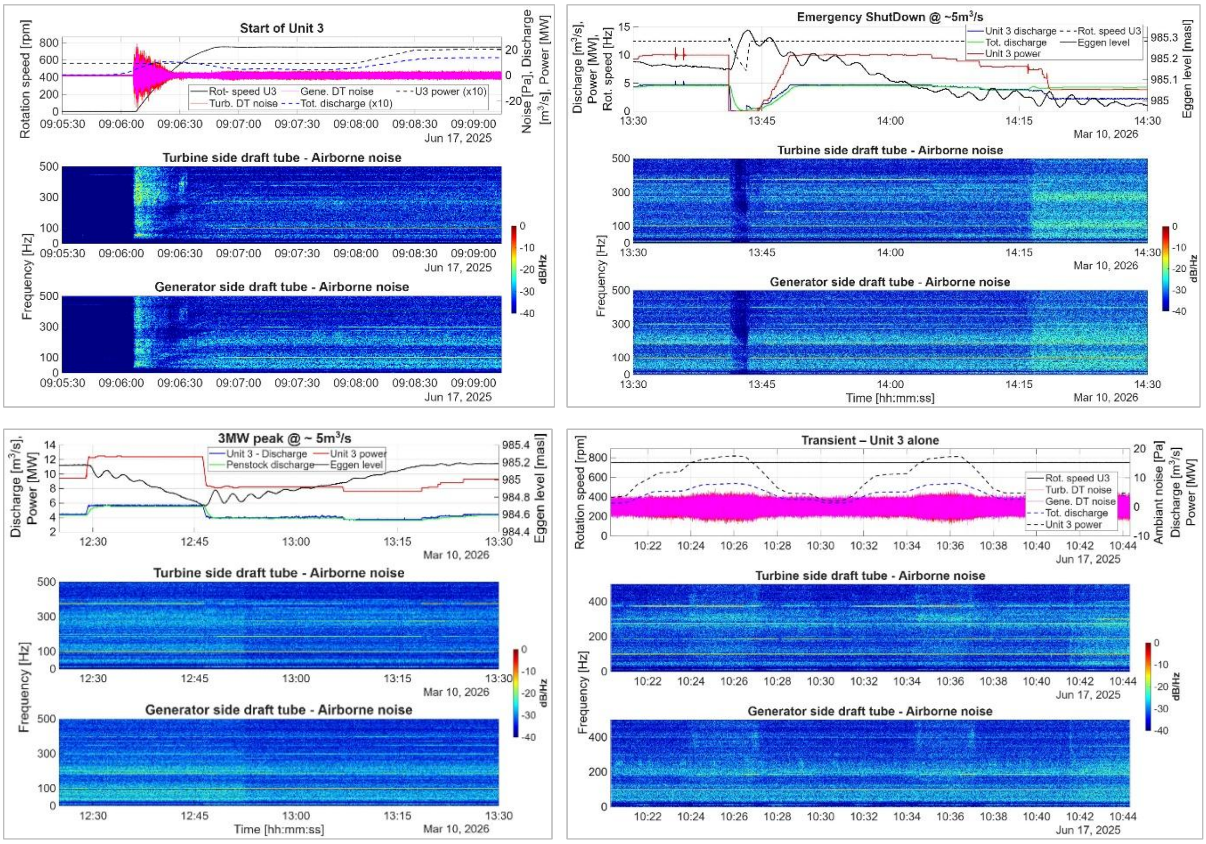

Figure 109 : Spectrograms of the airborne noise on the two draft tubes of the Unit 3 operated alone during a start-up (top-left), an emergency shutdown (top-right), a power peak of 3 MW with low inflow conditions (bottom-left) as well as during a sequence of two minimum-to-maximum and viceversa power transitions (bottom-right).

During the emergency shutdown sequence, a general decrease in airborne noise energy is observed. In contrast, the static pressure response exhibits a short-duration, slight increase in overall energy, following the variation in rotational speed. The fast restart sequence in the wake of the emergency shutdown appears less severe than a regular start-up, likely due to different hydraulic operating conditions (lower energy levels and a different opening required to reaccelerate the runner). The global energy increase observed shortly after 14:15 is induced by the start-up of Unit 2.

Finally, the 3 MW power peak performed with an inflow of approximately 5 m³/s does not show any significant change in airborne noise response. The slight increase in static pressure response amplitudes is attributed to the change in operating regime, as also observed during minimum-to-maximum power transitions.

In conclusion, from a frequency response perspective, the tested dewatering conditions do not exhibit any significant additional adverse effects compared to normal operation. However, this conclusion should be confirmed through a more detailed analysis of all recorded signals over a broader frequency range, as well as through long-term monitoring of the turbine's hydromechanical behaviour under ancillary service operation.

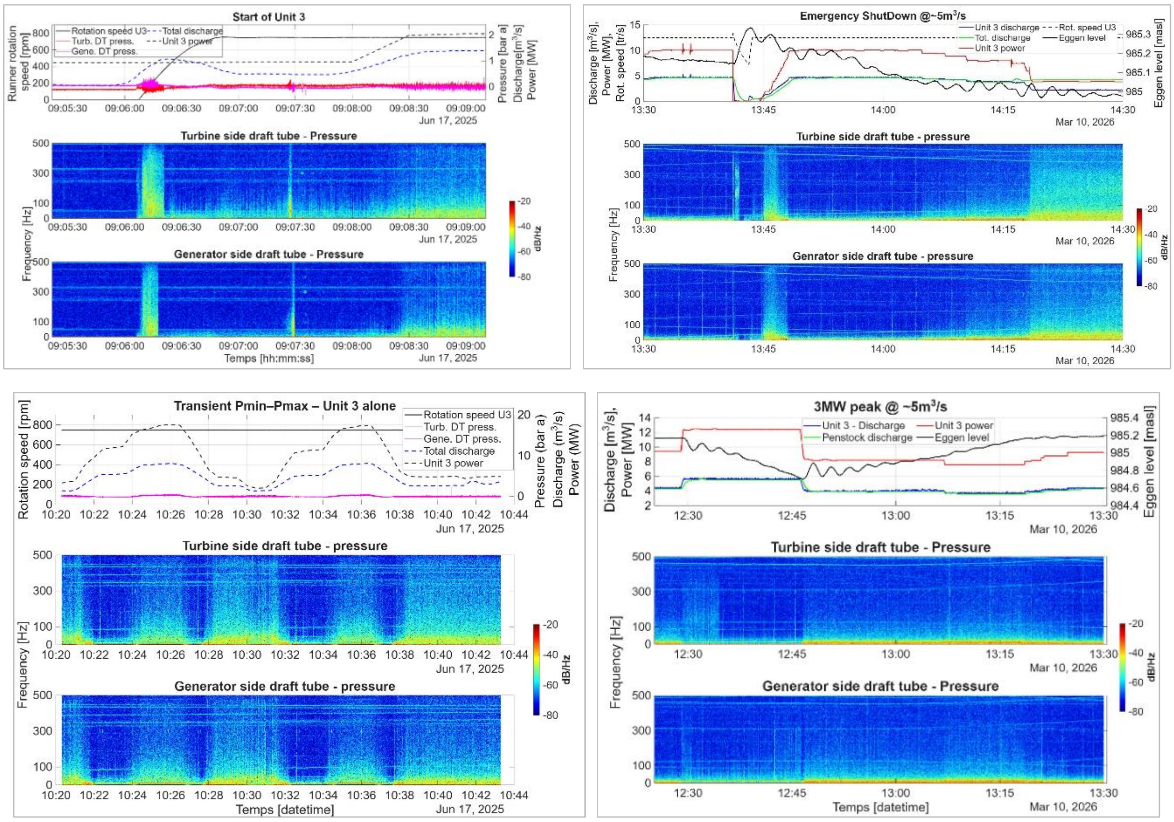

Figure 110 : Spectrograms of the static pressure on the two draft tubes of the Unit 3 operated alone during a start-up (top-left), an emergency shutdown (top-right), a power peak of 3 MW with low inflow conditions (bottom-left) as well as during a sequence of two minimum-to-maximum and viceversa power transitions (bottom-right).

Pressure regulator opening during emergency shutdowns

Knowing the dynamics of the pressure regulators is essential for the Hydro-Clone model to accurately predict the transient hydraulic behaviour of the power plant. To calibrate the Hydro-Clone 1D model, the displacement of the Unit 3 pressure regulator piston was recorded during three emergency shutdown (ESH) tests conducted under different operating configurations (see the power values prior to the shut-down trigger in Table 25). The ESH1 test was carried out with Unit 3 operating alone at full load. The ESH2 test was performed with all three units operating simultaneously at 5 MW. The ESH3 test was similar to ESH1, but with an initial power of 10 MW. In addition, two pressure regulator piston displacements were recorded during intentional draining phases.

Table 25 : Measured pressure regulator opening displacement and timing during the tested emergency shutdown and drain tests.

Test	P_{U1} [MW]	P_{U2} [MW]	P_{U3} [MW]	Max. displacement [mm]	Opening time [s]	Closing time [s]
ESH1	0	0	17	200	1.9	20.8
ESH2	5	5	5	71	0.8	4.9
ESH3	0	0	10	135	1.7	11.2
Drain1	0	0	10	21	2.6	1.9
Drain2	0	0	10	23	3.4	2.1

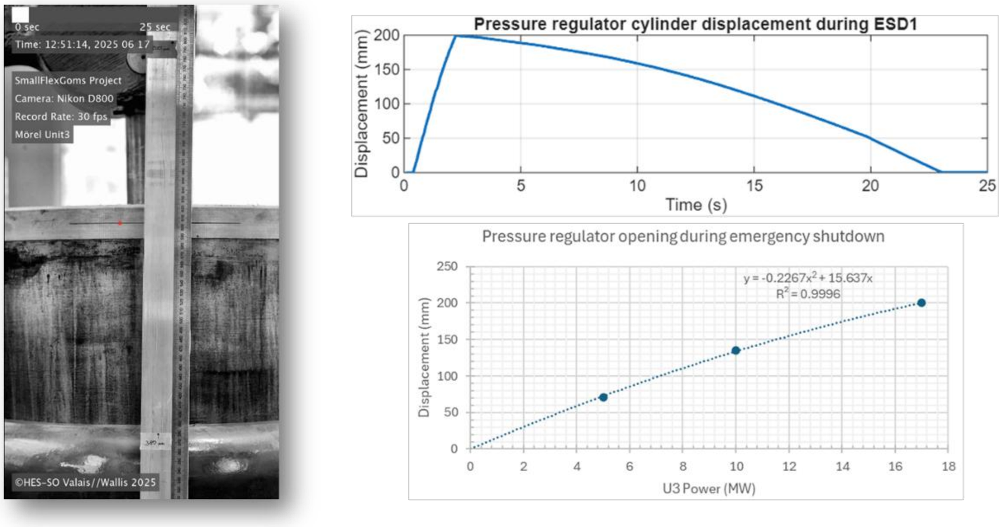

Figure 111 : Snapshot of the pressure regulator video (left) and the determined pressure regulator cylinder displacement (top-right) during the emergency shutdown ESH1 test; pressure regulator maximum opening as a function of Unit 3 power (bottom-right).

The piston displacement as a function of time was extracted from the video footage using a MATLAB code that tracks the dark line at the top of the moving cylinder (see the red marker in the photograph on the left-hand side of Figure 111). The resulting time-dependent displacement is shown in the top-right plot of Figure 111 for the ESH1 test, indicating a maximum displacement of 200 mm when Unit 3 was operating alone at full load (17 MW). The measured pressure regulator opening displacement and timing for all monitored emergency shutdown and drain tests are summarized in Table 25. Finally, the obtained relationship between the maximum piston displacement and the initial power of Unit 3 is presented in the bottom-right plot of Figure 111.

Validation of the operational limits of the power plant with respect to the identified storage potentials

Predictive simulations of power step changes were performed in the context of the Eggen overflow chamber dewatering to support the preparation of on-site tests and to validate the operational limits of the power plant with respect to the identified storage potentials. The simulated load cases were defined based on the expected test conditions, considering power regulation steps of 1, 2, and 3 MW for a single unit, with corresponding inlet discharges, under steady-state conditions at the defined reference water level. A loading and unloading rate of approximately 7.5 MW/min, measured on-site, was applied in the simulations to closely represent actual operating conditions.

The simulations were carried out under idealised conditions, assuming fully stabilised initial states, with both the surge tank and the Eggen overflow chamber at steady state prior to the transient. Although some discrepancies may arise when compared to measured data, the results provide a reliable indication of system behaviour and help to confirm the feasibility of the planned tests.

For instance, in the case of a 3 MW power increase, the simulations predict a noticeable variation in the water level of the Eggen overflow chamber. As illustrated in Figure 112 the load increase of Unit 3 induces significant oscillations in the surge tank, whereas the Eggen overflow chamber shows a relatively smooth and quasi-linear drawdown, with minor oscillations driven by surge tank dynamics. After approximately 900 seconds, corresponding to primary ancillary service requirements, a total level drop of about 0.75 m is observed.

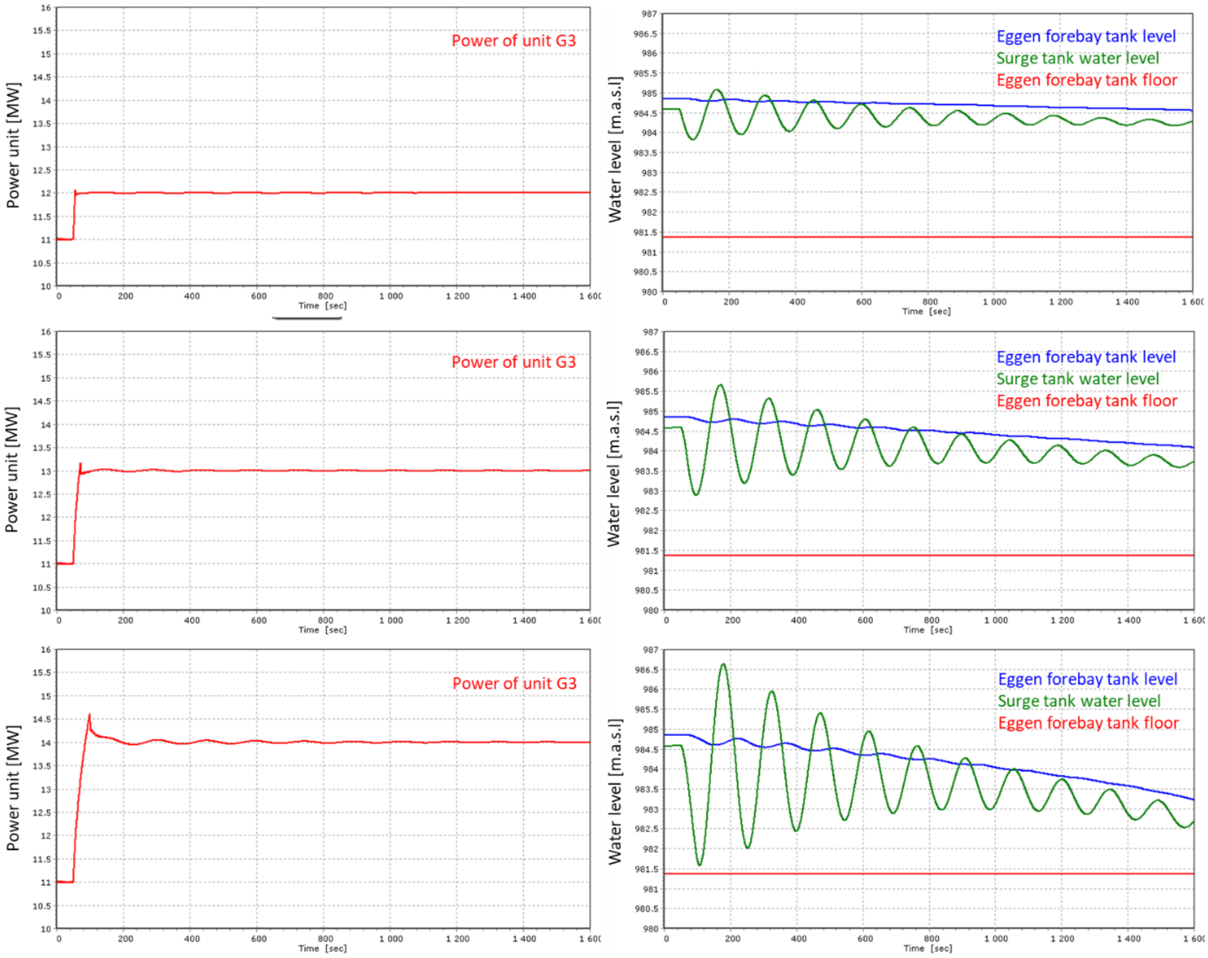

Figure 112 : Power regulation of Unit 3 (left); transient behaviour of the surge tank and Eggen chamber water level for a 1, 2 and 3 MW steps with Q_{in}=5 m³/s at 984.85 m a.s.l. (right).

3.6.5. Conclusion & perspectives

The data acquired under both free-run conditions and dedicated test sequences enabled a comprehensive characterization of the normal operation of the Pelton turbine at KW Merezenbach and one double-Francis unit at KW Mörel. The analysis provided a detailed overview of turbine behaviour under nominal head conditions, with the objective of identifying any potential impact of future dewatering operating modes. The recorded datasets were validated for both case studies, and statistical analyses were performed.

For the KW Merezenbach case, the acquired data allowed a detailed characterization of turbine behaviour under steady-state operating conditions. The upstream water level can be reliably estimated during normal operation, with an average deviation of approximately 0.2 mWC, using the static pressure measured upstream of the main inlet valve and the turbine discharge. However, this estimation is no longer valid under transient conditions, such as during primary ancillary services, due to the influence of the surge tank and the complex free-surface dynamics within the headrace tunnel. The overall condition of the turbine was further assessed through vibration measurements. The results indicate that the turbine operates without significant resonance or hydrodynamic disturbances across its full operating range.

No dewatering scenarios could be experimentally tested at KW Merezenbach due to the contraindications identified in WP3 and WP5. In addition, dewatering following the standard drawdown procedure could not be carried out due to operational constraints. Nevertheless, the acquired dataset remains highly valuable and provides a solid reference for detecting potential anomalies during normal operation.

At KW Mörel, Unit 3 and the Eggen overflow tank were instrumented to establish a comprehensive characterization of the machine's normal operation, to investigate the effects of primary ancillary services, and to monitor behaviour during emergency shutdown events.The primary ancillary service operating mode was expected to potentially induce significant overflow tank dewatering, increasing the risk of air entrapment, as described in WP3 and WP5.

The data acquired under both free-run conditions and dedicated tests at KW Mörel were validated, and statistical analyses were performed. These data enabled a comprehensive characterization of the normal operation of one of the installed double-Francis turbines. The analysis provided an extensive operational overview of the turbine under nominal head conditions, which was used to assess the effect of dewatering on turbine operation.

The performed dewatering tests indicate normal operation based on airborne noise, shaft displacement, draft tube static pressure or spiral case vibration monitoring, and represent a promising step toward ancillary service provision, pending additional validation. It was also demonstrated that the plant could deliver ±3 MW/min power peaks using automatic power regulation.

3.7 WP7– Virtual Power Plant

Lead: HEIG-VD, partners: HDE, ALPIQ, FMV, WSL

This work package focuses on the optimal design and operation of a Virtual Power Plant (VPP) composed of small-scale hydropower plants as well as distributed renewable energy sources such as wind and solar photovoltaic (PV) plants and Battery Energy Storage Systems (BESS). The goal is to optimize the revenue of the VPP from participating in electricity markets offering energy production and flexibility for provision of ancillary services.

The optimization process is divided into two main parts.

- The first part addresses the design of the VPP, including the selection of suitable resources (such as PV systems, battery energy storage systems, wind turbines, and hydraulic pump-turbines).
- The second part focuses on the operational optimization of the VPP components across multiple time horizons (weekly, daily, and intra-day), considering market conditions and uncertainties related to renewable generation and natural water inflows

3.7.1. Approach and Overall Problem Formulation

The optimal design of the VPP is developed through a practical and collaborative process with project partners (FMV and Alpiq). This involves defining a set of design schemes that account for geographical and technical constraints related to renovations, the feasibility of installing new pumps and hydropower turbines, and insights from existing studies on planned and prospective local wind and PV projects.

For each design scheme (*i.e.*, a VPP with given energy resources), a three-level optimization problem is formulated to find the optimal scheduling of controllable resources of the VPP across multiple time horizons. This optimisation problem allows us to estimate optimal annual revenue of the VPP from participating in different electricity markets and eventually estimate the OPEX of the VPP. Then OPEX can be compared with the CAPEX of a given design scheme for development of relevant business models to ensure the profitability of investing on new installations over their lifetime. In addition, to provide further insights on the profitability of various VPP schemes, a set of sensitivity analysis are performed by changing the size of different component of design schemes (e.g., power and energy capacity of batteries, peak installed PV power, etc.).

The abovementioned optimal operation problem must deal with the uncertainties related to the variabilities of the renewable generations as well as water inflow (discharge) and market prices across different time horizons. In this respect, first we formulated a deterministic optimization problem in which theses variables are known as input parameters of the optimization problem. The deterministic optimization problem provides an optimistic benchmark for estimation of annual revenue which is not realistic. Then, we formulated different variant of the optimization problem with scenario-based stochastic formulations. The uncertain variables are modelled through different set of scenarios using available historical data as well as measured and forecasted data of hydro and meteorological variables (solar irradiance, water discharge, wind speed, etc) provided by WSL in WP4 from mid-2024 onward for the specific case of KW Aegina – Alstafel.

A preliminary version of the VPP design problem formulation (including the objective function, decision variables, and key constraints) was formulated in 2023 following several meetings and discussions among the partners of WP7. An appropriate solution algorithm is also developed to solve the proposed problem formulation. In 2024, the mathematical problem formulation has been refined to better represent the technical and economic constraints for development of VPPs in the GOMS region following further advances in the project. In the revised formulation the feedback from the partners is integrated and additional constraints are modelled such as the financial risk of the VPP operation. The detailed mathematical formulation is available in the annex document "Virtual Power Plant Design - Problem Formulation". In 2025, the problem formulation is further revised to include the results of measured and forecasted hydro-meteorological variables provided by WSL and to benchmark an optimistic (but unrealistic) deterministic optimisation against different variants of stochastic optimisation formulations. The detailed formulation of the optimisation problems is presented in the deliverable document "Virtual Power Plant Design - Problem Formulation", D7.1.

The following are the main assumptions underlying the problem formulations and proposed solution algorithms:

The VPP will focus on three distinct electricity markets: day-ahead, intraday balancing, and flexibility market through provision of ancillary services.

The number of VPP design schemes is limited. As a result, we can calculate the profit and risk of each design scheme individually.

The VPP might consist of several existing and potential small hydro power plants, pumps, PVs, wind turbines, and battery energy storage systems.

There is a hydrological link constraint between small hydro power plants and pumps. Following consultations with FMV and other partners, this has been modelled through a set of variables representing the in/out flow of each reservoir as well as a set of variables to allocate each reservoir as up/down stream of a hydropower installation (turbine or pump).

Small hydro power plants, pumps, and energy storage systems participate in the flexibility market to provide flexibility products (e.g., Frequency Containment Reserve – FCR product for ancillary service market of Swissgrid). In this study, because of practical reasons, PVs and wind turbines do not curtail their power to participate in the flexibility market.

The VPP optimize its resources in day-ahead and ancillary service markets knowing the forecast with lead time of 24h. Furthermore, the VPP participate in intraday balancing market in which it minimizes the imbalance costs associated with the differences between the scheduled and real-time power production.

When we combine small hydro power plants, PVs, wind turbines, energy storage systems, and pumps into a single portfolio and centrally manage them within a VPP, there are several advantages.

- Firstly, by integrating small hydro power plants into a VPP scheme, it is possible to optimize their production and increase their potential profit in the day-ahead energy market.
- Secondly, the less reliable flexibility of the hydro power plants with small reservoir capacity can be combined with the more reliable flexibility of the battery energy storage systems, allowing them to meet the requirements of the flexibility market as well as environmental constraints (*e.g.*, limits related to hydropeaking).
- Thirdly, the flexibility of the small hydro power plants can be used to compensate for PV and wind turbine production imbalances due to forecast errors, resulting in increased profits in the day-ahead and intraday markets.
- Fourthly, the pumps can be used to transfer water multiple times to higher altitude hydro power plants, allowing them to provide and sell more flexibility if the price of flexibility is higher than the cost of energy in the day ahead.

The flowchart in Figure 114 describes the process of optimal VPP design. The process begins by generating a set of long-term annual scenarios, each of which represents a different possible hydro-meteorological condition (this is provided in WP4). The next step is to optimize the VPP operation for each scenario through a three-stage optimisation problem.

Once the VPP has been optimized for all scenarios, the profit and risk of all VPP schemes are calculated. The best scheme is then selected.

The overall objective of the proposed algorithm is to identify the following:

- The optimal VPP design scheme, including the optimal capacity of its generation and storage units.
- The optimal operating schedule for each generation and storage unit regarding various scenarios.

3.7.2. Three-stage optimisation problem

In the following, a brief description of problem formulation and proposed algorithm is presented. To optimally design the VPP, we must determine the optimal operation of the VPP components across different time horizons, considering the three mentioned markets. However, if we consider all time horizons in one optimization problem, it would be so large that it would be impossible to solve in a tractable manner. We employ a hierarchical approach to resolve the issue of tractability by estimating the optimal operation in three stages, namely, long-term (first stage), short-term or day-ahead (second stage), and real-time or balancing (third stage), keeping in mind that the number of VPP design schemes are limited.

The model of each stage includes its own objective function and set of constraints. The objectives are presented briefly as follows. The constraints are grouped regarding technical limits of assets and presented in subsection 3.7.2.4 (constraints). The detailed mathematical formulation is presented in the "Virtual Power Plant Design - Problem Formulation" deliverable D7.1. document.

3.7.2.1. Long term optimization model (first stage)

The first stage model is designed to determine the annual water level schedule for reservoirs associated with storage-based hydropower plants. Only these facilities are considerate due to their strong dependence on seasonal water availability, unlike run-of-river plants or Battery Energy Storage Systems (BESS), which operate on much shorter timescales.

The objective is to maximize annual revenue from participation in the day-ahead electricity market. This is achieved by optimizing the daily volumes of water either turbined or pumped at each plant. To discourage unnecessary water releases, a spillage penalty is incorporated into the objective function.

The decision variable represents the scheduled daily water level for each reservoir located upstream hydropower plant. Since intra-day dynamics are not modelled, all plants are assumed to operate as continuous systems, and no ancillary services are provided.

3.7.2.2. Day-ahead optimization model (second stage)

The second stage model focuses on optimizing the day ahead scheduling operational revenue of all resources within the VPP. It uses the annual schedule from the upper stage as input, breaking it down into a series of short-term optimization windows (typically 1 day). The optimizations should be executed sequentially to ensure dynamic updates of battery SOC and reservoirs water level, maintaining consistency across the year.

The objective is to maximize the total daily income generated by all resources, while adhering to the reservoir levels set by the upper-stage model. Any deviation from this schedule incurs a penalty. An additional spillage penalty is applied to discourage excessive water releases.

The decision variables correspond to the hourly scheduled power generation (or consumption) of each asset comprising the VPP.

3.7.2.3. Real time optimization model (third stage)

The third-stage model is only applied when performing stochastic or pseudo-stochastic second-stage optimization. It is executed immediately after each daily simulation. It serves two main purposes.

First, it updates the reservoirs' water levels by accounting for the actual measured water discharge volumes together with the turbined water volumes scheduled in the second stage. It also verifies whether each reservoir's water level remains within its operational limits. If this condition is not satisfied, the corresponding hydropower plants must be curtailed or shut down. This check is particularly important for assets with small reservoirs, which can be emptied or filled within a short time horizon

Second, it aims to reduce the overall VPP power imbalance mostly caused by renewable generation forecast errors. This is achieved by leveraging flexible assets such as BESS or hydropower plants with operational flexibility.

The objective is to minimize the deviation between the total power generation scheduled in the second stage and the actual measured power of each asset within the VPP. A penalty is applied to deviations in hydropower generation. This mechanism encourages the use of BESS flexibility before hydropower and allows also prioritization of which hydropower units should provide flexibility, and which should remain fixed.

The decision variables correspond to the actual measured power generation (or consumption) of each asset comprising the VPP.

3.7.2.4. Constraints

Since different optimisation models (*i.e.*, first, second, and third stages) share similarities in their constraints, here we present them grouped. As previously explained, the main distinctions arise from the time horizon, the temporal granularity, and the nature of the input data. In particular, ancillary services typically operate on another time scale than day-ahead markets (e.g., the FCR market is based on a 4-hour time step). Consequently, a second time index is introduced in the second stage, while it is not present in other stages.

The constraints are organized into several categories, which are summarized below. It is important to highlight that, as the focus of this project is on hydro power plants, the curtailment of solar and wind generation is not considered. Indeed, the wind and PV power generation are not modelled with controllable decision variables. Therefore, no explicit constraints are presented here for these resources.

Water reservoirs

- Water level dynamics tracks the evolution of reservoirs' water level considering all inflows and outflows. This includes natural discharge from surrounding areas, as well as inter-reservoir and plant interconnections, ensuring a comprehensive representation of water movement within the system.
- Final water level: Prevents the model from emptying every reservoir at the end of the optimization horizon, which would artificially maximize profit. It enforces that only the available water is turbinated or pumped. This constraint can be applied in two ways: either strictly, by requiring the final reservoir levels to match the initial levels, or more flexibly, by penalizing the difference between the initial and final levels.
- Reservoir State Definition (linearization): Define the operational state of each reservoir based on its current storage level, ensuring that water volumes remain within predefined operational limits. This constraint is required to model non-linear relation between power production and water flow of hydro power plant using performance tables which are defined separately for each reservoir state (net head) as schematically illustrated in Figure 113.

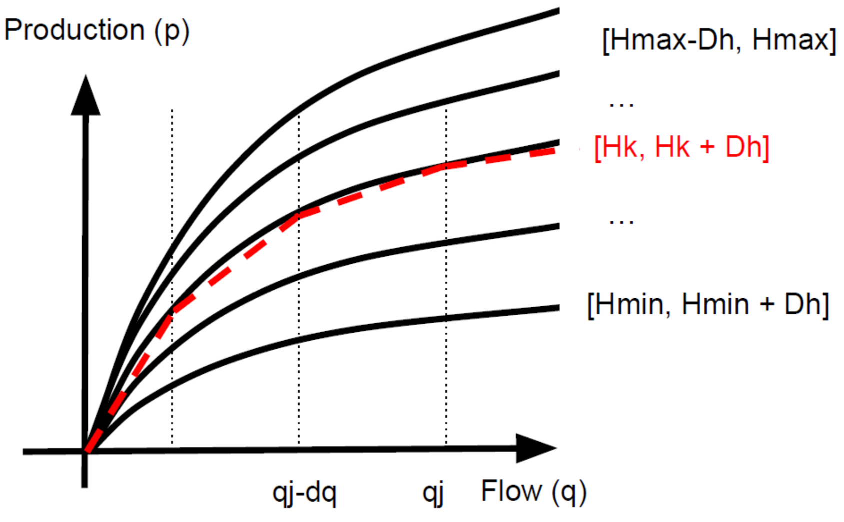

Figure 113: Hydropower performance linearization

Hydropower plants

- Operational Constraints: Ensure that each hydropower plant operates within its technical and capacity boundaries.
- Energy Conversion: Model the transformation of hydraulic energy (from water flow) into electrical energy, considering the current state of the upstream reservoir.
- On-off plant (Second Stage Only): Enforce a binary operational mode where the plant is either fully active at maximum flow or completely inactive with no water flow.
- Ancillary Services Provision (Second Stage Only): Guarantee that continuous-operation hydropower plants meet their assigned ancillary service reserve requirements.

BESS (second stage only)

- State of Charge (SOC) Dynamics: Model the evolution of the battery's SOC over time, based on charging and discharging actions.
- Operational Constraints: Ensure the battery operates within its defined power and energy capacity limits.
- Ancillary Services Provision: Ensure the battery contributes to meeting ancillary service reserve obligations.
- Mutual Exclusivity Constraint: Enforce that the battery can only operate in one mode at a time—either charging or discharging, but not both simultaneously.

Power imbalance (third stage only)

- Overall power imbalance: Calculate the positive or negative imbalance between the scheduled total power and the actual measured total power across the VPP[3].
- Hydropower imbalance: Calculate the positive or negative imbalance specifically between the scheduled hydropower and the actual measured hydropower.
- Short/long selection: Constraints that classify the VPP state as short (insufficient power) or long (excess power) relative to the actual measured power generation. These constraints ensure that the battery is not charged or discharged as by modifying the output of another flexible asset, to modify BESS capacity for future use.

[3] The calculation of balancing prices does not follow the new calculation method of swissgrid which is in place from January 2026.

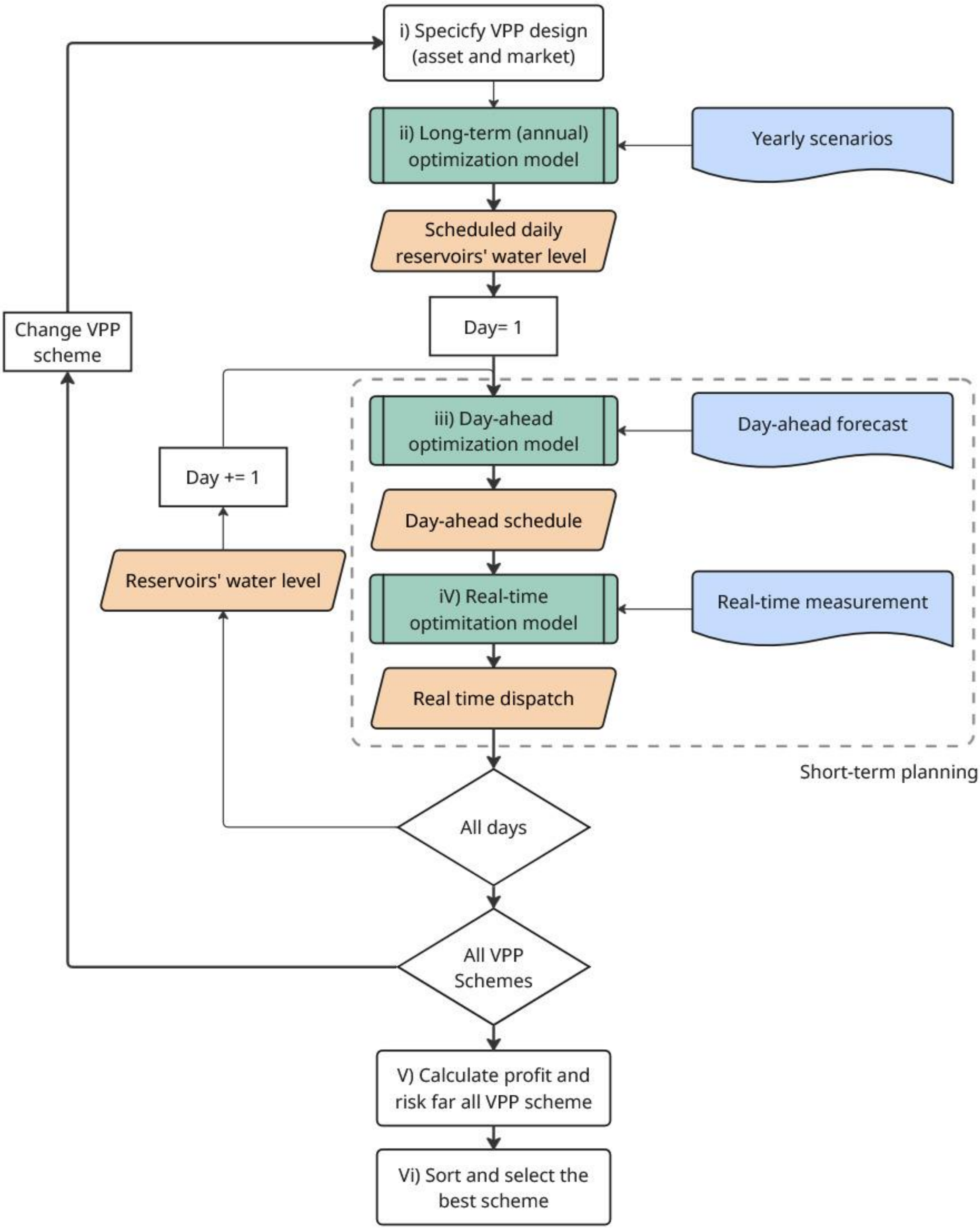

Figure 114 Proposed algorithm for the VPP design problem. The optimization stages are shown in green, the input data in blue, and the output data in orange.

3.7.2.5. Link between the stages

A key component of the proposed multi-stage optimization framework is the mechanism that links the first and second stages through water level scheduling in reservoir-based hydropower plants. After solving the first-stage stochastic optimization, a probabilistic schedule for reservoir water levels is obtained across the planning horizon. This schedule incorporates not only expected values but also quantile bounds that capture uncertainty in inflows, market prices, and operational constraints. When the first stage is treated as deterministic, these quantiles are instead represented as simple offsets.

In the second stage, which simulates day-ahead scheduling operations, a penalty term is introduced to encourage consistency to the scheduled water levels obtained from the first stage. This penalty discourages deviations from the first-stage schedule and ensures consistency between the two stages. Specifically, the penalty comprises two terms:

- Deviation penalty: This term penalizes the absolute deviation between the actual water level and the scheduled water level from the first stage.
- Quantile limit violation penalty: This term penalizes instances where the actual water level exceeds the upper quantile or falls below the lower quantile bounds derived from the first-stage stochastic results. For deterministic first stage runs, these quantiles are approximated by applying a fixed percentage deviation (e.g., ±5%) around the scheduled water level.

The penalty function can be expressed as:

$$PEN_1^b = \frac{\alpha^b_{\mathrm{AVG}}}{3600}\left(\overline{\Delta V^b} \cdot \overline{\pi_{\mathrm{DA}}} - \underline{\Delta V^b} \cdot \underline{\pi_{\mathrm{DA}}}\right)$$

$$PEN_2^b = -\underline{\pi_{\mathrm{DA}}} \sum_{q \in Q} \lambda^q_{\mathrm{Q}} \frac{\alpha^b_{\mathrm{AVG}}}{3600}\left(\overline{\Delta V^{b,q}_{\mathrm{Q}}} + \underline{\Delta V^{b,q}_{\mathrm{Q}}}\right)$$

Here, b denotes the upstream reservoir index and q represents the quantile limit number. The parameter α^b_{AVG} corresponds to the average efficiency of the hydro power plant associated with reservoir b. $\overline{\Delta V^b}$ and $\underline{\Delta V^b}$ denote the positive and negative reservoir final level deviation, respectively.$\overline{\Delta V^{b,q}_{\mathrm{Q}}}$ and $\underline{\Delta V^b}$ denote the reservoir water volume excess/deficit relative to the scheduled upper/lower quantile-based boundaries. $\overline{\pi_{\mathrm{DA}}}$ and $\underline{\pi_{\mathrm{DA}}}$ represent the low and high penalty market prices. Finally, λ^q_{Q} is the weighting factor applied to any violation of reservoir level limits.

This formulation maintains a linear penalty structure while effectively discouraging large deviations. It ensures that second-stage decisions remain aligned with the long-term planning of the first stage, while still allowing flexibility to respond to day-ahead data.

The performance of second-stage optimization is sensitive to the penalty market price, the reservoir water level limits and weighting factors parameters. These parameters must be carefully tuned to ensure that the second-stage solution remains close to the global optimum, while respecting the guidance provided by the first-stage schedule.lTo address this sensitivity, we propose a dynamic pricing strategy that adjusts to recent market conditions. For each simulation horizon (*e.g.*, one day), penalty prices are derived from historical DA market data using a fixed-size rolling window (*e.g.*, 14 days). Within this window, we compute selected upper and lower quantiles (*e.g.*, the 65th and 35th percentiles), which are then applied to penalize deviations between actual and scheduled water levels. This approach ensures that penalty signals reflect typical market behavior, avoiding distortions caused by extreme price events.lThree sensitivity analyses were conducted over the period from 2018 to 2024 to fine-tune these meta-parameters (*e.g.*, rolling window size, the market price quantile levels, and the penalty factor). These analyses are presented in detail in the results chapter. Their objective is to identify the parameter configurations that yield the most robust and economically efficient second-stage optimization outcomes.

3.7.2.6. Final penalty

Since the water level trajectories determined in the first-stage optimization are not strictly binding, reservoirs may complete the second-stage optimization with end-of-year water levels that deviate from the planned targets. A lower final water level indicates that more water has been turbined, leading to higher electricity generation and, in turn, greater revenue. Nevertheless, this can create a distortion in the income assessment, favouring strategies that take advantage of this flexibility.

To mitigate this issue, we propose introducing a final penalty to the yearly aggregated income. This penalty reflects the deviation between realized (second stage) and scheduled (first stage) final water levels at year's end. The penalty coefficient is derived from the yearly market price quantiles, as defined in the preceding sections, ensuring that the adjustment remains aligned with the yearly market dynamics.

3.7.3. Input Data and Parameters

The optimization model relies on two main categories of input data.

The first category includes physical system parameters, which define the static characteristics and operational limits of the system components. These parameters encompass maximum power capacities, reservoir and battery storage limits, and turbine efficiency curves that link energy output to water head. These values are considered fixed throughout the optimization process.

The second category consists of time-series data, which represent dynamic inputs that vary over time. VOne of the key components influencing VPP design is the treatment of market prices. We consider three types of market prices in our model.

The DA price for each hour is a unique value published by Swissgrid one day in advance. For each year (in the past), it is assumed that these prices are known for the second-stage optimization. For the first stage optimization, average daily prices are used.

The ancillary service market and particularly the FCR market operate differently. It does not rely on market clearing price mechanism determined by supply and demand intersections. Instead, prices are derived from multiple auctions through a pay-as-bid mechanism. These auctions occur at regular intervals, every four hours for primary control (FCR) and weekly for secondary control (aFRR). Given the small size of our VPP, we are unlikely to influence market outcomes significantly. Therefore, rather than modeling bidding strategies and auction dynamics, which would add complexity and shift the focus toward operational optimization, we adopt a simplified approach. We calculate the weighted average price of the bids awarded and define it as FCR market price and treat this average as a known parameter in the second stage. This allows us to estimate potential revenue from FCR market participation without simulating the full bidding process.nThe imbalance price is determined retrospectively by Swissgrid, after the actual imbalance volume has been assessed and the reserved FC (FCR, AFRR, and mFRR) power has been activated and compensated. Since this price is not known during the third stage of optimization, the model cannot incorporate it directly into the VPP's balancing decisions. As a result, the VPP may attempt to avoid penalties when imbalance prices are high, while potentially allowing larger imbalances when prices are low. Nevertheless, the model is designed to minimize imbalance volumes regardless of the price level.nThe imbalance price is determined retrospectively by Swissgrid, after the actual imbalance volume has been assessed and the reserved FC (FCR, AFRR, and mFRR) power has been activated and compensated. Since this price is not known during the third stage of optimization, the model cannot incorporate it directly into the VPP's balancing decisions. As a result, the VPP may attempt to avoid penalties when imbalance prices are high, while potentially allowing larger imbalances when prices are low. Nevertheless, tImbalance prices are published on a 15-minute basis. nCase studyt-Three hydropower plants were initially selected for the study: KW Merezenbach, KW Mörel, and KW Aegina – Alstafel. However, generating discharge flow data for KW Mörel would require simulating the entire upstream Rhône valley, making the necessary input data currently unavailable. Additionally, KW Merezenbach has a very limited rated power, reducing its relevance for the VPP optimisation study in WP7.

Consequently, KW Aegina – Alstafel has been utilized in this WP of the project. Near this plant, three wind turbines – each rated at 3.5 MW – have already been installed. According to FMV, a 9 MW photovoltaic (PV) power plant is also planned along the shores of Griessee Lake.

A key limitation of KW Aegina – Alstafel is its current on-off turbine configuration, which prevents continuous operation and excludes the plant from participating in ancillary service markets. To overcome this, a feasibility study is exploring an upgrade to a continuous-operation turbine, along with the potential addition of a pumping system and a downstream reservoir for the efficient capture and reuse of discharged water.

Therefore, the case study of WP7 analyses three core configurations for the Virtual Power Plant (VPP), with the downstream reservoir and the planned continuous turbine being hypothetically modelled due to the absence of real-world data:

- KW Aegina – Alstafel with an on-off turbine only (DT)
- KW Aegina – Alstafel with pump and on-off turbine (DTP)
- KW Aegina – Alstafel with pump and continuous turbine (CTP)

In addition to the hydropower plant, the VPP includes the existing wind farm and the planned PV installation. The study also investigates the integration of a Battery Energy Storage System (BESS) to enhance flexibility and market participation.

A VPP scheme can be conceived by combining three core configurations of hydro power plants and selecting wind and PV and BESS. For each VPP scheme, we evaluate the performance and economic benefits of VPP when participating in different energy and ancillary service markets.

The following operational scenarios are analysed:

- Participation in the Day-Ahead Energy Market (DA)
- Participation in the Primary Frequency Containment Reserve Market (FCR)
- Imbalance Cost Mitigation strategies

3.7.4. Data collection

Project partners provide needed input data, each in their own formats and structures. The first step involved processing and cleaning these datasets to ensure they were homogeneous and consistent for the optimization model. To manage this efficiently, a dedicated data scheme was developed, enabling all input data to be combined into a single, unified database that is directly integrated into our optimization pipelines.

The received data includes:

- HDE provided hydraulic performance tables for various head levels of the aforementioned power plants. These tables are generated with the RenovHydro program and give the optimal unit engagement to achieve the best efficiency, at each power level. The results are derived from the SIMSEN models, that incorporate head losses along the waterway as well as turbine characteristic curves. The losses in the generator and transformer are also considered.
- WSL provided two key types of data for KW Aegina – Alstafel: historical hydro-meteorological measurements covering 2006 to 2023 (including water discharge flow, surface temperature, global radiation, and wind speed), and ongoing daily data starting in June 2024. This ongoing data includes both six-day forecast scenarios and corresponding current measurements. These forecast scenarios are used as input for second stage stochastic optimisation.
- FMV contributed geometrical data of the reservoirs, as well as nominal specifications for the existing wind power plant and the planned photovoltaic (PV) installation in the region.
- Alpiq provided historical data on day-ahead energy market prices and ancillary service auction results for Switzerland and neighbouring countries (Germany, France, Austria, and Italy), encompassing various periods from 2015 through 2023. This data was further complemented by Swiss imbalance prices obtained from public ENTSO-E sources for the years 2024 and 2025.

3.7.5. Implementation

The formulated optimization problem has been implemented in a Python environment. In addition, a simple scenario generation procedure is implemented in Python to support stochastic optimization models. Implementation details (scalability, computation time, etc.) will be elaborated in the final version of the report.

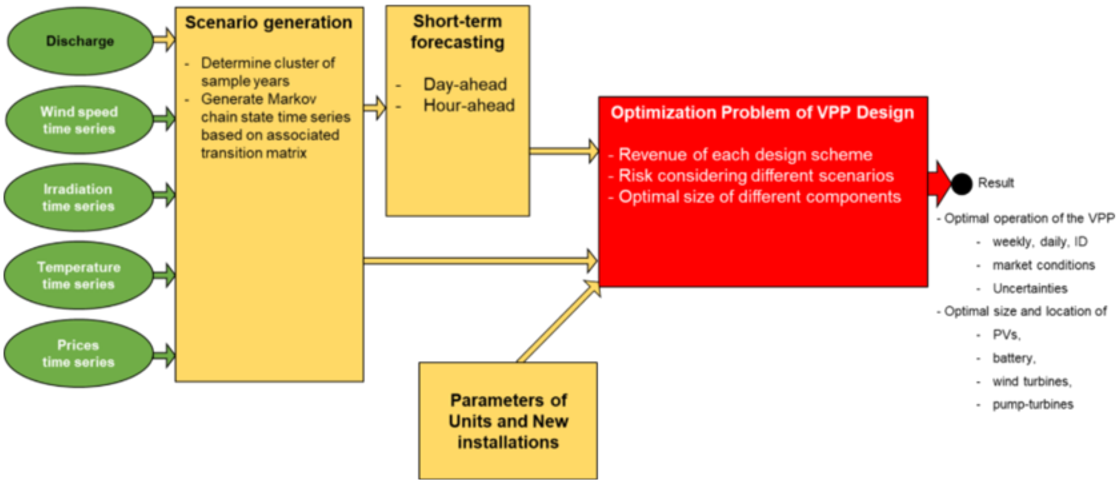

Figure 115 Implemented pipeline

3.7.6. Results of deterministic optimisation

In this section, we present the full deterministic first and second stage optimization results. As we detail the process and outline the expectations, we explore different design schemes for the hydropower plant, both with and without battery integration, considering the VPP participation in the DA market only, as well as in the FCR. As the optimization is fully deterministic, there is no forecast error associated with volatile assets such as photovoltaic turbines. Therefore, PV and wind turbines are omitted to focus uniquely on the hydropower plant results.

Optimization have been repeated for the years 2021, 2022, and 2023, as these are the only years that provide complete datasets for all input parameters (limited by ancillary services price data). However, they represent a good sample of input data heterogeneity, which enables meaningful interpretation of the results.

3.7.6.1. First stage result

Figure 116 and Figure 117 present the first-stage optimization results for the years 2021 and 2023, comparing system configurations of a turbine with and without pump. At this stage, all power plants are modelled as operating continuously; therefor, no distinction is made between continuous and discrete turbine operation. The results show that, in the absence of turbining or pumping, the upstream reservoir gradually fills, due to natural discharge inflows. When turbining occurs, water is transferred to the downstream reservoir, leading to a decrease in the upstream storage level and a corresponding increase downstream. . As the downstream reservoir has a smaller storage capacity, fills rapidly and, without pumping to empty it, remains at 100% capacity. This results in water spillage to maintain operational constraints and avoid exceeding storage limits..

The model generally behaves like an on/off system. Once market prices exceed a certain threshold, the plant tends to operate at full capacity to maximize income, while during intermediate price periods, partial operation may occur to ensure compliance with all constraints.

However, these price thresholds are not fixed and depend on water dynamics. Results for 2021 show that the model attempts to keep reservoirs as full as possible during the second part of the year to maximize income when prices are high. Due to the piecewise linearization of hydropower plant efficiency, maintaining high water levels later in the year also increases hydropower output and, consequently, revenues. This large gap between efficiency is smoothed in the second stage, where the state definition is more focused on the actual water level. In contrast, during 2023, higher prices at the beginning of the year lead the model to turbine as much as possible until the reservoir is emptied, then refill it during the remainder of the year.

In both cases, we observe that the model sometimes turbines at lower prices during certain periods, while in other periods, higher prices are not exploited. This behaviour ensures compliance with all constraints while still aiming at maximizing profit.

Figure 116: First-stage optimization results for the years 2021 (left) and 2023 (right) with a discrete turbine

The results with pumping capability highlight the additional flexibility that pumps bring to the VPP, allowing turbines to operate more actively compared to configurations without pumps, as expected. We also observe that turbine power output is higher because pumps require more energy to return water to the upstream reservoir than turbines generate when producing power. As anticipated, pump usage is less frequent during 2021 due to the prevailing market price structure.

Figure 117: First-stage optimization results for the years 2021 (left) and 2023 (right) with a discrete turbine and a pump

Table 26 reports the overall VPP income for the first stage. The most evident observation is the significant income discrepancy between years, driven by high volatility in DA market prices. We also note the impact of pumping: the more water is pumped, the greater the increase in income. The income calculation is normalised with reference to the baseline without any pump installation.

Table 26: First stage results summary

Year	Income without pump [%]	Income with pump [%]	Turbined volume diff [%]
2021	100	101.9	15.3
2022	100	106.3	24.9
2023	100	109.4	32.8

3.7.6.2. Second stage result

Figure 118 and Figure 119 show the second-stage optimization outcomes for the years 2021 and 2023 for a continuous turbine with pump, comparing the scenario where the VPPs are either selling energy solely on the DA market or also providing ancillary services on the FCR market using a 1 MW / 2 MWh battery. Since the battery's behaviour operates on a time scale close to a day, it is not appropriate to present results on a yearly basis, as daily variations cannot be clearly visualised. Figure 120 presents a two-week zoom to illustrate the battery's behaviour.

In this part, the downstream reservoir water level is no longer presented, as it is less relevant. Instead, we present the first stage scheduled reservoir level along with its limits. Since the first stage is deterministic, these limits are defined using a simple offset (i.e. 10%). As shown, the second stage measured water level closely follows the scheduled one. Because the first stage is deterministic, the second stage exhibits similar behaviour, with higher granularity.

We can also observe that the gap in turbine efficiencies across different water levels behaves more smoothly than in the first stage, as the reservoir states are consistently centred around the daily water level. Like the first stage, the continuous turbine also appears to operate in an on-off manner.

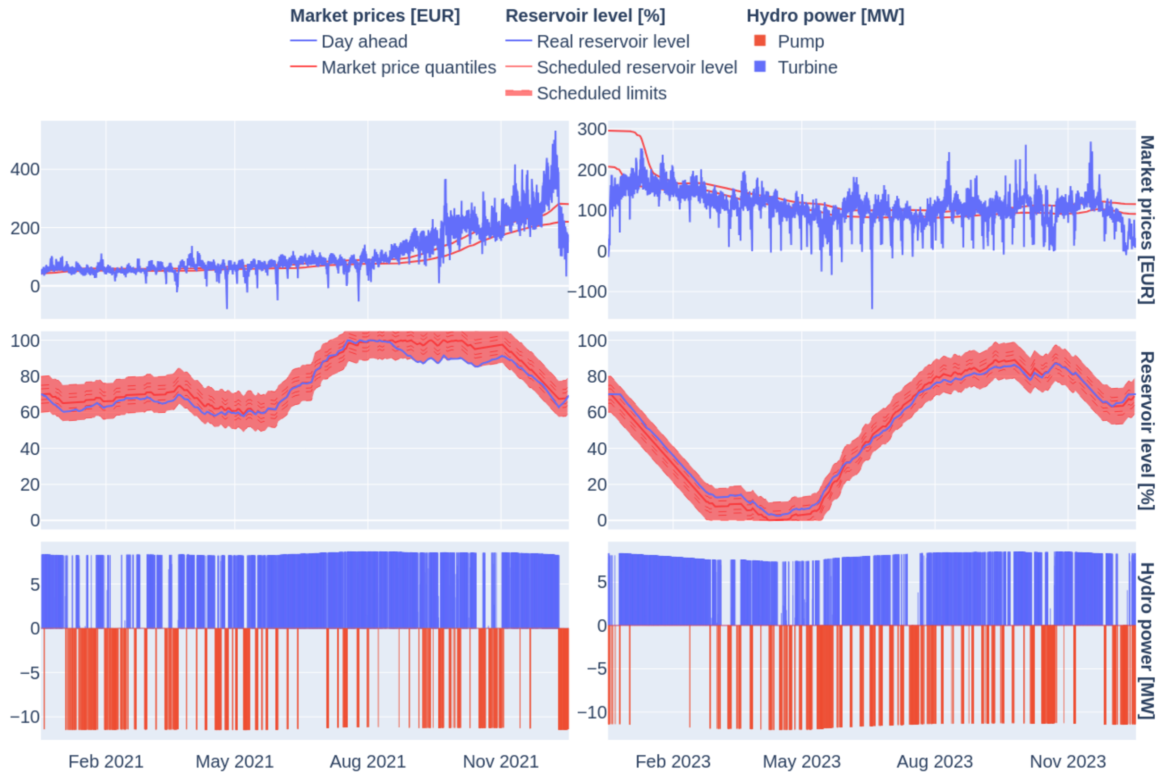

Figure 118: Second-stage optimization results for the years 2021 (left) and 2023 (right) with a continuous turbine, a pump and VPP only selling energy on DA market

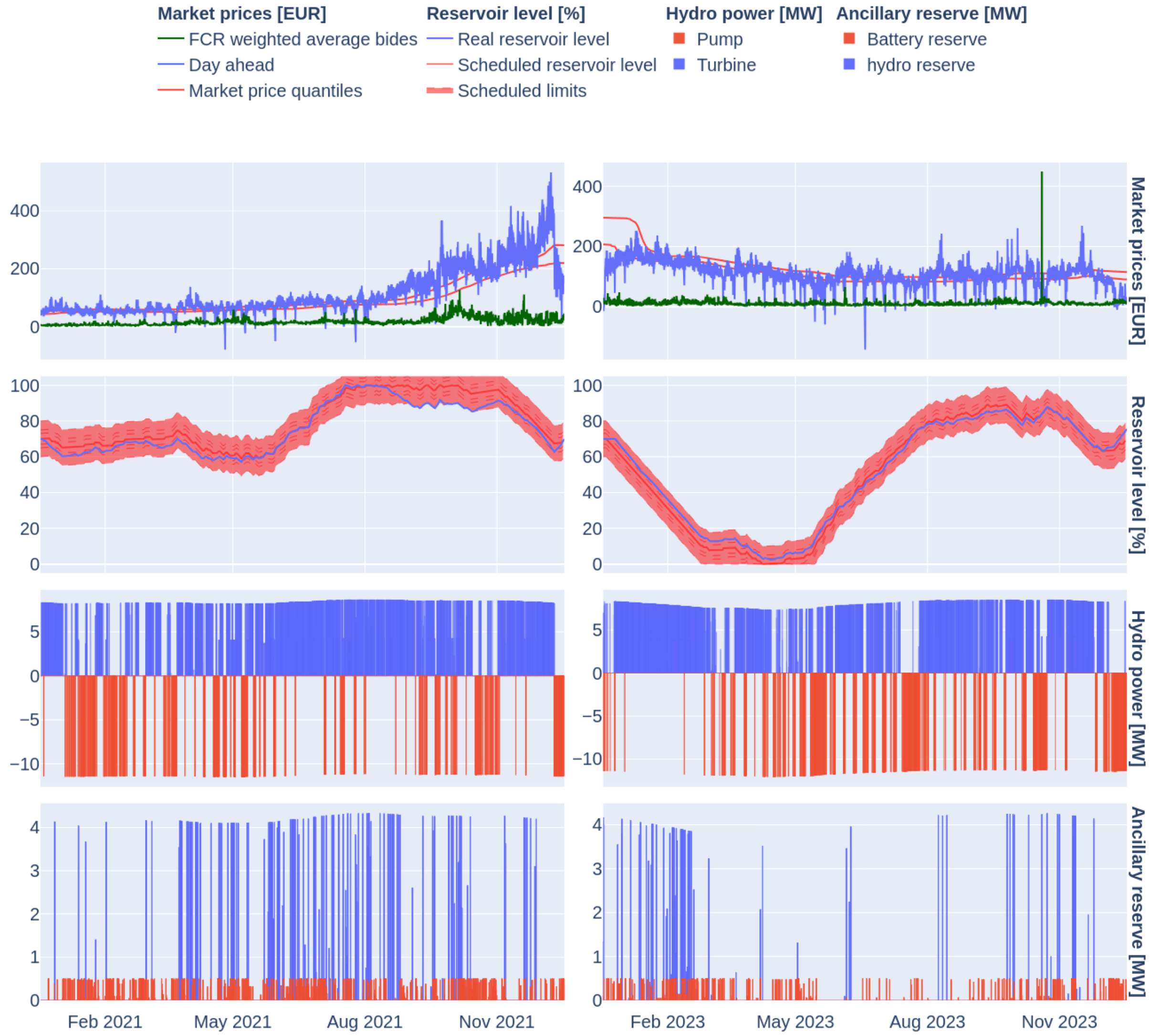

Figure 119: Second-stage optimization results for the years 2021 (left) and 2023 (right) with a continuous turbine, a pump, a 2 MW battery and VPP selling energy on DA market and ancillary reserve on FCR market

Figure 120 focuses on the first two weeks of October, highlighting the daily operational behaviour of the VPP. It is clearly observable that the battery typically completes one cycle per day, responding to the day-night price spreads in the DA market. Furthermore, the battery's operational pattern generally remains independent of the hydropower plant, which must adhere to the scheduled reservoir levels of the first stage. In the contrary, the battery's SOC is significantly more constrained and must be managed within strict operational bounds to ensure reliable performance.

Finally, we can also observe the impact of selling FCR reserves on the VPP. To trigger FCR reserve activation, the DA market price must be evaluated on a local average. In addition, FCR cleared price must reach their local peaks. We also observe that when FCR services are sold, the corresponding power output must be reduced to ensure the VPP can fulfil its commitment.

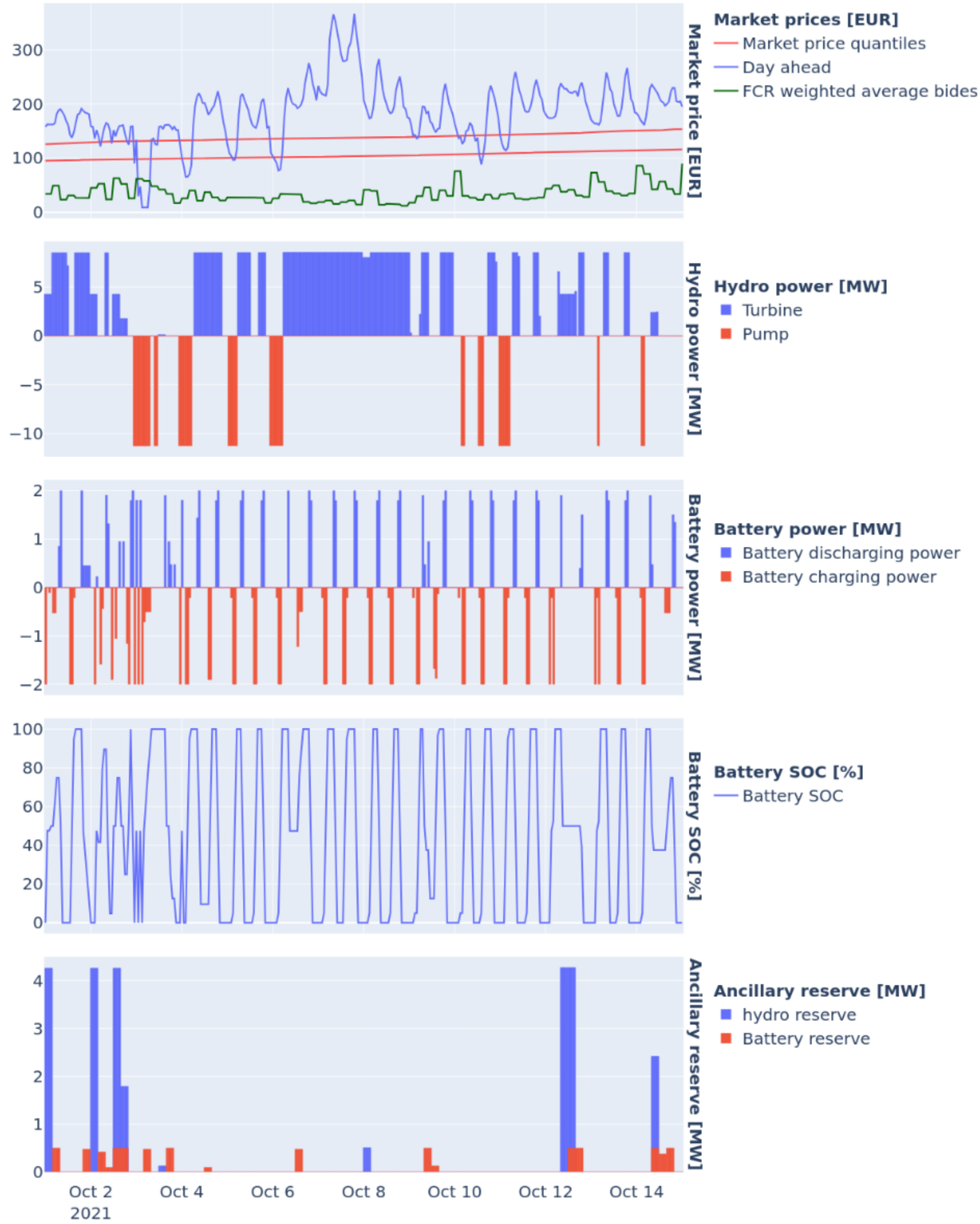

Figure 120: Two weeks zoom for second-stage optimization results for the year 2021 with a continuous turbine, a pump and a 2 MW battery.

Table 27 presents the summarized results for the deterministic second stage. The first result shows the VPP selling energy only on the DA market, while the last column refers to the continuous turbine also selling flexibility reserves on the FCR market. The FCR market is considered only with the continuous turbine, as discrete turbines cannot provide flexibility services.

For the same VPP configuration, income from the second stage is usually 3–10% higher than that from the first stage. This is quite understandable, given that the second stage benefits from higher granularity, allowing the optimization model to take advantage of daily market price fluctuations. Moreover, since we are dealing with a deterministic problem, the first stage has already maximized the possible income by knowing the prices in advance. The second stage simply follows the first-stage schedule and refines it further.

Table 27: Second stage summarized total income results for the year 2021 to 2023 expressed as a percentage of the yearly baselines (lowest income without new installations).

Year	Battery size	DT	DTP	CTP	CTP and FCR reserve
2021	-	100.0	103.0	103.0	105.6
	2 MW / 4 MWh	101.9	105.1	105.0	108.1
2022	-	100.0	109.1	109.1	112.8
	2 MW / 4 MWh	101.6	111.0	110.9	115.5
2023	-	100.0	119.7	119.7	124.7
	2 MW / 4 MWh	102.5	122.2	122.2	128.0

3.7.7. Stochastic vs Deterministic optimisation

When both stages are treated deterministically, Figure 116 illustrates the long-term changes in the reservoir volume alongside market prices. The reservoir remains at full capacity during the last 6 months of the year, coinciding with periods of high prices. For comparison, Figure 121 shows the actual reservoir volumes over different years. This highlights that the deterministic approach produces unrealistic volume profiles, as it effectively "knows" the evolution and the timing of peak prices in advance.

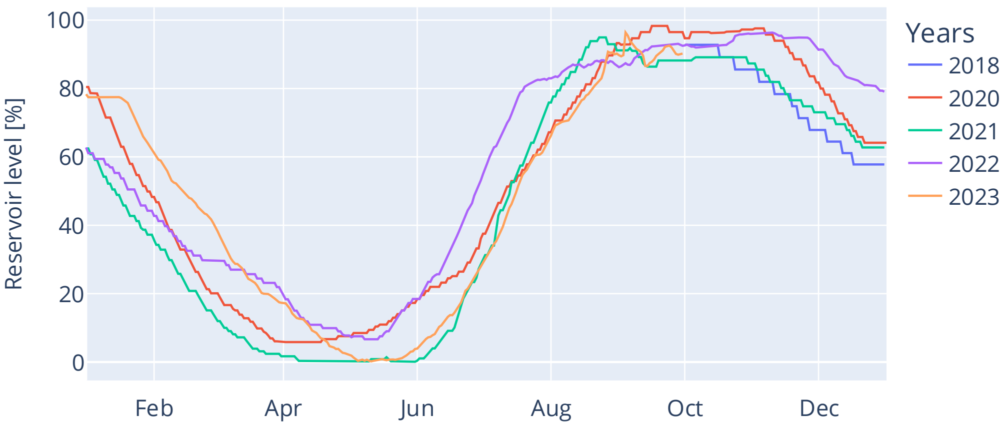

Figure 121: Measured KW Aegina – Alstafel reservoir level

3.7.7.1. Limits of deterministic models

The results of deterministic optimization model are heavily dependent on the selected scenario, including the market price or discharge flow, and fail to capture long-term uncertainties or variations in market prices in different years. Storage systems often appear underutilized, with full capacity rarely dispatched, and deviates from observed seasonal and intra-year storage volume variations in practice. Hydro reservoirs are treated as fixed or overly simplified resources, and their potential to provide flexibility and energy shifting is not fully exploited. Stochastic uncertainty from PV generation, wind generation, and market imbalances are typically not captured. Because the imbalance price is applied only after solving the deterministic optimization, the resulting schedule does not account for imbalance costs and is therefore sub-optimal. Finally, deterministic models cannot quantify risk, which is critical for planning VPP operations under uncertainty.

In deterministic model, the optimization is solved without explicitly including the imbalance price in the objective function or constraints. Once the optimization is complete, the imbalance between forecasted and actual production is calculated. The imbalance cost is then evaluated using the corresponding imbalance prices as follows:

Imbalance Cost = Long Price * Power Surplus + Short Price * Power Deficit

This approach captures the financial impact of the deviations from the forecasted schedule; however, because the imbalance prices are applied only after the optimization, the resulting dispatch schedule does not account for these costs and is therefore sub-optimal with respect to minimizing total costs.

It is worth noting that the imbalance price in Switzerland will be based a single price from 2026, whereas our calculations are based on the historical dual-sided prices.

3.7.7.2. Scenario generation process to support first-stage stochastic optimization

To fully support stochastic optimization, the current input data is insufficient to cover all potential outcomes. Therefore, a synthetic data set, which should accurately replicate the behavior of real data, must be created. This synthetic dataset focuses on time series for two domains:

- Weather measurements (e.g., river discharge).
- Market prices.

The time series must include the needed characteristics such as:

- **Regular trends:** seasonal, weekly, or daily patterns.
- **Extreme events:** punctual (i.e., water discharge peak from a storm) or prolonged (i.e., price increases following geopolitical events).
- The proposed method for generating this synthetic data is the Markov Chain algorithm, where the probability of the next event depends only on the current state. However, applying this algorithm directly to unprocessed data would yield poor results, necessitating a five-step workflow:
- **Data preprocessing:** Cleaning and reshaping the raw data to isolate and extract the key behaviors (trends, extremes) to be synthesized. This step ensures the data accurately reflects the critical features to be modeled.
- **Data digitization:** Transform continuous time series into a set of discrete states. This involves dividing the continuous range into bins that accurately represent the possible states. The number of bins should be adequate to properly define transitions without over- or undergeneralizing.
- **Transition matrix computation:** This matrix quantifies the probability of moving from any defined state to every other state based on historical patterns observed in the data. This matrix is critical because the entire synthesis relies on accurately capturing how states interact over time.
- **Data Synthesis**: Generate a new sequence of states using the transition matrix. Starting from a known or randomly chosen state, apply the transition probabilities to determine each subsequent state in the sequence.
- **Continuous time series Generation**: Convert the state sequence back into a continuous time series value. Typically, this step involves mapping each state to a statistical distribution (e.g., using a uniform distribution for normal trends or an exponential distribution to model extreme events).

3.7.7.3. First-stage stochastic optimisations

To produce a fully causal reservoir water level schedule, we now model the first stage as a stochastic optimization problem. We generated 200 representative scenarios capturing variations in reservoir discharge volumes and DA market prices. The model optimizes the total water turbined by the hydropower plants across all scenarios to maximize overall income.

To manage computational complexity and ensure reasonable solution times, each hydropower plant is modelled with a fixed average efficiency, independent of water flow or hydraulic head. This simplification allows the problem to be formulated as a linear optimization model, which can be solved efficiently regardless of the size of the decision space. The model is not intended to provide a precise estimate of the VPP total income, but rather to generate a reliable schedule for reservoir water levels. Crucially, this simplification does not compromise result accuracy, as the second stage of the model retains a detailed and piecewise-linear representation of hydropower efficiency.

After solving the stochastic optimization problem, the resulting reservoir volumes are presented in

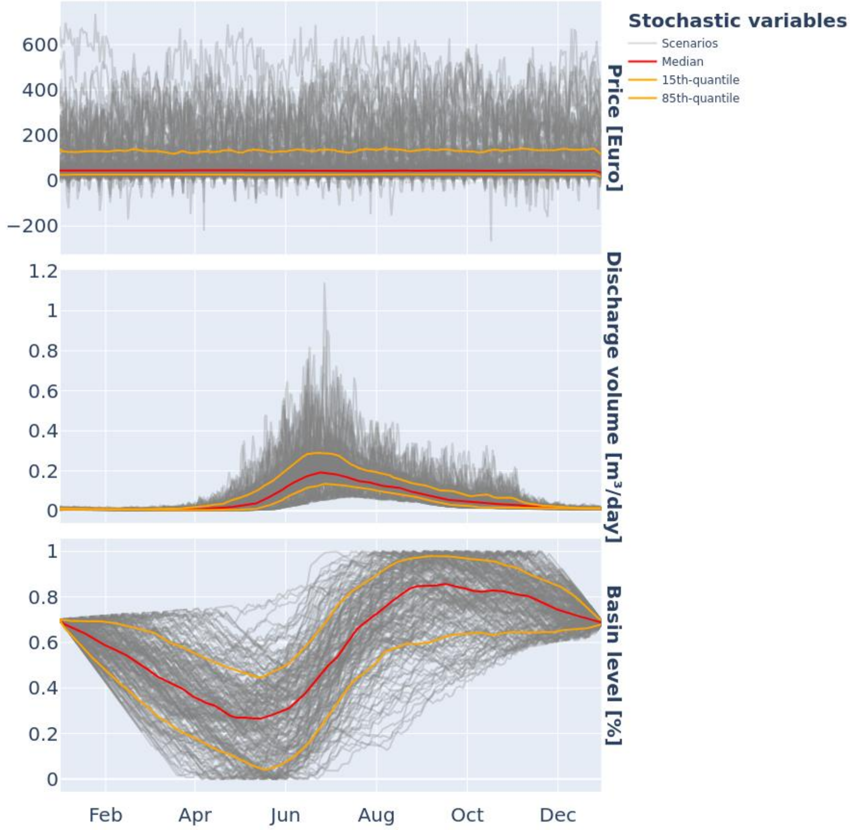

Figure 122 alongside market prices and discharge volumes. Compared to the purely deterministic approach, a larger portion of the reservoir's capacity is utilized throughout the year, particularly when contrasted with the year 2021 deterministic optimization. However, approximately 15% of the scenarios require water spillage, while 10% totally empties the reservoir during spring. These outcomes reflect the influence of extreme wet and dry year conditions.

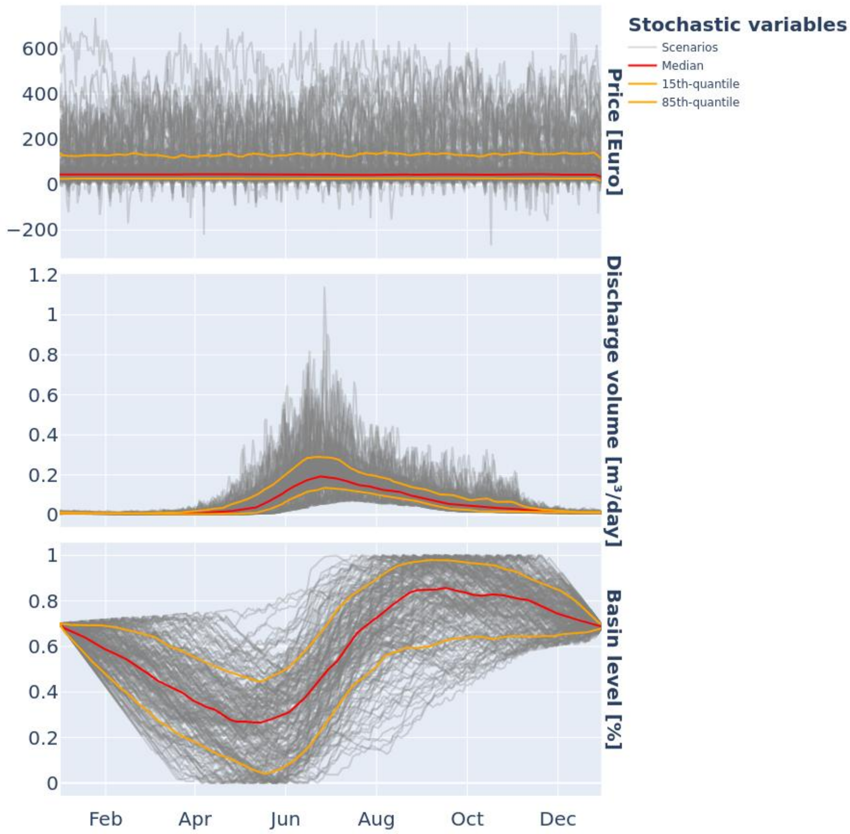

Figure 122 First-stage stochastic results considering a turbine with pump and 200 synthesized scenarios.

3.7.8. Sensitivity Analysis

In this section, a set of sensitivity analysis is performed to validate the robustness of the proposed optimization formulations and provide further insight into the impact of various input parameters and VPP design variables.

Three sensitivity analyses have been performed to evaluate the model's response to varying hyper parameters. These analyses were applied to two VPP design scheme: the discrete turbine (DT), and another combining the discrete turbine with the pump (DTP). In both cases, the VPP was modelled as participating exclusively in the DA market. The optimization was performed using a stochastic first stage and a deterministic second stage, without incorporating a third stage.

The sensitivity analysis was conducted over a time span from 2015 to 2023. For each year, we calculated the ratio of each parameter configuration's performance relative to the maximum value observed that year. An average ratio was then computed across all years. This method provides an indication of which parameter configuration performs best when considering a diverse set of input data across multiple years.

3.7.8.1. DA market prices' windows size

This analysis explores how the model responds to changes in the window size used to calculate DA market prices, which act as penalty factors for deviations in reservoirs water levels between the first and second stage optimization. To do that, we varied the window size from 7 to 182 days.

Table 28 presents the ratio of the annual maximum income to the selected income, averaged across all years. First, we observe that adding a pump to the VPP configuration increases income by more than 8%. Furthermore, the results clearly show that the best-performing configuration corresponds to a window size of six months. In nearly every year, this setting yields the highest outcomes.

We also observe that with a weekly window size, the second stage tends to follow the water level schedule from the first stage more closely. In contrast, a six-month window smooths out also weekly and monthly fluctuations, making the penalty factor more effective in a global optimization perspective. This effect becomes even more relevant when the first stage is stochastic and provides a general water level trend without accounting for day-to-day variations. The benefit of a longer window is particularly evident in years with oscillating day-ahead prices, as illustrated in

Figure 123.

Table 28: Summary of sensitivity analysis results based on window size used to evaluate market price penalties, expressed as a percentage of the baseline (lowest income)

Window size [days]	DT [%]	DTP [%]
7	100.5	101
14	101	100
28	103.9	104.3
56	109	113.6
112	114.7	118.5
182	117.8	120.9

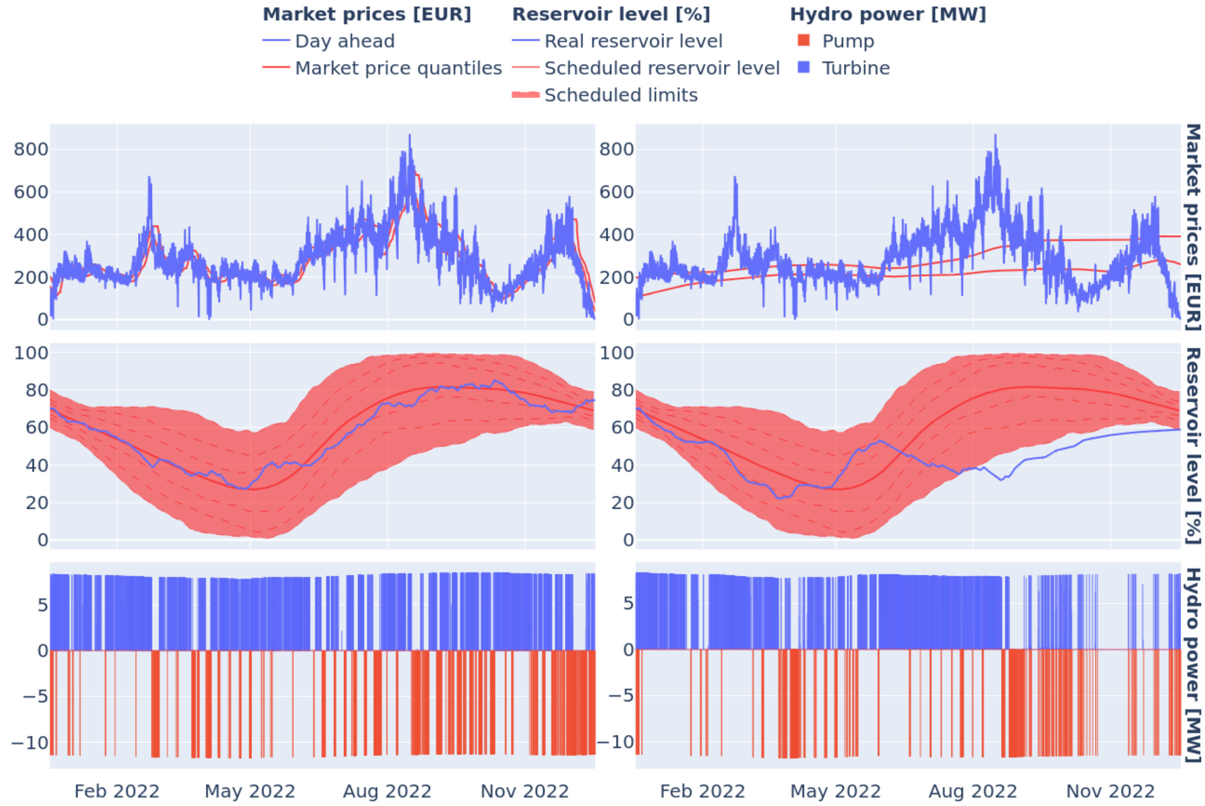

Figure 123: Second-stage optimization results for the year 2022, with the market price penalty factor using 7-day (right) and 182-day (left) window sizes.

3.7.8.2. DA market prices' quantiles

This analysis investigates how the model responds to variations in the DA market price quantiles used to generate the second stage penalty factors. To do that, we varied the quantile selection from the median to the 20th (lower) and 80th (upper) percentiles.

The results show that performance differences between these configurations are relatively small, with less than 2% variation across the tests. Moreover, the optimal quantile is not consistent between the two VPP configurations. The turbine-pump setup tends to favour the median quantile, while the single-turbine configuration performs better with more extreme quantiles.

Table 29 Summary of sensitivity analysis results based on quantiles used to evaluate market price penalties, expressed as a percentage of the baseline (lowest income)

Quantiles [low-high]	DT [%]	CTP [%]
50-50	103.7	109.9
40-60	103.7	110
35-65	105.4	112
25-75	105.2	111.3
20-80	104.7	110.6

As shown in Figure 124, using the median quantile leads to more binary, on/off behaviour in the optimization, which heavily depends on market price fluctuations and does not closely follow the scheduled water level. In contrast, wider quantiles give the model more flexibility to align with the water level schedule. Based on these observations, we chose to set the quantile range to the middle values, specifically the 35th and 65th percentiles, as a balanced compromise.

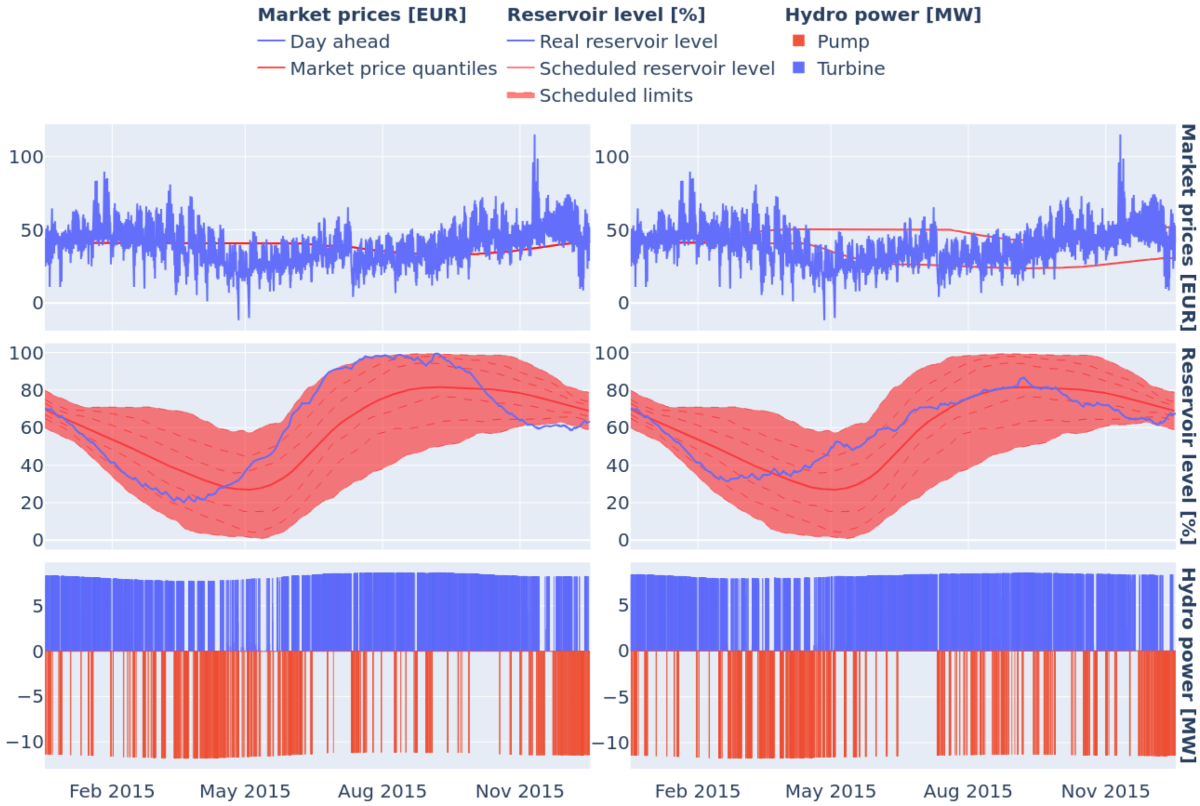

Figure 124: Second-stage optimization results for the year 2015, with the market price penalty factor using the 50 (right) and 20/80 percentiles (left).

3.7.8.3. Reservoir water levels' quantiles

This analysis explores how the model reacts to changes in the scheduled water level quantile threshold to generate the second penalty term. Specifically, we vary the quantile thresholds by setting their percentage deviations (both low and high) from the median as follows:

- Set 1: 45%, 15%, and 5%
- Set 2: 40%, 30%, and 15%
- Set 3: 45%, 35%, and 20%

In addition, we adjust the weights applied to these penalty term:

- Low weights: 0.3, 0.15, and 0.05
- High weights: 0.5, 0.3, and 0.1

Table 30 Summary of sensitivity analysis results based on quantiles used to evaluate water levels threshold for the second penalty term, expressed as a percentage of the baseline (lowest income)

Quantile's configuration	DT [%]		CTP [%]	
	Low	High	Low	High
1	103.3	101.8	110	107.5

2	103.9	102.2	110.7	107.9
3	106.1	102.6	112.9	108.6

The results suggest that model performance improves when the second penalty term is not overly restrictive. While this term plays a crucial role in preventing large deviations and keeping water levels within a realistic operational range, excessive penalization can reduce the model's flexibility. As illustrated in Figure 125, applying a narrow quantile range limits the model's ability to explore and identify the most optimal operational schedule.

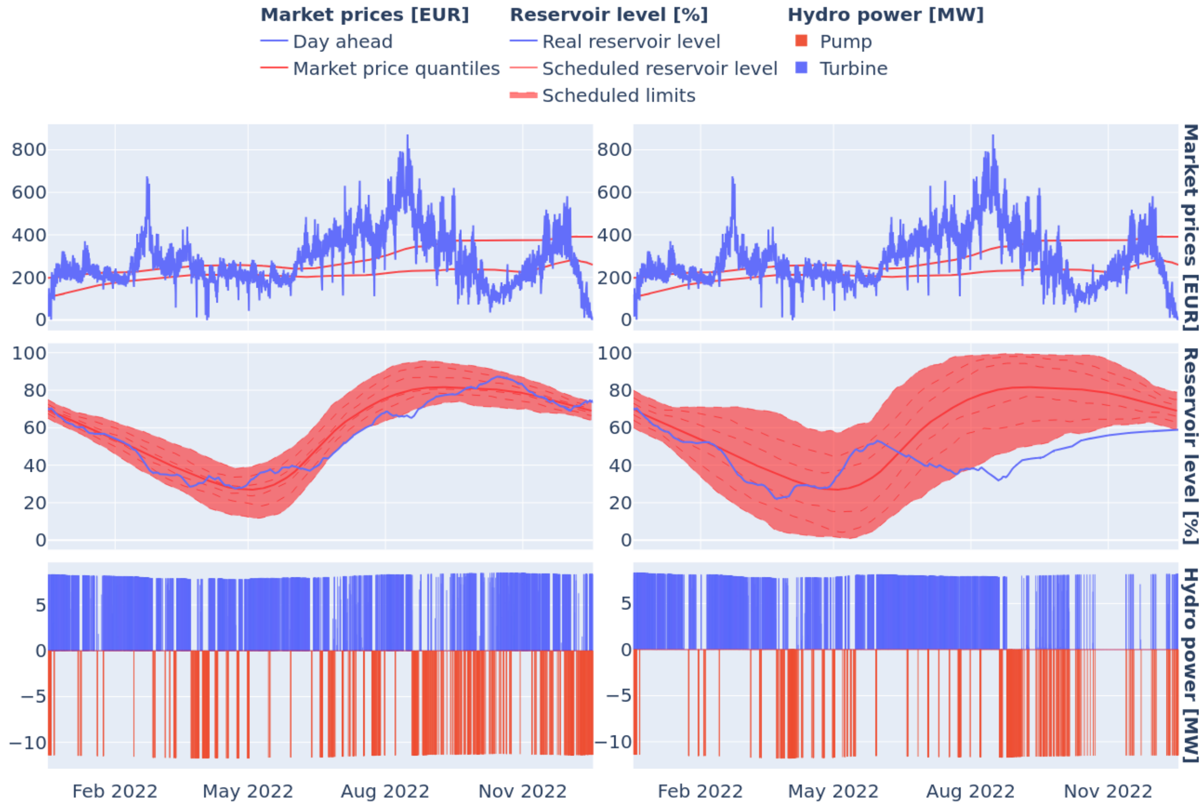

Figure 125 Second-stage optimization results for the year 2022, with the quantile configuration of (1 and high penalty) on the left, and (3 and low penalty) on the right.

3.7.9. First-stage stochastic second-stage deterministic results

In this section, we present an overview of the results obtained by considering a stochastic optimization problem in the first stage, followed by a deterministic optimization in the second stage, without incorporating a third stage.

We conducted tests using different VPP designs: discrete turbine (DT), continuous turbine with pump (CTP), and CTP with participation in the FCR market. The battery size was varied, and the optimization was performed for the years 2021, 2022, and 2023. Since the second stage remains deterministic, wind and PV generation are not included at this point, as their contribution would only act as an income offset without influencing the decision-making process.

We do not present the detailed evolution of the variables here, as these have already been thoroughly discussed in previous sections. Instead, the tables below summarize the total VPP income for each of the different VPP design schemes.

Table 31 Second stage summarized total income results for the year 2021, expressed as a percentage of the baseline (lowest income without new installations).

Battery size	DT	DTP	CTP	CTP and FCR reserve
-	100	113.6	113.6	118.3
1MW / 2MWh	101.4	115.3	115.2	119.7
2MW / 4MWh	103.1	116.4	116.6	121.8
5MW / 10MWh	107.2	121	121	127.3
1MW / 4MWh	102.4	116.4	116	121.3
2MW / 8MWh	104.7	118.3	118.5	124.2
5MW / 20MWh	111.8	125.5	125.8	133.8

As observed in the fully deterministic tests, selling flexibility to the FCR reserve is not profitable, even with a large 20 MWh battery. The main limiting factor is the low FCR price. To better understand the conditions under which FCR participation becomes viable, a sensitivity analysis will be conducted to determine the price threshold at which FCR market participation becomes profitable.

Table 32 Second stage summarized total income results for the year 2022, expressed as a percentage of the baseline (lowest income without new installations)

Battery size	DT	DTP	CTP	CTP and FCR reserve
-	100	102.9	103	109
1MW / 2MWh	101.1	104.1	104.1	110.6
2MW / 4MWh	102.3	105	105.1	112.2
5MW / 10MWh	105.5	108.3	108.3	117.1
1MW / 4MWh	101.7	104.5	104.7	111.9
2MW / 8MWh	103.4	106.4	106.3	114.8
5MW / 20MWh	108.5	111.2	111.3	123.7

Table 33 Second stage summarized total income results for the year 2023, expressed as a percentage of the baseline (lowest income without new installations)

Battery size	DT	DTP	CTP	CTP and FCR reserve
-	100	115.9	115.8	122.3
1MW / 2MWh	101.4	117.4	117.3	124.2
2MW / 4MWh	102.8	118.7	118.7	126
5MW / 10MWh	107	123	122.9	131.6
1MW / 4MWh	102.1	118.1	118	125.4
2MW / 8MWh	104.2	120.1	120	128.5

5MW / 20MWh	110.6	126.5	126.5	137.8

3.7.10. Imbalance penalty reduction

In this study, we aim to develop a model that integrates PV, wind power generation and water discharge flow uncertainties. The objective is to capture the stochastic nature of renewable energy production and hydrological variability to evaluate the response of the VPP, particularly with respect to the reduction of imbalance penalties. The analysis is based on 21 daily forecast scenarios provided by WSL in WP4. However, as the full stochastic model is still under development, the corresponding results cannot be presented at this stage. They will be included in the final report.

In the meantime, we have successfully implemented a model with pseudo-stochastic approximation. This model can be used to feed the third-stage optimization and support an imbalance penalty reduction analysis. To achieve this, we use the median of the scenario forecasts, resulting in a single representative forecast that drives the second-stage deterministic model. The output from this stage is then passed to the third-stage model, which aims to mitigate imbalance volumes using flexible resources.

Since the scenario data (measured and forecasted) from WSL does not cover a full calendar year, we processed it to generate a complete annual dataset. We then aligned this with the 2024 market prices, which offer the most comprehensive pricing data available. Although the dates between the scenario data and market prices are not fully consistent, this approach is sufficient for a proof-of-concept study. Further analysis will be possible once more complete data becomes available. Additionally, this study should be revisited once symmetric imbalance pricing [4] is firmly established in 2026 and a full year of consistent data is accessible.

3.7.10.1. Results

For this analysis, we consider a design scheme based on the continuous turbine with pump (CTP), complemented by different battery sizes. We also examine the effect of including or excluding the flexibility of the continuous turbine to reduce imbalance penalties.

Figure 126 presents result over a two-week period. In this figure, imbalance penalty prices are shown alongside DA market prices to provide a clearer comparison. When the VPP is short (*i.e.*, insufficient power generation), it incurs a penalty greater than the DA price. Conversely, when the VPP is long (*i.e.*, excess power generation), it receives compensation at a lower, potentially negative price. This highlights the critical importance of balancing the VPP as effectively as possible.

In the figure, red bars in wind and PV power generation indicate negative deviations between actual measured power and forecasted values, while green bars represent positive deviations. In case of VPP is short we can either discharge the battery or increase the continuous turbine power. However, as the battery is uniquely used for this purpose, we chose to prioritise its use before the use of the turbine.

[4] Swissgird new pricing mechanism, available at: https://www.swissgrid.ch/en/home/newsroom/newsfeed/20250328-01.html

Figure 126: Two-week zoom on third-stage optimization results, highlighting forecast errors and their reduction using a continuous turbine and a 2 MW / 4 MWh battery

The first observation is that the battery is less solicited compared to its use in energy arbitrage, completing less than one full charge-discharge cycle per day. The total number of cycles is 242 for the smallest battery and fewer than 50 for the largest one, whereas more than 500 cycles are typically observed when used for DA energy price arbitrage. If the VPP is short on energy during extended dispatch windows, a depleted battery becomes ineffective, as recharging is only possible through positive power imbalances, *i.e.*, when actual generation exceeds forecasted demand. This situation is clearly illustrated on the first day, when wind power forecasts were overestimated and the hydro turbine had to compensate alone for the resulting power imbalance within the VPP. A more advanced battery control strategy could be beneficial to enable the battery to provide additional services.

Another observation concerns the typical on/off behaviour of the hydro turbine even if it is a continuous one. This binary operation limits its ability to modulate power, as it can only increase output when inactive or decrease it when fully activated − without any intermediate control.

Table 34 Third stage summarized total income results taking in account imbalance penalties, expressed as a percentage of the baseline (lowest income without new installations).

Battery size	Without Hydro	With Hydro
-	100	106.7
1MW / 2MWh	106.7	112.2
2MW / 4MWh	108.6	113.8
5MW / 10MWh	110.7	114.8
1MW / 4MWh	108.0	113.1
2MW / 8MWh	110.1	114.8
5MW / 20MWh	112.6	116.3

Without considering CAPEX, the most efficient imbalance reduction is achieved by combining the hydro turbine with a 1 MW / 2 MWh battery. This configuration results in an income increase of over 12%. In comparison, further increases in battery capacity yield diminishing returns, where doubling the battery size leads to less than 2% income increase.

It is important to note that 2024 was one of the worst years in terms of imbalance penalty prices. Nevertheless, Table 38 shows the percentage of total absolute energy deviation relative to total annual energy, which is approximately 32 GWh. Using the smallest battery and the hydro turbine, the imbalance volume is reduced from 6% to 2%, demonstrating a significant improvement in operational performance.

Table 35 Third stage total absolute imbalance ratio relative to total VPP power, expressed as a percentage.

Battery size	Without Hydro	With Hydro
-	6.29	3.18
1MW / 2MWh	4.51	2.04
2MW / 4MWh	4.07	1.82
5MW / 10MWh	4.01	1.76
1MW / 4MWh	3.52	1.51
2MW / 8MWh	3.35	1.42
5MW / 20MWh	2.83	1.09

3.7.11. VPP design scheme summary

The following represent the final VPP design outcomes based on the comprehensive 2024 dataset, which was the only period where all necessary data were fully available. The conclusions are summarized below:

- The integration of a pump substantially enhances the VPP's profitability by enabling the execution of energy arbitrage.
- Operating a continuous turbine without flexibility provides no significant profit increase.
- Even without a battery, the turbine can largely reduce imbalance volumes.

- Small Battery makes the reduction of imbalance volumes even more profitable.
- As battery size increases, the strategy shifts toward the FCR market. A large battery provides the necessary capacity to maintain the required 50% SOC for symmetrical reserves while still having enough headroom to generate significant revenue from ancillary services.

Table 36 VPP design scheme results using 2024-year data, expressed as a percentage of the baseline (lowest income).

Battery size	DT	DTP	CTP	CTP and FCR	CTP and Imbalance
-	100	118.3	118.1	123.8	125.9
1MW / 2MWh	101.7	119.9	119.9	125.7	130.7
2MW / 4MWh	103.2	121.8	121.6	127.5	132.2
5MW / 10MWh	107.8	126.4	126.1	132.9	133.5
1MW / 4MWh	102.5	120.9	120.9	127.1	131.5
2MW / 8MWh	104.9	123.4	123.2	130.1	133.2
5MW / 20MWh	112.3	130.5	130.4	139.5	134.9

3.7.11.1. Results with Alpiq projection prices

In all these tests, historical price data from 2021 to 2025 are used. This approach provides a reliable indication of how our VPP would have performed in the past. However, for future VPP implementation, price evolution remains a significant sensitivity factor. For this reason, it is essential to test the VPP design using forecasted prices of the future. To achieve this, HEIG-VD has provided Alpiq with an executable optimisation model and Alpiq fed it with it's own DA and FCR price forecasts for year 2028. Since the imbalance mechanism changed in 2026, Alpiq did not have the long and short imbalance prices forecast required to populate the model. Therefore, we restricted the model's use to selling flexibility solely to the FCR market. To complete the simulation, we continued to use 2024 historical water data.

Table 37. VPP design scheme results using Alpiq 2028 DA and FCR price forecasts power, expressed as a percentage of the baseline (lowest income).

Battery size	DT	CTP	CTP and FCR
-	100	135.1	135.3
1MW / 2MWh	101.7	136.8	137.0
2MW / 4MWh	103.3	138.3	138.6
5MW / 10MWh	108.1	143.1	143.7
1MW / 4MWh	103.0	138.0	138.3
2MW / 8MWh	105.9	141.0	141.5
5MW / 20MWh	114.8	149.8	150.8

Regarding the results, we can observe a massive performance gap when utilizing both the turbine and the pump (exceeding 20%). This can be interpreted because of higher daily DA price fluctuations, which make energy arbitrage significantly more profitable. In contrast, participating in the FCR market adds only a marginal income. Since FCR market prices are predicted to be significantly lower than 2024 in comparison to DA market prices, the turbine does not frequently participate in ancillary services. This is due to the FCR market's requirement for symmetrical reserves, which forces the turbine to operate at mid-rated power to maintain flexible capacity in both directions. As DA price signals typically trigger either full turbine or full pump operation, the turbine only becomes suitable for FCR participation when the FCR price exceeds a specific opportunity-cost threshold.

3.7.11.2. Downstream reservoir volume sensitivity analysis.

Since the downstream reservoir is not yet built, we also performed a sensitivity analysis to determine which reservoir size would be most suitable considering the Griessee upstream water discharge. Because we lack CAPEX and OPEX data for this type of infrastructure, our sensitivity analysis strictly focuses on the benefits that adding this reservoir would bring to the power plant. To accomplish this, we ran our algorithm for the years 2021 through 2023, with the VPP with access to the DA and FCR market.

Table 38 Summary of sensitivity analysis results based downstream reservoir volume

reservoir volume [m³]	**CTP**	**CTP and FCR**
0	100.7	105.2
50’000	105.8	111.5
100’000	106.9	112.4
200’000	107.5	113.1
500’000	108.8	114.5
1’000’000	108.6	114.3
2’000’000	108.4	114.4
5’000’000	109.2	114.8

We can observe that adding a reservoir, even a small one, significantly improves the performance of the VPP. It enables intraday arbitrage by pumping water back when daily prices are low, which allows more water to be turbined during high-price periods. We can also see that the benefits consistently increase alongside the reservoir volume. However, these increases begin to saturate around 500’000 m³, which represent 1/36 the upstream reservoir volume.

This indicates that a larger reservoir would not significantly enhance our VPP's performance, while it would incur substantial costs. Note that we did not consider downstream rivers, which could be captured and pumped up to the Griessee reservoir for future use. In that scenario, the optimal volume could be greater, as retaining these downstream catchments would allow them to be pumped at the most optimal moments.

3.7.12. Summary and Conclusions

An optimal design and operational optimisation model for the virtual power plant (VPP) has been formulated, and corresponding solution algorithms have been implemented within a Python environment. Numerical tests were conducted using the KW Aegina – Alstafel hydropower plant as a representative case study. Input data provided by all partners were processed and harmonized into a unified data schema, enabling their direct integration into the VPP optimization framework. Various design configurations were explored, with a particular focus on leveraging flexibility.

In this optimisation framework, the annual revenue of VPP is maximised through a three-stage problem, combining both deterministic and stochastic methods to deal with uncertainties on hydro and meteorological forecasts as well as market prices. The first (long-term) stage sets the annual reservoir trajectories to maximise expected annual revenues from day-ahead energy market while limitting water spillage. The second (day-ahead) stage schedules the power setpoints of all flexible resources on an hourly basis to maximise the daily revenue, respecting the reservoir level trajectories imposed by the first stage and penalizing the deviations from them. The third (real-time) stage adjusts the reservoir levels using actual water inflow, checks the operational constraints, and minimises the imbalances with respect to the day-ahead plan.

To support the first-stage stochastic model, data synthesizers for market prices and weather data were developed. These tools enable the generation of a wide range of scenarios, allowing for robust testing even when input data is limited. Various sensitivity analysis is performed to test the robustness of the proposed optimisation models and find appropriate meta parameters.

The optimisation results are highly sensitive to electricity market prices and conditions. Integrating a pump significantly improves the VPP's profitability through energy arbitrage. Even without a battery, the turbine already substantially reduces imbalance volumes. A small battery further increases the value of this reduction. With a larger battery, the strategy shifts toward swissgrid's FCR market. For example, a VPP centred around the Aegina-Altstafel power plant can increase its revenue by 2 to 6% depending on the battery's size.

Overall, numerical results suggest that, for the case of KW Aegina – Altstafel VPP with wind, solar and battery energy storage systems around it, the flexibility of the hydropower plant is economically beneficial, especially in reducing imbalance penalties. However, the profitability of VPP participation in the FCR market depends significantly on the price of awarded bids.

3.8 WP8 – Development of the business model

The objective of Workpackage 8 is to develop a business model to evaluate the economic potential of the flexibility identified and tested within the SmallFLEX Goms project. This work relies on the technical results and data obtained.

The flexibility capacities characterized through experimental campaigns will be used to assess their market value under realistic operating and market conditions. Based on the flexibility potential identified for each plant, different valorisation scenarios will be considered, including optimization of production according to electricity market prices and participation in ancillary service markets.

For a run-of-river hydropower plant, flexibility is intrinsically constrained by the continuous inflow of water. Unlike a storage plant, the operator cannot freely decide when to generate or stop generating without immediately managing the hydraulic consequences. For this reason, the business model cannot be based only on expected revenues from ancillary services or avoided losses during negative-price periods.

When generation must be reduced while inflow continues, the water must be diverted either at the intake or within the hydraulic scheme toward the downstream river reach. This introduces a set of constraints that must be explicitly reflected in the business model.

When generation must be reduced while inflow continues, the water must be diverted either at the intake or within the hydraulic scheme toward the downstream river reach. This introduces a set of constraints that must be explicitly reflected in the business model.

- Technical constraints: feasibility of bypass arrangements in an existing plant, hydraulic transients, energy dissipation, vibration, noise, control performance, and physical integration into the existing layout.
- Environmental constraints: discharge velocity into the river, rate of water-level rise, and impacts on fish and the downstream aquatic environment.
- Safety constraints: sudden downstream water-level rise that may endanger people near the river, as well as risks for plant personnel and equipment.
- Economic constraints: investment costs, outage-related production losses, annual maintenance costs, and the uncertainty of electricity market prices over the relevant business horizon.

Conversely, if the goal is to quickly increase generation through flexibility, the hydraulic capacity of the intake, waterways, and generating units must be confirmed. The plant must be capable of increasing discharge without draining the intake basin, introducing air into the waterway, or creating unsafe operating conditions for the hydraulic system.

These constraints are part of the business model because they determine whether theoretical flexibility can be delivered in practice. Several of these aspects are addressed technically in the hydraulic work packages, in particular WP5 and WP6.

3.8.1. Case study: Mörel power plant

The Mörel power plant has been selected as the primary case study to assess a practical flexibility business model for a run-of-river scheme. The objective is not only to quantify theoretical market opportunities, but also to determine under which technical and economic conditions additional flexibility can be provided in a realistic way while simultaneously maintaining or improving plant security.

Accordingly, several technical options have been investigated, as presented below.

3.8.1.1. Bypass solution within the powerhouse

One option for providing downward flexibility is to install energy-dissipating valves on one or more branches between the main inlet valve and the spiral case. This arrangement would allow part of the inflow to be bypassed to the downstream river reach when turbine output must be reduced.

This option is attractive because it may create downward flexibility without immediately modifying the intake structures. However, it raises important questions regarding hydraulic transients, energy dissipation, vibration, noise, structural integration into the existing powerhouse, and downstream safety.

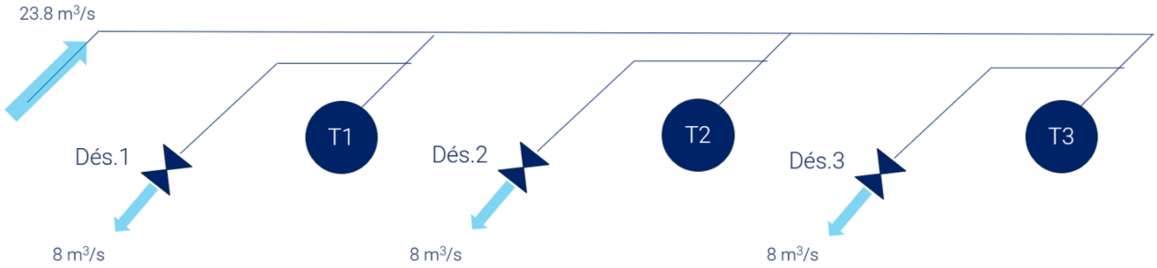

Figure 127: Schematic of the bypass system incorporated into the existing powerhouse.

3.8.1.2. Upgrade of the control and automation system

The control and automation system would need to be upgraded in order to be more reactive to satisfy the Swissgrid requirements for primary and secondary control. Response speed, control stability, instrumentation quality, and supervision logic are all critical for certification and reliable operation.

3.8.1.3. Verification of hydraulic capacity and safety

The hydraulic capacity of the waterways must be verified both for upward and downward flexibility. This includes the intake headrace system, penstock, transient behaviours, and downstream discharge arrangements. The goal is to ensure that flexibility can be provided without creating unacceptable risks for people, equipment, or the hydraulic scheme itself.

3.8.1.4. Unit replacement as an opportunity to enhance flexibility

If the generating units are replaced in the near future, flexibility can be improved further by integrating this objective into the electromechanical design. Unit replacement should therefore not be assessed only as an asset-renewal measure, but also as a strategic opportunity to improve the plant's market capability such as:

- Reduction of minimum operating power through design optimization
- Assessment of allowable start-stop cycles
- Synchronous condenser functionality

3.8.2. Cost structure associated with flexibility options

The business model shall consider at a minimum, the following items:

- Bypass equipment in the powerhouse.
- Civil works and hydraulic integration.
- Upgrading the control and automation systems.
- engineering studies.
- Maintenance caused
- Production losses during outages required for implementation.
- Necessary design optimization of the generating units.
- Possible costs related to environmental mitigation and downstream safety measures.

The following table provide a breakdown cost for each technical option discussed above.

Technical option	Cost
Powerhouse bypass/energy dissipation system	11%
Replacement of the control system	5%
Rehabilitation of the generating units	78%
Civil works in the tailrace channel	6%
Total	100%

3.8.2.1. Case 1 – Add a bypass in the powerhouse while keeping the existing units

In this case, flexibility is improved primarily through the installation of a bypass solution and an upgrade of the control and automation system, while the existing generating units are retained. The main advantage of this option is the lower initial investment compared with full unit replacement. However, the achievable flexibility remains limited by the existing unit design, especially at low load.

3.8.2.2. Case 2 – Integrate flexibility into future unit replacement

In this case, a lower minimum output, a wider operating range, improved start-stop capability, and possibly synchronous condenser functionality could be incorporated directly into the electromechanical design. This option is capital-intensive and should not be justified by flexibility revenues alone. It becomes more attractive when unit renewal is already foreseen within the next ten years. In that situation, flexibility becomes an additional benefit and a design criterion rather than the sole investment driver.

The following table summarizes the modifications required to enhance the operational flexibility of the power plant with the associated share of total investment cost.

Technical option	FCR	SRL	TRL	Negative prices	Lower min. output
Energy dissipation system		X	X	X	
Upgraded control system	X	X			X
Rehabilitated generating units					X
Necessary civil works		X	X	X	X
Cost	5%	22%	17%	17%	89%

Accordingly, the cost shares associated with SRL (22%), TRL (17%), and negative-price operation (17%) are significantly lower, while FCR (5%) requires only limited additional investment, mainly through the control system upgrade, bypass system and associated civil works.

3.8.3. Additional revenue due to flexibility

Based on the technical options assessed, namely the installation of a new bypass / energy dissipation system in the powerhouse, the upgrade of the control system, and the rehabilitation of the associated civil structures, the Mörel power plant could potentially provide:

- ±3 MW of symmetrical primary balancing capacity (FCR / FCR);
- Up to 30 MW of negative secondary balancing capacity (SRL / aFRR);
- Up to 30 MW of negative tertiary balancing capacity (TRL / mFRR).

The following table summarizes the relative contribution of each revenue stream to the total annual economic benefit of the flexibility measures. It indicates that most of the yearly value is generated by secondary and tertiary control reserves, while primary control reserve and avoided losses during negative-price periods make a smaller contribution.

Considering the uncertainty of the energy price market, the payback period ranges from 3 to 5 years, depending on the actual value of the energy market.

Given the uncertainty in the energy market, the payback period is estimated at 3 to 5 years, depending on actual market conditions.

Primary control reserve (±3 MW)	15%
Secondary control reserve (−30 MW)	44%
Tertiary control reserve (−30 MW)	38%
Avoided losses during negative prices	3%
Total	100%

3.8.4. Case study: Gletsch Oberwald power plant

Gletsch-Oberwald was selected as a case study to assess the impact of a potential solution aimed at maximizing primary control reserve (FCR) capacity by using the water volume in the galleries as a hydraulic reserve.

The power plant is currently certified for 1.6 MW of FCR. However, potentially the additional revenue that could be obtained by increasing the FCR capacity from 1.6 MW to 2.5 MW using the gallery water volume as temporary hydraulic storage for FCR provision.

From a technical perspective, the solution appears to be feasible and safe. However, its implementation may also lead to additional costs related to maintenance, monitoring, and operational supervision.

To check if this capacity increasing would be finically beneficial, the simulations were carried out over a five-year period from 2027 to 2031.

The results show that increasing FCR capacity provides only limited economic benefit. Although the reserve capacity can be increased, the corresponding gain in total revenue remains small. Moreover, the model indicates that, in some years, a higher FCR capacity, such as 2.6 MW, may even generate lower revenue than the current 1.6 MW configuration.

This is because reserving FCR imposes operating constraints that may reduce the value of energy sold on the day-ahead market. When day-ahead prices are high, or when the mobilizable water volume in the gallery is limited, it may be economically preferable to maximize generation rather than reserve part of the capacity for FCR. Consequently, the economic optimum does not necessarily coincide with the maximum FCR capacity.

Overall, the analysis indicates that the plant's business model should not be based primarily on FCR revenues, but rather on the actual technical flexibility of the scheme and on its ability to deliver this flexibility safely, reliably, and repeatedly.

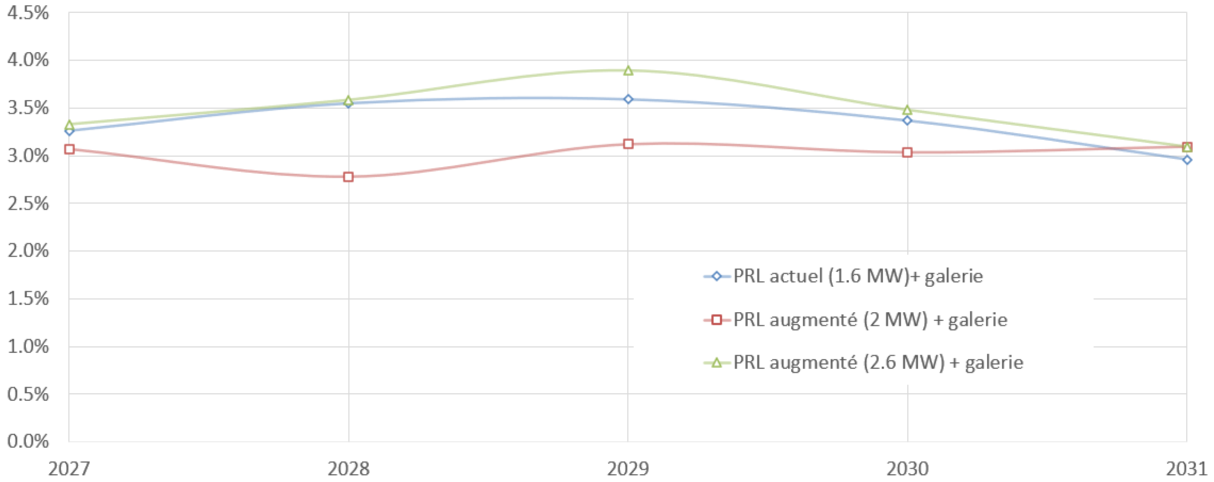

Figure 128: Difference in total revenue for FCR capacities of 1.6 MW, 2 MW, and 2.6 MW compared with the case involving day-ahead production only.

This can be explained by the fact that the conditions required to increase primary control reserve are only met during limited periods of the year. The Gletsch power plant is located downstream of the Rhône Glacier and typically operates under two main regimes.

3.8.5. In summer, during the melting season, the plant runs at full capacity, which leaves no available headroom to provide upward primary control reserve. In winter, when inflows are low, the operating power is too limited to offer downward reserve. rBenefits of implementing a pool of flexibility

Having a pool of small, flexible resources is highly beneficial when it comes to managing adjustments on a continuous, “as-needed” basis. In the context of primary frequency control, market requirements typically impose the sale of symmetrical capacity blocks of 1 MW. Individually, many small-scale assets cannot meet this threshold and therefore remain excluded from participation.

By aggregating these smaller flexibilities, it becomes possible to create a combined offering that meets market requirements. This pooling approach unlocks value from assets that would otherwise be unable to participate on their own. It also allows for optimization across different hydrological conditions: power plants located in separate catchment areas may face varying flow constraints at any given time. As a result, some units may be better suited to provide upward regulation (positive primary control), while others can deliver downward regulation (negative primary control).

Ultimately, this aggregation mechanism represents an effective solution to enable small hydropower plants to participate in ancillary services for grid regulation. Beyond improving system efficiency and resilience, it can also generate additional revenue streams, increasing the turnover of these plants by up to approximately 1% in the winter period.

FMV currently operates a pool of five small run-of-river power plants that together provide primary control. The objective is to expand this pool, particularly by taking into account the valuable results of this study.

3.8.6. Case study: VPP Aegina

The results presented in the previous section (3.7) are expressed in terms of revenue increase. They show that integrating a Virtual Power Plant (VPP), combining flexible hydropower assets and battery storage, can enhance operational performance and generate additional income.

However, these revenue gains are directly linked to significant investment projects. Unlocking such flexibility typically requires major infrastructure developments, such as dam heightening, pumped-storage installations, or battery systems. These projects involve substantial capital expenditures, as well as additional operational costs related to maintenance and system operation.

Therefore, the increase in revenue highlighted in this study should not be interpreted as net profit, but rather as an indication of the value created through improved flexibility and imbalance management.

From a business model perspective, the VPP acts as an enabling platform to aggregate assets, optimize their operation, and access new revenue streams. It also serves as a decision-support tool to evaluate the economic relevance of different investment options and system configurations.

A full profitability assessment would require a comprehensive analysis including investment costs, operational expenses, and market uncertainties. These aspects are beyond the scope of this report.

3.8.7. Conclusion

There is an important distinction between leveraging existing, “hidden” flexibility within current assets and developing new flexibility through large investments. The former can often be activated directly, with limited or no additional cost, making it immediately valuable. In contrast, investing solely to create new flexibility is generally not economically justified. However, when major investments are required for other strategic or operational reasons, it becomes highly relevant to integrate flexibility considerations into the design. In such cases, flexibility can be captured at marginal cost and significantly enhance the overall value of the project.

3.9 WP9 - Dissemination of the results

This work package aims to consolidate and disseminate the results of the project.

The results have been presented at several conferences and published in scientific journals (see Chapter 6). Additional publications are currently in preparation, including an article for the *Bulletin Electrosuisse*, planned for the June 2026 issue dedicated to hydropower.

To conclude the project, a public workshop has been organized on May 5, 2026, from 13:30 to 17:30 at Energypolis in Sion. This event was the occasion to present the final results to a broader audience and foster exchange with stakeholders.

4 Conclusions and outlook

The SmallFLEX Goms project provided a comprehensive assessment of the flexibility potential of small and medium-sized hydropower plants, combining real-scale implementation, modelling, forecasting and system integration approaches.

Implementation of flexible operation and identification of flexibility potential (WP1–WP3)

In WP1, a detailed protocol for flexible operation involving the dewatering of the KW Gletsch-Oberwald (KWGO) power plant was established based on the analysis of on-site data and operational constraints. Two main operating scenarios were investigated: (i) daily drawdown using a single turbine unit, and (ii) operation of both units with constant upstream water level regulation combined with primary grid control. In both cases, the storage capacity of the forebay chamber and the upper part of the penstock is mobilised to increase operational flexibility during periods of low inflow. From an economic perspective, operation in primary grid control mode at around 2 MW during dewatering appears to be the most promising scenario. The analysis of the on-site data acquired during several dewatering tests confirms that the existing instrumentation of the power plant is sufficiently robust to ensure continuous monitoring of such flexible operation modes. Monitoring remains essential to ensure safe and optimal performance under these conditions.

WP2 focused on the inventory and characterization of hydropower plants in the Goms region, enabling the ranking of installations according to their hidden flexibility potential. Based on both public and operator data, KW Mörel and KW Merezenbach were identified as the most promising candidates for further investigation, while KW Aegina–Altstafel was selected for further analysis in the context of hybridization and Virtual Power Plant integration.

WP3 assessed the flexibility potential of KW Merezenbach, KW Mörel and KW Aegina–Altstafel through detailed hydraulic analyses based on 1D transient modelling using SIMSEN. For KW Merezenbach, simulations indicate that dewatering up to 25–50% does not lead to critical transient behaviour, while higher levels may introduce conditions potentially leading to air entrainment, as further analysed in WP5. For KW Mörel, the use of the Eggen overflow chamber enables primary control operation with power steps of 1 to 3 MW using a single unit, whereas higher power levels with two units may lead to critical flow conditions. For KW Aegina–Altstafel, the integration of additional pumping capacity was investigated, identifying a promising configuration with a total capacity of approximately 12 MW. Emergency shutdown scenarios of the new pumping units were also analysed, supporting further developments within the Virtual Power Plant framework (WP7).

Forecasting and climate change impacts (WP4)

WP4 assessed the potential for flexible operation of small hydropower plants in the Goms Valley using advanced hydrometeorological forecasting tools and climate change scenarios. A state-of-the-art modelling framework was developed, combining an operational forecasting chain with a newly developed Toy Model for Energy Forecasting (Wisskott, 2025). This framework enables local-scale predictions of Run-of-River (RoR), photovoltaic (PV) and wind energy production. For operational applications, the results show that RoR forecasts reach approximately 70% usefulness for day-ahead planning, while PV forecasts achieve around 50% usefulness, with improved performance at longer lead times. In contrast, wind forecasts remain highly uncertain, with usefulness below 30%, which currently limits their operational applicability. Based on these findings, RoR and PV forecasts can be recommended for day-ahead and short-term flexible operation, whereas wind forecasts require further local calibration and validation before being used in practice. Future climate impacts were assessed using CH2018/HydroCH2018 frameworks across ten representative test areas in the Goms region. The results indicate that changes in total energy potential are primarily driven by modifications in hydrological response, particularly discharge and RoR production, while variations in solar radiation and wind remain relatively homogeneous across the region. A key finding is the seasonal complementarity between photovoltaic and hydropower production, with PV increasing in summer and RoR production being more significant in winter. This highlights the strong potential of hybrid systems combining hydropower and PV, especially when storage capacity is available. Pumped-storage solutions appear particularly promising for enhancing both flexibility and economic performance. Wind energy may also contribute to winter energy supply, when RoR production is limited, although its high variability remains a challenge. Finally, the study underlines that robust assessments of future hybrid energy systems strongly depend on the definition of realistic energy demand scenarios. Future work could build on the recently released CH2025 climate scenarios to further refine these analyses.

Air entrainment risks (WP5)

The outcomes of WP5 show that run-of-river hydropower plants (RoR-HPPs) can increase their operational flexibility by exploiting desanders and headrace waterways as unconventional storage volumes. However, this approach introduces the risk of air entrainment, which may compromise operational safety. A comprehensive review of the literature highlighted the main air entrainment mechanisms, including vortices, impingement jets and surface instabilities, as well as thresholds governing air transport. The critical pipe Froude number Fwc provides a useful criterion to exclude cases in which air pockets would be transported downstream; however, values below this threshold do not guarantee safe operation. Within the SmallFLEX Goms fleet, the pilot plant KW Gletsch-Oberwald represents a specific case, while for most other hydropower plants, emptying the power waterway is generally not advisable. The analysis of the KW Mörel plant demonstrates that the free-flow headrace tunnel contains a significant hidden storage volume, particularly at low discharges. Nevertheless, due to air entrainment mechanisms, the practical use of this volume remains strongly limited, as draining the Eggen overflow chamber may lead to air being entrained into the adjacent pressurised headrace. A similar conclusion applies to KW Merezenbach, where transitions to free-surface flow in the headrace pipe should be avoided. More generally, existing headrace tunnels operated under free-flow conditions can provide operational flexibility, provided that a backwater zone is used as a controlled storage volume. In contrast, converting fully pressurised headrace tunnels or pipes to free-surface flow in order to exploit additional storage volume is generally not recommended. Finally, potential mitigation measures such as the implementation of deaeration shafts could be considered to manage air entrainment in pressurised systems. These approaches would aim at safely exploiting hidden storage volumes, particularly in forebay areas, while maintaining operational safety. In this context, WP5 also provides a structured methodology that can serve as engineering guidance for assessing air entrainment risks in similar hydropower schemes.

On-site experiments and monitoring (WP6)

Within WP6, the data acquired under both normal operating conditions and dedicated test campaigns enabled a comprehensive characterization of the behaviour of the Pelton turbine at KW Merezenbach and the double-Francis turbine at KW Mörel. A detailed analysis of turbine operation under nominal head conditions was carried out to identify any potential influence of flexible operating modes, including dewatering. The recorded datasets were validated and used to perform extensive statistical analyses for both test cases. Due to operational constraints and identified contraindications, dewatering tests could not be performed at KW Merezenbach. However, the acquired dataset provides a solid reference for detecting potential anomalies during regular operation. At KW Mörel, measurements were successfully conducted under both standard and flexible operating conditions, including dewatering of the overflow tank. The Hydro-Clone system demonstrated its relevance as a physics-based digital twin for real-time monitoring of hydraulic transients at the Mörel hydropower plant. By combining a validated SIMSEN model with SCADA data, it provides predictive insights that enhance operational safety and support decision-making under dynamic operating conditions. While minor refinements are still ongoing, Hydro-Clone is expected to become a valuable tool for long-term monitoring and operation of hydropower plants. The performed dewatering tests indicate a normal turbine operation and open the perspective for ancillary service provision, pending additional validation. It was also demonstrated that the plant can deliver ±3 MW/min power peaks using automatic power regulation.

Virtual Power Plant and system integration (WP7)

WP7 focused on the development and application of an integrated optimisation framework for the design and operation of a Virtual Power Plant (VPP) combining small hydropower, photovoltaic, wind and battery storage systems. The methodology addresses both the optimal selection of system components and their coordinated operation over multiple time horizons, including long-term planning, day-ahead scheduling and real-time adjustments.

The optimisation framework relies on a three-stage approach, covering reservoir management, market participation and real-time imbalance correction under uncertainties in hydrology, weather conditions and electricity prices. The model accounts for cascaded hydropower systems with non-linear performance characteristics. To support stochastic optimisation, dedicated data generators for market prices and weather conditions were developed, enabling the creation of representative scenarios and robust sensitivity analyses.

The results show a strong dependence of system performance on market conditions. The integration of pumping capacity significantly improves profitability through energy arbitrage. Even without battery storage, hydropower operation already reduces imbalance volumes, while the addition of a battery further enhances system value. For larger storage capacities, the operational strategy shifts towards participation in ancillary service markets, particularly the Frequency Containment Reserve (FCR).

For the case study of the KW Aegina–Altstafel system, the results indicate that combining hydropower flexibility with wind, solar and storage systems provides clear economic benefits, mainly through the reduction of imbalance penalties. However, the profitability of participation in ancillary service markets remains highly sensitive to market price conditions.

Economic assessment and business model (WP8)

WP8 focused on evaluating the economic potential associated with the flexible operation of small hydropower plants, taking into account both market opportunities and technical feasibility constraints. The analysis was based on the flexibility capacities identified in previous work packages and assessed under realistic operating and market conditions.

The results highlight that, for run-of-river hydropower plants, flexibility is intrinsically constrained by continuous inflow and associated hydraulic, environmental and safety requirements. As a consequence, the business model cannot rely solely on expected revenues from electricity markets or ancillary services, but must explicitly account for the plant's ability to deliver flexibility under real operating conditions.

Several technical options were analysed to enable flexibility, including bypass solutions, control system upgrades and the integration of flexibility in the context of unit replacement. These options demonstrate that additional flexibility can be achieved, provided that the associated hydraulic and operational constraints are properly managed.

The economic assessment indicates that additional revenues from flexibility remain limited and strongly dependent on market conditions. While some value can be captured through improved operation, participation in ancillary services or reduction of imbalance penalties, these revenues alone are generally insufficient to justify dedicated investments in new flexibility.

Conversely, the results show that exploiting existing "hidden" flexibility within current infrastructures represents a cost-effective approach, offering immediate value with limited investment. In addition, the aggregation of multiple small hydropower plants through pooling strategies or Virtual Power Plant concepts enables access to ancillary service markets and improves the overall economic relevance of flexibility by combining distributed resources

Outlook

The results of the SmallFlex Goms project clearly indicate that the transition from technical feasibility to commercially viable deployment will require coordinated actions from both research and industry stakeholders. As immediate next steps, further research should focus on (i) refining and validating simplified modelling and forecasting tools for operational use, (ii) standardising the assessment methodology for hydraulic constraints and air entrainment risks, and (iii) testing scalability through pilot implementations across a broader portfolio of hydropower plants. In particular, the coupling between forecasting accuracy, storage availability, and real-time control strategies should be further optimised to enable automated and reliable flexibility provision.

At the same time, future developments should aim at reducing the cost and complexity of flexibility assessments. The methodologies developed in SmallFlex Goms are intended to provide transferable screening and evaluation tools, allowing plant owners to identify the most promising assets before engaging in detailed technical studies. In practice, this implies first assessing available hydraulic storage, operational constraints, ramping capability, aggregation opportunities and market-access conditions in order to determine whether a plant has sufficient technical and economic flexibility potential. Detailed investigations should therefore be reserved for assets with realistic deployment perspectives.

From an industrial perspective, the priority lies in translating these methodologies into deployable solutions. Plant operators and aggregators should jointly develop operational platforms integrating forecasting, monitoring, and dispatch optimisation, building on the demonstrated Virtual Power Plant concept. Equipment suppliers and engineering firms will play a key role in embedding flexibility considerations into refurbishment projects, ensuring that turbines, control systems, and waterways are designed or upgraded to safely accommodate dynamic operation. In parallel, pilot projects—particularly at sites such as KW Mörel—should be extended into pre-commercial demonstrators to validate revenue streams under real market conditions.

Achieving commercial viability will depend on the emergence of integrated service models, where aggregators or specialised flexibility operators take responsibility for pooling distributed hydropower assets, managing market participation, and guaranteeing performance towards system operators. Hydropower plant owners, in turn, would provide flexible capacity under contractual arrangements, reducing operational risk while accessing new revenue streams. This implies a clear allocation of roles: research institutions supporting methodology and validation, industrial partners delivering technical integration, and aggregators enabling market access and revenue optimisation.

Finally, regulatory and market frameworks must evolve to recognise and adequately remunerate distributed flexibility services. The results of SmallFlex Goms suggest that the most attractive business cases will not necessarily rely on dedicated new investments, but rather on the cost-effective exploitation of existing “hidden” flexibility within suitable hydropower assets, combined with aggregation and hybridisation strategies where relevant.

5 National and international cooperation

Within the framework of this project, collaborations outside the consortium were primarily developed in Work Package 4.

At the international level, WP4 collaborated with Prof. Dr.-Ing. Eva-Maria Königsheim and Artem Holovchack from the *Hochschule für Angewandte Wissenschaften Hamburg*. Prof. Königsheim is a lecturer in Power Engineering and Energy Storage Systems.

WP4 also collaborated with Maria-Helena Ramos, Research Director at the *French National Research Institute for Agriculture, Food and Environment (INRAE)* in Paris. Her research focuses on hydrometeorology, hydrological forecasting and ensemble prediction, as well as water resources management under past, present, and future climate conditions. During her nine-month fellowship at WSL, she co-supervised the work of Rona Schenk (ETH/WSL Master student).

In addition, WP4 hosted Dr. Domenico Micocci from the Department of Civil, Chemical, Environmental and Materials Engineering at the *University of Bologna* (Italy) for a six-month research stay. His work focused on the hybridization of hydropower with floating photovoltaic systems. This collaboration was further extended to his supervisors, Prof. Cristiana Bragalli and Prof. Elena Toth.

At the national level, WP4 highlights the strong synergies between the *Small-Flex Goms* project and the ETH initiative *Speed2Zero*, which aims to support the energy transition by addressing climate, energy, and ecological risks.

6 Publications and other communications

Haddad, Y. Y., Gudmundsson, L., Savelsberg, J., Garrison, J. B., Raycheva, E., Wechsler, T., Seneviratne, S. I. (2025). Recent climate impacts on run-of-river hydropower and electricity systems planning in Switzerland. Environmental Research Letters, 20, 084020 (10 pp.). https://doi.org/10.1088/1748-9326/ade4df

Holovchak, A. (2025). Climate model-based simulation analysis of hydropower plant potentials: Numerical experiments on water storage strategies and complementary photovoltaic integration. Bachelor's Thesis. Hamburg University of Applied Sciences (HAW Hamburg), Department of Information and Electrical Engineering, and Swiss Federal Research Institute WSL. Zurich.

Micocci, D., Bragalli, C., Toth, E., Wechsler, T., & Zappa, M. (2026). Vulnerabilities and opportunities of solar-hydro hybridization in a changing climate: A case study in Switzerland (paper ready for submission).

Micocci, D., Bragalli, C., Toth, E., Wechsler, T., & Zappa, M. (2025). Hybridization of an alpine pumped-storage hydropower plant with floating solar photovoltaics: a study from the water resource perspective. Renewable Energy, 253, 123530 (15 pp.). https://doi.org/10.1016/j.renene.2025.123530

Schenk, R. (2023). Complementing a hydropower plant with solar and wind power plants: a conceptual study in the canton of Valais. Master Thesis at WSL and ETH Zürich.

Streule, C., Lais A., Evers F., Münch-Alligné C. & Boes R. (2024). Flexibilisierung der Kleinwasserkraft durch Stollenspeicherung – Lufteintrag und -transport als limitierende Faktoren. In G. Zenz (Ed.), Wasserbausymposium Graz 2024 (9-17).

Streule, C., Lais A., Evers F., Münch-Alligné C. & Boes R. (2025). Flexibilisierung der Kleinwasserkraft durch Stollenspeicherung – Lufteintrag und -transport als limitierende Faktoren. Anwenderforum Kleinwasserkraft, Landquart 2024.

Streule, C., Lais A., Boes R. & Münch-Alligné C. (2025). Flexible Run-of-River Hydropower by Using Unconventional Storage Volumes in Headrace Tunnels and Penstocks – Limitations due to Air Entrainment. HYDRO 2025, Thessaloniki.

Wechsler, T., Stähli, M., Jorde, K., Zappa, M., & Schaefli, B. (2023). The future of Alpine Run-of-River hydropower production: climate change, environmental flow requirements, and technical production potential. Science of the Total Environment, 890, 163934 (13 pp.). https://doi.org/10.1016/j.scitotenv.2023.163934

Wechsler, T., & Zappa, M. (2024). CH-Kleinstwasserkraftwerke: ein schweizweiter Datensatz zu Kleinstwasserkraftwerken (≤ 300 kW). WSL.

Wechsler, T., Schirmer, M., & Bryner, A. (2025). Restwasser. Die Suche nach der angemessenen Menge - Festlegung, Wirkung und Anforderungen. Aqua & Gas, 105(3), 48-53.

References

Addor, N., Jaun, S., Fundel, F., & Zappa, M. (2011). An operational hydrological ensemble prediction system for the city of Zurich (Switzerland): skill, case studies and scenarios. Hydrology and Earth System Sciences, 15(7), 2327-2347. https://doi.org/10.5194/hess-15-2327-2011

Anwar, H. O., Weller, J. A., & Amphlett, M. B. (1978). Similarity of Free-Vortex at Horizontal Intake. *Journal of Hydraulic Research*, *16*(2), 95–105. https://doi.org/10.1080/00221687809499623

Bauer, L., & Matysik, S. (2023). Enercon E-82 E2 2.000. Retrieved July 28, 2023, from url: https://en.wind-turbine-models.com/turbines/835-enercon-e-82-e2-2.000.

Bernhard, L. & Zappa, M. (2012) Schlussbericht CCHydrologie: Teilprojekt WHH- CH-Hydro: Natürlicher Wasserhaushalt der Schweiz und ihrer bedeutendsten Grosseinzugsgebiete. Birmensdorf.

Bertola, N., Wang, H., & Chanson, H. (2018). Air bubble entrainment, breakup, and interplay in vertical plunging jets. *Journal of Fluids Engineering*, 140(9), 091301.

Bonalumi, M. ; Putzi, T. ; Federer, G. ; & Dupraz, C. (2021). Mitteilung 262: Wasserbau-Symposium 2021 / Band 1 (tech. rep.). Retrieved August 30, 2023, from url: https://henry.baw.de/items/aec66ae9-0003-45c7-8ab3-5b97f1b19a73.

Bottin, M., Berlandis, J. P., Hervieu, E., Lance, M., Marchand, M., Öztürk, O. C., & Serre, G. (2014). Experimental investigation of a developing two-phase bubbly flow in horizontal pipe. *International journal of multiphase flow*, *60*, 161-179.https://henry.baw.de/items/aec66ae9-0003-45c7-8ab3-5b97f1b19a73..

Brunner, M. I., Björnsen Gurung, A., Zappa, M., Zekollari, H., Farinotti, D., & Stähli, M. (2019). Present and future water scarcity in Switzerland: Potential for alleviation through reservoirs and lakes. *Science of the Total Environment, 666*, 1033–1047.

CH2018 – Climate Scenarios for Switzerland (Technical Report). (2018) (CH2018 Technical Report). National Centre for Climate Services. Zurich. https://www.nccs.admin.ch/nccs/en/home/climate-change-and-impacts/swiss-climate-change-scenarios/technical-report.html

Cronin, J., Anandarajah, G., Dessens, O., (2018). Climate change impacts on the energy system: a review of trends and gaps. Climatic Change 151, 79–93. https://doi.org/10.1007/s10584-018-2265-4

Delucchi M.A., M.Z. Jacobson. (2011). Providing all global energy with wind, water, and solar power, Part II: reliability, system and transmission costs, and policies, Energy Policy 39 1170–1190, https://doi.org/10.1016/j.enpol.2010.11.045

Duffie, J. A., & Beckman, W. A. (2013). Solar engineering of thermal processes. John Wiley & Sons. https://doi.org/10.1002/9781118671603

Egre, J.C. Milewski, The diversity of hydropower projects, Energy Policy 30 (2002) 1225–1230, https://doi.org/10.1016/S0301-4215(02)00083-6

Elektrizitätswerk Obergoms website (2025). https://www.ewobergoms.ch/energieproduktion/kw-merezenbach. Consulted on November 6th, 2025.

Enercon GmbH. (2016). E-82. Retrieved July 28, 2023, from url: https://www.enercon.de/en/ products/ep-2/e-82/.

Engeland, K., Borga, M., Creutin, J. D., François, B., Ramos, M. H., & Vidal, J. P. (2017). Space-time variability of climate variables and intermittent renewable electricity production– A review. Renewable and Sustainable Energy Reviews, 79 (May 2016), 600–617. doi: https://doi.org/10.1016/j.rser.2017.05.046

Escarameia, M. (2007). Investigating hydraulic removal of air from water pipelines. *Proceedings of the Institution of Civil Engineers - Water Management*, *160*(1), 25–34. https://doi.org/10.1680/wama.2007.160.1.25

Falvey, H. T. (1980). Air-water flow in hydraulic structures. *NASA STI/Recon Technical Report N*, *81*, 26429.

FOEN. (2021b). Hydro-ch2018: Auswirkungen des klimawandels auf die schweizer gewasser. hydrologie, gewasserokologie und wasserwirtschaft (tech. rep.). Federal Office for the Environment FOEN. Bern. Bern. https://www.nccs.admin.ch/nccs/en/home/climate-change-and-impacts/schweizer-hydroszenarien/synthesis-report%20.html

François, B., Puspitarini, H., Volpi, E., & Borga, M. (2022). Statistical analysis of electricity supply deficits from renewable energy sources across an Alpine transect. Renewable Energy,201 (P1), 1200–1212. doi: 10.1016/j.renene.2022.10.125.

Gardet. A. (1961). L'aménagement hydro-électrique du Merezenbach. *Bulletin technique de la Suisse romande*, 6, 69-79, March 25.

Gordon, J. L. (1970). Vortices at Intakes. *Water Power*, *22*(4), 137–138.

Gulliver, J. S., Rindles, A. J., & Linblom, K. C. (1986). Designing intakes to avoid free-surface vortices. *International Water Power and Dam Consturction*, *39*(9), 24–28.

Guittet, M. Capezzali, L. Gaudard, F. Romerio, F. Vuille, F. Avellan, Study of the drivers and asset management of pumped-storage power plants historical and geographical perspective, Energy 111 (2016) 560–579, https://doi.org/10.1016/j.energy.2016.04.052.

Gurung, A. B., Borsdorf, A., Füreder, L., Kienast, F., Matt, P., Scheidegger, C., Schmocker, L., Zappa, M., & Volkart, K. (2016). Rethinking Pumped Storage Hydropower in the European Alps. Mountain Research and Development, 36 (2), 222–232. doi: 10.1659/MRDJOURNAL-D-15-00069.1.

Holovchak, A. (2025). *Climate model-based simulation analysis of hydropower plant potentials: Numerical experiments on water storage strategies and complementary photovoltaic integration*. Bachelor's Thesis. Hamburg University of Applied Sciences (HAW Hamburg), Department of Information and Electrical Engineering, and Swiss Federal Research Institute WSL. Zurich.

Horton, P., Schaefli, B., & Kauzlaric, M. (2022). Why do we have so many different hydrological models? A review based on the case of Switzerland. Wiley Interdisciplinary Reviews: Water, 9(1), e1574. https://doi.org/10.1002/wat2.1574

Huss, M., & Hock, R. (2015). A new model for global glacier change and sea-level rise. *Frontiers in Earth Science, 3*(54).

Huss, M., Jouvet, G., Farinotti, D., and Bauder, A. (2010). Future high-mountain hydrology: a new parameterization of glacier retreat, Hydrol. Earth Syst. Sci., 14, 815–829, https://doi.org/10.5194/hess-14-815-2010.

Hunt J.D., Zakeri B., Lopes R., Barbosa P.S.F., Nascimento A., N.J. de Castro, R. Brandao, P.S. Schneider, Y. Wada. (2020). Existing and new arrangements of pumped-hydro storage plants, Renew. Sustain. Energy Rev. 129 109914, https://doi.org/10.1016/j.rser.2020.109914.

IPCC. (2012). Renewable energy sources and climate change mitigation: Special report of the intergovernmental panel on climate change (O. Edenhofer, R. P. Madruga, Y. Sokona, K. Seyboth, P. Matschoss, S. Kadner, T. Zwickel, P. Eickemeier, G. Hansen, S. Schlömer, & C. von Stechow, Eds.) [Intergovenmental Panel on Climate Change]. doi: https://doi.org/10.1017/CBO9781139151153

Jacob, D., Petersen, J., Eggert, B., Alias, A., Christensen, O. B., Bouwer, L. M., Braun, A., et al. (2014) EURO-CORDEX: New high-resolution climate change projections for European impact research. Reg. Environ. Chang. 14(2), 563–578. Springer Verlag. doi: https://doi.org/10.1007/s10113-013-0499-2

Jurasz J., Ciapała B.. (2018). Solar–hydro hybrid power station as a way to smooth power output and increase water retention, Sol. Energy 173 675–690, https://doi.org/10.1016/j.solener.2018.07.087

Kalinske, A. A., & Robertson, J. M. (1943). Closed Conduit Flow. *Transactions of the American Society of Civil Engineers*, *108*(1), 1435–1447. https://doi.org/10.1061/TACEAT.0005621

Karring, K., & Raeck, M. (2019). Wettbewerbsfähigkeit der Schweizer Wasserkraft: Studie im Auftrag des Bundesamtes für Energie (tech. rep.). Retrieved August 30, 2023, from url: https://pubdb.bfe.admin.ch/de/suche.

Kent, J. C. (1952). *The entrainment of Air by Water Flowing Through Circular Conduits with Downgrade Slopes* [PhD Thesis]. University of California.

Knauss, J. (1987). Prediction of critical submergence. In *Swirling flow problems at intakes*. Taylor & Francis.

Kneib, T., Silbersdorff, A., and Säfken, B. (2023). Rage against the mean – a review of distributional regression approaches. Econometrics and Statistics, 26:99–123.

Kroposki, B. Johnson, Y. Zhang, V. Gevorgian, P. Denholm, B.-M. Hodge, B. Hannegan, Achieving a 100% renewable grid: operating electric power systems with extremely high levels of variable renewable energy, IEEE Power Energy Mag. 15 (2017) 61–73, https://doi.org/10.1109/MPE.2016.2637122.

Lee, H., & Birol, F. (2020). Energy is at the heart of the solution to the climate challenge. Retrieved February 4, 2023, from url: https://www.ipcc.ch/2020/07/31/energy-climatechallenge

Lund, P.D., Lindgren, J., Mikkola, J., Salpakari, J., 2015. Review of energy system flexibility measures to enable high levels of variable renewable electricity. Renewable and Sustainable Energy Reviews 45, 785–807. https://doi.org/10.1016/j.rser.2015.01.057

Lustenberger, F., & Zappa, M. (2023). *Schlussbericht Klimastudie Wasserkraft Göschenen/Meienreuss.* WSL.

Mandal, N. K. & Bajracharya, T. R. (2021). Pelton Runner Erosion Due To Cavitation: A Case Study of Storage Hydropower Plant, Kulekhani First Hydropower Station. *Proceedings of 10th IOE Graduate Conference,* Institute of Engineering at Tribhuvan University, Nepal, 1213 - 1219

Manente, A. (2025): Auswertung der Sihl-Vorhersagesysteme für die Periode 2010-2025. Master Thesis at WSL and University of Zürich.

MeteoSchweiz**.** (2024). *Messdaten der Wetterstation Ulrichen (2006–2024)* [Datensatz]. Bundesamt für Meteorologie und Klimatologie MeteoSchweiz. https://www.meteoschweiz.admin.ch/ (Zugriff am 05.11.2025)

Micocci, D., Bragalli, C., Toth, E., Wechsler, T., & Zappa, M. (2026). *Vulnerabilities and opportunities of solar-hydro hybridization in a changing climate: A case study in Switzerland* (Draft — Supplementary information). Department of Civil, Chemical, Environmental, and Materials Engineering (DICAM), University of Bologna; Swiss Federal Research Institute WSL, Birmensdorf.

Micocci, D., Bragalli, C., Toth, E., Wechsler, T., & Zappa, M. (2025). Hybridization of an alpine pumped-storage hydropower plant with floating solar photovoltaics: a study from the water re-source perspective. Renewable Energy, 253, 123530 (15 pp.). https://doi.org/10.1016/j.renene.2025.123530

Möller, G. (2013). *Vortex-induced air entrainment rate at intakes* [PhD Thesis]. ETH Zurich. https://doi.org/10.3929/ETHZ-A-009932182

Moss, R. H., Edmonds, J. A., Hibbard, K. A., et al. (2010). The next generation of scenarios for climate change research and assessment. *Nature.*

Naudascher, E. (1991). *Hydrodynamic Forces: IAHR Hydraulic Structures Design Manuals 3. Routledge.*

Papadis, E., Tsatsaronis, G., 2020. Challenges in the decarbonization of the energy sector. Energy, 205, 118025. https://doi.org/10.1016/j.energy.2020.118025

Petrollese, M., Seche, P., & Cocco, D. (2019). Analysis and optimization of solar-pumped hydro storage systems integrated in water supply networks. Energy, 189, 116176. https://doi.org/10.1016/j.energy.2019.116176

Pothof, I., & Clemens, F. (2010). On elongated air pockets in downward sloping pipes. *Journal of Hydraulic Research*, *48*(4), 499–503. https://doi.org/10.1080/00221686.2010.491651

Pothof, I., & Clemens, F. (2011). Experimental study of air–water flow in downward sloping pipes. *International Journal of Multiphase Flow*, *37*(3), 278–292. https://doi.org/10.1016/j.ijmultiphaseflow.2010.10.006

Pulg, U., Lennox, R. J., Enqvist, M., Stranzl, S. F., Espedal, E. O., Schwarz, M., & Velle, G. (2024). Assessing the potential for gas supersaturation downstream of hydropower plants in Norway, Austria and Germany. Science of the Total Environment, 948, 174645.

Puspitarini, H. D., François, B., Zaramella, M., Brown, C., & Borga, M. (2020). The impact of glacier shrinkage on energy production from hydropower-solar complementarity in alpine river basins. Science of the Total Environment, 719, 137488. doi: https://doi.org/10.1016/j.scitotenv. 2020.137488

RGI Consortium. (2017) Randolph Glacier Inventory –A Dataset of Global Glacier Outlines: Version 6.0: Technical Report, Global Land Ice Measurements from Space. Colorado, USA. doi: https://doi.org/10.7265/N5-RGI-60

Rigby, R. A. and Stasinopoulos, D. M. (2005). Generalized additive models for location, scale

Rossa, A., Liechti, K., Zappa, M., et. al. (2011). The COST 731 Action: a review on uncertainty propagation in advanced hydro-meteorological forecast systems. Atmospheric Research, 100(2-3), 150-167. https://doi.org/10.1016/j.atmosres.2010.11.016

Rotach, M. W., Arpagaus, M., Dorninger, M., Hegg, C., Montani, A., & Ranzi, R. (2012). Uncertainty propagation for flood forecasting in the Alps: different views and impacts from MAP D-PHASE. Natural Hazards and Earth System Sciences, 12(8), 2439-2448. https://doi.org/10.5194/nhess-12-2439-2012

Schaefli, B., 2015. Projecting hydropower production under future climates: a guide for decision-makers and modelers to interpret and design climate change impact assessments. WIREs. Water 2, 271–289. https://doi.org/10.1002/wat2.1083

Schenk, R. (2023). Complementing a hydropower plant with solar and wind power plants: a concep-tual study in the canton of Valais. Master Thesis at WSL and ETH Zürich.

SFOE. (2021). Energy Strategy 2050 [Swiss Federal Office of Energy]. Retrieved August 9, 2023, from url: https://www.bfe.admin.ch/bfe/en/home/policy/energy-strategy-2050.html

SFOE. (2023). Hydropower [Swiss Federal Office of Energy]. Retrieved August 9, 2023, from url: https://www.bfe.admin.ch/bfe/en/home/supply/renewable-energy/hydropower.html/

SmallFLEX Project Report. Authors: Decaix, J., Münch-Alligné, C., Zordan, J., Manso, P., De Cesare, G., Alimirzazadeh, S., Avellan, F., Schmid, M., Weber, C., Aksamit, C., Vanzo, D., Bogner, K., Stähli, M., Dreyer, M., Nicolet, C., Crettenand, S. (2021). Demonstrator for flexible small hydropower plant. Swiss Federal Office of Energy. https://www.aramis.admin.ch/Dokument.aspx?DocumentID=67425 https://www.aramis.admin.ch/Dokument.aspx?DocumentID=67425

Speich, M. J. R., Bernhard, L., Teuling, A. J., & Zappa, M. (2015). Application of bivariate mapping for hydrological classification. *Journal of Hydrology, 523*, 804–821.

Spielhofer, R., Schwaab, J., & Grêt-Regamey, A. (2023). How spatial policies can leverage energy transitions - Finding Pareto-optimal solutions for wind turbine locations with evolution- ary multi-objective optimization. Environmental Science and Policy, 142, 220–232. doi: https://doi.org/10.1016/j.envsci.2023.02.016

Stasinopoulos, D. M., & Rigby, R. A. (2007). Generalized Additive Models for Location Scale and Shape (GAMLSS) in R. *Journal of Statistical Software*, *23*(7), 1–46. https://doi.org/10.18637/jss.v023.i07

Stasinopoulos, M. D., Kneib, T., Klein, N., Mayr, A., & Heller, G. Z. (2024). *Generalized Additive Models for Location, Scale and Shape: A Distributional Regression Approach, with Applications*. Cambridge: Cambridge University Press. Spielhofer, R., Schwaab, J., & Grêt-Regamey, A. (2023). How spatial policies can leverage energy transitions - Finding Pareto-optimal solutions for wind turbine locations with evolution- ary multi-objective optimization. Environmental Science and Policy, 142, 220–232. doi: https://doi.org/10.1016/j.envsci.2023.02.016

Staubli, T., Abgottspon, A., Weibel, P., Bissel, C., Parkinson, E., Leduc, J., & Leboeuf, F. (2009). Jet quality and Pelton efficiency. *Proceeding of Hydro-2009*.

Steeb, N., Badoux, A., Bialek, R., Bogner, K., Hug Peter, D., et. al. (2022). Vorhersage und Warnung von Unwettern in der Schweiz. Das Zusammenwirken von Bund und Kantonen anhand von zwei Fallbeispielen im Jahr 2020. Wasser, Energie, Luft, 114(2), 98-104.

Talley, J. D., Worosz, T., Kim, S., & Buchanan, J. R. (2015). Characterization of horizontal air–water two-phase flow in a round pipe part I: Flow visualization. *International Journal of Multiphase Flow*, *76*, 212–222. https://doi.org/10.1016/j.ijmultiphaseflow.2015.06.011

Thirunavukkarasu, M., Sawle, Y., & Lala, H. (2023). A comprehensive review on optimization of hybrid renewable energy systems using various optimization techniques. https://doi.org/10.1016/j.rser.2023.113192

Viana, F., Pardo, R., Yánez, R., Trallero, J. L., & Joseph, D. D. (2003). Universal correlation for the rise velocity of long gas bubbles in round pipes. *Journal of Fluid Mechanics*, *494*, 379–398. https://doi.org/10.1017/S0022112003006165

Viviroli, D., Zappa, M., Gurtz, J., & Weingartner, R. (2009). An introduction to the hydrological mod-elling system PREVAH and its pre- and post-processing-tools. Environmental Modelling and Software, 24(10), 1209-1222. https://doi.org/10.1016/j.envsoft.2009.04.001

Wechsler, T., Stähli, M., Jorde, K., Zappa, M., & Schaefli, B. (2023). The future of Alpine Run- of-River hydropower production: Climate change, environmental flow requirements, and technical production potential. Science of the Total Environment, 890. doi: https://doi.org/10.1016/j. sci-totenv.2023.163934

Weitkamp, D. E., and Katz, M. (1980). A Review of Dissolved Gas Supersaturation Literature. Transactions of the American Fisheries Society, 109(6), 659-702.

Wickenhäuser, M. (2008). *Zweiphasenströmung in Entlüftungssystemen von Druckstollen* [PhD Thesis]. ETH Zurich. https://doi.org/10.3929/ETHZ-A-005595457

Wickenhäuser, M., & Kriewitz, C. R. (2009). Air-water flow in downward inclined large pipes. *Water Engineering for Sustainable Environment: 33rd IAHR Congress*.

Wilks, D. S. (2011). Chapter 8 - Forecast verification. In D. S. Wilks (Ed.), Statistical methods in the atmospheric sciences (Vol. 100, pp. 301–394). Academic Press. https://doi.org/10.1016/B978-0-12-385022-5.00008-7

Wisner, P., Mohsen, F. N., & Kouwen, N. (1975). Removal of Air from Water Lines by Hydraulic Means. *Journal of the Hydraulics Division*, *101*(2), 243–257. https://doi.org/10.1061/JYCEAJ.0004201

Wisskot, R. (2026). SmallFLEX Goms: Toy Energy Modeling: Framework Model Structure and R Code Documentation. Technical Report for SmallFLEX Goms. WSL, Birmensdorf.

Zappa, M., & Vogt, S. (2007). Hochwasser-Vorhersagesysteme der neusten Generation im Praxis-Test. In C. Hegg & J. Rhyner (Eds.), Forum für Wissen: Vol. 2007. Warnung bei aussergewöhn-lichen Naturereignissen (pp. 25-31). Eidgenössische Forschungsanstalt für Wald, Schnee und Landschaft

Zappa, M., Beven, K. J., Bruen, M., et al. (2010). Propagation of uncertainty from observing systems and NWP into hydrological models: COST-731 Working Group 2. Atmospheric Science Letters, 11(2), 83-91. https://doi.org/10.1002/asl.248

Zappa, M., Jaun, S., Badoux, A., et al. (2010). IFKIS-Hydro Sihl: ein operationelles Hochwasservorhersagesystem für die Stadt Zürich und das Sihltal. Wasser, Energie, Luft, 102(3), 238-248.

Zappa, M., Jaun, S., Germann, U., Walser, A., & Fundel, F. (2011). Superposition of three sources of uncertainties in operational flood forecasting chains. Atmospheric Research, 100(2-3), 246-262. https://doi.org/10.1016/j.atmosres.2010.12.005

Zappa, M., Rotach, M. W., Arpagaus, M., et al. (2008). MAP D-PHASE: real-time demonstration of hydrological ensemble prediction systems. Atmospheric Science Letters, 9(2), 80-82. https://doi.org/10.1002/asl.183

Zekollari, H., Huss, M., and Farinotti, D.: Modelling the future evolution of glaciers in the European Alps under the EURO-CORDEX RCM ensemble, The Cryosphere, 13, 1125–1146, https://doi.org/10.5194/tc-13-1125-2019, 2019

Zukoski, E. E. (1966). Influence of viscosity, surface tension, and inclination angle on motion of long bubbles in closed tubes. *Journal of Fluid Mechanics*, *25*(4), 821–837. https://doi.org/10.1017/S0022112066000442

Appendix

Appendix A - Proposal of a logical scheme for flexible operation with dewatering of KWGO.